THE COMPUTER SIMULATION AND PREDICTION OF ROCK FALL

by

James Richard Ashfield
School of Engineering
University of Durham

A thesis submitted to the University of Durham for the degree of Doctor of Philosophy.

June 2001

Abstract

This thesis deals with the study of rock falls using a mathematical model, codified for computer use, entitled GeoFall. GeoFall, which was developed by the author, allows predictions to be made of rock fall trajectories, run out distances and kinetic energies for a rock of any arbitrary shape. Its main purpose is to assist in the design of remedial works. The mathematical model is based on rigid body mechanics, and analyses a fall in 2D space using a new theory of impact dynamics developed by Brach (1991). The main features and algorithms of the program are presented in this thesis. The performance of GeoFall was evaluated by comparing actual rock fall events described in several published papers with the output created by GeoFall. Also the output from GeoFall has been compared with the output from other rock fall simulation programs used to simulate the documented rockfalls.

A new rock slope inventory system entitled the Rock Fall Risk Assessment System (RFRAS) has been developed by the author to determine the rock fall risk at specific rock fall sites. It consists of three phases of inspection, the slope survey, and the preliminary and detailed rating phases. The detailed rating phase uses 13 parameters that when assessed, evaluated and totalled, numerically differentiates slopes from the least to the most hazardous producing an overall rating in the range 21-1926. It not only allows the relative risk of rockfall between slopes to be assessed but it also categorises the rock fall risk and the potential number of future rockfalls. It has been tested on 18 slopes at ten locations in County Durham.

The final part of the thesis details a new laboratory based procedure that can be used to determine the coefficients of restitution for any type of rock material. The normal coefficient of restitution has been determined for seven different types of rock, and the tangential coefficient of restitution has been determined for a local sandstone. Some tentative correlations between the normal coefficient of restitution and the rocks physical properties, such as its Unconfined Compressive Strength (UCS) have been presented.

Acknowledgements

I wish to express my sincere thanks to my supervisor, Dr. John Wilson, for his advice, guidance, encouragement and professional dedication throughout this research. His patience and time spent reviewing this thesis has been invaluable.

I would also like to thank my parents for their continual support and encouragement.

Declaration

This thesis is the result of my own work. No part of this thesis has been submitted for any other degree in this or any other University.

James Richard Ashfield

Durham

June 2001

Contents

Chapter 3: Computer Simulation of Rock Fall

Chapter 4: Rock Slope Inventory Systems

Chapter 5: The Algorithms used in GeoFall

Chapter 6: Computer Simulation of Rock Fall using GeoFall

List of Figures

List of Tables

List of Maps

Notation

A_x	Acceleration along x axis	(ms^{-2})
A_y	Acceleration along y axis	(ms^{-2})
A_t	Acceleration tangential to slope region	(ms^{-2})
A	Area	(m^2)
a_j	Area of the j_{th} triangle	(m^2)
a_t	Tangential acceleration	(ms^{-2})
c'	Distance from the origin to the centroid along the x axis	(m)
d'	Distance from the origin to the centroid along the y axis	(m)
d_a	Distance to apex	(m)
d_c	Distance to centroid along baseline from point of contact	(m)
d_d	Distance to centroid normal to baseline from point of contact	(m)
Γ	Defined by equation 5.39	(m^3)
D_n	Post impact normal distance	(m)
d_n	Pre impact normal distance	(m)
d_v	Distance to vertex	(m)
e	Restitution coefficient	
e_n	Normal coefficient of restitution	
e_t	Tangential coefficient of restitution	
f	Shape factor	
g	Acceleration due to gravity	(ms^{-2})
h	Height	(m)
h_a	Height of triangle apex	(m)
I_c	Moment of area about the centroid	(m^4)
I_p	Polar moment of area about rock centroid	(m^4)
$I_{x'}$	Moment of area about the x axis	(m^4)
$I_{y'}$	Moment of area about the y axis	(m^4)
I_x	Moment of area about the x axis in relation to the centroid	(m^4)
I_y	Moment of area about the y axis in relation to the centroid	(m^4)
J_p	Moment of inertia about point of contact	(kgm^2)
J_c	Moment of inertia about centroid	(kgm^2)
m	Rock mass	(kg)
M	Moment Impulse	(Nms)
P	Force impulse	(Ns)
r	Radial distance from centroid	(m)
R	Rolling radius	(m)
S_x	Distance travelled in x direction	(m)
S_y	Distance travelled in y direction	(m)
t	Time interval	(s)
V_{et}	Post impact velocity of point of contact	(ms^{-1})
v_{et}	Pre impact velocity of point of contact	(ms^{-1})
v_x	Horizontal velocity	(ms^{-1})
V_n	Normal velocity after impact	(ms^{-1})
v_n	Normal velocity before impact	(ms^{-1})
V_t	Tangential velocity after impact	(ms^{-1})
v_t	Tangential velocity before impact	(ms^{-1})
v_y	Vertical velocity	(ms^{-1})
x', y'	Rock nodes as defined in an arbitrary local co-ordinate system	(m)

x, y	Rock nodes as defined about the centroid	(m)
X, Y	Co-ordinates of the rock nodes	(m)
X_c, Y_c	Centroid position	(m)
X_p, Y_p	Co-ordinates of the point of contact	(m)
X_s, Y_s	Co-ordinates that define the slope	(m)
z	Rock thickness	(m)
Δ	Defined by equation 5.40	(m^3)
ΔE	Change in energy head	(kgm^2s^{-2})
$\Delta x'$	Distance from the origin to centroid in the x' direction	(m)
$\Delta y'$	Distance from the origin to centroid in the y' direction	(m)
$\Delta \Pi$	Change in potential energy	(m)
Φ	Anticlockwise angle from the x axis to current position	(rad)
Λ	Clockwise angle from x axis to slope region	(rad)
α	Angle of incidence	(deg)
μ_d	Co-efficient of dynamic sliding friction	
μ_r	Co-efficient of rolling resistance	
μ_s	Co-efficient of static sliding friction	
θ	Anticlockwise angle from the x axis	(rad)
ρ	Density	(kgm^{-3})
ω	Angular velocity before impact	(rad s^{-1})
Ω	Angular velocity after impact	(rad s^{-1})

Chapter 1

Introduction

1 Introduction

1.1 Rock fall

The movement of surface rocks can occur chiefly in three ways: by rockslide, rock toppling and rock fall. Rockslides involve either a large mass of rock sliding as a single unit or a large mass of individual rocks sliding on a failure surface and moving as a whole with little interaction between individual rocks or a large collection of rocks flowing as debris avalanches with considerable interaction. In all of these cases, resistance to motion is provided by shear forces and contact of the rock mass with the slope surface is maintained. Rock toppling is the movement produced by the rotation about its base of a large block or column of blocks. Rock fall occurs when a single rock or boulder or a small group of independently moving rocks, becomes dislodged from an exposed face or slope and moves downwards by means of some combination of sliding, rolling, bouncing or free fall under the action of gravity. Both rockslides and rock toppling may act as precursors to rock fall.

Essentially rock fall is a phenomenon influenced mainly by processes that are active near the surface (Bjerrum and Jorstad, 1968) resulting generally in very rapid movement. The size of rock involved in a rock fall may range from pebbles to huge blocks with masses of hundreds of tonnes (Spang, 1987) and there is no generally accepted size of rock characteristic of rock fall. Furthermore, rock falls can occur in all rock types ranging from granite to mudstone, there being no simple correlation between rock strength and rock fall susceptibility.

Rock fall presents a potential hazard to settlements and buildings, civil engineering and quarrying sites, transport routes and people living, working or enjoying their leisure on or near the base of steep slopes and cliffs. Very large rocks are capable of catastrophic damage with a potentially large loss of human life. Even a rock fall comprising small pebbles provides for the possibility of a significant hazard for traffic.

Rock fall in rock slope engineering is an increasing problem today for the engineer because modern requirements are for high rock cuts. It is obviously more severe in mountainous regions but is not necessarily restricted to these areas. Frequently funds are not available to cope properly with the problem because the construction of a highway or railway route through rugged and mountainous territory may well involve

large tracts of rocky terrain with adjacent slopes ranging up to several hundreds of metres in height. When broken rock is present, the risk of rock fall is comparatively high and the budget set for work undertaken to reduce the hazards to achieve and maintain an acceptable level of safety must necessarily be limited. Because rock falls are unpredictable and incapable of being analysed with any precision, the concept of a factor of safety is not appropriate. The current approach is to use a rock slope inventory system to predict the rock fall risk to highway users and then, by means of a computational simulation, to attempt to predict their likely paths in order to make decisions about measures required to mitigate their effects.

1.2 Factors causing rock fall

The factors causing rock fall can be divided into two categories: structural and environmental. Of the structural factors, clearly a potentially loose rock mass must exist on the surface of the slope. In the case of a pebble or boulder, this will have undergone a previous movement. In the case of a rock mass, it must be sufficiently fissured to produce potentially unstable blocks. The slope on which the rock or boulder is situated must be steep enough to promote instability and to encourage continued movement resulting from this.

Environmental factors generally act as triggering forces but may also influence the structure of the surface and hence induce instability. Physical and chemical weathering are the chief agents primarily responsible for rock fall. Joints or discontinuities formed by planes of weakness or previous deformation provide egress for water and vegetation. This further reduces joint strength by a combination of frost and root wedging, erosion and increased porewater pressures producing a reduction of cohesive strength and frictional resistance to motion by reducing normal rock to rock forces. Water pressure acting within joints can have an important affect with similar results. Heavy rainfall can itself act as a trigger by producing a forceful stream of water or by erosion of stabilising material. Particularly dangerous is differential weathering in which a weak rock is removed leaving a more resistant rock unsupported as an overhanging ledge.

Earthquakes are another common source of environmental trigger but any source of groundborne vibration will suffice. Manmade vibration, due to blasting, operating of

construction plant and machinery, the process of excavation itself and passing traffic can all effectively trigger rock fall. Movement of people and animals on the slope can also act as triggers.

1.3 Factors affecting rock fall

Once rock fall has been initiated, its behaviour is influenced chiefly by the slope geometry, material and surface cover and the rock geometry and material properties (Ritchie, 1963).

Slope geometry can be divided into slope inclination, slope length, surface roughness and lateral variation. The first two factors are very important. The slope inclination defines zones of acceleration and deceleration and the slope length determines the distance over which the rock is accelerated or decelerated. As noted by Pfeiffer and Bowen (1989) and Wu (1985), surface irregularities alter the angle at which a rock impacts the surface and thus are significant in determining the character of the bounce. The effect of lateral variability is usually to channel falling rocks in a certain direction - for example down a gully, which could effect the velocity of the rocks. The material properties and nature of the covering of the slope influence the behaviour of the bounce, which is generally defined in terms of the normal and tangential coefficients of restitution of the rock on the slope.

Rock properties that affect rock fall behaviour are its size, strength, shape, and mass. Mass and size are important because a larger and heavier rock has greater momentum, is less likely to lodge among irregularities and will therefore travel further down slope. Shape and strength are also important. A spherical rock will obviously travel further than an angular one, as will a rock that does not break apart on impact.

1.4 Rock fall mitigation

There are two main approaches to overcoming the rock fall problem: protection and stabilisation. In both cases the objective is to prevent rocks causing damage to transport routes or buildings and threatening human life but the methods used are very different.

Protective measures are used to deal with rocks that are already in motion. The method of protection must allow for the sizes of rocks involved as the cost of

protection increases rapidly with increasing size and the rate at which fallen rock accumulates (Peckover 1975). Methods used include relocation of the railway or highway, the construction of interception ditches on the slope and shaped ditches immediately adjacent to the vulnerable utility. Wire mesh blankets offer an economical solution for protection from rocks 0.6 to 1.0m in diameter. These serve to restrain loose rocks and guide falling ones into the ditches below. Catch nets, fences and walls can be used to intercept bouncing rocks 0.6m to 1.0m in diameter either part way up a slope or in front of the vulnerable utility. Finally rock sheds and tunnels provide the ultimate protection against rock fall where stabilisation or other methods are not effective or economical.

Stabilisation involves preventing the rocks moving in the first place. Techniques used include scaling to remove loose rock in a safe manner, and trimming to remove small ragged areas, which would otherwise require repetitive scaling operations. Presplit blasting in the original construction of a cutting or slope leaves a more stable slope. Careful design of the slopes can prevent the problem of rock fall occurring.

Other stabilisation methods include drainage, to prevent the build up of water pressure, and the prevention of weathering by the application of shotcrete. Finally individual rocks and rock masses can be prevented from moving by the use of rock bolts, dowels, anchors and buttresses.

1.5 Rock slope inventory systems

Over the past decade various rock slope inventory systems have been developed. The purpose of these systems is to assess the rock fall risk to a highway user by considering the combined effects of the trigger mechanisms that act upon the jointed rock mass and the risk of a falling rock hitting a passing vehicle. The various parameters that trigger rock fall are either subjectively or numerically assessed and are assigned a value based upon the relative risk. A total value is then calculated based upon the value received for each parameter. This allows a comparison of rock fall risk between rock slopes and also determines the level of risk at that site.

1.6 Computer programs to simulate rock fall

Numerous analysis of rock fall have been developed over the last 30 years, the first of which is probably attributable to Ritchie (1963). Most of these have led to computer simulation of rock fall, which are normally restricted to two dimensions, but some extend to three dimensions.

The rock is generally treated as an indestructible, massive rigid body of simple shape, usually having some circular form. In some cases point masses or particles are used, occasionally a polygonal or an ellipsoidal shape is adopted and more rarely a fully three-dimensional form.

Normally the slope surface profile is formed by a continuous piecewise linear set of segments, cells or regions, each of which is an intersection of the slope surface and the vertical plane in which the rock moves. The rock is set in motion by commencing to slide or roll from its initial position on the slope surface or by being dropped or thrown from some initial position above the slope surface. The subsequent motion of the rock under gravitational action consists of some combination of resisted surface movements (sliding or rolling) and aerial motion consisting of trajectories separated by bounces where impact between the rock and the slope occurs. Air resistance is usually neglected. The surface motions and impacts are governed by mathematical equations based on established laws of mechanics and hypotheses based on energy and momentum laws. The latter may not be consistent with the former. The majority of rock fall programs use rolling resistance (μ_r), sliding friction (μ_d), and restitution coefficients to determine the surface motion and impact characteristics. A combined coefficient of restitution (e) or separate normal (e_n) and tangential (e_t) coefficients may be used to calculate rebound velocities.

Most computer simulations allow for some sort of random behaviour and allow for multiple rock fall paths to be produced. Graphical output is used to show the multiple paths and to summarise the analysis of the results of the simulation.

1.7 Thesis aims and objectives

The aims and objectives of this Thesis are threefold;

a) to write a leading edge rock fall simulation program to overcome the shortcomings of existing programs,

b) to develop a new rock slope inventory system to analyse the risk from rock fall slopes,

c) to determine coefficients of normal and tangential restitution using a repeatable laboratory method.

1.7.1 GeoFall

GeoFall is a general two-dimensional rock fall simulation program, which was written by the author over a period of approximately 14 months. A demonstration version containing the example simulations illustrated in this thesis is contained in a pocket in the rear cover. The various motions of the rock are linked to form complete rock fall paths, and the rock is assumed to behave as a rigid body that remains intact during rock fall. Any slope geometry may be modelled including re-entrants and closed profiles such as caverns. Various rock fall shapes are permitted which include a sphere, disc, ellipse, and several polygonal shapes. The user may also generate any rock shape of their choosing. Translational and rotational velocities after impact are related to those before impact by coefficients of normal and tangential restitution. Rolling and sliding are also modelled by a coefficient of rolling resistance and friction, a combination roll-slide is not possible and rocks may only slide on one surface. Surface roughness is set by randomly varying the angle of the slope. Kinetic energy, velocity, bounce height envelopes and the rock fall distribution are all determined by the program at slope locations pre set by the user. The effectiveness of user defined rock fall nets may also be determined.

1.7.2 The Rock Fall Risk Assessment System (RFRAS)

Previous rock slope inventory systems have concentrated on the estimation of rock fall risk to highway users. The RFRAS has been developed and tested by the author over a period of four months. The purpose of the RFRAS is to allow the practising

engineer to be able to assess the level of risk of rock fall from any rock slope. Once the risk of rock fall has been determined then the slopes at high risk of rock fall may be modelled on a rock fall simulation program such as GeoFall. The simulation program thus provides an accurate means of determining the consequences of a rock fall event whilst the RFRAS determines the likelihood of a rock fall event.

If more than one rock slope is to be assessed then the rating obtained from the RFRAS provides a subjective comparison between slopes. This allows a cost and benefit analysis to be made so that funds may be allocated accordingly.

1.7.3 Laboratory determined coefficients of restitution

Previous methods used to determine the coefficients of restitution have been based on either back analysis of rock fall events using computer simulation or in-situ filming of triggered rock falls.

In order to overcome the shortcomings of back analysis and in-situ testing a repeatable and accurate laboratory test is required, allowing the coefficients of restitution to be determined in a controlled environment.

The method chosen to determine the coefficients of restitution for various rock types was an air table combined with video equipment. Disks of rock were cored and floated on a bed of air, which provided a frictionless surface. The disks were then fired, with no spin, at a large immobile piece of the same rock type, and the rock allowed to rebound. The pre and post impact trajectory was recorded using high-speed video equipment, allowing the coefficients to be calculated.

1.8 Thesis Structure

This thesis is split into nine chapters and contains four appendices.

The Introduction in chapter one provides a brief overview on the subject of rock fall and the aims and objectives of this thesis. Chapter two is a general literature review which compares and contrasts the causes of rock fall, methods of stabilisation and protection, rock slope inventory systems, expert systems, geographical information systems and the use of finite element modelling. The third chapter compares and contrasts existing programs and the coefficients that are used in their formulation. In chapter four various rock slope inventory systems including the Rock Fall Risk

Assessment System (RFRAS) are described in detail. The main algorithms used in the GeoFall program and their verification are described in detail in chapter five. In chapter six GeoFall has been used to model rock falls described in the literature. Where another computer program has been used to simulate the rock fall event then the output has been compared to that produced by GeoFall. A laboratory method that uses an air table and a floating disk of rock has been developed to determine the coefficients of restitution for several types of rock and is described in chapter seven. In chapter eight the main findings have been discussed. Chapter nine presents the conclusions and recommendations for further work.

Chapter 2

General Literature Review

2 General literature review

2.1 Causes of rock fall

Tectonic activity such as folding and thrust faulting produces steep escarpments prone to rock fall. At the rock mass scale, tectonic activity controls joint orientation and micro fracturing, both of which result in kinematically feasible rocks. In addition many large rock falls are triggered by earthquake induced ground accelerations which cause fracturing of the rock mass and loss of friction across inter block discontinuities.

In order to identify slopes subject to rock fall one must have a basic understanding of the causes and mechanisms of rock fall. Several papers on rock fall inventory studies have been published all of which have attempted to correlate rock fall magnitude and frequency with a variety of potential causal mechanisms.

McCauley et al. (1985) visited 92 sites in California to assess the cause of rock fall. They also sent a questionnaire to the California Department of Transportation maintenance personnel. The information gathered from this was used to examine the causes of rock fall, to identify corrective methods that were used, and to determine the effectiveness of the methods chosen. Figure 2.1 shows the trigger mechanisms of 1308 rock falls recorded by the California Department of Transport. Because of the diverse topography and climate within California, their records provide a useful guideline of the stability condition of rock slopes and the causes of rock falls.

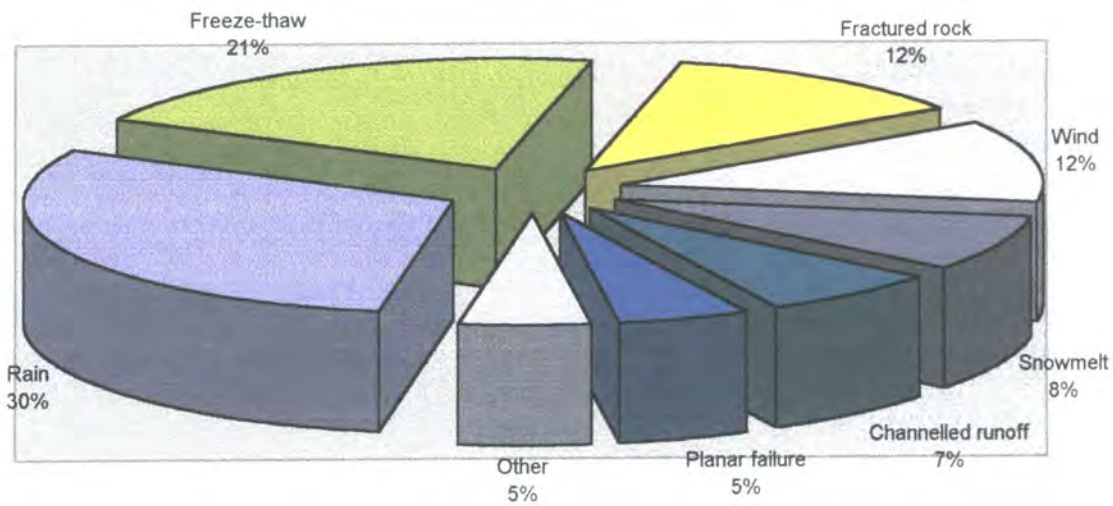

Figure 2.1: Causes of rock falls on highways in California.

Luckman (1976) collected rock fall frequency, temperature and precipitation data in Jasper National Park, Alberta during the period May to October 1969. The study area was Surprise Valley, a small alpine catchment bounded by massive vertical cliffs (180 to 400m high) cut in dolomite with valley floor temperatures ranging from -12°C in January to 15°C in June, and total annual precipitation averaging 400mm. Luckman found that rock fall frequency showed a distinct seasonal pattern, with spring and autumn maxima separated by a period of low activity in which rock fall events could be correlated with major storms. In addition to studying broad seasonal variations, Luckman also looked at diurnal frequency data for a west and east facing slope. The west facing site was found to have an equal hourly probability of rock fall between the hours 10.00 and 20.00, whereas the east facing slope was more likely to produce rock fall events during the hours in which it was exposed to sunlight.

Gardner (1980) also studied frequency magnitude relationships of rock fall in the Canadian Rocky Mountains. His study area was located in Highwood Pass, Alberta, 80km south west of Calgary. Highwood Pass cuts through 800m high north east facing fault scarps some 2185m above sea level. Mean annual temperatures were slightly below freezing and precipitation averaged 700mm, falling mainly as snow. Data collection during June, July and August 1975-77 involved observation of low magnitude events and the field mapping of rock fall deposits. The data was used to calculate a frequency of 0.83 events per hour of observation, with an increase in frequency during the afternoon. Gardner also proposed a tentative correlation, based on observations in Highwood Pass, between geological structure, slope aspect, temperature, moisture conditions and rock fall frequency. Seventy five percent of all rock falls were found to occur on north facing slopes cut in easily weathered, discontinuous rocks. In the Canadian Rocky Mountains, northern slopes exhibit increased freeze thaw activity that probably accounts for the increased rock fall frequency. The study also showed that rock fall increased on warm days when snow and ice patches melted suggesting that joint water pressure played an important role in rock fall initiation. Both Luckman and Gardner show that freeze thaw cycles and precipitation are the primary causes of rock falls in the Canadian Rocky Mountains.

In a similar study in County Antrim, Northern Ireland, Douglas (1980) collected rock fall data for cliffs in olivine flood basalt. The basalt contained a set of vertical cooling joints and showed evidence of extensive micro fracturing. Rock fall data was recorded

on a weekly basis from 1968-72; temperature and rainfall data was also collected. Douglas found that low magnitude, high frequency rock fall activity showed seasonal maxima in November, December, February, and March with a positive linear correlation between rock fall and the number of freeze thaw events.

Peckover and Kerr (1977) also studied the effects of seasonal weather on movement of rock slopes. They noted that rock fall occurred principally during November to March when the mean temperature was at or slightly below freezing, freeze thaw cycles were taking place and the rock saturated from an accumulation of precipitation. When the temperature was above freezing between March and November the frequency of rock falls varied more or less in proportion to the amount of rainfall.

On a similar theme, Jennings and Costin (1978) investigated the seasonal movement of blocks of stone through snow creep over a period of thirteen years. Snow creep is the dragging of boulders across a rock surface due to the movement of thick layers of snow. Some of the stones were found precariously balanced on the edge of vertical drops and show that snow creep is a possible cause of rock fall.

These rock fall inventories suggest that climate and geology exert a fundamental control on rock fall activity, in particular that freeze thaw cycles and precipitation are the main causal mechanisms of rock fall in temperate climates.

2.2 Remediation methods

Once the slopes and rock cuts that require remedial work have been identified, appropriate hazard mitigation techniques must be chosen. These take the form of either stabilisation or protection methods.

Stabilisation methods are designed to prevent the movement of rock blocks, whereas protection methods assume the block is going to fall and are designed to control its direction and speed. Ten common methods of stabilisation and six methods of protection are illustrated in Figure 2.2.

Several reviews of rock fall protection and stabilisation measures have been published by Fookes and Sweeney (1976), Peckover and Kerr (1977), Spang (1987) and Wyllie and Norrish (1996). Each review divides rock fall stabilisation and protection measures into distinct categories; for example Spang refers to 'passive' and 'active' protection whilst Fookes and Sweeney describe a time sequence of remedial measures.

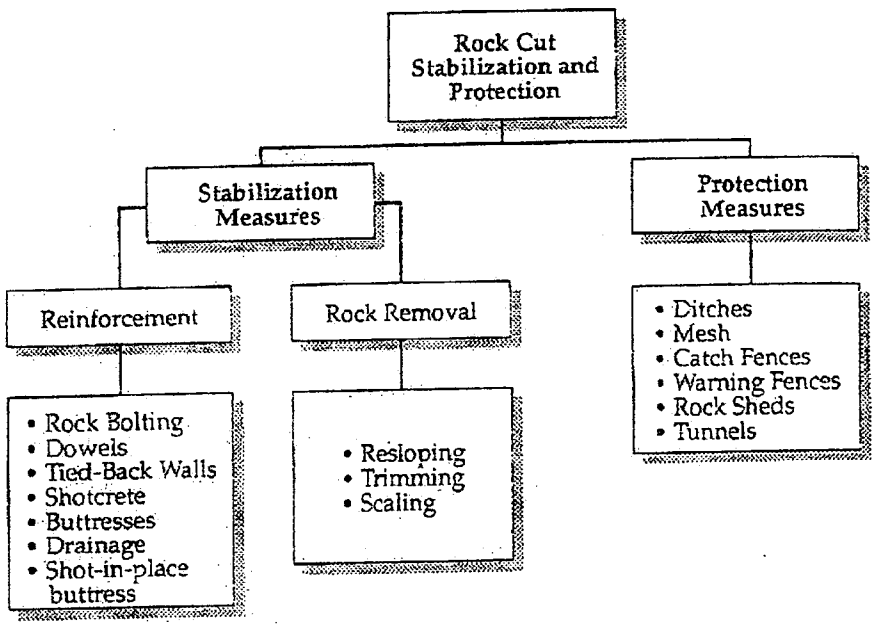

Figure 2.2: Slope stabilisation and protection methods (Wyllie and Norrish, 1996).

2.2.1 Methods of slope stabilisation

Stabilisation methods fall into two categories, reinforcement and rock removal. Figure 2.2 lists ten of the more common stabilisation methods. It is important that the appropriate method is used for the particular conditions at each site.

2.2.1.1 Rock reinforcement

Figure 2.3 shows a number of reinforcement techniques that may be implemented to secure potentially loose rocks. The common feature to all of these techniques is that they minimise the relaxation and loosening of the rock mass that may take place because of excavation and unloading. Reinforcement of rock slopes is most effective if it is installed before excavation, a process known as pre-reinforcement. For example, installation of rock bolts at the crest of a cut before excavation prevents relaxation and loosening of the rock slope upon subsequent excavation.

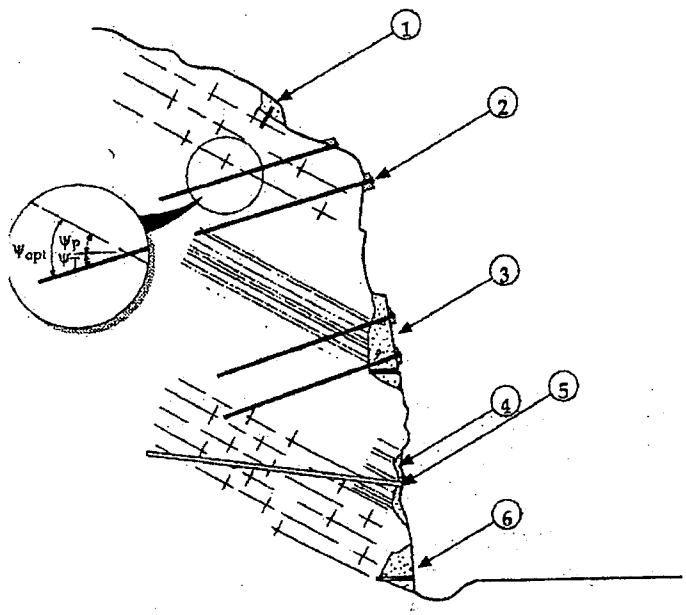

Figure 2.3: Rock reinforcement (Wyllie and Norrish, 1996).

2.2.1.1.1 Rock bolts

A rock bolt consists of a steel rod, which is inserted into a pre-drilled hole in the rock mass. It is fixed either by grouting or by an expansion bolt. The exposed end passes through a steel plate designed to spread the compressive force caused by the tensioning of the rod.

Rock bolts are installed across potential failure surfaces and anchored in the sound rock beyond the surface. The application of a tensile force in the bolt, which is transmitted into the rock by a reaction plate at the rock surface, produces compression in the rock mass and modifies the normal and shear stresses across the potential failure surface.

2.2.1.1.2 Dowels

Dowels are composed of lengths of reinforcing steel grouted into holes drilled into the underlying, stable rock, with a cap of reinforced concrete encasing the exposed steel. The reinforcing steel dowels used to anchor the concrete to the rock are usually about 25mm in diameter, embedded about 0.5m into sound rock, and spaced about 0.5 to 0.8m apart.

2.2.1.1.3 Tieback walls

A tieback wall is a reinforced concrete wall that is constructed over the area of fractured rock, holes for rock bolts are then drilled through sleeves in the wall.

Tieback walls are used where there is a potential for a sliding failure in closely fractured rock. Finally, the rock bolts are installed and tensioned against the face of the wall. The wall acts as both protection against ravelling of the rock and as a large reaction plate for the rock anchors.

2.2.1.1.4 Shotcrete

Shotcrete is a pneumatically applied, fine aggregate mortar that is usually placed in a 75 to 100mm layer. Zones or beds of closely fractured or degradable rock can be protected by applying a layer of shotcrete to the rock face. The shotcrete controls both the fall of small blocks of rock and progressive ravelling that will produce large, unstable overhangs on the rock face. However, shotcrete provides little support against

sliding of the overall slope; its primary function is surface protection. It is important that drain holes be drilled through the shotcrete to prevent the build up of water pressure behind the face.

2.2.1.1.5 Buttresses

A buttress is a large mass of usually lightly reinforced concrete that is built in a cavity of the slope face. The buttress serves two functions: to retain and protect areas of weak rock and to support the overhang. Buttresses should be designed so that the thrust from the rock to be supported loads the buttress in compression. In this way, bending moments and overturning forces are eliminated, and there is no need for heavy reinforcement of the concrete.

2.2.1.1.6 Drainage

Drainage is usually provided by means of lined or unlined drain holes drilled into the rock mass which serve to reduce water pressures.
The most important factor in the design of drain holes for rock slopes is to locate them so that they intersect the fractures that are carrying the water.

2.2.1.1.7 Shot in place buttresses

On landslides where the surface of a rupture is a well-defined geological feature such as a continuous bedding plane, stabilisation may be achieved by blasting this surface to create a shot in place buttress. The friction angle of the broken rock is greater that that of the smooth and planar bedding surface because of the greater effective roughness of the broken rock. Fracturing of the rock also enhances drainage.
The method of blasting involves drilling a pattern of holes through the sliding surface and placing an explosive charge at the level that is just sufficient to break the rock.

2.2.1.2 Rock removal

Stabilisation of rock slopes can be accomplished by the removal of potentially unstable blocks. Figure 2.4 shows several removal methods including;

a) resloping zones of unstable rock,

b) trim blasting overhangs, and

c) scaling individual blocks of rock.

In general, rock removal is a preferred method of stabilisation because the work eliminates the hazard and no future maintenance is required. However, removal should only be used if it is certain that the new face will be stable.

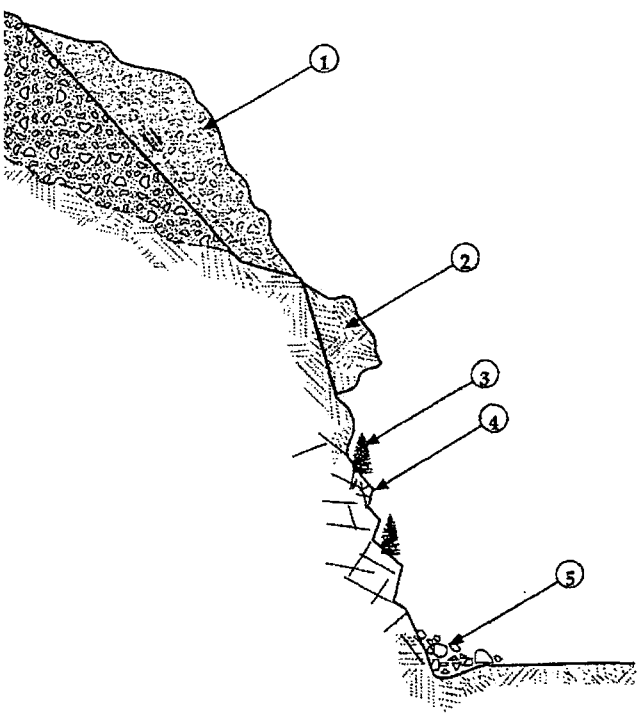

Figure 2.4: Rock removal methods for slope stabilisation. (Wyllie and Norrish, 1996).

2.2.1.2.1 Resloping

When there is overburden or weathered rock in the upper portion of a cut, it is often necessary to cut this material at an angle flatter than that of the more competent rock below. Careful attention should be given to investigating this condition because the thickness and properties of the overburden or weathered rock can vary considerably over short distances.

2.2.1.2.2 Trimming

Failure of a portion of a rock slope may form an overhang on the face, which may be a hazard if it were to fall. Trimming involves drilling, light blasting, and scaling in order to remove dangerous blocks.

2.2.1.2.3 Scaling

Scaling describes the removal of loose rock, soil, and vegetation on the face of a slope using hand tools such as scaling bars, shovels, and circular saws. On steep slopes workers are usually supported by ropes anchored at the crest of the slope and tied to a climbing harness.

2.2.2 Protection measures against rock falls

An effective method of minimising the hazard of rock falls is to let the rock falls occur and to control their distance and direction of travel. Several methods of rock fall control and protection are listed in Figure 2.2. These include catchment ditches and barriers, wire mesh fences, mesh hung on the face of the slope and rock sheds. A common feature of these protection structures is their energy absorbing characteristics, which either stop the rock fall over some distance or deflect it away from the facility that is being protected. It is possible to control rocks with diameters as large as 2 to 3m falling from heights of several hundred metres and striking with energies as high as 1 MJ. Rigid structures such as reinforced concrete walls or fences with stiff attachments to fixed supports are rarely appropriate for stopping a falling rock.

2.2.2.1 Ditches

A catch ditch at the toe of the slope is often a cost-effective means of stopping rock falls when there is adequate space for it. Perhaps the first significant work in the study of rock fall ditch design at its time was attributable to Ritchie (1963). Fookes and Sweeney (1976), Whiteside (1986) and Badger and Lowell (1992), have all produced ditch design charts based on Ritchie's work. Fookes and Sweeney published a design chart summarising Ritchie's work which related slope height and angle to ditch height and width, but they were however conservative in their interpretation of the original data. Whiteside published a corrected chart (Figure 2.5, which provides a good basic design criterion for rock trap ditches.

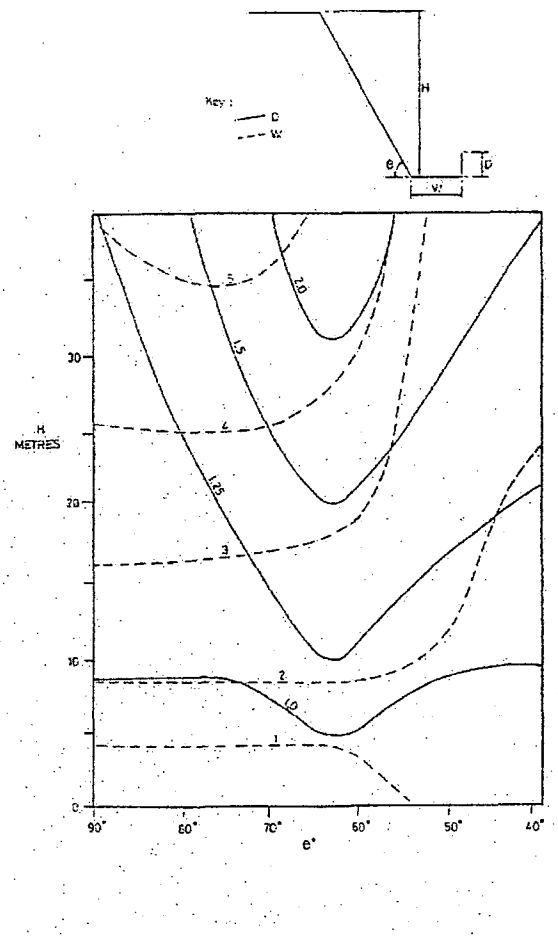

Figure 2.5: Fookes and Sweeney ditch design chart, with modifications according to Whiteside (1986).

Badger and Lowell concluded that an increase in slope height results in a larger run out distance and greater rebound heights, whereas, an increase in slope angle results in smaller rebound heights but greater run out distances.

2.2.2.2 Draped mesh

A draped mesh consists of a wire mesh hung on the face of a rock slope, which can be an effective method of containing rock falls close to the face and preventing them from bouncing onto the road. Because the mesh absorbs some of the energy of the falling rock, the required dimensions of any ditch at the toe of the slope are considerably reduced.

Chain link mesh is suitable on steep faces for controlling rock falls with dimensions less than about 0.6m, and woven wire rope may be suitable for rock with dimensions up to 1m. For larger blocks, ring nets may be used.

2.2.2.3 Barriers

A variety of barriers such as concrete, gabion, earth barrier or suspended tyre barrier (attenuators) can be constructed to either enhance the performance of excavated ditches or to form catchment zones at the toes of slopes. The function of a barrier, which is often combined with a ditch, is to form a vertical face particularly at the base of a slope that traps rolling rocks or rocks having small bounce heights. Without the presence of the barrier such rocks can roll up the sloping outer side of the ditch.

2.2.2.4 Gabions and concrete blocks

Gabions are rock filled baskets, typically measuring one metre square in cross section, that are often constructed on site with local waste rock. Advantages of gabions are the ease of construction on steep slopes and irregular foundations and their ability to sustain considerable impact from a falling rock. Concrete barriers are also used extensively on transportation systems for rock fall containment because they are often readily available and can be placed quickly. Concrete blocks are somewhat less resilient to impact than gabions.

2.2.2.5 Mechanically Stabilised Earth Barriers (MSE)

Various earth barriers have been constructed by Hearn et al. (1995) using geofabric and soil layers, each about 0.6m thick, built up to form a barrier of up to four meters in height. By wrapping the fabric around each layer it is possible to construct a barrier with a vertical front and back face; the impact face can be strengthened by such materials as railway sleepers, gabions, and rubber tyres. An MSE barrier can stop rocks as heavy as 14 tonnes, possessing kinetic energies in the order of 1400kJ. MSE barriers provide the best protection against large boulders with high kinetic energies.

2.2.2.6 Nets, fences and attenuators

During the 80's various nets and fences suitable for installation on steep rock faces, in ditches, and on talus run out zones were developed and tested. A common feature of all of these designs is that they deform upon impact and exhibit energy absorbing characteristics. When a rock collides with a net, there is deformation of the mesh, which then engages energy absorbing components over an extended time of collision. This significantly increases the capacity of these components to stop rolling rocks and allows the use of lighter, lower cost elements in construction. The angular velocity of the block is significant in determining the amount of damage at the point of impact.

Care must be taken in the assembly of these structures since incorrect torque on the bolts of the friction brakes may result in total collapse of the structure (Peila et al, 1988).

Peila et al. concluded that the kinetic energy, maximum deflection, the force transmitted to the foundations and precise assembly instructions must always be included in the design of a rock fall fence.

2.2.2.6.1 Woven wire rope nets

Nets are constructed with either woven wire rope mesh or ring mesh. They can be located either in the ditch beside the road, railway, or on the steep slope above it. The components of these nets are a series of posts anchored to the foundation with grouted bolts. Additional support for the posts can be provided by up slope anchor ropes incorporating friction brakes that are activated during high-energy events, which help disperse the forces.

2.2.2.6.2 Flex post rock fall fence

The flex post system (Hearn et al, 1995) is composed of a series of posts constructed of bundles of seven wire pre-stressed strands grouted into lengths of steel pipe. A portion of the strand bundle is left ungrouted, forming a flexible spring element that can withstand large rotations of the post without damage. When small rocks strike the fence, the energy is absorbed by the mesh and wire stays; for larger rocks, the mesh is stretched taut and the posts bend. The fence then rebounds to its vertical position.

2.2.2.6.3 Fences on talus slopes

Rock falls down talus slopes tend to roll and stay close to the slope surface. In these circumstances a lightweight chain link fence placed either on the slope or along the outside edge of the ditch will decelerate or catch the rock.

2.2.2.6.4 Rock fall attenuators

When rocks fall down a narrow gully or chute bounded by stable rock walls, it is possible to install a variety of relatively lightweight fences that slow down and absorb the rock fall energy. The general method of construction is to install a pair of rock bolts to support a wire rope from which the fence spanning the gully is suspended. For small rock falls a chain link mesh is draped from the anchor rope. Falling rocks are gradually brought to a halt as they bounce and roll under the mesh.

For rocks as large as 1m, an attenuator fence utilising waste automobile tyres developed by Hearn et al. (1995) in conjunction with the Colorado Department of Transport has proved to be successful in a number of installations. The fence consists of a wire rope from which a number of steel rods are suspended each holding a stack of tyres mounted on rims. The stacks of tyres are arranged so that they form a continuous barrier across the chute. When the attenuator is struck by a falling rock, the kinetic energy is dissipated by a combination of the compression of the rubber tyres and the movement of the stacks of tyres, which swing on the suspension cable rope. The prototype models were found to be effective up to 81kJ. Rock fall attenuators do not capture boulders; falling boulders are slowed down and come to rest further down slope.

2.2.2.7 Warning fences

Fences and warning signals that are triggered by falling rocks are sometimes used to protect railways and roads. The warning fence consists of a series of timber posts and cantilever crossarms that support rows of wires spaced about 0.5m apart. At least one wire will be broken by rocks rolling or bouncing down the face. The wires are connected by a signal system that displays a red light when the wire is broken.

2.2.2.8 Rock sheds or tunnels

In areas of extreme rock fall hazard where stabilisation work would be very costly, construction of a rock shed or even relocation of the highway or railway into tunnels may be justified. On shallow slopes, the roof of a rock shed is angled such that rocks may roll over it rather than to withstand a direct impact. If there is a steep slope above the rock shed then the roof material must be designed to withstand impact loads.

2.3 Rock slope inventory systems

Effective management of unstable rock slopes on a road network requires knowledge of their location and the risk posed to the road user. Existing stability assessment and risk evaluation systems use variable approaches and are dominated by subjective judgement. In addition they are usually undertaken on a reactive basis, prompted by rock falls. As a consequence road users may be exposed to risk before problems are assessed, comparison of results is difficult, budgetary problems arise as incidents are largely unforseen, and prioritisation of funds is impossible.

In order to assess these problems various empirical rock slope inventory systems have been developed by Brawner and Wyllie (1975), Pierson (1992), McMillan and Matheson (1997) and Franklin and Senior (1997). The purpose of these systems is to evaluate the rock fall risk by considering the combined effects of the various rock fall trigger mechanisms that act upon the rock jointing.

Blocks of falling rock pose a significant hazard to buildings and transport arteries in the vicinity of degrading rock slopes. In particular, rock falls from road cuts deposit large boulders on the road pavement causing potentially fatal road accidents. Rarely, falling rocks may hit a moving or stationary vehicle.

Several rock falls from slopes adjacent to highways in British Columbia, Canada, resulted in several fatalities to road users. These cases set a legal precedent as to the acceptable risk from rock fall whilst using a highway. The argillite slope that one of the rock falls originated from was assessed by Bunce et al. (1997) using the Rock Fall Hazard Rating System (RHRS) developed by Pierson. The documented rock fall history onto the highway was appraised. In order to determine the rock fall frequency the damage to the pavement below the slope was mapped to identify the number, size and distribution of the depressions caused by rock fall impacts. This is the first recorded instance that rock fall frequency has been assessed by using roadway damage.

Risk analysis procedures suggested by the Canadian Standards Association (CAN/CSA, 1991) provided the framework for a rock fall hazard assessment onto the highway. The probability of an impact on a stationary vehicle, a moving vehicle and the risk of death from a rock fall were all appraised.

In the argillite cut the probability of death during a single use was of the order of $6x10^{-8}$ and the annual probability of a rock fall causing a death was $8x10^{-2}$. A daily commuter was subject to a risk of $3x10^{-5}$ per year, which is comparable with the risk of death from fire or drowning. Bunce et al. concluded that on highway routes through rock slopes, with a limited budget, the remediation of the areas can be prioritised by the RHRS and that the public should be prepared to accept a reasonable level of risk.

The Oregon Department of Transport (ODOT) began to discuss the need for a rock slope inventory system in 1984. As part of an initial literature survey, a study by Brawner and Wyllie (1975) was reviewed. It contained rating criteria and a scoring method that grouped rock fall sections into either A, B, C, D or E categories based upon the potential and expected effect of a rock fall event. ODOT adopted a similar assessment approach as part of the preliminary rating of rock fall areas.

In a subsequent study, Wyllie (1987) outlined a more detailed procedure for prioritising rock fall sites. Wyllie's method included specific categories for evaluation and used an exponential scoring system. This became the prototype for Oregon's RHRS and in 1989 ODOT completed the development of an effective RHRS which was tested at over 3000 sites. Pierson (1992) presented the final version in a paper.

The RHRS is a two stage system, the first stage or preliminary slope rating is based upon that by Brawner and Wyllie, whilst the second detailed rating phase is based on the exponential system presented by Wyllie. The RHRS was intended to be a proactive

tool that allowed transportation agencies to rationally address rock fall hazards rather than to react to rock fall accidents. It provides a method of targeting limited construction funds available by numerically differentiating the apparent risk at rock fall sites. Much of the RHRS is subjective and proper training in its application is necessary to ensure consistency of ratings between different users. The RHRS is strictly only applicable to highways and cannot be used to assess rock fall risk on railways and the like. No discrimination is made between the probability of a rock fall and the consequences of a rock fall. Since 1988 Washington State Department of Transport has used the RHRS to address rock fall problems on existing facilities around the state (Badger and Lowell, 1992). The purpose was to assess a large number of areas where rock fall had occurred and to objectively rate the slopes in terms of potential hazard.

A similar rock slope inventory system called RHRON has been developed by the Ontario Ministry of Transportation (Franklin and Senior, 1997) which was modelled on the RHRS system. The exponential weighting system as used in the RHRS was removed from RHRON and the number of parameters was increased from twelve to twenty. The RHRON system rates each parameter from zero (no problem) to nine (imminent collapse) and consists of a basic rating and a detailed rating phase. The basic rating phase is used for preliminary screening. The detailed RHRON is only applied to the more dangerous sites. The final value obtained allows the user to distinguish between the least and most dangerous sites.

In a more recent paper McMillan and Matheson (1997) have developed a two stage approach to identifying and classifying rock slope risks. The first stage of this system derives a Rock Slope Hazard Index (RSHI) from rapid standardised field data collection. The RSHI is defined as the potential for failure multiplied by the consequences of failure. This acts as a coarse sift eliminating slopes with a low risk potential from the later second detailed assessment stage and has the same purpose as the preliminary rating phases used in the RHRS and RHRON. The second more detailed stage derives a Rock Slope Hazard Rating (RSHR) from detailed field surveys. This is a more detailed and comprehensive measure of the risk posed by an unstable rock face and is derived from the sum of the two risks posed by all of the potential failures on that slope. It is a semi-probablistic method based on the principles of quantitative risk analysis. The system has been field tested on 179 rock slopes in West

Lothian, Scotland. The results were used to classify the slopes according to the requirement for future action.

2.4 Expert systems

Palassi and Franklin (1998) have developed an expert system called ROFEX which is based on the rock slope inventory system RHON. Having assigned a hazard rating using RHON, ROFEX makes use of information stored in a database to provide suggestions of alternate methods of hazard mitigation. ROFEX guides in the selection of methods to match the given rock conditions. The treatments can be designed and costs estimated by using empirical design methods stored in ROFEX.

Under a research grant administered by the Washington State Transportation Commission (WSTC) and the Federal Highway Administration (FHWA), WSDOT and Washington State University developed an expert system entitled the Unstable Slope Management System (USMS). The USMS is a computer program consisting of a database and algorithms that prioritise unstable slopes and is described briefly in the paper by Badger and Lowell (1992). Unstable slopes not only include rock fall but also landslides, embankment failures, debris flows etc. The algorithms are developed from the expert shell system CLIPS, a language developed by the National Aeronautics and Space Administration. The USMS identifies factors such as the cause of instability, cost of repair, use of road, and safety to motorists that determine the importance of a failure site. The USMS develops a list of priority ranked sites from which mitigation work can be selected.

2.5 Geographical Information Systems (GIS)

Rock slope inventory systems and expert systems can be combined with data concerning regional climate, geology, land use and traffic distribution in a GIS, which can then be used to aid risk analysis. Navarro and Wohl (1994) describe the use of a GIS to evaluate the risk potential of geological hazards in Medelin, Columbia. Several factors including geology, topography, hydrology and land use were put into the GIS as map based data layers. Boolean overlay techniques were then used to apply risk ratings, on a scale of one to ten, to each data layer. The influence of each factor was

subjectively weighted according to each hazard. Ultimately, the product of the weighting value and the category weighting was used to define the risk rating for an individual site. The GIS software was then used to combine the hazard rating with details of local infrastructure and planning criteria, making the program an excellent decision support tool for land use planners.

2.6 Distinct/Finite element modelling of rock slopes

If a large development is to be situated near an unstable rock slope, it is important to investigate the response of the rock mass to various static and dynamic loads. Distinct element modelling packages are particularly well suited to assessing the stability of discontinuous rock masses. Perhaps the most popular distinct element formulation is UDEC (Universal Distinct Element Code) which simulates the response of discontinuous media subjected to static or dynamic loading. UDEC, in common with the Distinct Element Method (DEM), treats a discontinuous medium as a series of blocks interacting through deformable joints. The discontinuities form boundary conditions between blocks, and individual blocks can be constrained to behave as rigid or deformable material. In the latter case each block is subdivided into a mesh of finite difference elements, each of which deform according to a prescribed stress-strain law (which may be linear or non linear).

Finite element modelling techniques have also been applied to rock slopes. For example, Huang et al. (1990) used a finite element code to analyse the stress distribution in large rock masses that form dam abutments in China.

2.7 Recent Developments

Assigning numbers to geology requires a delicate balance between the commonly held opinion that geology cannot be quantified and the over optimistic view that every physical quantity can be described in precise mathematical terms. In reality, many geological characteristics cannot be quantified precisely, and educated guesses must be made based upon logic and experience. Hoek (1999) has shown that, with care, rational engineering decisions can be made in spite of the limitations of the input data.

Chapter 3

Computer Simulation of Rock Fall

3 Computer simulation of rock fall

With the development of computers in recent years, several programs have been written to predict rock fall trajectory paths. A number of these have been obtained and the interface, formulation and output critically appraised by the author. Rockfall programs are very useful for the planning and design of defence works. However, the detailed applicability of these programs is in part constrained by inadequate field and experimental data for the dynamic parameters, which govern the rock fall motion. A number of researchers have used in-situ testing to determine these critical parameters, however they must be used with caution since the definition, or methodology used to calculate these parameters varies.

3.1 Computer programs to simulate rock fall

Numerous analyses of rock fall have been developed over the last 30 years, the first of which is probably attributable to Ritchie (1963). Most of these have led to computer simulation of rock fall, which are normally restricted to two dimensions, but some extend to three dimensions.

The rock is generally treated as an indestructible, massive rigid body of simple shape, usually having some circular form. In some cases point masses or particles are used, occasionally a polygonal or an ellipsoidal shape is adopted and more rarely a fully three dimensional form.

Normally the slope surface profile is formed by a continuous piecewise linear set of segments, cells or regions, each of which is an intersection of the slope surface and the vertical plane in which the rock moves. The rock is set in motion by commencing to slide or roll from its initial position on the slope surface or by being dropped or thrown from some initial position above the slope surface. The subsequent motion of the rock under gravitational action consists of some combination of resisted surface movements (sliding or rolling) and aerial motion consisting of trajectories separated by bounces where impact between the rock and the slope occurs. Air resistance is usually neglected. The surface motions and impacts are governed by mathematical equations based on established laws of mechanics and hypotheses based on laws of

energy and momentum. Most computer simulations allow for some sort of random behaviour and allow for multiple rock fall paths to be produced. Graphical output is used to show the multiple paths and to summarise the analysis of the results of the simulation.

A survey of computer programs which simulate rock fall was undertaken by Fornaro et al. (1990). In all they considered 15 codes, reviewing and comparing the important features of the majority, and developed their own simulation program. More recently Giani (1992) presented a review of mathematical models of rock fall which form the algorithms for computer simulations. The existing analytical formulations may be divided into two categories: rigorous methods, and lumped mass methods (Hungr and Evans, 1988).

3.1.1 Rigorous methods

The Distinct Element Method (Cundall, 1971) and the analytical procedure proposed by Descoudres and Zimmermann (1987) are examples of rigorous rock fall analysis methods.

In the rigorous method, the size and shape of the blocks are assumed to be known, and all the block movements, including those involving the block rotation are considered. The block flies through the air with a ballistic trajectory and the translational and rotational velocity is transferred by the block impact at the slope surface contact. The impact impulse changes both the translational and angular velocity according to a very complex condition set. This depends on the corner block shape at the surface contact, on the rotation angle at the impact point, on the roughness of the slope surface, and on the elastic deformations. Since it is difficult to schematise all these things, the rigorous methods are distinguished on the basis of the simplified hypotheses assumed in order to describe the block impact phenomenon.

3.1.2 Lumped mass methods

In the lumped mass method, the single block is considered to be a simple point mass or particle. The particle flies through the air with a ballistic trajectory and the air resistance is usually neglected. As the block contacts the slope surface, the normal component of the velocity is changed in sign and reduced by a coefficient of normal

restitution (e_n) and the tangential component of this velocity is reduced by a tangential coefficient of restitution (e_t).

Lumped mass methods do not take the rotational moments into account. The two restitution coefficients are assumed as overall values which take all the impact considerations, including the deformation work, the contact sliding and the transfer from rotational to translational moment and vice versa, into account.

3.1.3 Rock fall simulation programs

Perhaps the earliest of the true rock fall simulation models was that developed by Piteau (1976). This program uses a slope divided into straight line segments and laws of motion to determine where a rock particle will impact the ground. At the point of impact the velocity of the rock normal and parallel to the slope is attenuated by the use of normal and tangential coefficients of restitution. The program produces velocity and bounce height probability distributions from random surface variations.

In the computer program described by Falcetta (1985) a two dimensional simulation is used with the rock modelled as a polygonal block. A piece wise linear, partially plastic force-displacement law characterised by three parameters is used to model the impact of the rock with the slope surface. This program was used to evaluate the risk of rock fall at sites in Haute-Savoie in France.

Wu (1985) produced a point mass computer program called ROCKSIM. This work was prompted by four major landslides and rock falls that occurred in North Carolina in 1980 and caused severe interruption to traffic flow. A coefficient of normal and tangential restitution was used to estimate the velocity of the rock as it starts the trajectory after impact. This was the first rock fall study to have developed coefficients of restitution. The restitution coefficients are normally distributed with respect to the slope surface and air resistance is neglected. A two stage research project provided the required field data. The data was derived from drop tests with spheres of various materials undertaken on inclined platforms of wood and rock and in-situ tests on rock slopes. A movie camera was used to film the rock trajectories from which the coefficients of restitution could be derived. The mean and standard deviation values were then calculated.

In the simulation program, energy was removed from the falling rock by randomly selected restitution coefficients and frictional resistance due to sliding on the slope surface. As a result of the use of the ROCKSIM program to analyse the slopes above a roadway in North Carolina susceptible to rock fall, the original route was changed in favour of another which was virtually isolated from predicted rock falls.

Chan et al. (1986) developed a mathematical model based on Newtonian mechanics to estimate boulder velocity and to predict boulder barrier interaction. This program was used in the design of rock fall barriers at the base of a boulder field in Hong Kong. It is capable of modelling octagonal and spherical shaped rocks. The algorithm uses a combined coefficient of restitution and a coefficient of friction to determine energy losses. Three types of motion may be modelled, namely rotation, rotation with sliding and bouncing.

After carrying out numerous experiments on rock fall in the Ticino region of Switzerland (at sites where serious damage had occurred as a result of a previous rock fall) and recording the motion of the rocks on cine film, Bozzolo and Pamini (1986) recognised, in common with many other researchers in the field, the importance of the influence of the rotation on its motion especially during impact. Although using an essentially two-dimensional representation of the motion in their simulation programs SASS and MASSI, the rock shape was modelled as an ellipsoid. Sliding and rolling resistances were provided by frictional models and the laws of rigid body mechanics were applied to the impact with a single coefficient of restitution being chosen from two possible values to control any consequent energy loss. The sole difference between the programs is that in MASSI the rock is treated consistently as a rigid body whereas in SASS it is treated as a point mass to determine its point of impact with the slope. Some randomness was introduced in the programs by varying the slope angle from its idealised value within a range of extremes. Both programs were subsequently used to investigate a variety of protection schemes for these sites with a view to designing protection to be incorporated in remedial works.

Spang (1987) describes a program called STEPCHILD which has a very similar formulation to Piteau's program but differs principally in that it allows a sliding mode with both static and dynamic friction. Multiple runs can be performed by varying the input data parameters but it is unclear if this is performed randomly. The computer

program was used to optimise the location of passive protection measures adjacent to a children's playground.

The computer program produced by Descoudres and Zimmerman (1987) was originally written as a fully three dimensional code but subsequently a two dimensional version was implemented as in most cases they considered that the added complication of a fully three dimensional analysis was not warranted. The rock could be represented either as a polygonal block or an ellipsoid and the slope surface by bi-linear quadrilaterals (3-D) or by straight lines (2-D).

The mechanics of impact are governed by coefficients of restitution, which have limiting values, friction at the contact point between the rock and slope surface and elasto plastic deformation of the ground. During any motion, which involves contact with the slope, sliding or rolling may take place imposing kinematic constraints on the equations of motion. These are solved by a numerical time stepping integration procedure. The program has been used to investigate the risk of damage from a site above the Rhone valley in France, which was unstable and prone to rock, fall. Variation of the rock fall paths is introduced by varying the initial position of the rock.

ROCKFALL is a simple lumped mass simulation program written in BASIC by Hoek (1987), which is purely deterministic and allows only a single rock to fall. The main program interface is shown in Figure 3.1. Both sliding and rolling surface motion are permitted and resisted by frictional forces. This latter feature leads to some inconsistency with the basic premise but the major advantage is its simplicity and, if required, the easy accessibility of the source code which is written in BASIC. Data may be entered in a plain text file or through the programs simple interface. The data file must be stored in the root directory of a specified drive otherwise an error occurs. The program does not work for re-entrant slopes.

Kozanis (1995) modified Hoek's program with a new interface written in Borland C++, which is illustrated in Figure 3.2. Whilst the program is visually more appealing, the interface is actually less user friendly.

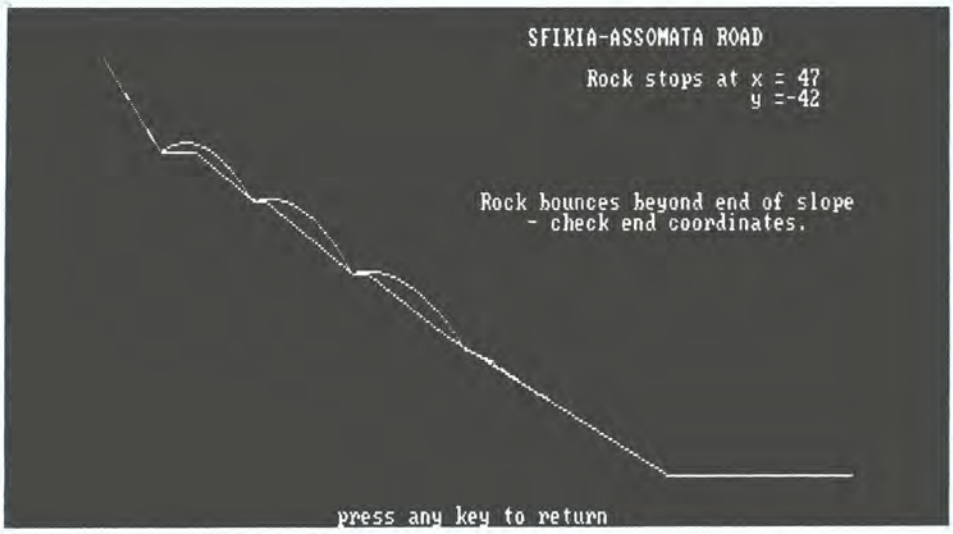

Figure 3.1: Output from the author's use of Hoek's program.

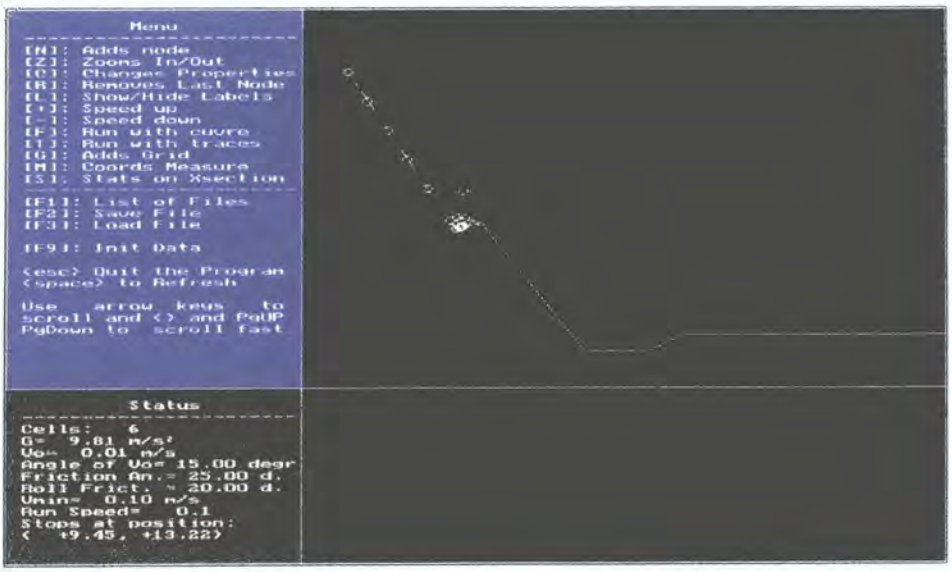

Figure 3.2: Output from the author's use of Kozanis' program.

Although the algorithms for the simulation described by Hungr and Evans (1988) are similar to those described above for earlier point mass programs, the significance of their work is the introduction of two useful concepts, the rock fall shadow and the energy line. The former relates to a limiting state formed by the characteristic talus slope profile produced by innumerable previous rock falls and marks out a danger zone at the base of the slope. Hungr and Evans used the energy line to plot the total energy head of a falling rock to illustrate the energy losses during the motion. The point of intersection of this line with the slope denotes the final resting place of the

rock. Their model was capable of using constant or random restitution coefficients and was used to investigate rock falls, which occurred at three locations in British Colombia.

Sofianos et al. (1988) used a two dimensional version of a distinct element program (Cundall, 1971) to simulate rock fall which had occurred near Argos in Greece. The rock was represented as a square block with interactions between corners and edges of the block and slope surface governed by a combination of Rayleigh and hysteretic damping to dissipate the kinetic energy acquired by the rock.

The principal feature of the rock fall simulation program described by Paronuzzi (1989) was the introduction of a randomly chosen combination of a single restitution coefficient and a corresponding rebound angle to model the bounce of a rock on impact with a slope. Both parameters were assumed to have probability density functions, which were particular forms of beta distributions (Johnson and Kotz, 1975). Data justifying this assumption and later used in the program were derived from experimental data of Bozzolo and Pamini (1982). Paronuzzi used the program to simulate rock fall, which had occurred as a result of an earthquake at two locations (Casletto Tunnel and Mount Pulineto in the Friuli region of the Italian frontier with Switzerland) and to investigate the effects of a variety of possible protective measures. The computed results were also compared with those obtained from back analysis at those sites.

The Colorado Rock Fall Simulation Program (CRSP) was developed by Pfeiffer et al. (1989) for use by the Colorado Department of Transport (CDOT) to model rock falls near vulnerable highways. The program is two dimensional and allows for a variety of rock shapes of circular form (Figure 3.3). Impacts are governed by a velocity dependant law, which dissipates the kinetic energy of the rock subject to a kinematic constraint, that immediately before the rock separates from the surface it is rolling. Continuous rolling motion is treated as a succession of small bounces. Although the restitution coefficients are constant on each portion of the slope, randomness in the motion is introduced at impact by a surface roughness parameter which is related to the rock size and is used to vary the nominal slope angle up to a limiting value.

CRSP is a DOS program that has been written in BASIC. Data may be entered in a plain text file or through the program interface. All values are in Imperial units. The program models spheres or disc shaped rocks and does not allow for re-entrant slope

profiles. A further limitation to the program is that rock travel must be from the left of the screen to the right.

The software has been used by Pfeiffer et al. at Glenwood Canyon and West Rifle, Colorado, to determine the optimum position for rock fall protection measures. Washington State Department of Transport (WSDOT) has also used CRSP to aid in rock fall mitigation design (Badger and Lowell, 1992). The program provided WSDOT with design information for the necessary length on a tunnel portal extension, rock fall protection fence placement, and ditch design verification.

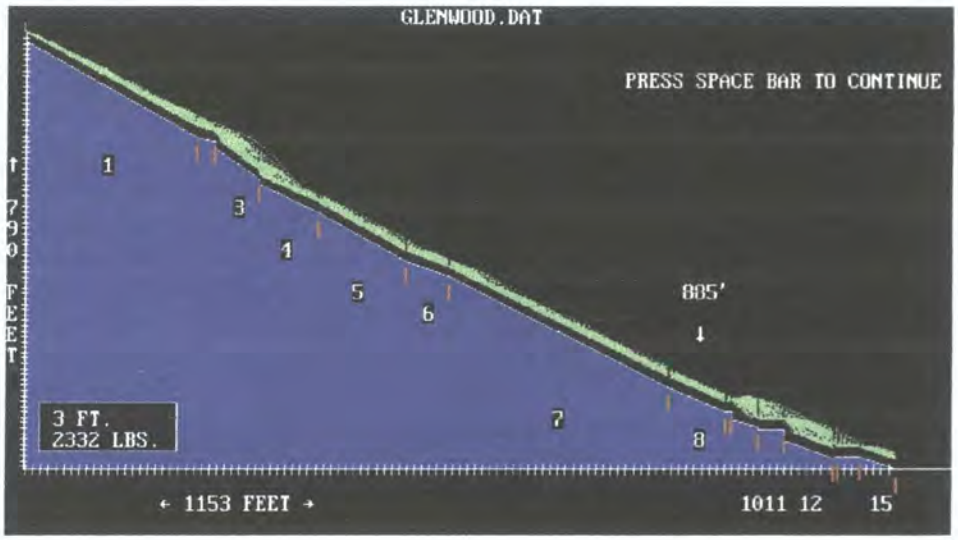

Figure 3.3: Output from the author's use of CRSP.

Fornaro et al. (1990) opted to develop a simple simulation model for rock fall in the hope that this approach would lead to a practical and effective solution. The model included a frictional resistance to rolling motion. This was defined as the work done by frictional forces per unit length along the slope per mass unit of the rock. The speed of the rebounding rock was calculated by probabilistic coefficients of normal and tangential restitution. Also included was the possibility of a rock fragmenting on impact. If fragmentation occurred then a smaller block with a new starting velocity was obtained using the stochastic numerical simulation. The air resistance was considered negligible. It was recognised the most difficult aspect of simulation was to identify and estimate values for the parameters affecting rock fall.

The computer program developed by Kobayashi et al. (1990) was used to simulate rock falls triggered by earthquakes on several sites in California. Only rolling and

bouncing motion of rocks of basically circular form are considered. Rolling motion is governed by a combination of frictional and viscous resistance. Impact is modelled by laws based upon the conservation of momentum modified by limiting frictional forces at the contact point and a coefficient, which determines the efficiency of collision, which is equivalent to a normal coefficient of restitution. This model was used because it favours bouncing motion. A degree of randomness in the motion is achieved by varying the height of the slope surface at the point of impact.

A program developed by Robotham et al. (1995) was used in the assessment of risk from active and abandoned quarry slopes, using the Monte Carlo method to simulate the potential risk of rock fall. The program makes the following simplifying assumptions; slope geometry is two dimensional, rock blocks remain intact and retain their original mass during travel, blocks are spherical, and angular velocity is not considered.

The mean and standard deviations for the coefficients of restitution are required for each slope and it is assumed that these are normally distributed. The surface roughness of a slope region is simulated by the use of a set of sub regions over the length of the original slope region. The projected length of each sub region is equal to the radius of the simulated block or, where the diameter of the block is less than half the measured wavelength, the projected sub region length is equal to one quarter of the wavelength. The inclination of each sub region is varied at random such that the amplitude of the sub regions roughness does not exceed the measured maximum amplitude of the slope region.

The French 'Bureau de Recherches Geologiques et Minieres (BRGM) and the laboratoire 'IMAGIS' jointly developed a computer program which models rock block trajectories in three dimensions (Leroi et al, 1996). This work was based on a physical formulation of the ballistics and the impact with the ground, in solid mechanics. The program considers the real 3D topology of the site, the real geometry of the blocks, the geomechanical properties of the materials involved and their associated behaviour laws with their possible fragmentation and interaction. Furthermore, the program enables the interaction between several blocks, impact with buildings, and randomized initial conditions or rebound parameters that help the delimitation of hazard areas. Future developments may include a better graphics interface, physical

validation (based on scaled models and real landslides), and finer equations to model fragmentation of blocks.

This simulation has been integrated into the 3D 'FABULE' software developed by IMAGIS and is illustrated in Figure 3.4.

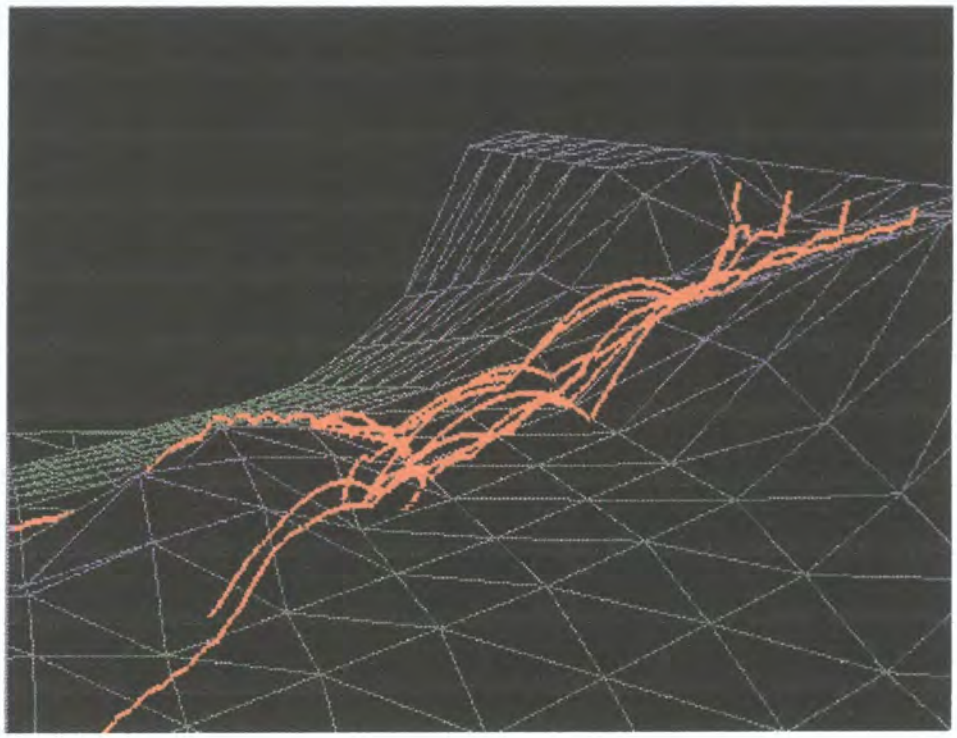

Figure 3.4: 3D Rock fall simulation developed by IMAGIS.

A computer program entitled 'rock fall demo', written by a company called Geoplan is briefly described in a paper by Zhou et al. (1996). A favourable correlation was obtained between the computer simulated and in-situ rock velocities. Based upon company experience the angular kinetic energy accounts for 10-15% of the transitional energy. The total kinetic energy of the falling blocks was calculated from the translational kinetic energy, which was then multiplied by a factor of 1.2 to account for the angular momentum.

Figure 3.5 shows the main screen plot of a simple DOS program called Tumble. Slope and rock data is entered in a plain text file that is then opened in the program. The program is capable of modelling rocks of any shape, however some results can be dubious since the rock sometimes gains more energy than it initially possessed.

Several simulations may be run but since the program produces no output data it is of little practical use.

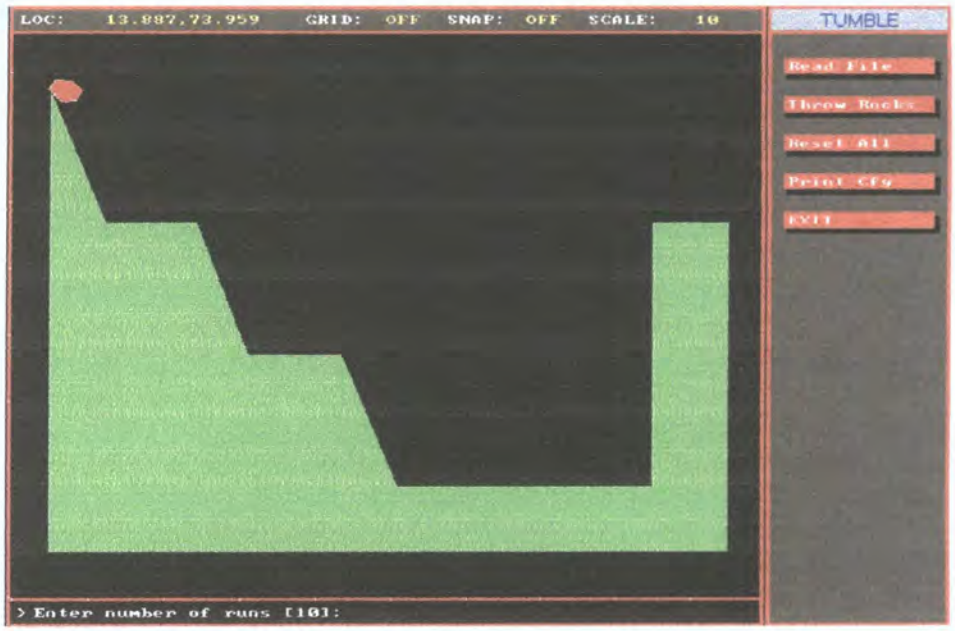

Figure 3.5: Output from the author's use of Tumble.

The computer program ROXIM (Wilson, 1996) is a general two dimensional rock fall algorithm in which the various motions of the rock are linked to form complete rock fall paths (Figure 3.6). One simulation may be chosen from a set of five based upon algorithms published by authors of existing rock fall simulation programs. These include ROCKFALL (Hoek, 1987), CRSP (Pfeiffer and Bowen, 1989), ROCKFALL (Paronuzzi, 1989), an untitled program described by Kobayashi et al. (1990) and the program MASSI (Bozzolo and Pamini, 1986). A new simulation entitled DURSIM, written by Wilson, may be used.

In all the simulations the rock is assumed to behave as a rigid body which remains intact during rock fall. Various rock shapes are permitted which include a point mass, a circular disc or cylinder, a sphere, an ellipsoid and a double cone. With the exception of the point mass, translational and rotation velocity are considered.

Data is entered either into a simple plain text file or through the programs user interface. The contents of the text file are complicated by the fact that different simulation modes require different input parameters. Depending on the simulation used, various attributes, which may be assigned random properties, are required for

each region on the slope profile. Any type of slope profile may be generated. The user may input data in either imperial or metric units.

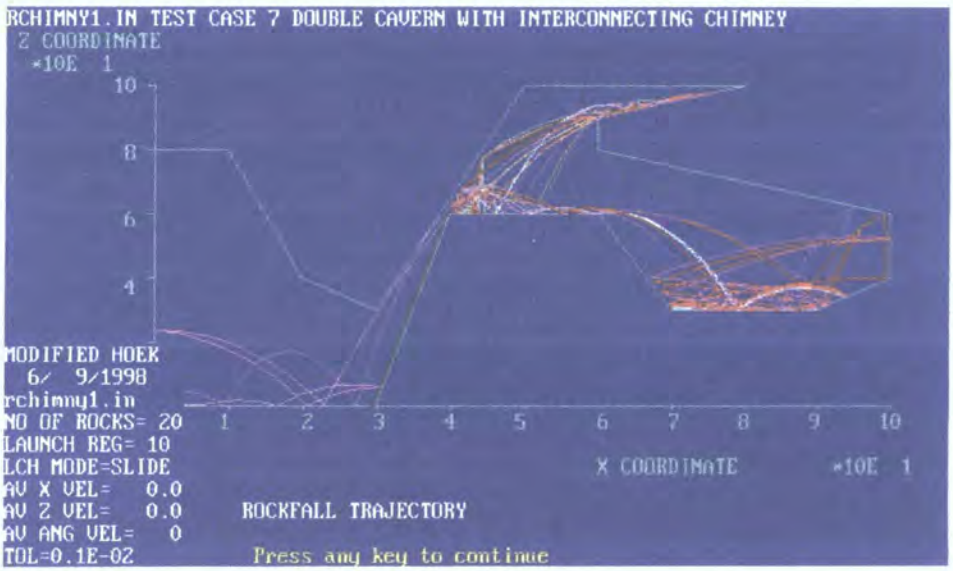

Figure 3.6: Output from the author's use of ROXIM.

The first Windows rock fall program was written by Stevens (1996). There are two versions of the program, RocFall 2.0 and 3.0 as illustrated in Figures 3.7 and 3.8. These are both two dimensional and only model rocks as particles. Angular velocity is only considered in version 3.0 of the program. Slope surface materials are chosen by the user and the program uses typical coefficients of restitution which are pre-set in the program and cannot be altered by the user. In version 3.0 if the user so chooses, impacts may be governed by a velocity or rock mass dependant law. The coefficient of sliding friction may be entered or determined from the tangential coefficient of restitution.

The program supports both imperial and metric units and CRSP files may be imported into the program. Surface roughness is set by randomly varying the angle of the slope. Energy, velocity and bounce height envelopes for the entire slope are all determined by the program as are the location of rock endpoints. Distributions of energy, velocity and bounce height are also calculated along the slope profile. Any number of user-defined barriers may be placed at any angle or location on the slope. The response of barriers to rock impact is user-definable, with a coefficient of restitution for each barrier.

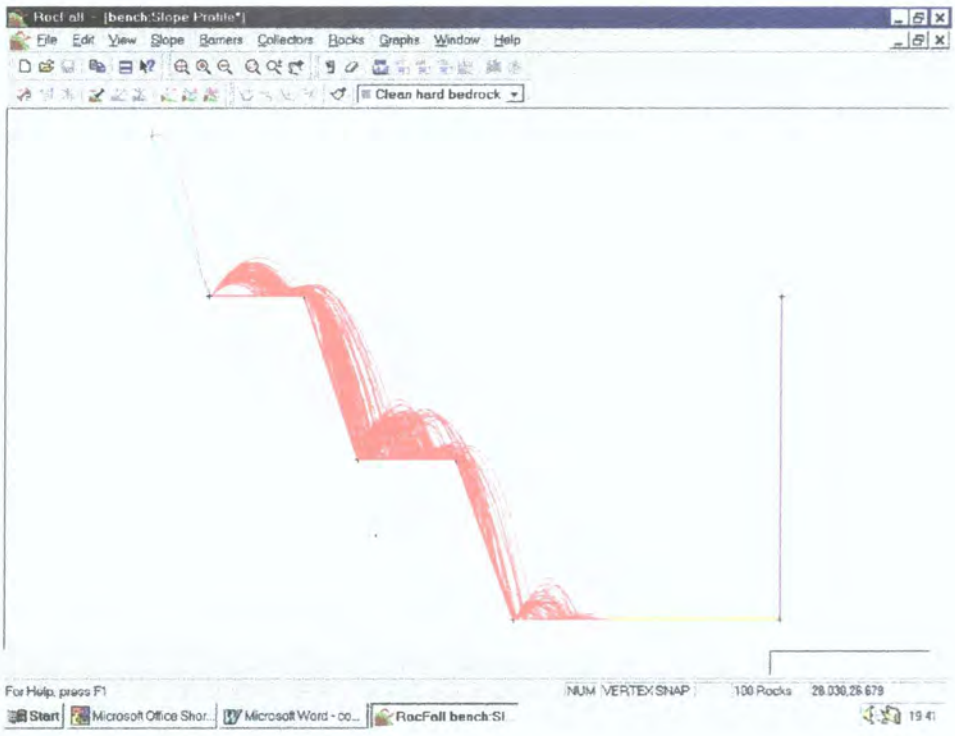

Figure 3.7: Output from the author's use of RocFall 2.0.

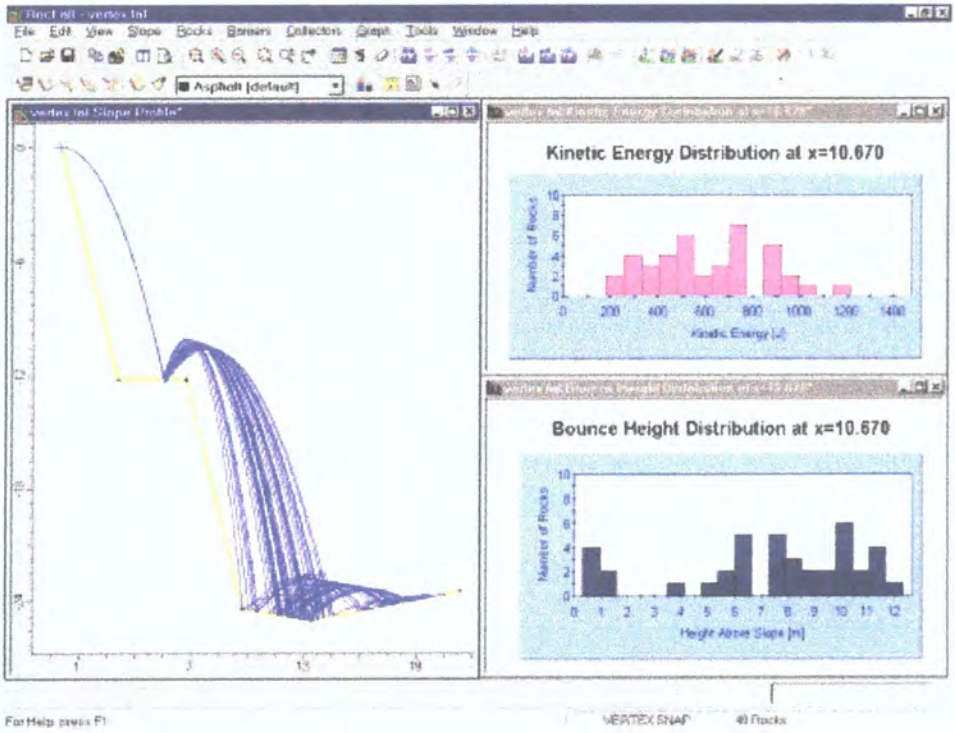

Figure 3.8: Output from the author's use of RocFall 3.0.

3.2 Critical parameters in modelling rock fall

Pfeiffer and Bowen (1989) present several coefficients of restitution for use with their program CRSP depending on the nature of the slope surface (Table 3.1). Their results have been determined through in-situ testing and back analysis. These coefficients must be used with caution since their formulation is not standard. The normal coefficient of restitution is modified by a velocity dependent scaling factor, which is incorporated to adjust for the increased frictional resistance due to an increase in the normal force. A friction function is used to adjust the tangential coefficient of restitution according to the velocity of the rock at the point of contact.

Slope material	Normal coefficient of restitution (e_n)	Tangential coefficient of restitution (e_t)
Hard surface paving	0.37-0.42	0.87-0.92
Bedrock or boulders with little soil or vegetation	0.33-0.37	0.83-0.87
Talus with little vegetation	0.30-0.33	0.83-0.87
Talus with some vegetation	0.30-0.33	0.80-0.83
Soft soil slope with little vegetation	0.28-0.32	0.80-0.83
Vegetated soil slope	0.28-0.32	0.78-0.82

Table 3.1: Coefficients of restitution presented by Pfeiffer and Bowen (1989).

Hoek (1990) presents some coefficients of restitution that have been determined from tests carried out by various North American Transportation Departments for various slope surface types and materials (Table 3.2). The coefficients have been derived using the Monte Carlo method, which models the rock as a sphere, and does not consider angular velocity. Although Hoek's formulation is very different to that of Pfeiffer and Bowen's the coefficients of restitution are very similar.

Slope material	Normal coefficient of restitution (e_n)	Tangential coefficient of restitution (e_t)
Clean, hard rock	0.53	0.90
Asphalt roadway	0.40	0.90
Bedrock outcrops with hard surfaces and large boulders	0.35	0.85
Talus cover	0.32	0.82
Talus cover with vegetation	0.32	0.80
Soft soil some vegetation	0.30	0.80

Table 3.2: Coefficients of restitution presented by Hoek (1990).

Several in-situ rock fall tests were carried out by Azzoni et al. (1991). The slopes chosen were of different geological and geomorphological features and the purpose of these tests were to investigate the different types of motion of various strength, shape and sizes of rock. The tests were carried out at the following sites in Italy; a quartzite quarry near Strozza, a gneiss quarry in the Luserna area, an abandoned limestone quarry at Cagliari, an orthogneiss quarry in Iselle and a natural slope in Val Malenco. Three or more video cameras were placed along each test slope at different lateral positions depending upon the length of the slope and the morphological condition of the site. A movie camera was also placed in a frontal position in order to evaluate the lateral movement of the falling rock.

The recorded rock falls were analysed in the laboratory using digitisation software. This allowed the computation of pre and post impact velocities and rotations. The coefficients of normal and tangential restitution, and the rolling friction coefficient were calculated from the results and are presented in Table 3.3.

Site	Surface material	Rock Type	Restitution Coefficients		Rolling friction coefficient
			(e_n)	(e_t)	(μ_r)
Strozza	Rock/thin debris	Quartzite	0.45-0.85	0.45-0.75	0.97±0.184
	Fine debris	Quartzite	0.30	0.66	0.75±0.159
Cagliari	Earth & debris	Limestone	0.62	0.66	0.39±0.117
Val Malenco	Coarse debris	-	1.22	0.80	0.88±0.24
Luserna	Rock	Gneiss	-	-	1.31±0.163
Iselle	Coarse debris	Orthogneiss	-	-	0.84±0.301

Table 3.3: Restitution and rolling friction coefficients presented by Azzoni et al. (1991).

The coefficients of restitution were calculated by Azzoni et al. using a method applied by Hungr and Evans (1988). This correlates the total energy head loss ΔE during an impact to the angle of incidence α and absolute velocity v_{abs} prior to impact, with the normal (e_n) and tangential (e_t) coefficients of restitution as defined by Hungr and Evans. The acceleration due to gravity is denoted by g.

$$\Delta E = \frac{v_{abs}^{\ 2}}{2g}\left[\left(\frac{e_t^{\ 2} + e_n^{\ 2}\tan^2\alpha}{1+\tan^2\alpha}\right) - 1\right] \qquad \textbf{3.1}$$

This method is based upon the assumption that the rock is a point mass which has no pre or post rotational velocity and its moment of inertia is zero. The coefficient of rolling friction is based on the inclination of the energy line during the rolling motion. The rolling motion of the blocks in the field was actually a series of small multiple collisions caused by the irregularity of the rock shape and the slope surface.

The values of normal and tangential coefficients of restitution are much higher than those presented by Hoek, and Pfeiffer and Bowen. The normal coefficient of

restitution of 1.22 calculated for the Val Malenco slope, implies that the rock gained energy through impact with the slope. This would only have been possible if an explosion had occurred on impact. Again the values presented by Azzoni et al. (1991) must be used with caution since it is unclear which methodology and definition has been used to calculate the coefficients of restitution.

Giani (1992) presents some values for the coefficients of restitution based on several in-situ tests on an abandoned quarry face (Table 3.4). The coefficients of normal restitution are similar to those presented by Hoek and Pfeiffer and Bowen, whilst the coefficients of tangential restitution are more comparable with those of Azzoni et al. (1991). Again is unclear exactly how the normal and tangential coefficients of restitution have been defined.

Slope material	Normal coefficient of restitution (e_n)	Tangential coefficient of restitution (e_t)
Bedrock	0.50	0.95
Bedrock covered by large blocks	0.35	0.85
Debris formed by uniformly distributed elements	0.30	0.70
Soil covered by vegetation	0.25	0.55

Table 3.4: Coefficients of restitution presented by Giani (1992).

Robotham et al. (1995) conducted several in-situ tests in an abandoned chalk and limestone quarry to derive the relevant coefficients of restitution for several different slope materials. The tests included dropping rock blocks to fall freely onto inclined bare rock surfaces and onto slopes consisting of vegetated quarry waste. Rock blocks were also pushed over the slope crests. Fifty eight rocks were pushed over three pre-selected slopes, two of which had been formed by restoration blasting and the third by production blasting. Rock blocks of two size ranges ($0.2m^3$ and $0.05m^3$) were used. Each test was filmed to enable the determination of rock fall travel times. The coefficients of restitution, which are presented in Table 3.5 were derived using the same method used by Hoek (1990), the values obtained however, are slightly lower.

Slope material	Normal coefficient of restitution (e_n)	Tangential coefficient of restitution (e_t)
Limestone face	0.315	0.712
Limestone scree, partially vegetated	0.303	0.613
Uncovered limestone blast pile	0.315	0.712
Chalk face	0.276	0.835
Vegetated chalk scree	0.271	0.596

Table 3.5: Coefficients of restitution presented by Robotham et al. (1995).

In a more recent paper Azzoni et al. (1995) conducted several in-situ tests to determine the rolling friction and restitution coefficients of two quarry slopes.

Their coefficient of rolling friction is defined as the tangent of the angle of the slope at which a block can be considered to move with a steady velocity (Statham, 1979). On a slope steeper than this angle the block will accelerate, while on flatter slopes it decelerates and finally comes to rest. The values of the rolling friction coefficients were evaluated through back analysis of two experimental tests, carried out with blocks of two different shapes and volume (a prismatic block, approximately $1.2m^3$ in volume, and a spherical one of $0.3m^3$). Since the rolling friction coefficient depends on the surface roughness of the slope in relation to the size of the falling block, two different values were determined.

Their coefficient of restitution (e) is defined as the ratio of the post and pre impact kinetic energy values (Bozzolo and Pamini, 1982) and their results are presented in Table 3.6. The values of the rolling friction coefficients are very different to those presented by Azzoni et al. (1991), because they have been calculated using two very dissimilar methods.

Slope material	Restitution coefficient (e)	Rolling friction coefficient (μ_r)	
Block size		0.3 m^3	1.2 m^3
Rock (limestone)	0.75-0.90	0.40-0.45	0.40
Fine angular debris and earth, compacted	0.55-0.60	0.50-0.60	0.40
Fine angular debris and earth, soft	0.35-0.45	0.70-0.80	0.60-0.70
Medium angular debris with angular rock fragments	0.45-0.50	0.60-0.70	0.50-0.60
Medium angular debris with scattered trees	0.40-0.50	0.7-1.0	
Coarse angular debris with angular rock fragments	0.55-0.70	0.65-1.2	0.60-0.80
Earth with grass and some vegetation	0.50-0.60	0.55-0.65	0.45-0.50
Ditch with mud	<0.20	0.85	
Yard (artificially compacted ground)	0.50-0.65	0.50-0.65	
Road	0.75	0.40-0.45	

Table 3.6: Coefficients presented by Azzoni et al. (1995).

Chau et al. (1998) conducted several in-situ tests to determine the coefficients of restitution and the static (μ_s) and dynamic (μ_d) sliding friction of rock blocks on several slope materials. Cuboid and angular fragments were dropped onto slope surfaces made of soil, rock, shotcrete and soil containing rock fragments. Their results are presented in Table 3.7. Their normal and tangential coefficients of restitution for a rock slope compare well with those presented by Pfeiffer and Bowen (1989), Hoek (1990) and Giani (1992). The value of the normal coefficient of restitution for a soil slope is high whilst the tangential coefficient is low, compared to those of Pfeiffer and Bowen, Hoek and Giani. Again it is unclear exactly how the normal and tangential coefficients have been defined.

Slope material	Normal coefficient of restitution (e_n)	Tangential coefficient of restitution (e_t)	Coefficient of dynamic sliding friction (μ_d)	Coefficient of static sliding friction (μ_s)
Rock	0.487	0.910	0.576±0.130	0.909±0.240
Soil	0.393	0.567	0.562±0.0867	1.033±0.195
Shotcrete	0.453	0.737	0.559±0.118	0.764±0.162
Rock/soil	-	-	0.557±0.054	0.733±0.194

Table 3.7: Coefficients presented by Chau et al. (1998).

Chapter 4

Rock Slope Inventory Systems

4 Rock slope inventory systems

Effective management of unstable rock slopes on a road network requires knowledge of their location and the risk posed to the road user. Existing stability assessment and risk evaluation systems use various approaches and are dominated by subjective judgement. In addition, they are usually undertaken on a reactive basis, prompted by rock falls. Consequently road users may be exposed to risk before problems are assessed, comparison of results is difficult, budgetary problems arise as incidents are largely unforeseen, and prioritisation of funds is impossible.

In order to assess these problems various empirical rock slope inventory systems have been developed by Brawner and Wyllie (1975), Pierson (1992), McMillan and Matheson (1997) and Franklin and Senior (1997). The purpose of these systems is to evaluate the rock fall risk by considering the combined effects of the various rock fall trigger mechanisms that act upon the rock jointing and the risk of a falling rock to road users.

4.1 Rock Fall Hazard Rating System (RHRS)

Early work on rock slope inventory systems by Brawner and Wyllie (1975) and Wyllie (1987) was developed by Pierson (1992) into a process for the rational management of rock slopes along transportation systems, which has been named the Rock Fall Hazard Rating System (RHRS). The RHRS consists of three phases of inspection, the slope survey, and the preliminary and detailed rating phases.

4.1.1 Slope survey

The slope survey is an essential feature of the RHRS that allows an agency to accurately determine the number and location of its rock fall sites. For the RHRS, a rock fall section is defined as any uninterrupted slope along a highway where the level and occurring mode of rock fall are the same.

4.1.2 Preliminary RHRS

The purpose of the preliminary rating, illustrated in Table 4.1 is to group the rock fall sections inspected during the slope survey into three broad more manageable categories, A, B and C, corresponding to high, moderate and low risk, respectively. Without this step, many additional hours would be spent applying the detailed rating at sites with only a low to moderate chance of a rock fall occurring.

		Preliminary rating		
Rating System	RHRS	**A**	**B**	**C**
	RFRAS	**H**	**M**	**L**
Criteria	Estimated potential for rock on roadway	**HIGH**	**MODERATE**	**LOW**
	Historical rock fall activity			

Table 4.1: The preliminary rating system.

4.1.3 Detailed RHRS

The detailed rating system which is summarised in Table 4.2, is the third step in the RHRS and is usually only applied to sites that receive an A grade in the preliminary rating phase. Note that all quantities in the Table are in Imperial (British) units.
Altogether, there are twelve parameters, which must be measured or assessed as shown in the table. The four columns on the right hand side of the Table correspond to logical breaks in the increasing risk associated with each parameter. Of these parameters, only ten contribute to the rating depending on which of the geological characteristics predominate (Case 1 or Case 2). For five of these parameters (1, 3, 4, 5, and 10), an exponent, x, is evaluated using the formulae shown in Table 4.3. The remaining parameters require a subjective assessment corresponding to integer values of the exponent x in the range 1 to 4. The score in points, S, for each parameter is then obtained from Equation 4.1.

$$S = 3^x \qquad \textbf{4.1a}$$

subject to limits,

$$x \le S \le 100 \qquad \textbf{4.1b}$$

Thus for the integer exponents, the score ranges from 3 to 81 points.

Parameter Number	Parameter			RATING CRITERIA AND SCORE			
				3 POINTS	9 POINTS	27 POINTS	81 POINTS
1	SLOPE HEIGHT			25 Feet	50 Feet	75 Feet	100 Feet
2	DITCH EFFECTIVENESS			Good catchment	Moderate catchment	Limited catchment	No catchment
3	AVERAGE VEHICLE RISK			25% of the time	50% of the time	75% of the time	100% of the time
4	PERCENT OF DECISION SIGHT DISTANCE			Adequate sight distance, 100% of low design value	Moderate sight distance, 80% of low design value	Limited sight distance, 60% of low design value	very limited sight distance, 40% of low design value
5	ROADWAY WIDTH INCLUDING PAVED SHOULDERS			44 Feet	36 Feet	28 Feet	20 Feet
6	GEOLOGICAL CHARACTER	CASE 1	JOINT STRUCTURAL CONDITION	Discontinuous joints, favourable orientation	Discontinuous joints, random orientation	Discontinuous joints, adverse orientation	Continuous joints, adverse orientation
7			ROCK FRICTION	Rough, irregular	Undulating	Planar	Clay Infilling, or slickensided
8		CASE 2	EROSION STRUCTURAL CONDITION	Few differential erosion features	Occasional differential erosion features	Many differential erosion features	Major differential erosion features
9			DIFFERENCE IN EROSION RATES	Small difference	Moderate difference	Large difference	Extreme difference
10	BLOCK SIZE VOLUME OF ROCKFALL/EVENT			1 Foot 3 Cubic yards	2 Feet 6 Cubic yards	3 Feet 9 Cubic yards	4 Feet 12 Cubic yards
11	CLIMATE AND PRESENCE OF WATER ON SLOPE			Low to moderate precipitation; no freezing periods; no water on slope	Moderate precipitation or short freezing periods or intermittent water on slope	High precipitation or long freezing periods or continual water on slope	High precipitation and long freezing periods or continual water on slope and long freezing periods
12	ROCK FALL HISTORY			Few falls	Occasional falls	Many falls	Constant falls

Table 4.2 Summary sheet of the RHRS (Pierson, 1992).

(Note: 1 foot (ft)=0.3128 m; 1 cubic yard = 0.828 m^3)

When all the parameters have been evaluated and scored, ten are selected which are totalled. Comparison between the total values obtained through the rating system allows an agency to numerically differentiate rock slopes from the least to the most hazardous since slopes with higher scores present the higher risk. Furthermore, an

exponential system provides a rapid increase in score that distinguishes the more hazardous sites. This allows greater flexibility in evaluating the relative impact of each variable.

Parameter		Exponent, x
1	Slope Height	$\frac{\text{Slope Height}\,(ft)}{25}$
3	Average Vehicle Risk , AVR (%)	$\frac{\text{Average daily traffic}\,(cars/day)\times\text{slope length}\,(miles)}{24\,(hours/day)\times\text{posted speed limit}\,(mph)}\times 100$
4	Sight Distance	$\frac{120-\left[\frac{\text{Actual sight distance}\ (ft)}{\text{Decision sight distance}\ (ft)}\times 100\%\right]}{20}$
5	Roadway width	$\frac{52-\text{Roadway width}(ft)}{8}$
10	Block size	Block size(ft)
	Volume	$\frac{\text{Volume}\,(cubic\ yards)}{3}$

Table 4.3: Exponent formulas.

The following sections explain or clarify the assessment procedure.

4.1.3.1 Slope height

Slope height represents the vertical height of the slope, not the slope distance.

4.1.3.2 Ditch effectiveness

The effectiveness of the ditch is measured by its ability to restrict a falling rock from reaching the roadway. The assessor should consider the following,

a) slope height and angle,
b) ditch width, depth and shape,
c) anticipated volume of rock fall event, and
d) impact of launching features on the falling rock.

4.1.3.3 Average Vehicle Risk (AVR)

The AVR measures the percentage of time that a vehicle will be present in the rock fall hazard zone. The result directly relates to the significance of the route and the potential hazard by approximating the likelihood of a vehicle being present and thus being involved in a rock fall incident.

4.1.3.4 Sight distance

The Decision Sight Distance (DSD) is the length of roadway that a driver must have to make a complex or instantaneous decision. It is defined as the shortest distance along a roadway for which a 6 inch object is continuously visible and is related to the speed limit, as recommended by the American Association of State Highway and Transportation Officials AASHTO (Table 4.4). The DSD is critical when obstacles on the road are difficult to perceive or when unexpected or unusual manoeuvres are required.

Posted speed limit (mph)	Decision Sight Distance (ft)
25	375
30	450
35	525
40	600
45	675
50	750
55	875
60	1000
65	1050

Table 4.4: Recommended Decision Sight Distances AASHTO (1990).

4.1.3.5 Roadway width

Roadway width is measured perpendicular to the highway centreline from edge of pavement to edge of pavement. This measurement represents the available room to

avoid a rock fall, and should be the minimum width when roadway width is not constant.

4.1.3.6 Geological character

If joints, bedding planes and other structural features are present and are the primary causes of instability, the geological character is dominated by the joint structure (Case 1). If differential erosion is the dominant cause of instability then erosion features govern the geological character (Case 2). If both jointing and erosion features are present, then both cases must be assessed and scored but only the highest is considered in the rating.

4.1.3.7 Structural condition

Structural condition refers to whether slope instability is controlled by joint orientation or differential erosion features. If jointing is the predominant structural condition then the orientation and continuity of the joint sets must be assessed and scored. If differential erosion is the predominant structural condition then the number of erosion features must be assessed and scored.

4.1.3.8 Rock friction

Rock friction directly affects the potential for a rock to move relative to another. The rock fall potential is greater where joints contain highly weathered or hydrothermally altered products, where movement has occurred causing slickensides or fault gouge to form, where open joints dominate the slope or where joints are water filled.

4.1.3.9 Difference in erosion rates

The rate of erosion directly relates to the potential for a future rock fall event. As erosion progresses, unsupported or oversteepened slope conditions develop.

4.1.3.10 Block size or volume of rock fall per event

If individual blocks are typical of the rock fall, the block size should be used for scoring. If a mass of blocks tends to be the dominant type of rock fall, the volume per event should be used

4.1.3.11 Climate and presence of water on slope

Water and freeze thaw cycles contribute to the weathering and movement of rock materials. If water is known to flow continually or intermittently from the slope, the slope is rated accordingly.

4.1.3.12 Rock fall history

Historical information is best obtained from the maintenance personnel responsible for the slope.

4.1.3.13 Total rating

The rating of the detailed RHRS is evaluated as the sum of the scores of ten of the twelve parameters. This gives a numerical rating ranging from 30 to 1000. The higher the rating the more likely a rock fall is to hit a vehicle.

4.1.4 System limitations

The RHRS provides agencies with a method to address their rock fall problems by giving a numerical comparison of risk between slopes. The slope evaluation process is as straightforward as possible, however there is still range of values a slope could receive, depending upon consistency between assessors.

4.2 Ontario Rock slope inventory system (RHRON)

A similar rock slope inventory system called RHRON has been developed by the Ontario Ministry of Transportation (Franklin and Senior, 1997). RHRON was modelled on the RHRS system developed by Pierson (1992). The exponential weighting system used in the RHRS was removed from RHRON and the number of parameters was increased from 12 to 20 to include information on face looseness, water table height and intensity of jointing in the rock mass.

The RHRON system assumes that different degrees on instability can be recognised by a trained observer and rated on a scale from zero (no problem) to nine (imminent collapse) and consists of a basic rating and a detailed rating phase. The basic rating phase is used for preliminary screening.

The detailed RHRON is only applied to the more dangerous sites. It is defined identically to the basic RHRON rating, however it assesses the parameters using a more comprehensive set of observations. The final value obtained allows the user to distinguish between the least and most dangerous sites.

4.3 Rock Slope Hazard Rating (RSHR)

McMillan and Matheson (1997) have developed a two-stage system, defining a hazard rating and a hazard index to identify and classify rock fall risk.

The first stage of the system derives a Rock Slope Hazard Index (RSHI) from rapid standardised field data collection. The Rock Slope Hazard Index is defined as the potential for failure multiplied by the consequences of failure. This acts as a preliminary rating procedure incorporating three standard data collection forms, which describe a variety of primary and secondary parameters. Primary parameters establish the potential for failure and include safety factor, discontinuity spacing, failure plane dimension, rock mass strength and hydrological measurements. Secondary parameters such as rock trap size, slope profile, carriageway width, sight line distance, remedial work effectiveness and traffic density influence the severity of a rock fall event. In the RSHI system an index value of <1 does not represent a serious risk and would be ignored. Conversely, slopes and cuts with RSHI values in excess of ten require detailed inspection, while a value of 100 suggests the need for immediate action. Slopes with intermediate values (1-10) require detailed investigation within five years.

The second more detailed stage derives a Rock Slope Hazard Rating (RSHR) from detailed field surveys. The RSHR aims to provide a comprehensive assessment of the risk posed by an unstable rock face. It is derived by considering all potentially unstable blocks on the slope. An overall probability of slope failure can be determined from factor of safety data pertaining to each kinematically feasible rock block. It is defined as the ratio of the number of analysis results with a value <1 to the total number of analyses undertaken. In each case, it is assumed that the probability of failure along an individual plane is reduced in proportion to any stabilisation devices installed along the discontinuity. In order to calculate the final hazard rating an estimate of the likelihood of a block hitting a vehicle is combined with the probability

of failure value. Assuming a braking distance of 40m the probability of a driver hitting a rock varies with the available decision sight distance. McMillan and Matheson suggest values of 0.75, 0.3 and 0.05 for sight distances of 40-60m, 60-100m and >100m respectively. Data concerning the available sight distance and probability of rock fall can thus be combined to calculate the probability of a vehicle hitting a boulder on a particular stretch of road.

4.4 Rock Fall Risk Assessment System (RFRAS)

Previous rock slope inventory systems have concentrated on the estimation of rock fall risk to highway users. The RFRAS was developed by the author to enable the practising engineer to assess the level of risk of rock fall from any rock slope. Once the risk of rock fall has been determined then the slopes at high risk of rock fall may be modelled on a rock fall simulation program such as ROXIM, CRSP or GeoFall. **The simulation program thus provides an accurate means of determining the consequences of a rock fall event whilst the RFRAS determines the likelihood of a rock fall event.**

If more than one rock slope is to be assessed then the rating obtained from the RFRAS provides a subjective comparison between slopes. This allows a cost and benefit analysis to be made so that funds may be allocated accordingly.

4.4.1 Description of the RFRAS

The RFRAS is based upon the RHRS developed by Pierson (1992) and consists of three phases of inspection, the slope survey, and the preliminary and detailed rating phases. The slope survey allows the engineer to divide the slope into zones of approximately uniform rock fall risk. The preliminary rating acts as a coarse sift so that the detailed rating system is not applied to sites with a low rock fall risk. The scheme uses 13 parameters with an exponential scoring system based on five grades. Each parameter is assessed as one of these grades, which represent the degree of risk and are rated exponentially as 1, 3, 9, 27 and 81. The detailed rating system includes 13 parameters that when assessed, evaluated and totalled will numerically differentiate slope zones from the least to the most hazardous. The RFRAS produces an overall rating in the range 21-1296 and allows the relative risk of rock fall between

slopes to be assessed. It also categorises the rock fall risk as either none, low, moderate, high, or very high and the potential number of future rock falls as none, few several, many or continual.

4.4.2 Slope survey

The slope survey is an essential feature of the RFRAS that allows the number and location of potential rock fall sites to be accurately determined. For the RFRAS, a rock fall zone is defined as the surface area of the slope for which the occurring mode of rock fall is the same.

Accurate delineation of each rock fall zone is important. The slope surface area defines the assessment zone and extends not only laterally along the slope but also vertically. This allows for the separate assessment of features such as different rock strata with different joint orientations. Zones may not overlap.

4.4.3 Preliminary RFRAS

The purpose of the preliminary rating (Table 4.1) is to group the rock fall zones inspected during the slope survey into three broad, more manageable categories H, M and L, which correspond to high, moderate and low risk. Little is gained by adding intermediate stages, as consistency is important. The preliminary rating is a subjective evaluation of the rock fall potential and requires judgements by experienced personnel.

The preliminary rating is a critical step in the RFRAS, especially when there are a large number of zones to consider. Initially the H rated zones should be evaluated with the detailed rating system. This will economise the effort whist directing it towards the most critical areas. The M rated zones should be evaluated as time and funding allows and the L rated zones should receive no further attention.

Without the preliminary rating, many hours would be spent applying the detailed system to sites with only low to moderate chance of producing a hazardous condition.

All rock fall zones that receive an 'H' rating must be photographed. To assist in the assessment of the preliminary rating a field booking sheet has been prepared and is illustrated in Figure 4.1.

RFRAS Booking Sheet 1

Photo

Preliminary rating

Initial risk	Estimated potential for rock fall	H	M	L	
	Historical rock fall	H	M	L	(Circle as appropriate)

Zone location

Co-ordinates defining zone

	x	y	z	x	y	z	
1							5
2							6
3							7
4							8

Co-ordinate system used

Zone description

Comments

Figure 4.1: Booking sheet 1.

This booking sheet allows the assessor to record the preliminary rating, the zone location, to define the boundary of the zone in an arbitrary co-ordinate system, to describe the zone and to add further comments.

The zone is described by a series of x, y, and z co-ordinates that define the three dimensional boundary in a linear piece wise manner. The co-ordinate system chosen to define this boundary may be either arbitrary or any conventional system such as the Ordnance Survey system and must be recorded on the booking sheet.

4.4.4 Detailed RFRAS

Before decisions can be made on how to rate a rock fall zone, the criteria used to assess each parameter must be well understood and carefully considered. To aid in understanding, narratives for each parameter are included. Some parameters require a subjective evaluation, whereas others can be directly measured and then evaluated. A summary and field booking sheet for the detailed RFRAS is presented in Table 4.5 and Figure 4.2 respectively.

4.4.4.1 Joint orientation (P_1)

The combinations of joint orientations and that of the slope face determine whether rock fall is kinematically feasible. A very adverse joint orientation is one in which block, planar, wedge or toppling failure is kinematically feasible and angles of dip or plunge are high (usually >20°). An adverse joint orientation is one in which block, planar, wedge or toppling failure is kinematically feasible and the angle of dip or plunge of the discontinuities is between 5 and 20°. A favourable joint orientation refers to a slope that contains no adversely orientated discontinuities. The angle of dip or plunge is between -5 and 5°. A very favourable joint orientation refers to a slope that contains no adversely orientated discontinuities and the angle of dip or plunge is steeply dipping into the face (usually <-5°). If the rock slope contains randomly orientated joints and some scattered blocks with adversely orientated joints, but no dominant adverse pattern is present, then the joint orientation is classed as random. If the rock slope exhibits a dominant joint pattern, bedding plane or other discontinuity with a persistence greater than 3m in length then the joint is classed as continuous.

[This Page Intentionally Left Blank]

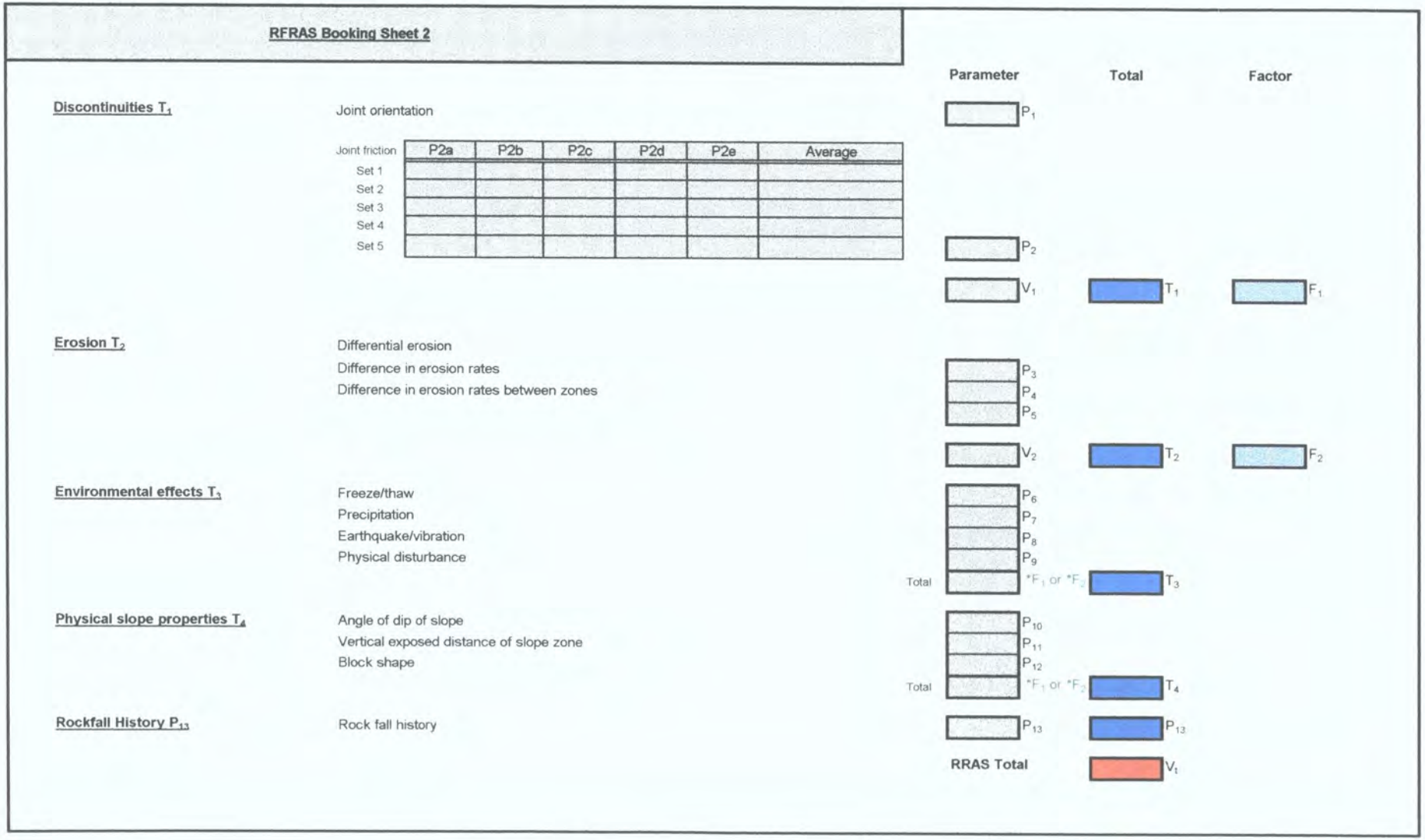

Figure 4.2: Booking sheet 2.

4.4.4.2 Joint friction (P_2)

Rock friction directly affects the potential for a block to move relative to another. Both the macro and micro-roughness of the surfaces govern friction along a discontinuity surface. Macro-roughness is the degree of undulation of the joint relative to the direction of possible movement. Micro-roughness is the texture of the surface. The rock fall potential is greater in areas where the joint contains a highly weathered or hydrothermally altered material, where joints have been subject to movement forming slickensides or fault gouge, or where the joints are open or water filled.

4.4.4.2.1 Separation or aperture (P_{2a})

The distance between joint faces determines not only rock friction but also the likelihood of frost wedging, root wedging and the build up of water pressure. This parameter is especially critical in situations where a release joint is present.

4.4.4.2.2 Joint roughness (P_{2b})

The joint surface may only be categorised as undulating if the two surfaces are locked together requiring asperity displacement to shear the two surfaces, otherwise the joint is considered as planar.
Note that if the aperture distance is greater than 5mm then the joint roughness is of little significance compared to the shear properties of the infill. If this is the case then the joint roughness is scored as either planar or undulating.

4.4.4.2.3 Joint infilling (P_{2c})

The type and thickness of material between the joint faces largely determines the shear resistance of the discontinuity set.

4.4.4.2.4 Mean fracture spacing (P_{2d})

The mean fracture spacing of the discontinuity set is assessed and scored.

4.4.4.2.5 Joint water (P_{2e})

The presence of joint water reduces rock friction and if flow rates are high, seepage pressures will tend to push the block towards the free face. The amount of water seepage through the joint set due to ground water is assessed.

4.4.4.3 Differential erosion (P_3)

If erosion is non uniform then rock blocks will eventually be undermined resulting in overhanging blocks or flakes of rock to fall. The difference in hardness between layers and the spacing of release joints are critical to the stability of the slope.

4.4.4.4 Difference in erosion rates (P_4)

As erosion progresses, unsupported or over-steepend slope conditions develop. The impact of the common physical and chemical erosion processes, as well as the effects of human actions, should be considered. The degree of hazard caused by erosion should reflect how quickly the erosion is occurring; the size of blocks, blocks, or units being exposed; the frequency of rock fall events; and the amount of material released during the event. If erosion features take many years to develop then the difference in erosion rates is classed as small. Slopes that are near equilibrium with their environment are covered in this category. If differential erosion features develop over a few years then the difference in erosion rates is classed as medium. If the difference in erosion rates is such that noticeable changes in the slope develop annually then the difference in erosion rates is classed as large. Erosion rates that allow rapid and continuous development of erosion features are classed as extreme.

4.4.4.5 Difference in erosion rates between zones (P_5)

The undercutting of a zone reduces the amount of support to the base of the rock blocks and consequently a block may simply fall from the undercut section. In a heavily jointed rock mass, the overlying rock may tilt towards the open face through displacement in the joint system. If the zone that is being assessed is undercut by a softer or weaker layer then the degree of overhang (B) in relation to the release jointing (A) is critical to the stability of the overlying rock mass (Figure 4.3).

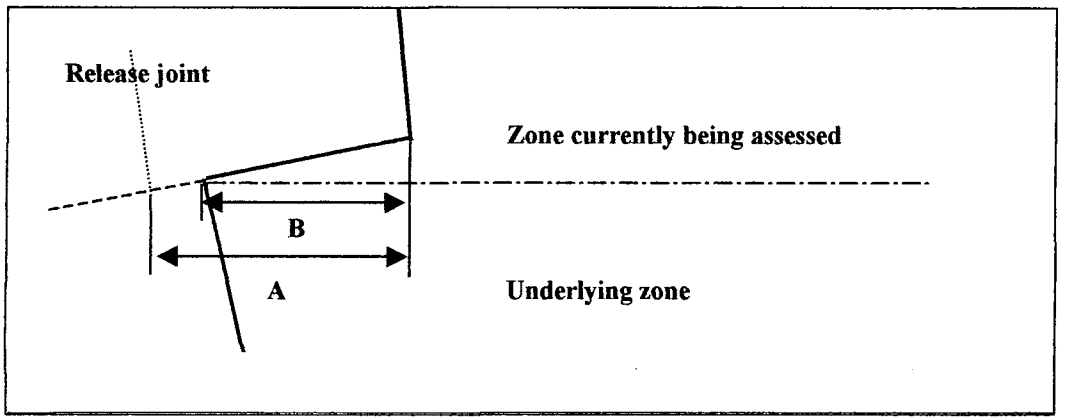

Figure 4.3: Parameters A and B defining the difference in erosion rates between zones.

4.4.4.6 Freeze/thaw (P_6)

The cyclic freeze/thaw action in the jointing system results in the widening of discontinuities. The gradual opening of the release joints results in rock blocks that are slowly pushed forwards towards the slope face, eventually leading to a rock fall. The widening of jointing due to freeze/thaw action also allows the ingress of water and tree roots. The greater the separation between joint faces the faster the joint surfaces will weather. The number of freeze/thaw cycles that the slope is subjected to in a year is estimated if no meteorological data is available. This category is only scored if water is present in the joint system over the periods that freeze/thaw is possible.

4.4.4.7 Precipitation (P_7)

Large quantities of rainfall onto a slope cause a reduction in rock friction, increase seepage pressures and are vital to freeze thaw cycles.

4.4.4.8 Earthquake/vibration (P_8)

The Mercalli earthquake intensity index is used to assess the vibration intensity in the vicinity of the slope zone. This may be estimated based upon experience or seismic records. The greater the intensity of the vibration the higher the dynamic loads will be on individual blocks.

4.4.4.9 Physical disturbance (P_9)

This parameter encompasses disturbance from sources such as animals, wind and vegetation (root wedging). It requires a subjective evaluation based upon the likelihood that these effects will instigate a rock fall. The assessor must consider the risk of animal life disturbing a rock based upon the type and number of animals. In some cases such as on sea cliffs, the presence of sea birds may contribute to instability.

The action of wind force on exposed blocks must be assessed based upon the maximum likely wind force the slope zone will be subjected to. The likelihood of a rock being disturbed by the wind is low, however wind forces also contribute to the adverse effects caused by root wedging. The expansion of roots may cause the aperture spacing of the discontinuity to increase. This is especially detrimental to stability if the root is growing in a release joint. The rate or growth and influence of the root system must be assessed. The effect of wind acting on the foliage may cause a lever action to develop in the root system rock blocks being de-stabilised.

4.4.4.10 Dip of slope face (P_{10})

The angle of dip of the slope face is measured and scored. The steeper the rock face the greater the risk of rock fall.

4.4.4.11 Vertical exposed distance of slope zone (P_{11})

This is the total distance of the exposed slope zone measured from the bottom to the top of the zone. The greater the value the more likelihood of a rock fall since more rocks will be exposed on the face.

4.4.4.12 Block shape (P_{12})

The typical shape of the rock is assessed using Figure 4.4. If the slope consists of more than one dominant rock shape then both are scored but only the highest scoring is used in the rating.

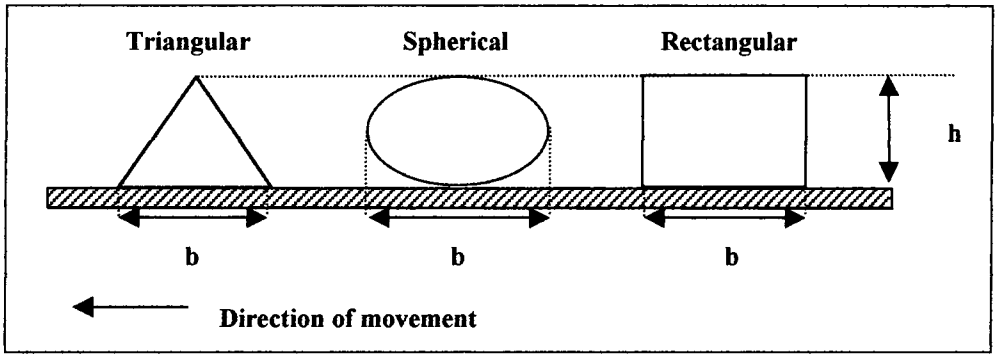

Figure 4.4: Block shape.

4.4.4.13 Rock fall history (P_{13})

Historical information is best obtained from the maintenance personnel responsible for the slope because they directly represent the known rock fall activity at the site. There may be no history available at new sites or ones where documentation practices are poor. Historical information is an important check on the potential for future rock falls.

If rock falls only occur a few times a year or less, or only during severe storms then the rock fall history parameter P_{13} is classed as rare. If rock falls occur regularly and can be expected several times a year and during most storms then the rock fall history parameter P_{13} is classed as few. The rock fall history parameter P_{13} is classed as many if rock fall occurs frequently during a certain season, such as the winter or spring wet period, or the winter freeze/thaw etc. This category is for sites where frequent rock falls occur during a certain season and are not a significant problem during the rest of the year. This category may also be used where severe rock fall events have occurred.

If rock falls occur frequently throughout the year then the rock fall history parameter P_{13} is classed as continual. This category should also be used for sites where severe rock fall events are common.

4.4.4.14 Discontinuities (T_1)

The orientation of discontinuity sets within a rock mass is a critical parameter for rock slope stability. Of secondary importance are the friction and cohesion parameters of the discontinuities, which determine the likelihood of toppling, sliding or falling of individual rock blocks. Joint orientation (P_1) and joint friction (P_2) are assessed and scored using the criteria presented in Table 4.5.

Each joint set present in the rock is assessed and scored as the mean of five sub parameters P_{2a} to P_{2e}. This procedure is repeated for each joint set. P_2 is the value of the highest scoring average. V_1 is calculated from Equation 4.2 and is subject to a maximum value of 100 points.

$$V_1 = 2P_1 + P_2 \qquad \textbf{4.2a}$$

subject to the condition that,

$$V_1 \leq 100 \qquad \textbf{4.2b}$$

The total value (T_1) for the discontinuities is calculated from Equation 4.3.

$$T_1 = V_1 \times 3.24 \qquad \textbf{4.3}$$

The joint condition factor (F_1) is calculated thus;

$$F_1 = \frac{V_1}{100} \qquad \textbf{4.4}$$

4.4.4.15 Erosion (T_2)

Because rock fall is caused by a loss of support either locally or throughout the slope, erosion features such as oversteepened slopes, unsupported rock units, or exposed resistant rocks on a slope may eventually lead to a rock fall event. Common slopes that are susceptible to this loss of support are layered units consisting of easily weathered rock that erodes, undermining more durable rock. Differential erosion may also widen jointing resulting in columns of unsupported rock blocks.

V_2 is the sum of parameters P_3, P_4, and P_5 subject to a maximum value of 100 points.

$$V_2 = P_3 + P_4 + P_5 \qquad \textbf{4.5a}$$

subject to the condition that,

$$V_2 \leq 100 \qquad \textbf{4.5b}$$

The total (T_2) for the erosion features is calculated from Equation 4.6.

$$T_2 = V_2 \times 3.24 \qquad \textbf{4.6}$$

The erosion condition factor (F_2) is calculated thus;

$$F_2 = \frac{V_2}{100} \qquad \textbf{4.7}$$

4.4.4.16 Environmental effects (T_3)

The total (T_3) is calculated as follows;

If $F_1 \geq F_2$ then,

$$T_3 = F_1(P_6 + P_7 + P_8 + P_9) \quad \textbf{4.8}$$

If $F_2 > F_1$ then,

$$T_3 = F_2(P_6 + P_7 + P_8 + P_9) \quad \textbf{4.9}$$

4.4.4.17 Physical slope properties (T_4)

The total (T_4) is calculated as follows;

If $F_1 \geq F_2$ then,

$$T_4 = F_1(P_{10} + P_{11} + P_{12}) \quad \textbf{4.10}$$

If $F_2 > F_1$ then,

$$T_4 = F_2(P_{10} + P_{11} + P_{12}) \quad \textbf{4.11}$$

4.4.4.18 Total RFRAS value V_t

The total RFRAS value (V_t) is calculated as follows;

$$V_t = T_1 + T_2 + T_3 + T_4 + P_{13} \quad \textbf{4.12}$$

The potential for future rock fall may be determined by reference to Table 4.6.

Total RFRAS value (V_t)	Likely number of future rock falls	Rock fall risk
<63	None	None
63-200	Few	Low
201-349	Several	Moderate
350-705	Many	High
>705	Continual	Very high

Table 4.6: Rock fall potential and risk.

4.4.4.19 System limitations

The RFRAS provides agencies with a method to address their rock fall problems by providing a relative rating between slope zones. For the most part this relative rating is subjective. The slope evaluation process is as simple as possible, however, there is still a range of values a slope could receive. Much depends upon the ability of the assessor and how consistently they interpret and apply the rating criteria.

Agencies will always be expected to react to rock fall accidents no matter where a particular zone appears on the RFRAS priority list, but the tendency to overreact must be resisted. Sites where an accident has occurred should be re-evaluated with the detailed rating system to determine if the rock fall incident has increased or decreased the rock fall potential. The level of investment at the site should be consistent with new potential relative to that on other sites.

4.4.5 Testing of the RFRAS

The RFRAS has been applied to 18 slopes at ten sites in and around County Durham. All of the rock slopes were photographed and the potential for rock fall estimated and compared to the degree of risk predicted by the final RFRAS value. In order to simplify the calculation of the RFRAS total (V_t) a Visual Basic program entitled GeoRisk has been developed by the author. The slope locations, photographs and GeoRisk computed totals are included in Appendix 1. The final RFRAS value, calculated potential risk, estimated potential risk, and rock fall history, are all presented in Table 4.7. This allows a direct comparison to be made between the degree of risk predicted by a trained observer and the RFRAS. In theory, the historical rock fall should be a good indicator of the likelihood of future rock falls. However, this will not always be the case since an unstable slope may stabilise after a rock fall event, especially if differential erosion was the primary cause of the rock fall.

Location	Slope No.	OS. Grid reference	Preliminary Rating		Detailed Rating		
			Potential for future rock fall	Historical rock fall	V_t	Likely future rock fall	Rock fall risk
Running Waters	1	NZ 433500, 540300	Moderate	Moderate	291	Several	Moderate
	2				309		
	3				327		
	4		High	High	389	Many	High
Nr Running Waters	5	NZ 433550, 540300	Low	Low	187	Few	Low
	6	NZ 433600, 540300			177		
Nr. Wingate	7	NZ 366000, 382000			85		
Finchale	8	NZ 297000, 472000			111		
	9	NZ 292000, 473000			124		
	10	NZ 289000, 473000			176		
Pittington	11	NZ 333000, 442000	Moderate	Moderate	348	Several	Moderate
	12		Low	Low	201	Few	Low
High Moorsley	13	NZ 334000, 455000	High	High	739	Continual	Very High
Eppleton Quarry	14	NZ 358000, 485000	Moderate	Moderate	215	Several	Moderate
Quarrington	15	NZ 330000, 379000	High	High	850	Continual	Very High
	16	NZ 333000, 378000			845		
Cassop Vale	17	NZ 339000, 383000			660	Many	High
Wingate	18	NZ 374000, 375000			393		

Table 4.7: Summary of field data.

Chapter 5

GeoFall: Program Structure, Algorithms and Verification

5 GeoFall: Program structure, algorithms and verification.

5.1 Introduction

GeoFall is a general two dimensional rock fall simulation program in which the various motions of the rock are linked to form complete rock fall paths. The rock is assumed to behave as a rigid body, which remains intact during rock fall. Any slope geometry may be modelled including re-entrants and closed profiles such as caverns. Various rock fall shapes are permitted which include a sphere, disc, ellipse, and several polygonal shapes. The user may also generate any rock shape of their choosing. Translational and rotational velocities are considered and impacts governed by coefficients of normal and tangential restitution. Rolling and sliding are also modelled by a coefficient of rolling resistance and friction, a combination roll-slide is not possible and rocks may only slide on one surface. Surface roughness is set by randomly varying the angle of the slope. Kinetic energy, velocity, bounce height envelopes and the rock fall distribution are all determined by the program at slope locations pre set by the user. The effectiveness of user defined rock fall nets may also be determined. A users guide to GeoFall is included in Appendix 2.

5.2 Structure

GeoFall consists of six main algorithms, namely, projectile, rolling and sliding motion, impact checks, determination of the mode of travel, and the time step algorithm. The interaction between these algorithms is illustrated in Figure 5.1.

A rock modelled in GeoFall always begins as a projectile. The position of the rock is checked for impact with the slope. If the rock has not hit the slope then its position after a small time increment is calculated until impact with the slope occurs. The subsequent post impact mode of travel is determined and may be projectile, rolling or sliding motion.

A rock continues to bounce, roll or slide until impact with the slope occurs or other criteria have been met. If the rock cannot move by any of the three modes of travel then it has ceased moving and is considered 'dead', the program is then reset, ready for a new rock fall simulation.

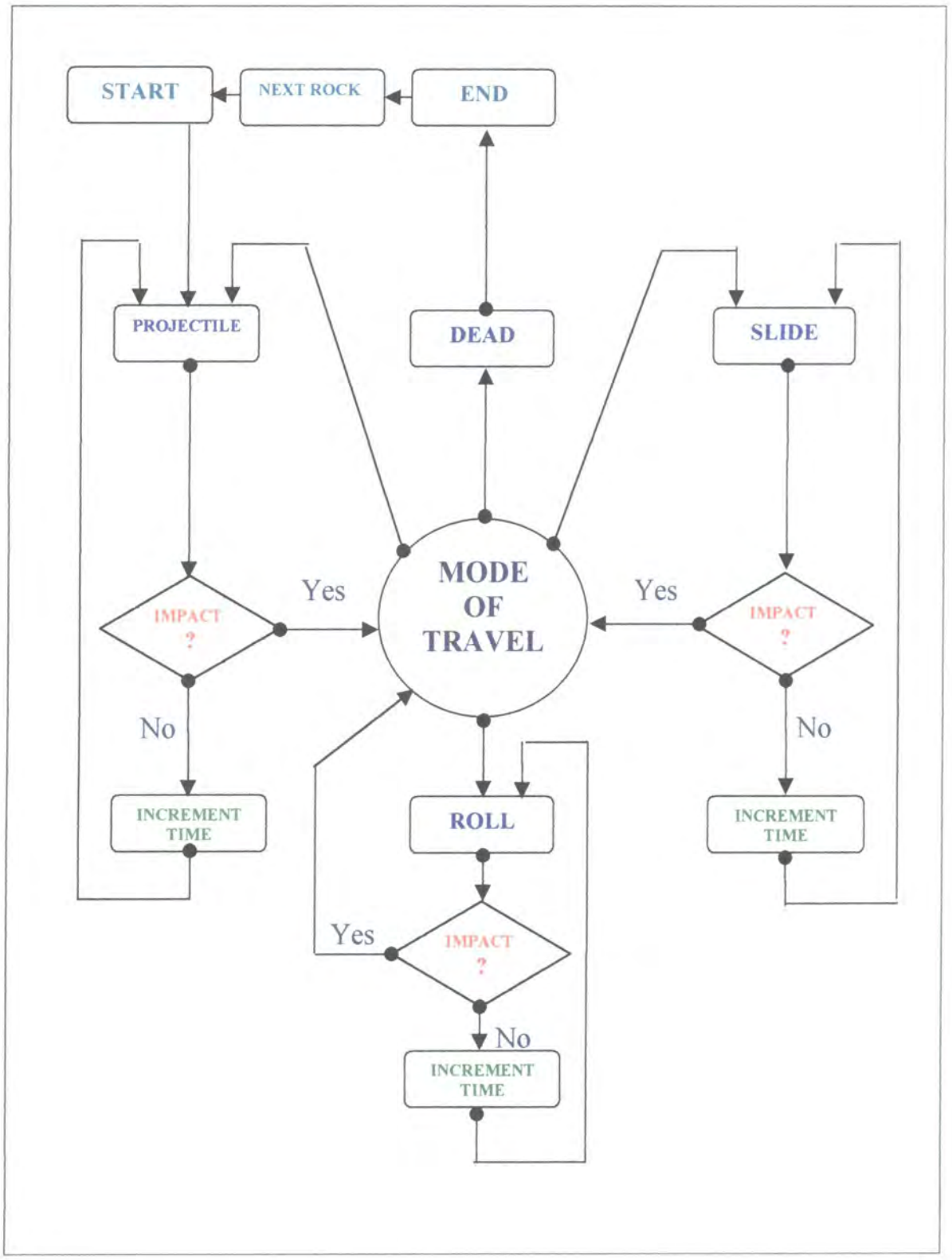

Figure 5.1: Basic program flow diagram.

5.3 Algorithms

5.3.1 The time step method

The position of a rock after a given amount of time may be calculated, whether it is rolling, sliding, bouncing or falling. Once the simulation has started then the new rock position after a small amount of time is calculated. This new position is checked for possible impact with the slope, change of mode of travel, collision with rock fall nets and other criteria that determine whether the rock has lost energy, stopped or changed mode of travel. If none of the criteria has been met then the rock will continue to roll, bounce, fall or slide ad infinitum. The smaller the increment of time or time step between successive position calculations the more accurate the rock fall model will be theoretically. However, the smaller the time step the more computation is required and as such there is a trade off between speed of execution and accuracy. If the time step is very small then rounding errors will start to become significant due to the order of accuracy of the program variables.

Figure 5.2 illustrates the principle of the time step method. A spherical rock is in free fall after rolling over a cliff edge. The time step in this instance is one second and its position has been calculated every second up to the point of impact. The total time up to and including impact in this instance is seven seconds. This time is known as the elapsed time and is defined as the time elapsed from the initial movement of the rock. The user of the program may set the time step. The need for a smaller time step is governed by one or more of the following factors.

a) Speed of execution.

   The smaller the time step is, the greater numbers of iterations are required for a given simulation.

b) Acceptable accuracy of results.

   If the time step is large then the orientation of the rock upon impact will be less exact.

c) The size of the slope.

   If the slope is of great extent and the velocity of the rock is low then the total elapsed time of a rock fall simulation may be quite high. The result of this is that a large number of iterations or time steps are needed.

d) The number of regions defining the slope.

For each time step the position of the rock is calculated. This position is compared with the position of the slope to determine whether the rock has penetrated the slope profile. The greater the number of regions that define the slope, the greater the number of impact checks that are required.

e) The speed of the rock.

If the rock is travelling at high speed then the distance covered in any given time step can be quite high. The result is that the geometry upon impact and position before impact may be unacceptable. This is especially true if the rock has a high angular velocity.

f) The geometry of the rock.

The greater the number of nodes that define the rock, the greater the number of impact checks that are required.

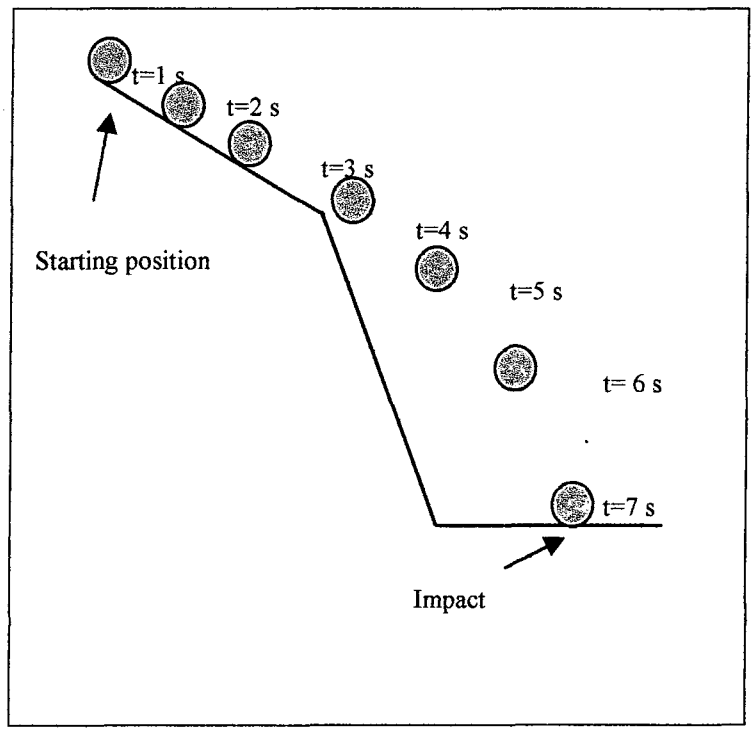

Figure 5.2. The time step method.

5.3.2 Global and local co-ordinate systems

GeoFall uses a local and global co-ordinate system. The global co-ordinate system is used to define the slope surface profile, and the rock's centroid position after any given time interval relative to an arbitrary datum (Figure 5.3). The slope profile is represented by a number of continuous piece wise linear regions defined in an anti clockwise manner so that the solid slope is always to right and the air to the left. The slope may be open, as shown in the Figure, or closed as in a cavern. Each joint or node between regions is numbered sequentially.

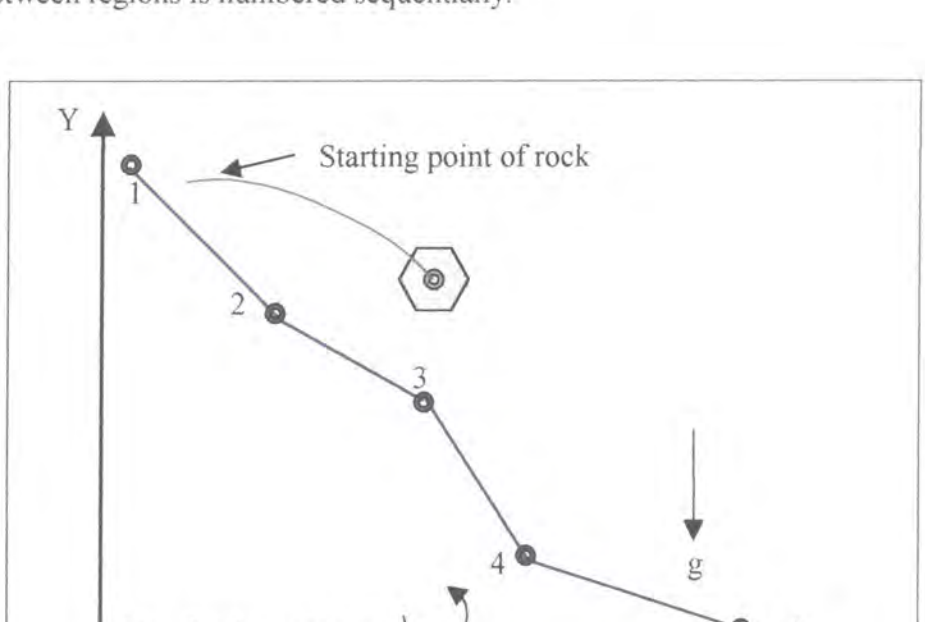

Figure 5.3: The global co-ordinate system.

Two local co-ordinate systems exist. The first is used to define the rock shape about an arbitrary origin, and the second to define the rock shape about its centroid. The Cartesian co-ordinates of the rock nodes are all relative to the origin and are denoted as x', y' and x, y for each respective co-ordinate system. The local co-ordinate system is parallel to the global co-ordinate system. Figure 5.4 illustrates a rock that has been defined by four points or nodes about an arbitrary origin 0. Point 2 for example, in the Figure is defined about this arbitrary local origin as (x'_2, y'_2).

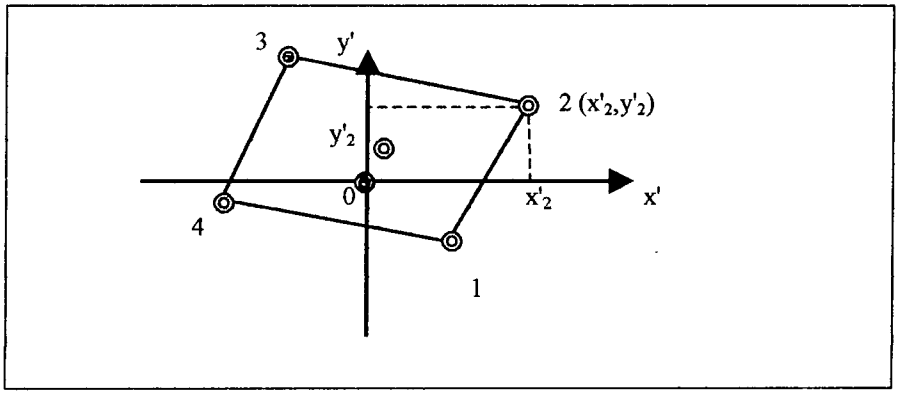

Figure 5.4: The local co-ordinate system.

5.3.2.1 Conversion between co-ordinate systems

It is essential that the co-ordinates of the rock nodes can be converted from the local to the global co-ordinate system. If the global co-ordinates of the rock centroid are known, and if the co-ordinates of the rock nodes in the local system are defined relative to the centroid, then the two co-ordinate systems can be superimposed to calculate the global co-ordinates of each rock node. Figure 5.5 illustrates a rock defined by three nodes (1, 2 and 3) about its centroid. Node 2 has co-ordinates (3,1) and the centroid has co-ordinates (0,0) in the local system. The position of the centroid in the global co-ordinate system is (10,15). By superposition, the global co-ordinates of point 2 are calculated by adding the local co-ordinates of point 2 (3,1) to those of the centroid (10,15), thus obtaining (13,16).

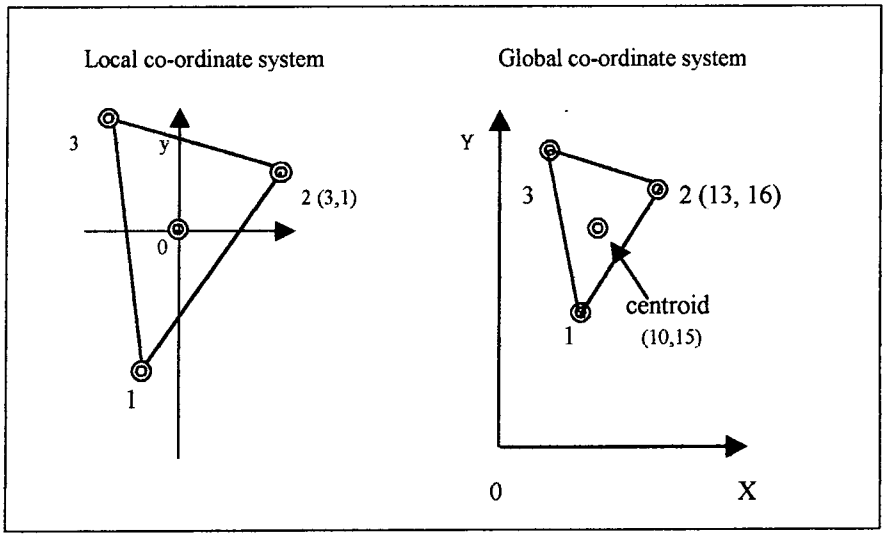

Figure 5.5: Superposition of co-ordinate systems.

5.3.3 Calculation of the area of a triangle

Many of the algorithms used in GeoFall are based upon the properties of triangles. Consider the triangle illustrated in Figure 5.6. The co-ordinates of the triangle have been defined from the origin in an anti clockwise manner and an arbitrary Cartesian co-ordinate system (x',y') chosen. The co-ordinates of the triangle nodes are (x_1',y_1'), (x_2',y_2') and (x_3',y_3') respectively. The area of the triangle (A) is given by Equation 5.1.

$$A = \frac{1}{2}\left[\left(x_3'y_1' - x_1'y_3'\right) + \left(x_1'y_2' - x_2'y_1'\right) + \left(x_2'y_3' - x_3'y_2'\right) \right] \qquad \textbf{5.1}$$

For a triangle whose vertex is at the origin;

$$A = \frac{1}{2}\left(x_1'y_2' - x_2'y_1'\right) \qquad \textbf{5.2}$$

If the rock nodes are numbered sequentially anti clockwise then the calculated value of A will be positive. If the nodes are numbered in a clockwise manner then the calculated area will be negative in value.

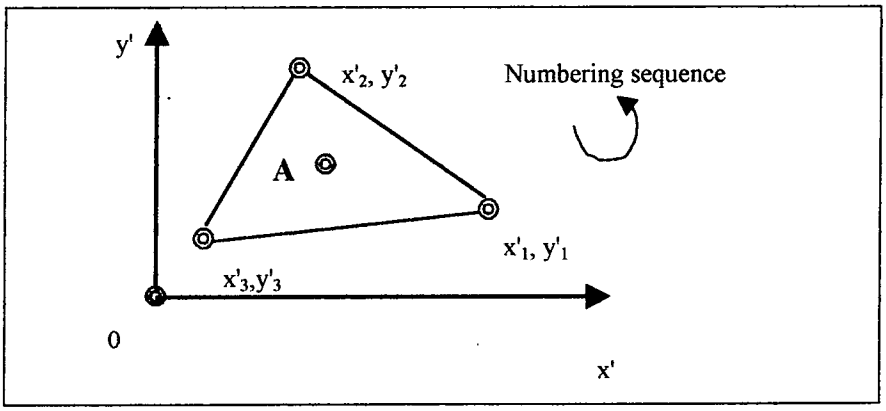

Figure 5.6: Calculation of area for a triangle.

5.3.4 Calculation of the area of an irregular shaped rock

An irregular shaped rock as illustrated in Figure 5.7, is defined relative to the arbitrary origin with its nodes numbered in an anti clockwise manner. The origin can be anywhere but it is convenient to use a point close to the estimated centroidal position for illustrative purposes. By drawing radial lines from the arbitrary origin to the rock nodes we can divide the rock into j triangles having areas a_1 to a_n where n is the total number of rock nodes. The total area of the rock (A) is the summation of the areas a_1 to a_n.

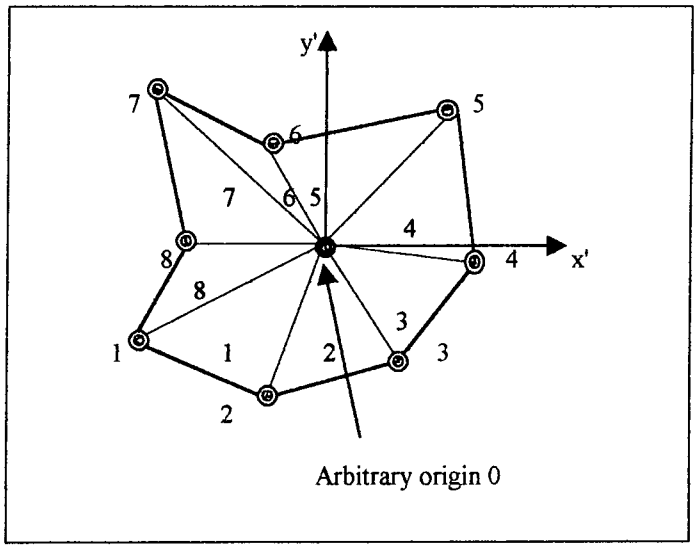

Figure 5.7: Division of the rock into triangles.

For the j_{th} triangle, from Equation 5.2;

$$a_j = \frac{1}{2}\left(x'_j y'_{j+1} - x'_{j+1} y'_j\right) \qquad \textbf{5.3}$$

This procedure is repeated for the other triangles so that the total area of the rock A may be calculated thus,

$$A = \sum_{j=1}^{n} a_j \qquad \textbf{5.4}$$

5.3.5 Calculation of the centroid position for a triangle

The co-ordinates of the position of the centroid (c',d') of the triangle illustrated in Figure 5.8 are given by Equations 5.5 and 5.6.

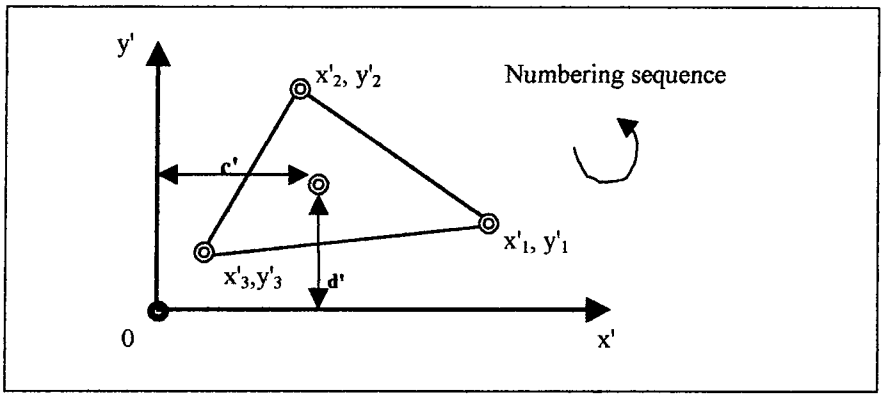

Figure 5.8: Calculation of triangle centroid.

$$c' = \frac{1}{3}(x'_1 + x'_2 + x'_3) \qquad \textbf{5.5}$$

$$d' = \frac{1}{3}(y'_1 + y'_2 + y'_3) \qquad \textbf{5.6}$$

For a triangle whose vertex is at the origin (such as any triangle shown in Figure 5.7);

$$c' = \frac{1}{3}(x'_1 + x'_2) \qquad \textbf{5.7}$$

$$d' = \frac{1}{3}(y'_1 + y'_2) \qquad \textbf{5.8}$$

5.3.6 Calculation of the centroid position for an irregular shaped rock

For the j_{th} triangle shown in Figure 5.7 the horizontal distance c'_j and the vertical distance d'_j from the origin to the centroid of the triangle may be calculated using the following equations;

$$c'_j = \frac{1}{3}\left(x'_j + x'_{j+1}\right) \qquad 5.9$$

$$d'_j = \frac{1}{3}\left(y'_j + y'_{j+1}\right) \qquad 5.10$$

The moments of area for each triangle $I_{x'}$ and $I_{y'}$ about the x and y axis respectively, are calculated as the area of the triangle multiplied by the perpendicular distance of the centroid from the origin as shown in Figure 5.8. Thus,

$$I_{x'j} = a_j d'_j \qquad 5.11$$

$$I_{y'j} = a_j c'_j \qquad 5.12$$

The total moment of area about the x axis is the sum of all the moment areas of each triangle about the x axis. Similarly the total moment of area about the y axis is the sum of all the moment areas of each triangle about the y axis. Thus,

$$I_{x'} = \sum_{j=1}^{n} a_j d'_j \qquad 5.13$$

$$I_{y'} = \sum_{j=1}^{n} a_j c'_j \qquad 5.14$$

The values of $\Delta x'$ and $\Delta y'$ give the horizontal and vertical distances to the centroid from the chosen origin .

$$\Delta x' = \frac{\sum_{j=1}^{n} a_j c'_j}{A} \qquad 5.15$$

$$\Delta y' = \frac{\sum_{j=1}^{n} a_j d'_j}{A} \qquad \textbf{5.16}$$

It is convenient to move the arbitrary origin to the centroid position such that all of the rock nodes are defined around the centroid. The centroid then becomes the new origin.

Figure 5.9 illustrates a simple rock that has had the origin of its local co-ordinate system shifted to the position of the centroid.

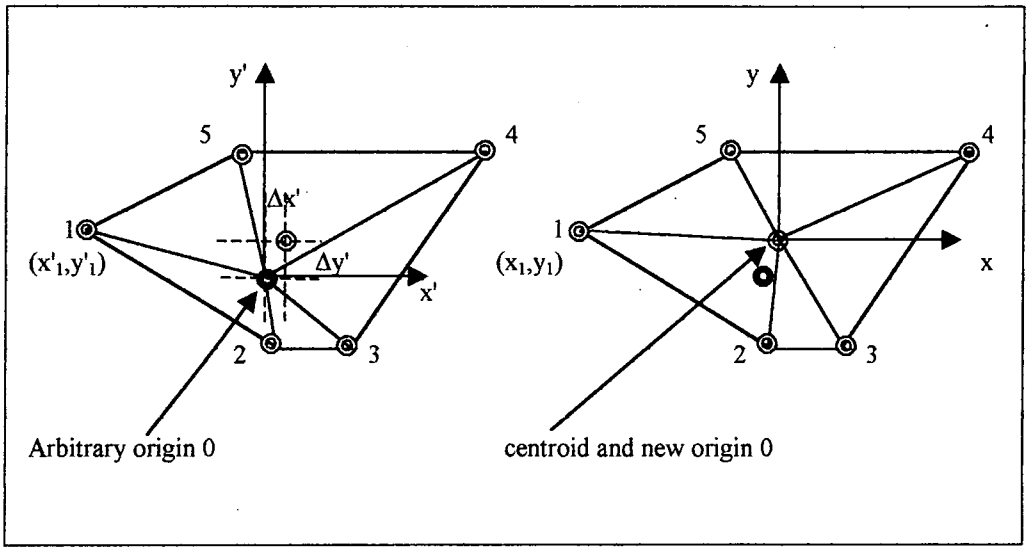

Figure 5.9: Shifting the co-ordinate system to the centroid position.

The co-ordinates of rock node i (x'_i, y'_i) thus become (x_i, y_i), where;

$$x_i = (x'_i - \Delta x') = x'_i - \frac{\sum_{j=1}^{n} a_j c'_j}{A} \qquad \textbf{5.17}$$

$$y_i = (y'_i - \Delta y') = y'_i - \frac{\sum_{j=1}^{n} a_j d'_j}{A} \qquad \textbf{5.18}$$

Note that this method works for any shaped rock including those that contain re-entrant corners.

5.3.7 Calculation of the moment of area for a triangle

The determination of the moment of area for the rock is necessary in order to calculate the moment of inertia. The moment of inertia governs both the rock's behaviour on impact and the rotational kinetic energy. Both the moment of area and inertia may be determined by dividing the rock into a series of triangles.

Consider the triangle illustrated in Figure 5.10. A local Cartesian co-ordinate system is chosen with its origin at one vertex of the triangle and with its base line rotated about an anticlockwise angle θ from the x axis. Distance d_v is the length of the base line, distance h_a is the height of the triangle from the base line to the apex and distance d_a is the distance to the apex measured along the base line.

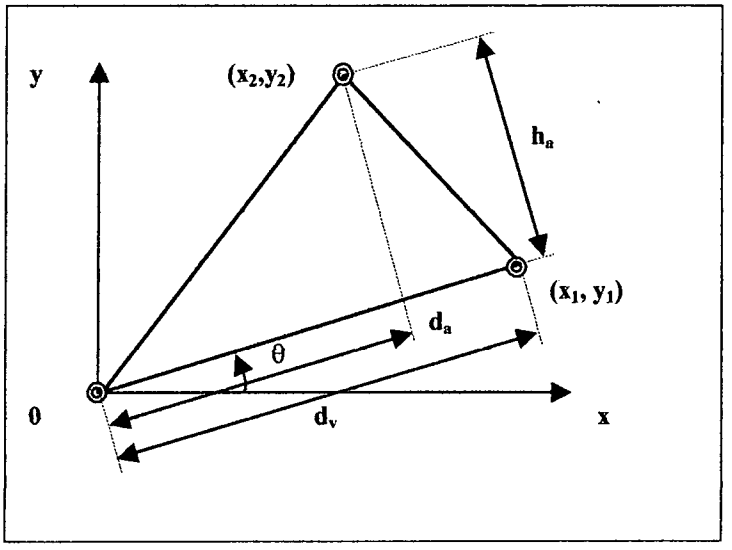

Figure 5.10: A triangle rotated by an amount θ.

If the rock nodes x_1, y_1 and x_2, y_2 are ordered in an anticlockwise manner from the origin then distances d_a, d_v and h_a may be calculated thus,

$$d_a = x_2 Cos\theta + y_2 Sin\theta \qquad \textbf{5.19}$$

$$d_v = x_1 Cos\theta + y_1 Sin\theta \qquad \textbf{5.20}$$

$$h_a = -x_2 Sin\theta + y_2 Cos\theta \qquad \textbf{5.21}$$

For any given shape the polar moment of area I_p is the sum of the parallel moments of area I_x and I_y .

Defining I_x as the moment of area of the triangle about the x axis, I_y as the moment of area of the triangle about the y axis and I_p is the polar moment of area about the vertex at the origin, we have

$$I_x = \frac{d_v h_a^{\,3}}{12} \qquad \textbf{5.22}$$

$$I_y = \frac{d_v h_a}{12}\left(d_v^{\,2} + d_a d_v + d_a^{\,2}\right) \qquad \textbf{5.23}$$

By the perpendicular axis theorem,

$$I_p = I_x + I_y \qquad \textbf{5.24}$$

5.3.8 Moment of inertia for an irregular polygonal rock

For an irregular polygon divided into j triangles with a common vertex at its centroid the moment of area I_c about the centroid is given by;

$$I_c = \sum_{j=1}^{n} I_{pj} \qquad \textbf{5.25}$$

Extending this definition to a rock in the form of an irregular polygon of uniform density ρ and thickness z, the moment of inertia of the rock about its centroid J_c is given by,

$$J_c = \rho z \sum_{j=1}^{n} I_{pj} \qquad \textbf{5.26}$$

$$J_c = \frac{m}{A} \sum_{j=1}^{n} I_{pj} \qquad \textbf{5.27}$$

This method works for any shaped rock including those that contain re-entrant corners.

5.3.9 Moment of inertia for simple geometrical shapes

For simple rock shapes it is more convenient to use standard formulae listed in Table 5.1 rather than the method described in section 5.3.8.

Rock shape	Parameter	Definition	Moment of Inertia J_c	
Sphere	r	radius	$\frac{8}{15}\rho\pi r^5$	$\frac{2}{5}mr^2$
Disc	r	radius	$\frac{1}{2}\rho\pi r^4 z$	$\frac{1}{2}mr^2$
Square	b	side length	$\frac{1}{6}\rho\pi b^4 z$	$\frac{1}{6}mb^2$
Rectangle	b	breadth	$\frac{bh}{12}\left(b^2+h^2\right)\rho z$	$\frac{m}{12}\left(b^2+h^2\right)$
	h	height		
Ellipse	a	semi major axis	$\frac{\pi ab}{4}\left(a^2+b^2\right)\rho z$	$\frac{m}{4}\left(a^2+b^2\right)$
	b	semi minor axis		

Table 5.1: Standard formulae for polar moments of inertia J_c about the centroid.

5.3.10 Rock shapes

GeoFall contains thirteen standard polygonal shapes which the user may chose from. The rock size and shape is defined in a local co-ordinate system where the origin is at the first defined node. Its base is formed by the line joining nodes one and two which are parallel to the x axis as shown for the triangular rock in Figure 5.11. The dimensions of the chosen rock a, b, c and h are entered and from these the co-ordinates of each rock node relative to the first node may be calculated. The co-ordinates of the rock nodes are defined in an anticlockwise manner and have been summarised in Tables 5.2 and 5.3.

It is not possible in GeoFall to model a true sphere, disc, semi-circle or ellipse and so a pseudo model is used. Figure 5.12 illustrates the top right quadrant of a sphere. A nominal value of five points per quadrant was chosen, which divides the boundary of the rock into 21 points. The centre of the circle is taken as the origin and all points are defined relative to this. The radius along the x axis has been split into five equal divisions. From equation 5.28 the corresponding value on the y axis can be determined and a series of co-ordinates obtained which define the rock perimeter (Table 5.4).

$$y = \sqrt{r^2 - x^2} \qquad \textbf{5.28}$$

An ellipse is modelled in a similar manner to that of a sphere or disc. For each value of x the corresponding value on the y-axis can be determined from equation 5.29, where a is the length of the major axis and b is the length of the minor axis. A series of co-ordinate values defining the rock perimeter is thus obtained.

$$y = \sqrt{b^2 - \frac{b^2 x^2}{a^2}} \qquad \textbf{5.29}$$

This method of splitting each quadrant of a sphere or ellipse into five divisions is only used to define the rock perimeter and to determine whether impact with the slope has occurred. The area, mass and moment of inertia are calculated using the standard formulae given in Table 5.1.

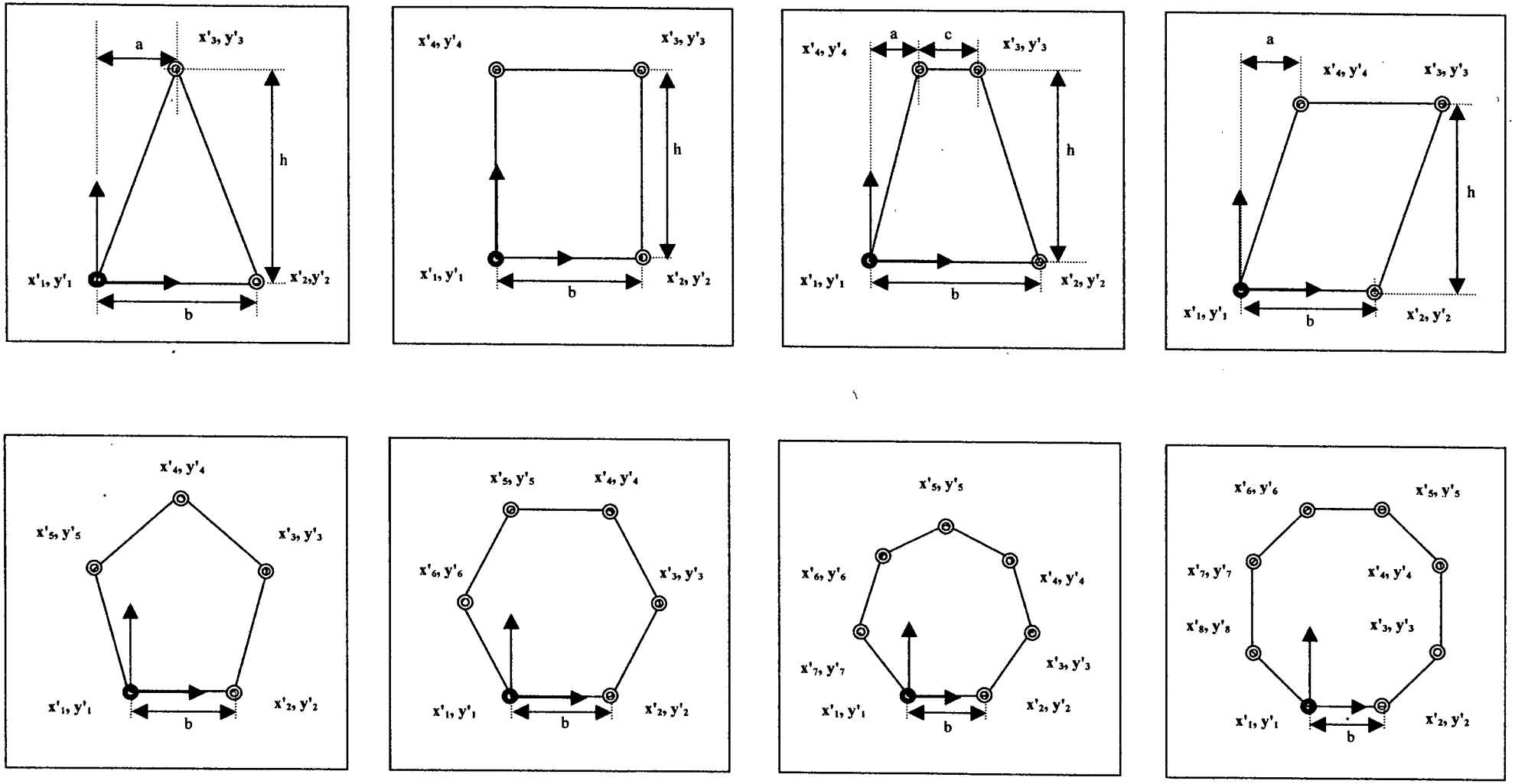

Figure 5.11: Nodes defining polygonal rock shapes.

x'	Triangle	Trapezoid	Rectangle	Square	Parallelogram	Pentagon	Hexagon	Septagon	Octagon
x'_1	0	0	0	0	0	0	0	0	0
x'_2	b	b	b	b	b	b	b	b	b
x'_3	a	a+c	b	b	a+b	b+bCos (3π/5)	b+bCos (2π/6)	b+bCos (2π/7)	b+bCos (π/4)
x'_4		a	0	0	a	b/2	b	b+ bCos (2π/7)-bCos (3π/7)	b+bCos (π/4)
x'_5						bCos (3π/5)	0	b/2	b
x'_6							-bCos (2π/6)	-b/2-bCos (π/7)	0
x'_7								-bCos (2π/7)	-bCos (π/4)
x'_8									-bCos (π/4)

Table 5.2: Co-ordinate matrix defining the rock perimeter.

y'	Triangle	Trapezoid	Rectangle	Square	Parallelogram	Pentagon	Hexagon	Septagon	Octagon
y'_1	0	0	0	0	0	0	0	0	0
y'_2	0	0	0	0	0	0	0	0	0
y'_3	h	h	h	b	h	bSin (3π/5)	bSin (2π/6)	bSin (2π/7)	bSin (π/4)
y'_4		h	h	b	h	bSin (3π/5)+bSin (π/5)	2bSin (2π/6)	bSin (2π/7)+bSin (3π/7)	b+bSin (π/4)
y'_5						bSin (3π/5)	2bSin (2π/6)	bSin (2π/7)+bSin(3π/7) +bSin (π/7)	2bSin (π/4)+b
y'_6							bSin (2π/6)	b+ bCos (2π/7)-bCos (3π/7)	2bSin (π/4)+b
y'_7								bSin (2π/7)	b+bSin (π/4)
y'_8									bSin (π/4)

Table 5.3: Co-ordinate matrix defining the rock perimeter.

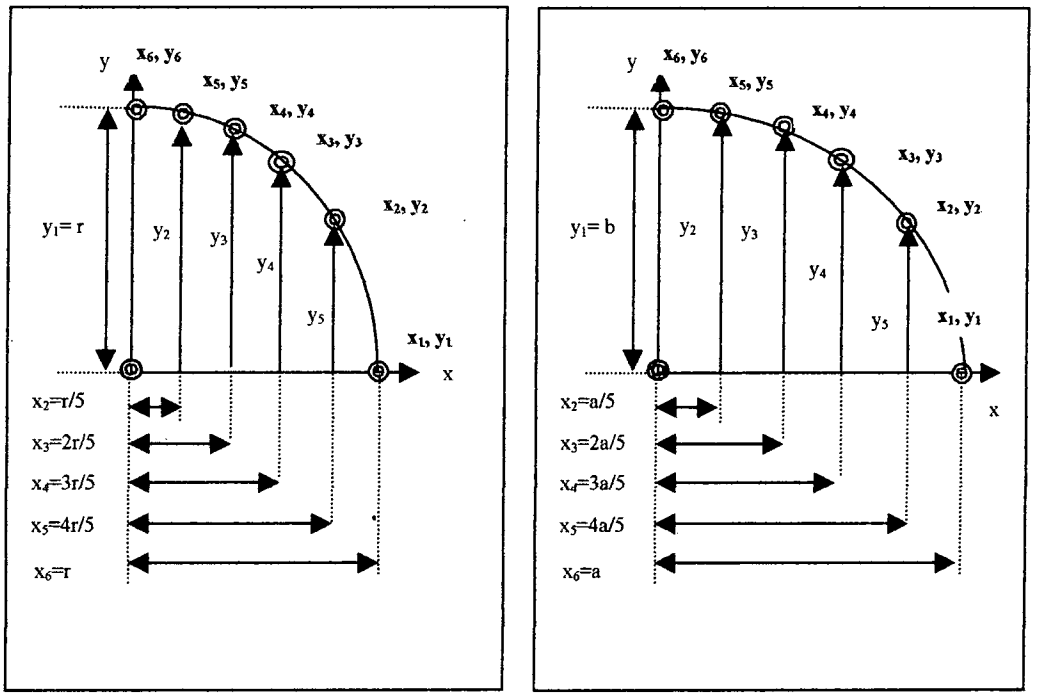

Figure 5.12: The top right quadrant of a sphere and an ellipse.

x	Disc/sphere	Ellipse	y	Disc/sphere	Ellipse
x_1	r	a	y_1	0	0
x_2	$\frac{4r}{5}$	$\frac{4a}{5}$	y_2	$\frac{3r}{5}$	$b\sqrt{\frac{9}{25}}$
x_3	$\frac{3r}{5}$	$\frac{3a}{5}$	y_3	$\frac{4r}{5}$	$b\sqrt{\frac{16}{25}}$
x_4	$\frac{2r}{5}$	$\frac{2a}{5}$	y_4	$r\sqrt{\frac{21}{25}}$	$b\sqrt{\frac{21}{25}}$
x_5	$\frac{r}{5}$	$\frac{a}{5}$	y_5	$r\sqrt{\frac{24}{25}}$	$b\sqrt{\frac{24}{25}}$
x_6	0	0	y_6	r	a

Table 5.4: Co-ordinates defining the first quadrant of a disc/sphere and ellipse.

5.3.11 Impact checks

Figure 5.13 shows a rock about to impact a slope region defined by nodes 1 and 2 of an enclosed cavern. It is essential that an algorithm exists to determine impact of a rock node against a slope region for each time step. Without a robust algorithm it is possible that the rock may imbed or pass through the slope. By using Equation 5.2 to calculate the area of a triangle a robust and effective algorithm has been developed. It is also essential that this algorithm can be used regardless of the complex topography of the slope, which may contain re-entrant corners, vertical cliffs and the like. This allows the user to define any slope, including those completely enclosed, such as caverns, or partially constricted excavations, such as bell pits.

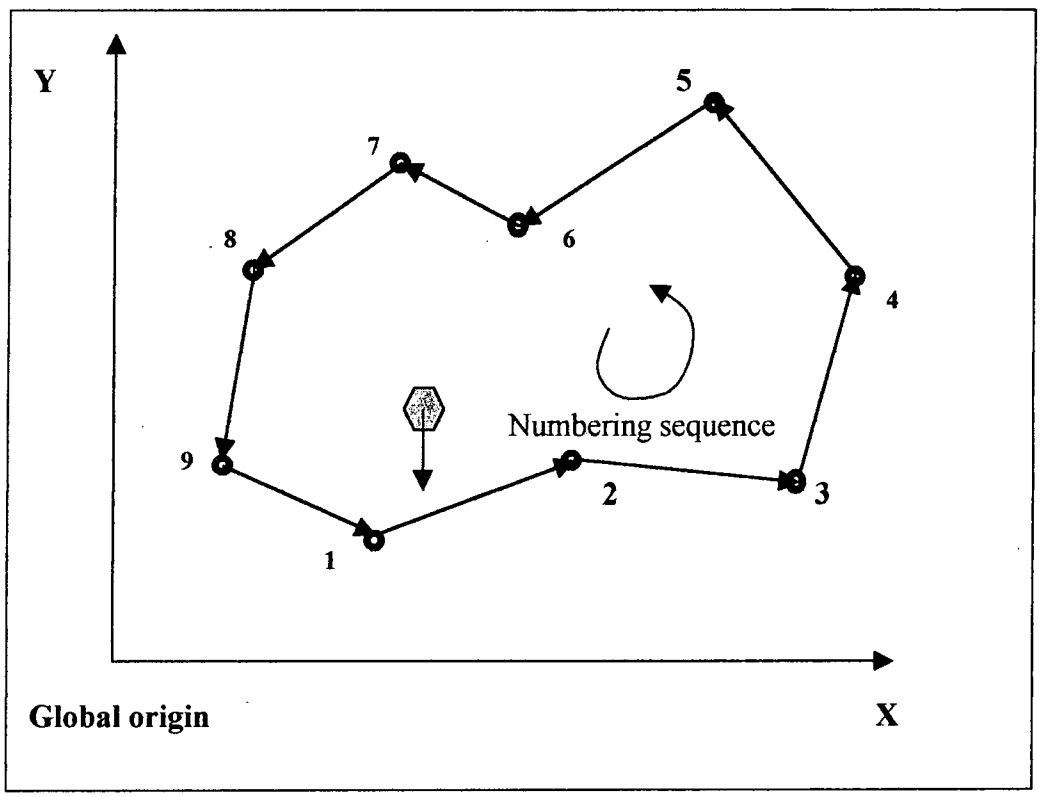

Figure 5.13: A closed slope surface profile.

5.3.11.1 Impact of a rock node against the slope

Figure 5.14 depicts a slope region defined by nodes (1-2) and two positions at the beginning, A and end, B of a time step of a typical node in the rock. Point A is prior to impact and B after impact. If a triangle is constructed such that the slope region is the base line of the triangle and the rock node in either position is the apex, then the area may be calculated using Equation 5.2. If the nodes of the triangle form an anticlockwise sequence (1-2-A) then the calculated area will be positive, and if they form a clockwise sequence, as shown by triangle (1-2-B) after impact, the area will be negative. A zero area means that the node must lie on the slope region or its projection as shown in Figure 5.15. Impact may have occurred if the area of the triangles changes in sign from positive to negative. Thus, an additional check is necessary since it is possible that the rock node may pass from one side of the slope region to the other without actually passing through it.

In order to check whether a false impact has occurred two sets of additional triangles are used. The base line of both triangles and its sense are defined from the previous rock node position, A to the current rock node position, B. The triangle apex being either the start or the end point of the slope region. By using the previous convention and formula, for a rock node to have passed through the slope region as shown in Figure 5.14 the first area (A-B-1) must be ≤ 0 and the second area (A-B-2) must be ≥ 0. When no impact has occurred as shown in Figure 5.15, both the areas of the triangles have the same sign. The current rock position is then tested for a facet of the rock striking a slope node, and impact of the rock against a net.

If impact has not occurred then the time step is advanced and the new position of the rock calculated. If the rock strikes the slope then the rock is moved back to its position prior to impact and the post impact velocities calculated using the impact equations defined by Brach (1991).

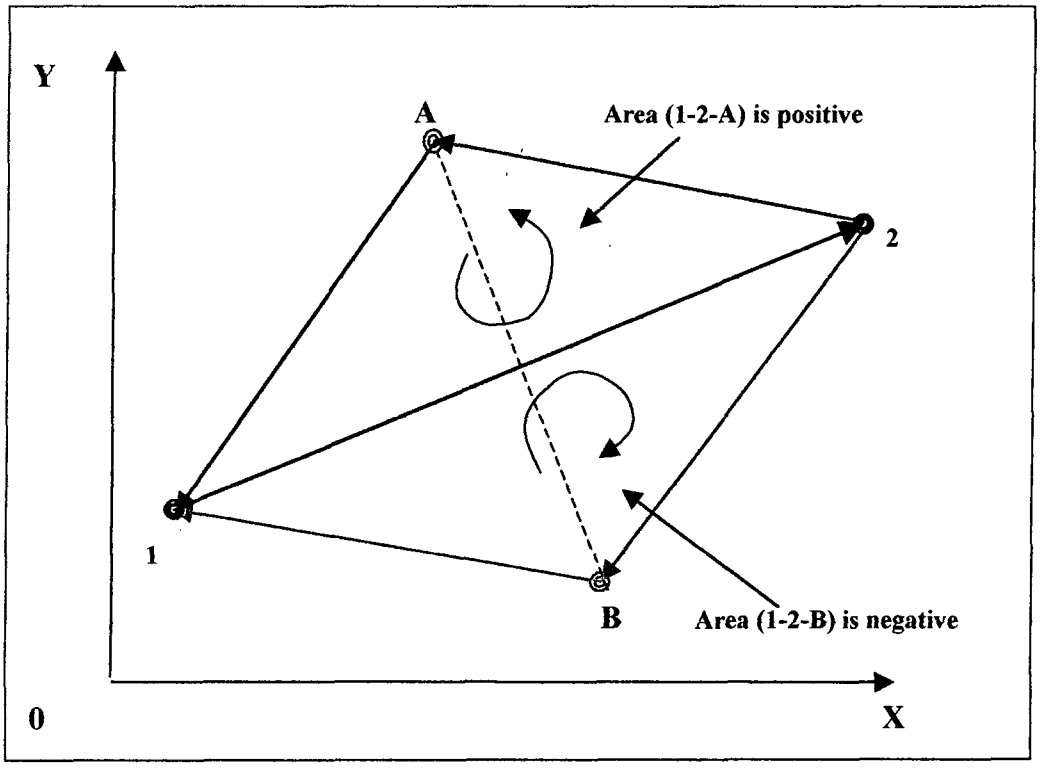

Figure 5.14: Change in sign of area defining possible impact.

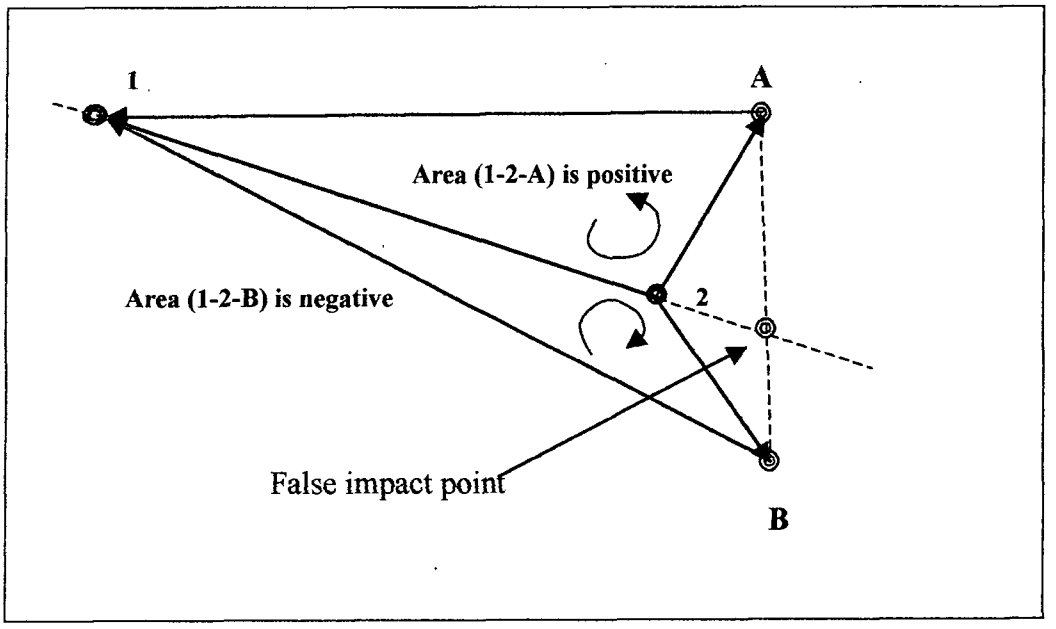

Figure 5.15: Change in area creating a false impact.

5.3.11.2 Impact against a flat

As well as the possibility of a rock node hitting the slope it is equally possible that a flat on the rock may strike a node on the slope surface as illustrated in Figure 5.16.

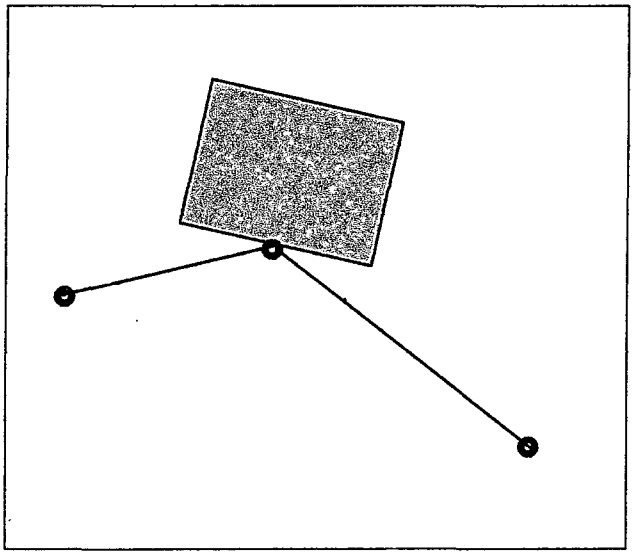

Figure 5.16: Impact against a flat of the rock.

Figure 5.17 illustrates a section of a slope defined as (1-2-3). One of the flat edges of the rock is depicted as line (A-B). In order to determine whether a true impact has occurred six criteria must be met. These criteria as before are based upon the signs of the areas of six different triangle combinations.

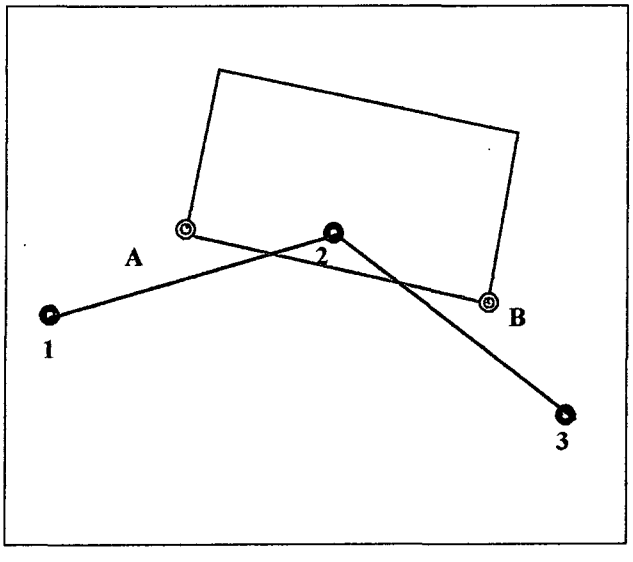

Figure 5.17: Impact against a flat face of the rock.

Criterion 1: The area of triangle 1-2-3 <0

Criterion 2: The area of triangle A-B-2 ≥0

Criterion 3: The area of triangle 1-2-A >0

Criterion 4: The area of triangle 1-2-B <0

Criterion 5: The area of triangle 2-3-A <0

Criterion 6: The area of triangle 2-3-B >0

5.3.11.3 Impact against a net

The method to detect impact with a net is similar to that used to check whether a rock node has penetrated the slope surface. The difference is that the centroid is used in place of the rock node and this may pass through the net in either direction.

Figure 5.18 illustrates a net that is defined by a pair of nodes 1 and 2. The base of the net is point 1 and the top of the net point 2. The previous centroid position is defined as point A and the current position as point B. If the net is used as the base line for a triangle and the apex is either one of the two centroid positions then two triangles may be defined as (1-2-A) and (1-2-B) respectively. Thus the area of (1-2-A) will be positive whilst that of (1-2-B) will be negative. If the rock passes from right to left through the net then the signs of the triangular areas will have been reversed.

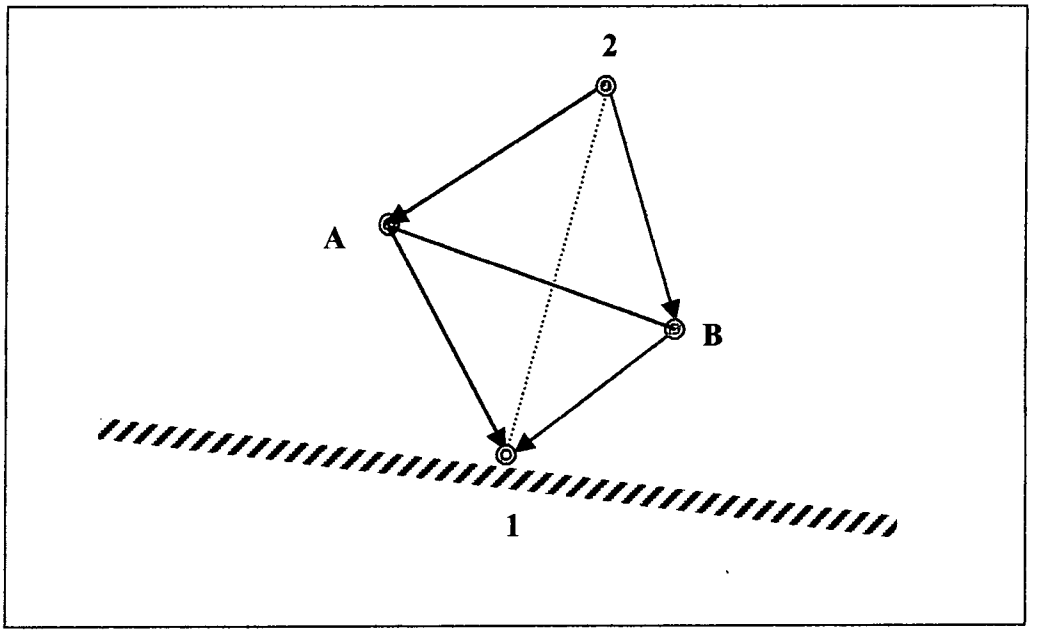

Figure 5.18: Areas of triangles produced by impact against a net.

A second check is necessary to make sure that the rock has passed through the net rather than over it. A line (A-B) from the previous to the current centroid position is used as a base line for a pair of triangles. The apex of each triangle is the top and bottom of the net These two triangles are depicted as (A-B-1) and (A-B-2) respectively. Thus the area of (A-B-1) will be negative whilst that of (A-B-2) will be positive. If the rock passes from right to left through the net then the signs of the triangle areas will have been reversed.

For impact to have occurred two sets of four criteria must be met depending upon the direction of travel of the rock.

For a rock passing from left to right the following criteria must be met for impact to have occurred.

Criterion 1: The area of triangle 1-2-A ≥ 0

Criterion 2: The area of triangle 1-2-B < 0

Criterion 3: The area of triangle A-B-1 ≤ 0

Criterion 4: The area of triangle A-B-2 ≥ 0

For a rock passing from right to left the following criteria must be met for impact to have occurred.

Criterion 1: The area of triangle 1-2-A ≤ 0

Criterion 2: The area of triangle 1-2-B > 0

Criterion 3: The area of triangle A-B-1 ≥ 0

Criterion 4: The area of triangle A-B-2 ≤ 0

The previous and current positions of the rock centroid are used rather than those of the rock nodes themselves. This ensures that the centroid has passed through the net and guards against the possibility that the rock has merely clipped the net. This produces a safer design since partial impacts are treated as if they had not passed through the net.

5.3.12 Impact dynamics

The most complex part of any rock fall simulation program is the analysis of the impact between a rock and the slope and the calculation of rock velocities before and after impact. Generally, a simple rock shape such as a disc or sphere is chosen so that simple rules of dynamics may be used to analyse the impact, however it is not possible to use these equations with very complex/irregular shapes possessing or obtaining angular velocity. Many of the existing rock fall impact analyses are overcomplicated and inconsistent thus, a new consistent theory of impact dynamics was required in order to model any planar rigid body impact such as that developed by Brach (1991). Brach uses several coefficients of which only the coefficient of normal restitution e_n and coefficient of tangential restitution e_t are used in this analysis of impact.

5.3.12.1 The normal coefficient of restitution (e_n)

If two particles strike each other normally with initial normal velocities v_{1n} and v_{2n} then they will rebound with final velocities V_{1n} and V_{2n} given by,

$$-e_n = \frac{V_{2n} - V_{1n}}{v_{2n} - v_{1n}} \qquad \textbf{5.30}$$

where e_n is the normal coefficient of restitution as defined by Brach.

In the case of a rock particle striking a massive slope, the slope velocity prior to and after impact will be zero such that;

$$-e_n = \frac{V_n}{v_n} \qquad \textbf{5.31}$$

Only the velocities of the particle are non zero and therefore the subscripts have been dropped. If the particle rebounds from the surface then $0 < e_n \leq 1$. For a perfectly elastic rebound $e_n = 1$ whilst for a completely inelastic impact (no rebound) $e_n = 0$. If the particle passes through a barrier, such as a pane of glass which may offer some or no resistance to impact, then $-1 \leq e_n < 0$ and the initial direction of travel is thus unaffected.

The coefficient of normal restitution e_n is generally treated as a constant. However in practice it depends upon many factors such as the particle shape, material and initial velocities. Values must be determined experimentally or analytically. For most engineering applications e_n varies with initial normal velocities as shown in Figure 5.19. It is apparent that as the approach velocity increases the coefficient of restitution e_n approaches an asymptote and further increases in velocity do not change the value of e_n providing there is no permanent deformation.

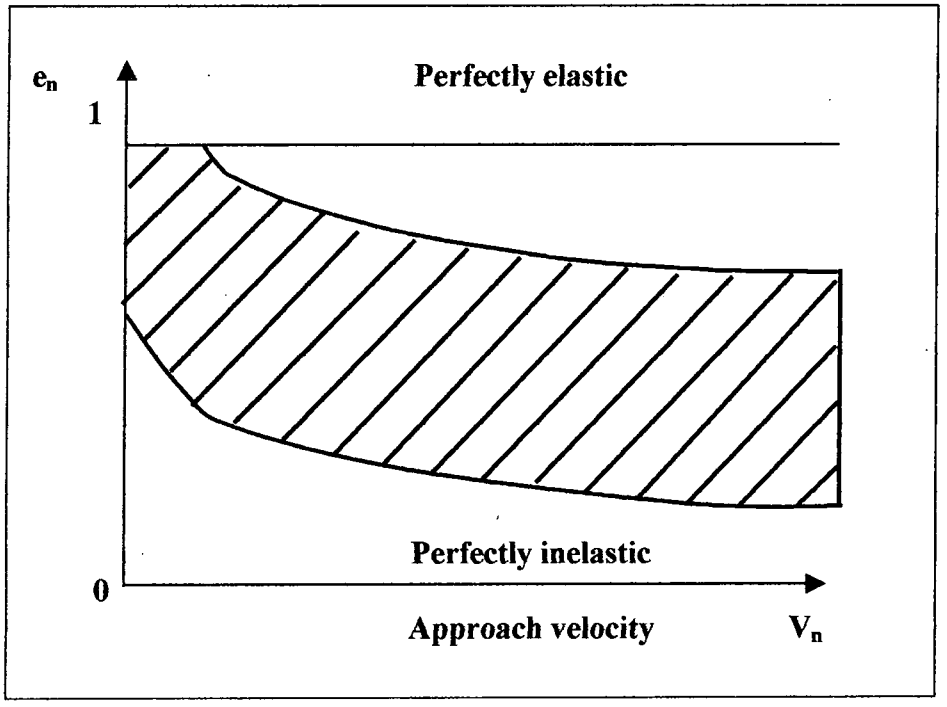

Figure 5.19: Variation of e_n with approach velocity (Brach, 1991).

5.3.12.2 The coefficient of tangential restitution (e_t)

There is some valid argument and also experimental evidence to indicate that significant shearing effects, or what can be termed tangential elastic effects, exist during some impacts (Brach, 1991).

When tangential restitution occurs the corresponding coefficient e_t allows the tangential rebound velocities after an impact to be calculated. If two particles strike each other with initial tangential velocities v_{1t} and v_{2t} then they will rebound with final velocities V_{1t} and V_{2t}.

$$-e_t = \frac{V_{2t} - V_{1t}}{v_{2t} - v_{1t}} \qquad \textbf{5.32}$$

Again considering the impact of a rock particle with a massive slope which is considered fixed then the values of V_{2t} and V_{2t} will be zero such that;

$$-e_t = \frac{V_t}{v_t} \qquad \textbf{5.33}$$

again dropping the subscripts.

If the particle rebounds from the surface then $-1 \le e_t < 0$. For a perfectly elastic rebound e_t= -1 whilst for a completely inelastic rebound e_t = 0. Negative values of the tangential restitution coefficient can be regarded as retardation rather than rebound. Although Brach shows that the coefficient of tangential restitution and the coefficient of dynamic friction μ_d can be considered equivalent, it must be kept in mind that they represent different physical effects such as elasticity and friction. This equivalence for a particle is determined by,

$$\mu_d = \frac{1+e_t}{1+e_n}\frac{v_t}{v_n} \qquad \textbf{5.34}$$

Values of e_t between -1 and 0 have a direct correspondence to values of μ_d. In particular, e_t = -1 implies no tangential effects, that is μ_d=0.

5.3.12.3 Rigid body impact theory

If two rigid bodies collide, the velocities of the bodies before and after impact are related by restitution coefficients in a similar manner to those for particles. When one of the two colliding rigid bodies is significantly more massive than another, its velocity changes may be considered negligible. In the case of rock fall the rock slope is massive and therefore remains stationary before, during and after impact. Figure 5.20 shows a rock striking a rock slope with a common tangent and normal at (X_p, Y_p), point (X_c, Y_c) is the mass centre or centroid position. The two components of force impulse P_{In}, P_{It}, and the moment impulse M_I as defined by Brach, are externally applied and are considered known. The corresponding impulses at the point of contact P_n, P_t, and M are unknown. If no permanent deformation occurs during the impact

then the corresponding initial and final dimensions of the body are given by d_c and d_d. Distance d_d is defined as the perpendicular distance from the slope to the rock centroid (X_c, Y_c). Distance d_c is measured from the point of impact (X_p, Y_p) to the rock centroid (X_c, Y_c) along the line of the slope. Because it has been assumed that no deformation occurs on impact the moment of inertia before impact is equal to that after impact.

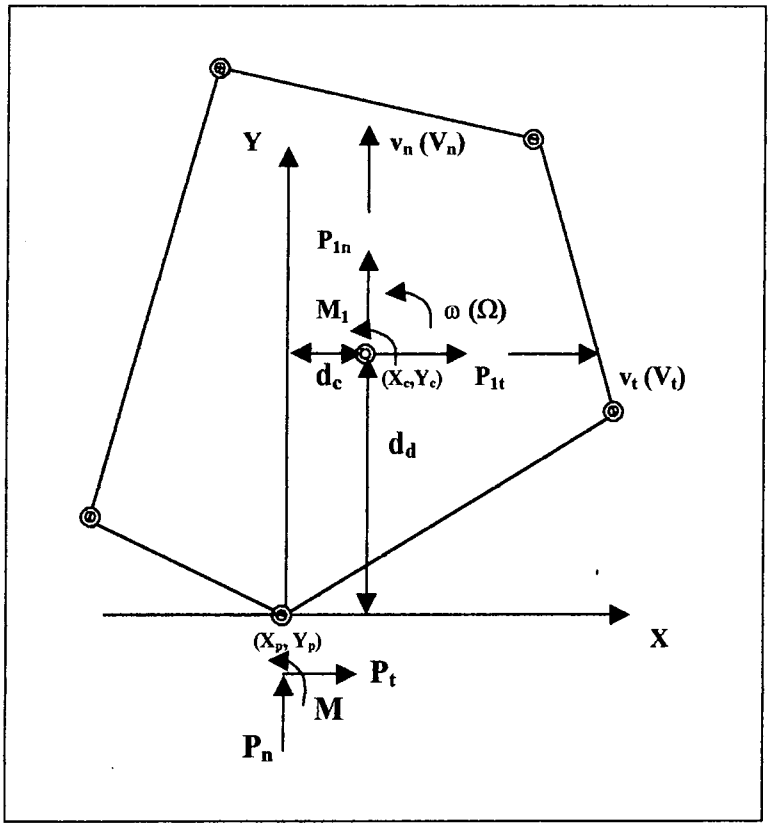

Figure 5.20: Diagram and co-ordinates of rigid body.

The initial normal, tangential and angular velocities before impact are v_n, v_t and ω respectively. The final normal, tangential and angular velocities after impact (in brackets) are V_n, V_t and Ω respectively. To simplify the analysis the external impulses P_{1t}, P_{1n} and M_1 are considered negligible and are treated as zero. With these simplifications, the principle of impulse and momentum along the two co-ordinate axes provides two equations.

$$P_n = m(V_n - v_n) \qquad \textbf{5.35}$$

$$P_t = m(V_t - v_t) \qquad \textbf{5.36}$$

Brach (1991) shows that the angular impulse and momentum are related by:

$$J_c(\Omega - \omega) = \frac{P_n}{1+e_n}d_c + \frac{e_n P_n}{1+e_n}d_c - \frac{P_t}{1+e_n}d_d - \frac{e_n P_t}{1+e_n}d_d + M \qquad \textbf{5.37}$$

This provides an expression for the unknown moment M, which can be written as

$$\frac{M}{J_c} = (\Omega - \omega) - \Gamma P_n + \Delta P_t \qquad \textbf{5.38}$$

where,

$$\Gamma = \frac{d_c + e_n d_c}{(1+e_n)J_c} \qquad \textbf{5.39}$$

$$\Delta = \frac{d_d + e_n d_d}{(1+e_n)J_c} \qquad \textbf{5.40}$$

At this point six unknowns exist. These are V_n, V_t, Ω, P_n, P_t and M. The three impulses can be eliminated using Equations 5.35-5.40 from which Brach presents three new equations.

$$V_n = -e_n(v_n + d_c\omega) - d_c\Omega \qquad \textbf{5.41}$$

$$V_t = -e_t(v_t - d_d\omega) + d_d\Omega \qquad \textbf{5.42}$$

$$\Omega = \frac{-m\Gamma(v_n + e_n v_n + e_n d_c\omega) + m\Delta(v_t + e_t v_t - e_t d_d\omega) + \omega}{m\Gamma d_c + m\Delta d_d + 1} \qquad \textbf{5.43}$$

The value of Ω may be substituted into Equations 5.41 and 5.42 to calculate V_n and V_t.

5.3.12.4 Velocities and distances for an inclined slope

For the case of an inclined slope (Figure 5.21), the calculation of velocities and dimensions of the rigid body in a global co-ordinate system is performed as follows.

$$d_c = (X_c - X_p)Cos\theta + (Y_c - Y_p)Sin\theta \qquad \textbf{5.44}$$

$$d_d = -(X_c - X_p)Sin\theta + (Y_c - Y_p)Cos\theta \qquad \textbf{5.45}$$

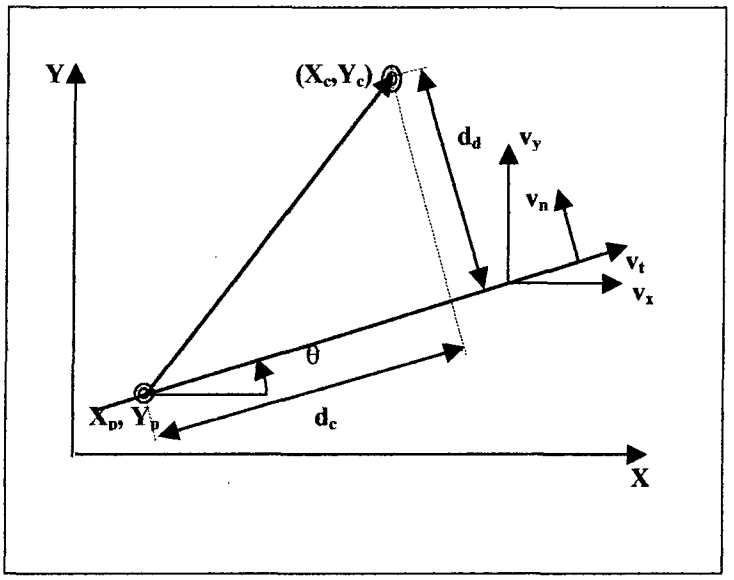

Figure 5.21: Calculation of d_c, d_d, v_n, v_t, v_y and v_x.

$$v_n = v_y Cos\theta - v_x Sin\theta \qquad \textbf{5.46}$$

$$v_t = v_y Sin\theta + v_x Cos\theta \qquad \textbf{5.47}$$

$$v_y = v_t Sin\theta + v_n Cos\theta \qquad \textbf{5.48}$$

$$v_x = -v_n Sin\theta + v_t Cos\theta \qquad \textbf{5.49}$$

5.3.13 Projectile Motion

If no part of the rock perimeter is in contact or embedded in the slope then the rock is acting as a projectile. Standard formula (Croft & Hart, 1988) may be applied to determine the position of the rock after any given time interval. These formulae do not take into account aerodynamic drag which is neglected. The amount of aerodynamic drag is very difficult to determine and becomes less significant as the rock mass increases.

Figure 5.22 illustrates the sign convention used and depicts the centroid of a rock which possess an initial vertical velocity V_{yo}, horizontal velocity V_{xo} and angular velocity ω_o.

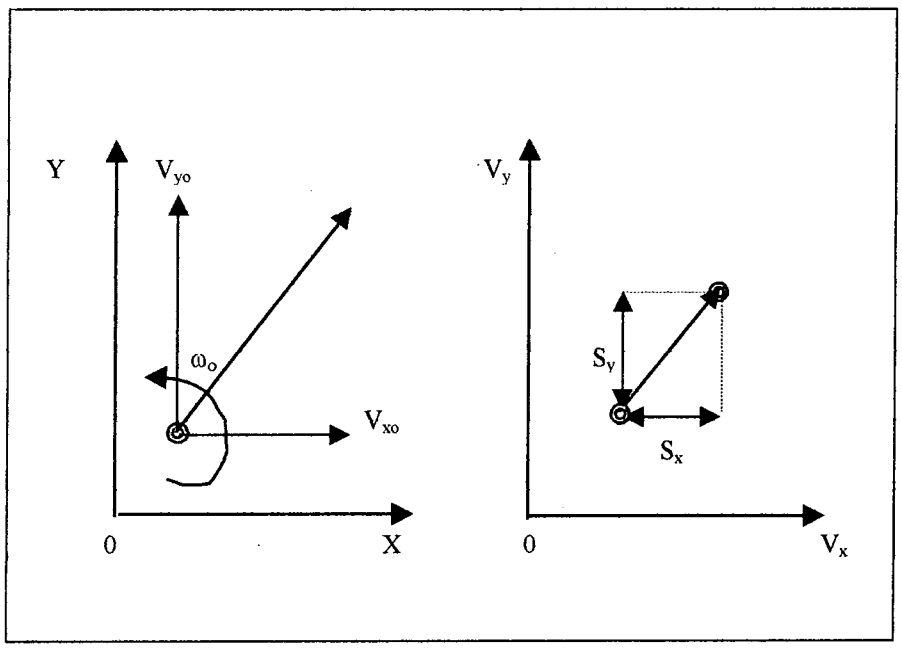

Figure 5.22: The distance travelled by a projectile.

5.3.13.1 Vertical motion

Using standard formula (Croft & Hart, 1988) the vertical velocity V_y, vertical acceleration A_y and vertical distance travelled S_y can be calculated for a given time interval t. Vertical motion is influenced by the force of gravity g and consequently the vertical acceleration A_y is equal to -g.

$$S_y = V_{xo}t - \frac{1}{2}gt^2 \qquad \textbf{5.50}$$

$$V_y = V_{yo} - gt \quad \textbf{5.51}$$

$$A_y = -g \quad \textbf{5.52}$$

5.3.13.2 Horizontal motion

The horizontal velocity V_x, horizontal acceleration A_x and horizontal distance travelled S_x can be calculated using formula similar to those used for vertical motion. Horizontal motion is not influenced by the force of gravity and consequently the horizontal acceleration A_x is zero.

$$S_x = V_{xo}t \quad \textbf{5.53}$$

$$V_x = V_{xo} \quad \textbf{5.54}$$

$$A_x = 0 \quad \textbf{5.55}$$

5.3.13.3 Calculation of the rock centroid position after time t

Consider a projectile illustrated in Figure 5.23 that starts from a local origin with an initial vertical V_{yo} and horizontal velocity V_{xo}. After a time interval t the rock will have travelled a vertical distance S_y and a horizontal distance S_x. Thus the distance travelled from the local origin after any given time interval may be calculated using Equations 5.50 to 5.55. The position of the rock at the end of the time interval is simply the initial position of the centroid (X_{co}, Y_{co}) plus the distance moved during the time interval, as given by Equations 5.50 and 5.53. The position of the rock is unaffected by the angular velocity ω which is assumed unchanged.

$$X_{c(t)} = X_{co} + S_x \quad \textbf{5.56}$$

$$Y_{c(t)} = Y_{co} + S_y \quad \textbf{5.57}$$

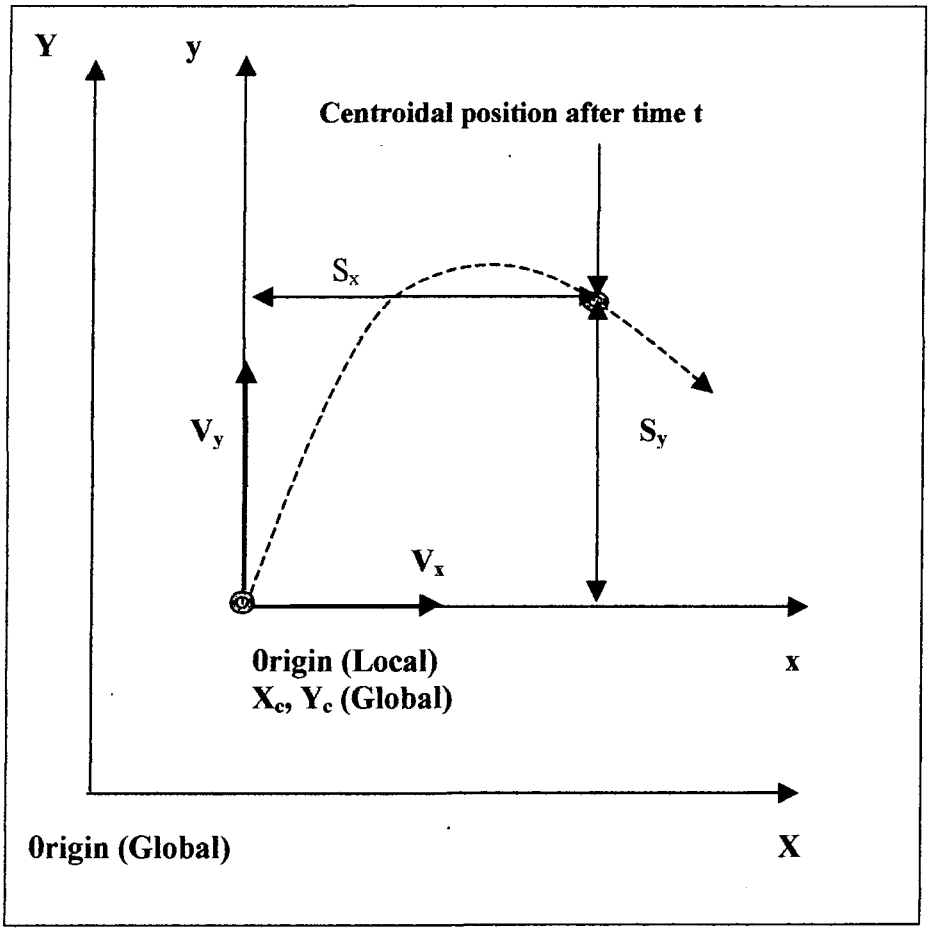

Figure 5.23: The rock centroid position after time t.

5.3.13.4 Angular velocity

If the rock possesses an angular velocity ω then it will effectively spin around the position of its centroid. If the position of the centroid is known then the positions of the rock nodes can be calculated relative to the centroid. If a rock has no vertical or horizontal velocity but possesses only an angular velocity ω, then the angle through which it rotates after a given time interval t is ωt.

The rock nodes (x_i, y_i) are defined around the centroid position in a local co-ordinate system. The new local co-ordinates for any given rotation may be calculated as follows.

a) Define all the angles θ_i from the origin to the i_{th} rock node in an anticlockwise manner from the horizontal x axis.

b) For the i_{th} rock node (x_i, y_i) calculate the radial distance r_i (Figure 5.24).

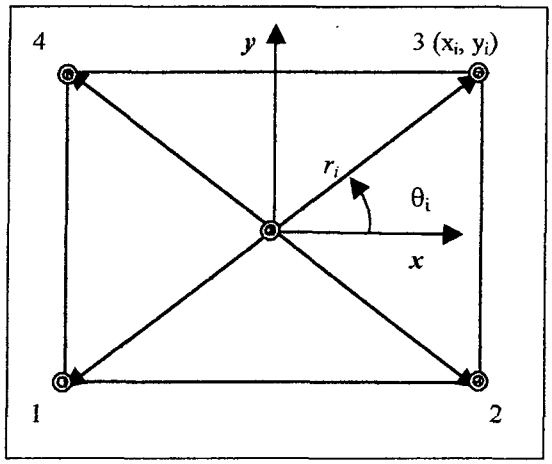

Figure 5.24: Calculation of radial distances, r_i.

where,

$$r_i = \sqrt{x_i^2 + y_i^2} \qquad \textbf{5.58}$$

c) The new angle from the horizontal x axis to the rock node *i* after a given time increment t is defined as Φ_t. Figure 5.25 illustrates one of the rock nodes x_i, y_i that has rotated anticlockwise about its centroid from its previous position x_{io}, y_{io}.

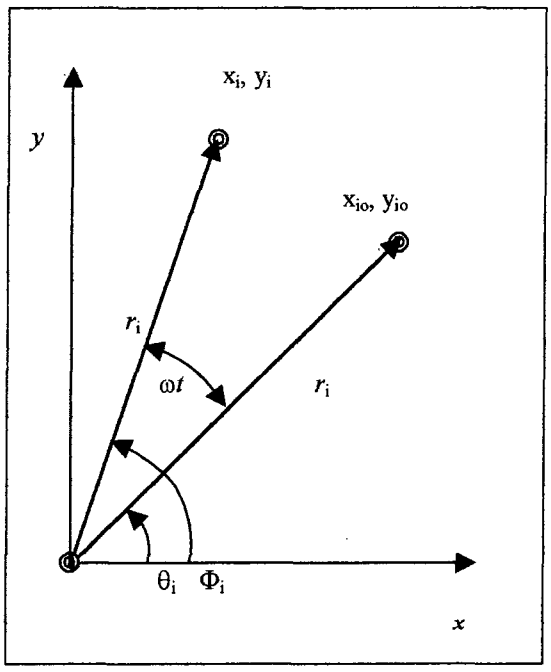

Figure 5.25: Rotation of a node *i* in time interval t.

$$\Phi_i = \theta_i + \omega t \qquad \textbf{5.59}$$

d) The new local co-ordinates of the rock nodes (x_i,y_i) may now be calculated.

$$x_i = r_i Cos\Phi_i \qquad \textbf{5.60}$$

$$y_i = r_i Sin\Phi_i \qquad \textbf{5.61}$$

e) By superposition the global co-ordinates of the i_{th} rock node X_i, Y_i may be calculated from the global co-ordinates of the centroid (X_c, Y_c) plus the local co-ordinates of the i_{th} node (x_i, y_i).

The new position of the centroid is given by Equations 5.56 and 5.57. The new global position of the i_{th} rock node (X_i, Y_i) is;

$$X_i = X_c + S_x + r_i Cos\Phi_i \qquad \textbf{5.62}$$

$$Y_i = Y_c + S_y + r_i Sin\Phi_i \qquad \textbf{5.63}$$

5.3.14 Rolling Motion

Three types of rolling motion exist depending upon the rock shape and the conditions of contact with the slope. If the rock is polygonal then the rock will rotate either about a node or about a point on one of its facets. A circular rock however may roll along its circumference. In all three cases, rolling is assumed to take place without slipping

5.3.14.1 Polygonal rock rolling on a node

For the case of a polygonal rock rotating about one of its nodes in contact with the slope region without slipping then the rock is termed to be rolling on a node.
The principle of conservation of energy can be used to calculate the angular velocity after a time interval t. The new angular velocity can be calculated in eight stages.

a) The rolling radius R is defined as the distance from the rock node in contact with the slope region (X_p, Y_p) to the centroid (X_c, Y_c) of the rock (Figure 5.26).

$$R = \sqrt{(X_c - X_p)^2 + (Y_c - Y_p)^2} \qquad \textbf{5.64}$$

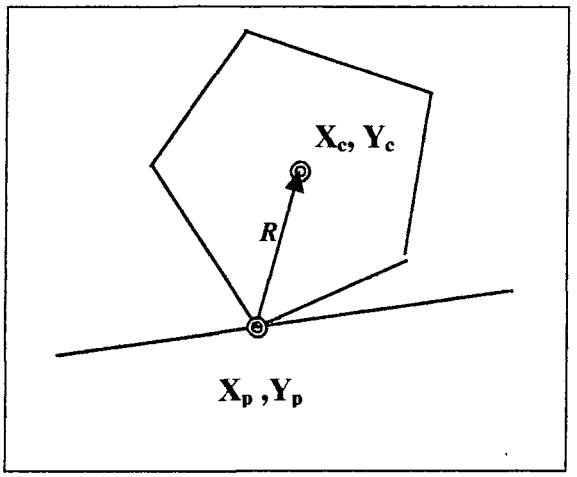

Figure 5.26: Calculation of the rolling radius, R.

b) The moment of inertia J_p is calculated about the point of rotation.

$$J_p = mR^2 + J_c \qquad \textbf{5.65}$$

c) The radial distances R_i from the point of contact (X_p, Y_p) to the i_{th} rock node (X_i, Y_i) must be calculated.

$$R_i = \sqrt{(X_i - X_p)^2 + (Y_i - Y_p)^2} \qquad \textbf{5.66}$$

d) The anticlockwise angles θ_i from the horizontal to the i_{th} rock node must be calculated. Figure 5.27 shows θ_i for a typical node.

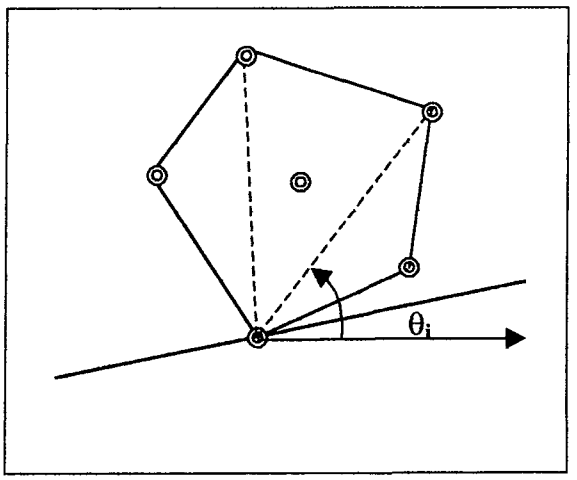

Figure 5.27: Calculation of anticlockwise angles θ_i.

e) **Assuming that the angular velocity ω is constant for a given time increment *t* the amount of rotation is ωt.** This assumption is virtually true if the time step is small. Thus, the angle from the horizontal x axis to the i_{th} rock node after a time interval t is defined as Φ_i (Figure 5.28) and calculated from Equation 5.59.

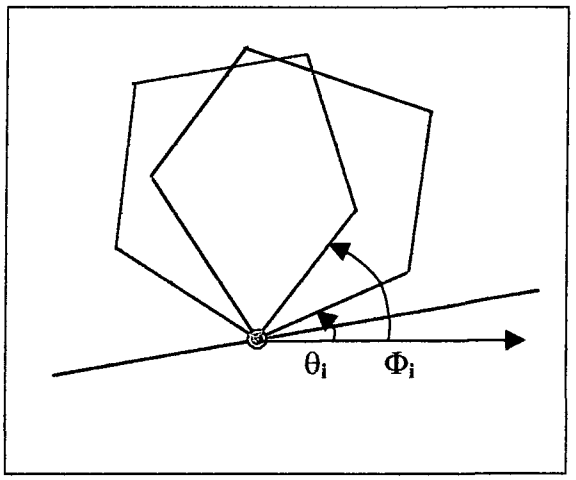

Figure 5.28: Calculation of new anticlockwise angles Φ_i.

f) The new global co-ordinates (X_i, Y_i) for the i_{th} rock node may be calculated thus,

$$X_i = X_p + Cos\Phi_i R_i \qquad \textbf{5.67}$$

$$Y_i = Y_p + Sin\Phi_i R_i \qquad \textbf{5.68}$$

g) The local co-ordinates of the rock nodes in relation to the centroid must also be recalculated (Figure 5.29). If the anticlockwise angles from the x axis to the rock node are calculated, and the radial distances r_i known, then by using Pythagoras the x and y co-ordinates of the rock nodes (x_i, y_i) can be calculated.

$$x_i = Cos\Phi_i r_i \qquad \textbf{5.69}$$

$$y_i = Sin\Phi_i r_i \qquad \textbf{5.70}$$

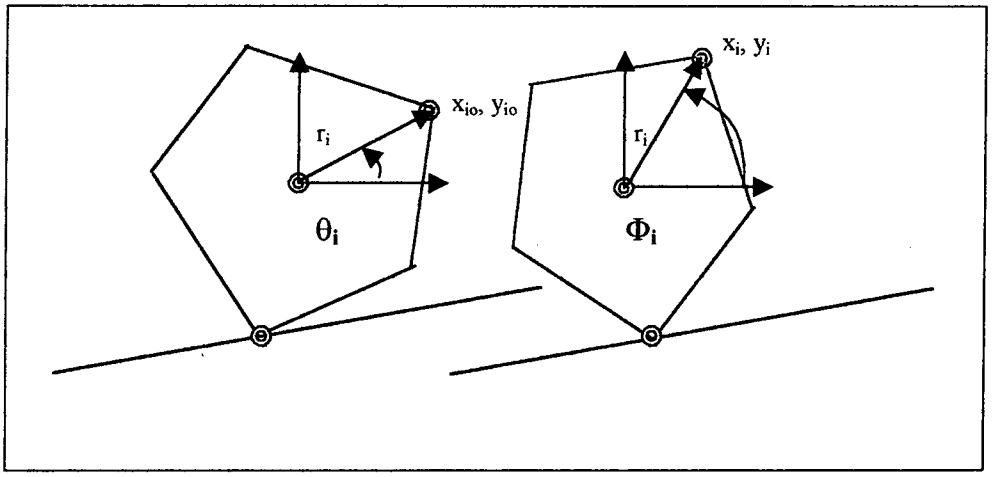

Figure 5.29: Calculation of new local co-ordinates of rock nodes (x_i, y_i).

h) The change in potential energy $\Delta\Pi$ as illustrated in Figure 5.30 is given by Equation 5.71.

$$\Delta\Pi = mgh \qquad \textbf{5.71}$$

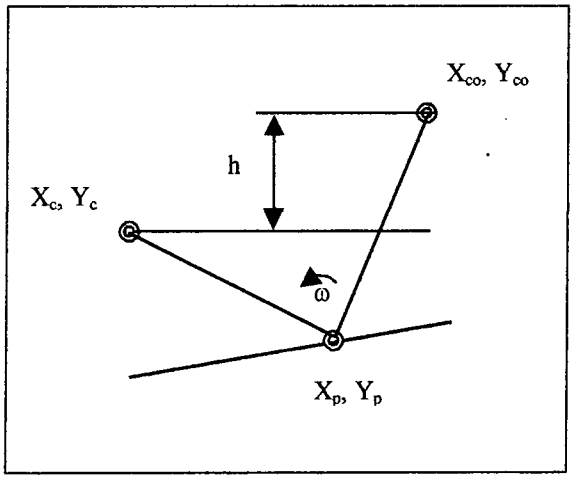

Figure 5.30: Change in potential energy.

By using the principles of the conservation of energy the sum of the kinetic energy and the potential energy must remain constant for any given degree of rotation.

Thus,

$$\frac{1}{2}J_c\omega_o^2 + mgY_{co} = \frac{1}{2}J_c\omega^2 + mgY_c \qquad \textbf{5.72}$$

By rearrangement of Equation 5.72 the angular velocity ω after a small time increment *t* may be calculated.

$$\omega = \sqrt{\omega_o^{\,2} + \frac{2mg(Y_{co} - Y_c)}{J_c}} \qquad \textbf{5.73}$$

The sign of ω is lost in the calculation and so it is assumed that the rock rotates in the same direction that it was doing so previously. However, problems occur when the square root term is negative in value since this cannot be resolved.

This situation only occurs when,

$$\frac{1}{2} J_c \omega_o^{\,2} < mgh \qquad \textbf{5.74}$$

Thus the presumption that the rock is rotating in the same direction that it was previously doing is wrong and the sign of ω must be the opposite to that of ω_o.

If ω = 0 then the rock cannot rotate and so requires a small 'push'.

5.3.14.2 Polygonal rock rolling on a facet

If the rock is rotating without slipping about a point on one of its sides whilst in contact with a node on the slope then the rock is termed to be rolling on a facet.
By using the principle of conservation of energy the new angular velocity after a time interval can be calculated in eight stages, similar to the previous analysis for rotating about a rock node.

a) The rolling radius R is defined as the distance from the point of contact with the slope region (X_s, Y_s) to the centroid (X_c, Y_c) of the rock (Figure 5.31).

$$R = \sqrt{(X_s - X_c)^2 + (Y_s - Y_c)^2} \qquad \textbf{5.75}$$

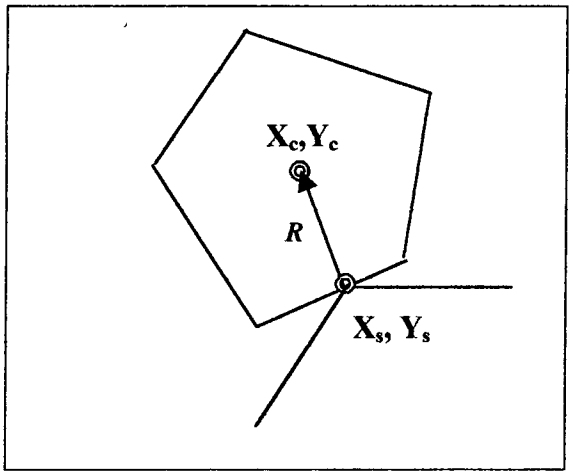

Figure 5.31: Rolling radius R.

b) The moment of inertia J_c is calculated using Equation 5.65, the only difference being that the point of rotation is no longer a node but a point on one of the faces of the rock.

c) The radial distances R_i from the point of contact (X_s, Y_s) to the i_{th} rock node X_i, Y_i must be calculated.

$$R_i = \sqrt{(X_i - X_s)^2 + (Y_i - Y_s)^2} \qquad \textbf{5.76}$$

d)-e) As for rolling on a node.

f) The new global co-ordinates (X_i, Y_i) of the rock nodes may be calculated.

$$X_i = X_s + Cos\Phi_i R_i \qquad \textbf{5.77}$$

$$Y_i = Y_s + Sin\Phi_i R_i \qquad \textbf{5.78}$$

g)-h) The new local co-ordinates and the new angular velocity are calculated using Equations 5.69 to 5.74.

5.3.14.3 Rolling motion of a sphere or disc

The previous method used to calculate rolling on a node or a facet is not ideally suited to that of a sphere or disc. Most irregular shapes rotate on a corner and then skip or bounce down a slope. A circle or disc rotates along the whole of its circumference and so a rolling model based upon rolling resistance μ_r (Grosjean, 1991) is more realistic and can be implemented relatively easily.

A rock may only roll if the anticlockwise angle to the slope region θ is either in the range $0^\circ \leq \theta \leq 90^\circ$ or $270^\circ \leq \theta \leq 360^\circ$. Figure 5.32 illustrates a slope region with a circular shaped rock resting upon it. For rolling to occur the normal velocity V_n to the slope must equal zero. Its initial velocity tangential to the slope is V_{to} and its final velocity is V_t. The acceleration down the slope is A_t. For the rock shown in the figure the initial velocity and final velocity will both be negative i.e: down slope.

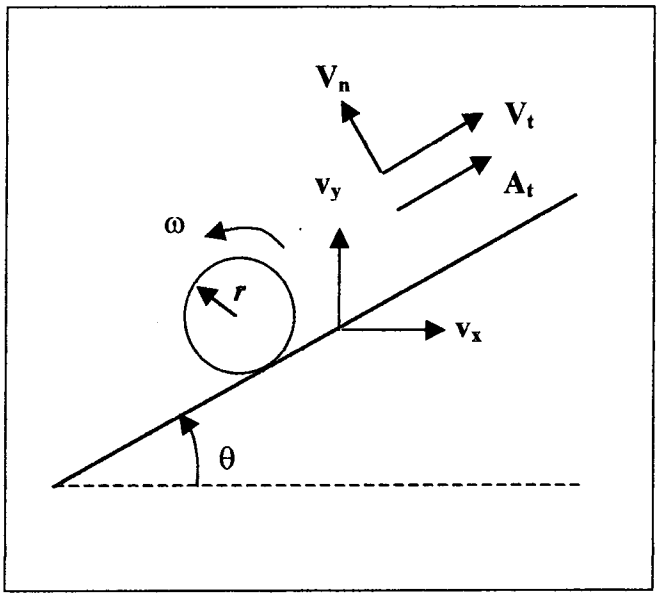

Figure 5.32: Rolling motion sign convention.

The initial velocity V_{to}, the final velocity V_t and the distance travelled S_t after a time interval t are calculated as follows,

$$V_{to} = -\omega r \qquad \textbf{5.79}$$

where r is the radius of the rock.

$$V_t = V_{to} + A_t t \qquad \textbf{5.80}$$

$$S_t = V_{to}t + \frac{1}{2}A_t t^2 \qquad \textbf{5.81}$$

If $V_{to} = 0$ and $A_t = 0$ then the rock cannot roll.

Once the tangential velocity V_t has been calculated it may be resolved into its vertical V_y and horizontal components V_x by the following formula,

$$V_y = V_t Sin\theta \qquad \textbf{5.82}$$

$$V_x = V_t Cos\theta \qquad \textbf{5.83}$$

5.3.14.3.1 Rolling on slopes where θ is between 0° and 90°

For the rock illustrated in Figure 5.32 the acceleration down slope A_t acting under the influence of gravity g will be,

$$A_t = fg(\mu_r Cos\theta - Sin\theta) \qquad \textbf{5.84}$$

where the shape factor, f is 2/3 for a disc and 5/7 for a sphere (Grosjean, 1991).

Two special cases exist where the above formula may not be applied or require modification.

If V_{to} is negative (rolling down slope) and A_t is positive (deceleration/retardation) then Equation 5.80 is still applicable, but if V_t becomes greater than zero, the rock must come to rest, otherwise the rock will accelerate back up the slope.

If V_{to} is positive (rolling up slope) and A_t is positive (deceleration/retardation) then Equations 5.80 and 5.81 are no longer applicable since the rock will accelerate up the slope.

In this case;

$$V_t = V_{to} - A_t t \qquad \textbf{5.85}$$

$$S_t = V_{to} - \frac{1}{2}A_t t^2 \qquad \textbf{5.86}$$

If V_{to} becomes negative then the rock has come to rest.

5.3.14.3.2 Rolling on slopes where θ is between 270° and 360°

The acceleration down slope A_t acting under the influence of gravity g will be;

$$A_t = -fg(\mu_r Cos\theta + Sin\theta) \qquad \textbf{5.87}$$

Two special cases exist where Equations 5.80 and 5.81 may not be applied or require modification.

If V_{to} is positive (rolling down slope) and A_t is negative (deceleration/retardation) then Equation 5.80 is still applicable, but if V_{to} becomes less than zero the rock must come to rest, otherwise the rock will accelerate back up the slope.

If V_{to} is negative (rolling up slope) and A_t is negative (deceleration/retardation) Equations 5.80 and 5.81 are no longer applicable since the rock will accelerate up the slope and Equations 5.85 and 5.86 must be used. If V_t becomes positive then the rock has come to rest.

5.3.14.3.3 Cessation of rolling

A check is needed to determine whether the circular or disc shaped rock has rolled off a cliff or other surface protuberance. Figure 5.33 illustrates a rock that is about to roll over an edge, it is at this point that the rock may no longer be in contact with the slope and may either go into free fall or if its velocity V_t is low it may rotate about the corner. The transition of motion in this instance occurs when the point of contact X_p equals or exceeds $X_{s(2)}$.

$$X_p = X_c + (Sin\Lambda.R) \qquad \textbf{5.88}$$

If the rock is rolling from left to right on region number n then the rock will stop rolling on that slope region when,

$$X_p \geq X_{s(n+1)} \qquad \textbf{5.89}$$

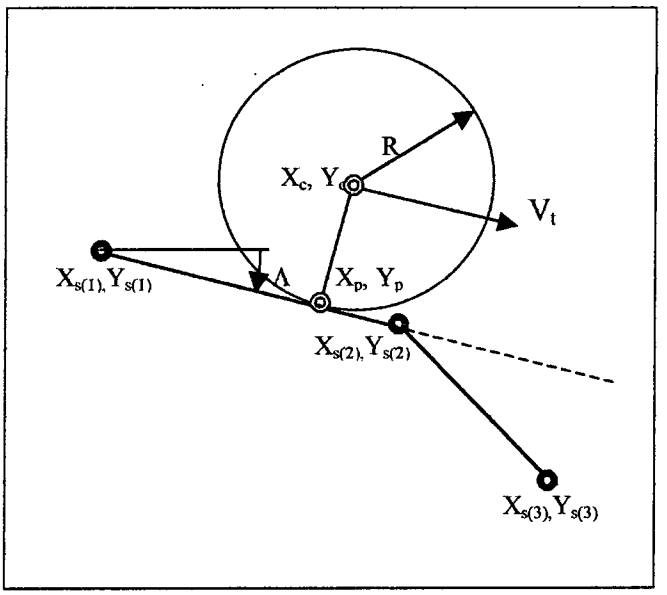

Figure 5.33: Rolling off a slope region.

If the rock is rolling from right to left on region number n then the rock will stop rolling on that slope region when,

$$X_p \leq X_{s(n)} \qquad \textbf{5.90}$$

5.3.15 Sliding

Sliding is only possible if the rock has faceted sides and because of this fact spherical and disc shapes rocks cannot slide. For sliding to transpire the rock must also have zero angular velocity ω, else a combination of a roll/slide will occur. For a rock sliding on a flat edge a coulomb friction model may be used and a coefficient of dynamic friction μ_d introduced.

A rock may only slide if the anticlockwise angle to the slope region θ is either in the range $0^\circ \leq \theta \leq 90^\circ$ or $270^\circ \leq \theta \leq 360^\circ$.

Figure 5.34 illustrates a slope region with a rectangular shaped rock resting upon it. For sliding to occur the normal velocity V_n and angular velocity ω must equal zero. Its initial velocity tangential to the slope is V_{to} and its final velocity is V_t. For a rock initially at rest V_{to} is zero. The acceleration down the slope is A_t. For the rock shown in Figure 5.34 the initial velocity and final velocity will both be negative i.e: down slope.

The velocity V_t after a time interval t may be calculated from Equation 5.80.

If $V_{to} = 0$ and $A_t = 0$ then the rock cannot slide.

Once the tangential velocity V_t has been calculated it may be resolved into its vertical V_y and horizontal components V_x from Equations 5.82 and 5.83.

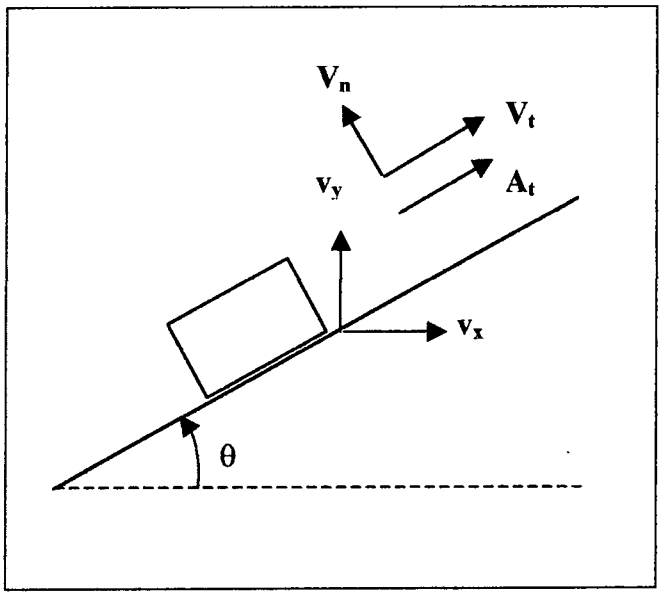

Figure 5.34: Sliding motion sign convention.

5.3.15.1 Sliding on slopes where θ is between 0° and 90°

For the rock illustrated in Figure 5.34 the acceleration down slope A_t acting under the influence of gravity g will be;

$$A_t = g(\mu_d Cos\theta - Sin\theta) \qquad \textbf{5.91}$$

If Tan θ < μ_d then the rock cannot slide.

5.3.15.2 Sliding on slopes where θ is between 270° and 360°

The acceleration down slope A_t acting under the influence of gravity g will be;

$$A_t = -g(\mu_d Cos\theta + Sin\theta) \qquad \textbf{5.92}$$

If -Tan θ > μ_d then the rock cannot slide.

5.4 Algorithm verification

It is essential that the algorithms work correctly since the output of GeoFall may be used as a decision making tool for Geotechnical Engineers.

Several slopes were set up in GeoFall to model projectile, rolling and sliding motion. By using the debugging tools included in Visual Basic the position and velocity could be measured for each advancement of the time step. The velocities after 20 time steps (0.2s) were then compared to those calculated by hand and the results have been presented in Appendix 3.

The motion of the rock has been tested for all possible directions of travel. For projectile and rolling motion the rock may move from, left to right upwards or downwards, or, right to left upwards or downwards. The rock may only slide downwards from left to right, or right to left.

Chapter 6

Computer Simulation of Rock Fall

Using GeoFall

6 Computer simulation of rock fall using GeoFall

GeoFall has been used to model a number of rock fall events described in several published papers. These include the modelling of actual events using published data and comparing the outcome of GeoFall with that of other rock fall simulation programs. The rock fall simulations are presented in order of significance based upon the quality of the available data, which is summarised in Table 6.1.

6.1 Rock falls in British Columbia, Canada

Hungr and Evans (1993) studied four significant rock falls that occurred in British Columbia, Canada. These are listed in Table 6.1. Three caused significant structural damage to houses whilst the fourth caused damage to a car. There were several fatalities as a result of these rock falls.

6.1.1 Sunnybrae

Sunnybrae is a small community in the British Columbia interior on the shore of the Shuswap Lake. The community lies 350m above sea level directly beneath the precipitous faces of Bastion Mountain, which extends to 1300m above sea level. The cliffs are made up of metamorphosed limestone of the Sicamous formation. The steep, sparsely forested slopes extending from the foot of the cliffs down towards the lakefront are underlain by schistose bedrock units, thinly mantled by fine grained talus derived from the same rock. The bedrock is exposed in numerous small cliffs and outcrops on the slope.

At 1:50 on November 23rd, 1983, a disc shaped boulder 6m in diameter and 2m thick became detached from near the base of the limestone cliffs, rolling and bouncing 790m before coming to rest. It partly destroyed a house at the north end of Sunnybrae and killed two inhabitants.

Reference	Site Location		Rock shape	Rock size	Outcropping Material	Coefficients of restitution			
						e_n	e_t	m_r	Remediation
Hungr and Evans (1993)	Sunnybrae	British Columbia, Canada	Disc	6m Φ 2m thick	Bedrock with talus covering	0.5	0.8	0.577	None
	Hedley		Sphere	3m Φ					
	Squamish Highway		Rectangular	0.7 by 1 by 2m thick		0.7	0.9		
	Barnhartvale		Sphere	1m Φ					Catchment ditch
Pfeiffer and Bowen (1989)	Glenwood Canyon	USA	Disc	2m Φ 0.6 m thick	Granitic bedrock with sparse vegetation and a thin soil cover	0.35	0.85	No Data	Rock fall net
					Talus with scattered areas of low shrubs	0.32	0.81	No Data	None
Robotham et al. (1995)	Limestone Quarry	UK	Sphere	0.3m Φ	Limestone bedrock	0.315	0.712	No Data	None
					Partially vegetated limestone scree	0.303	0.613	No Data	None
	Chalk Quarry			0.6m Φ	Chalk face	0.276	0.835	No Data	None
					Vegetated chalk scree	0.271	0.596	No Data	None
Zhou et al. (1996)	Dahekou	Sichuan, China	Various	Various	Limestone bedrock	No Data	No Data	No Data	2 rock fall nets
Mercer (1882)	Craig y Dref, central section	Gwynedd, Wales, UK	Sphere	2m Φ	No Data	No Data	No Data	No Data	Rock fall net
	Craig y Dref, western section				No Data	No Data	No Data	No Data	Gabion Wall
Sofianos et al. (1988)	Argos	Pelopponese, Greece	Rectangular	4 by 1.5 by 1.2m thick	No Data	No Data	No Data	No Data	None

Table 6.1: Summary of available data.

6.1.1.1 Rock fall simulation

Hungr and Evans modelled the Sunnybrae rock fall by using a program which treats the rocks as a point mass. The coefficients listed in Table 6.1 have been used in the following rock fall simulation carried out by Hungr and Evans and the output trajectories are presented in Figure 6.1.

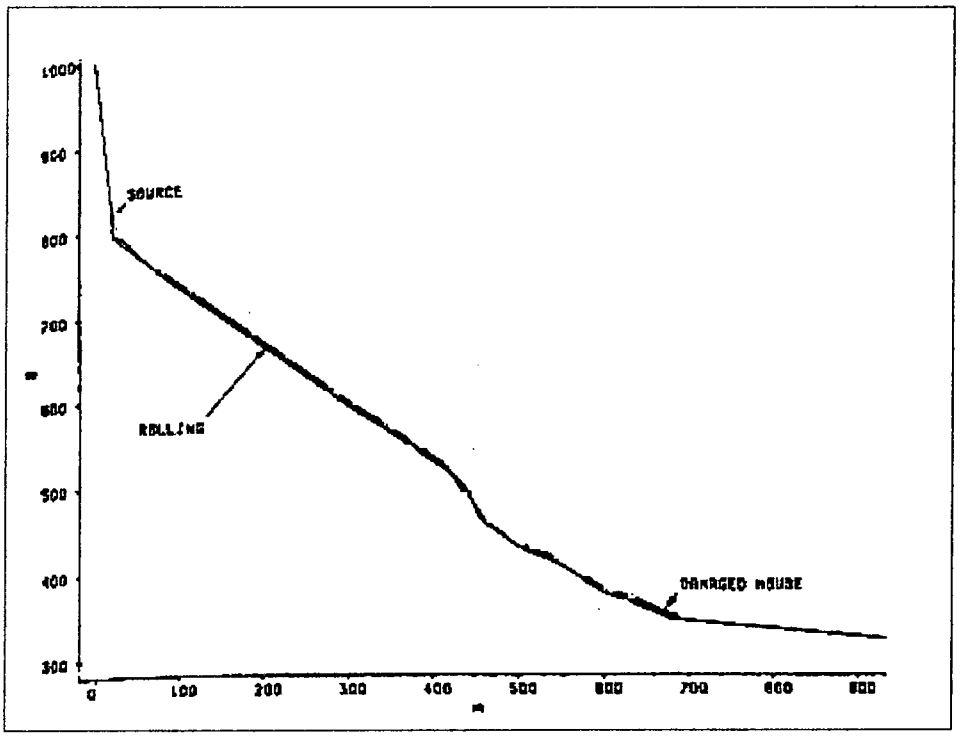

Figure 6.1. Sunnybrae rock fall simulation (after Hungr and Evans).

The rock fall at Sunnybrae was also modelled using GeoFall. A disc shaped rock 6m in diameter and 2m thick was used in the simulation since this closely matches the shape of the boulder involved. Figure 6.2 shows the trajectory paths of fifty rocks, all of which have passed through the area where the damaged house was situated. The mode of travel at the location of the damaged house is predominantly bouncing or rolling with the rocks possessing high kinetic energies.

The slight differences between the two sets of trajectories are largely due to Hungr and Evans' program modelling the rock as a point mass rather than as a discrete 2m thick, 6m diameter disc.

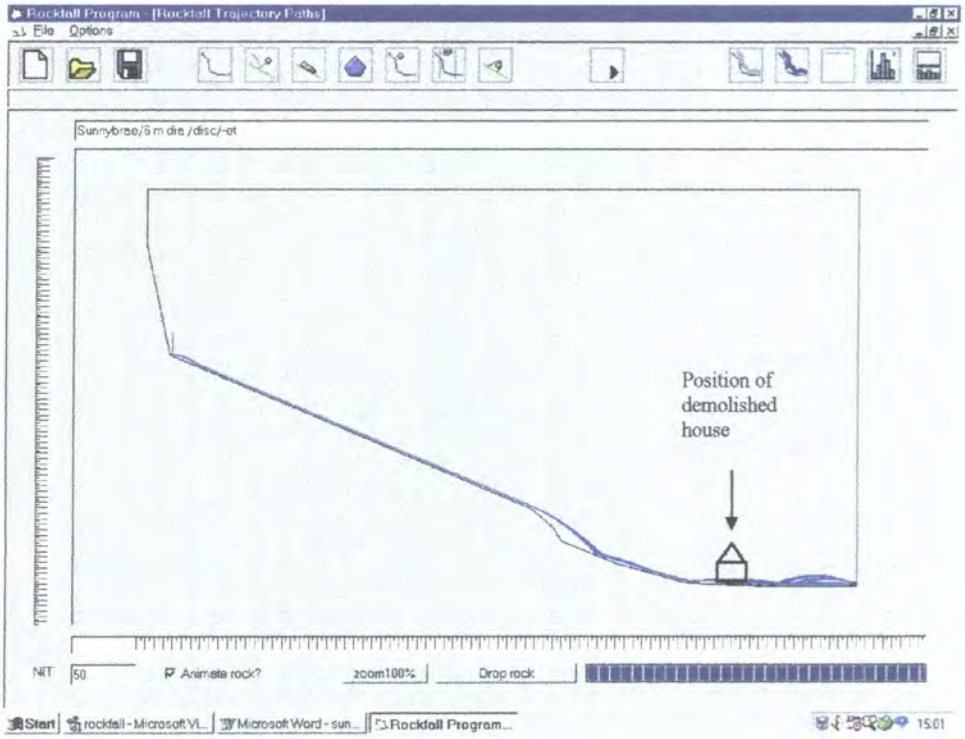

Figure 6.2. GeoFall simulation of the Sunnybrae rock fall.

6.1.2 Hedley

Hedley is a small mining community located in the Similkameen valley in the interior of British Columbia. Part of the community was situated directly beneath the rock faces and talus slopes of Stemwinder Mountain.

A 3m diameter spherical rock fell from the slope of Stemwinder Mountain and struck the town at 1:00 on January 17th, 1939 killing two people and damaging several houses.

6.1.2.1 Rock fall simulation

Figure 6.3 shows the Hedley rock fall simulated by using their program with the same parameters as those listed in Table 6.1. The rock fall at Hedley was also modelled in GeoFall using the parameters listed in Table 6.1. Figure 6.4 shows the trajectories of fifty simulated runs. All of the rock trajectories have passed through the area of the damaged house situated on the outskirts of the town of Hedley. The rocks have gained high kinetic energies whilst rolling down the steep mountainside.

The output trajectories of GeoFall and Hungr and Evans' program both predict the impact of the boulder with the outlying town houses.

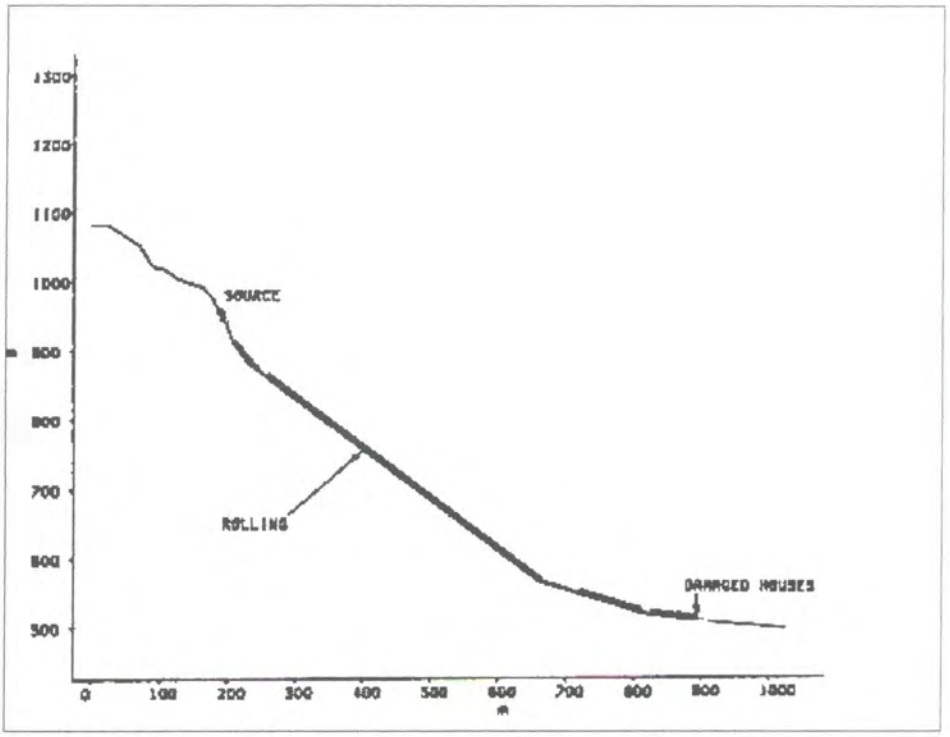

Figure 6.3 Hedley rock fall as simulated by Hungr and Evans.

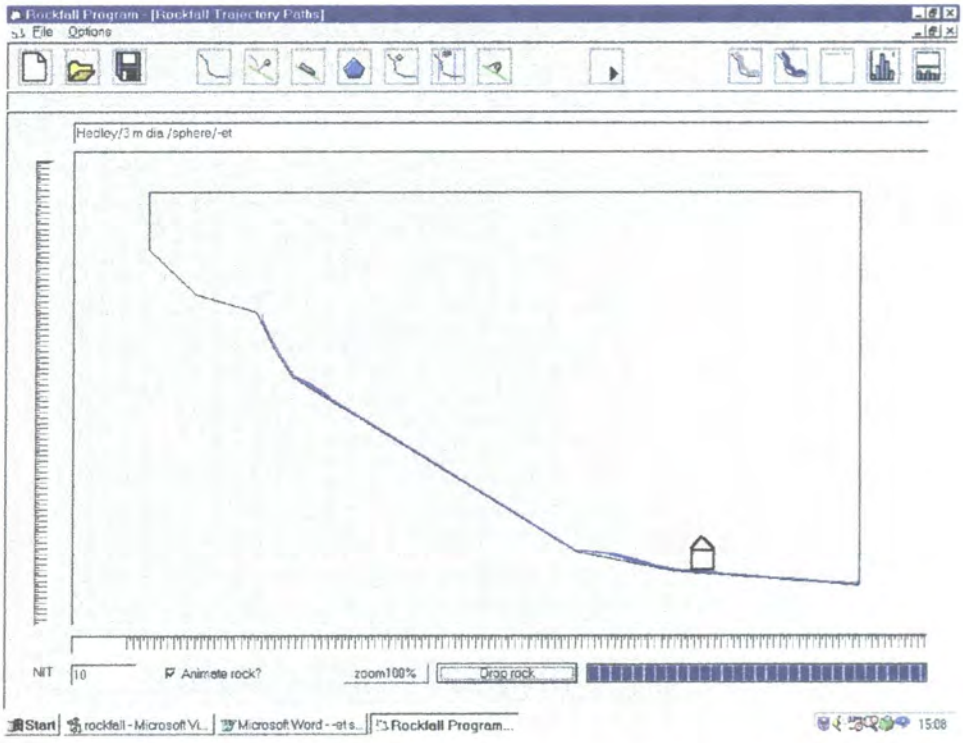

Figure 6.4 A GeoFall simulation of the Hedley rock fall.

6.1.3 Squamish highway

A rectangular boulder of metamorphosed tuff measuring approximately 0.7 by 1 by 2m thick, detached by toppling from a narrow shelf above the Squamish highway. Several short bounces occurred on bare rock. The boulder then traversed a steep snow covered shelf and fell over the edge of the steep rock cut, to land directly on the roof of a car. The passenger was killed instantly and the driver injured.

6.1.3.1 Rock fall simulation

The coefficients listed in Table 6.1 are those for the Squamish highway slope used in Hungr and Evans' program, the output of which is presented in Figure 6.5. They modelled the rock as a point mass rather than as a discrete rectangular block.

The rock fall event at Squamish highway was also modelled in GeoFall using a rectangular shaped rock measuring 0.7 by 1 by 2m thick. Their choice of a coefficient of normal restitution of 0.7 seems very high for bare bedrock, which is generally no higher than 0.5, the value chosen in the GeoFall simulation.

Figure 6.6 shows the trajectory paths of fifty rocks. There is a much larger spread in trajectories than with the previous simulation because of the rectangular shape of the rock. A slight change in angular velocity causes a change of geometry upon impact and thus affects the rebound trajectory, the greater the spread in angular velocities the greater the spread in the rock fall trajectories. GeoFall has predicted that an area of up to forty metres from the base of the cliff is at high risk of rock fall and that the car may have been struck by this rock if it was anywhere in this region.

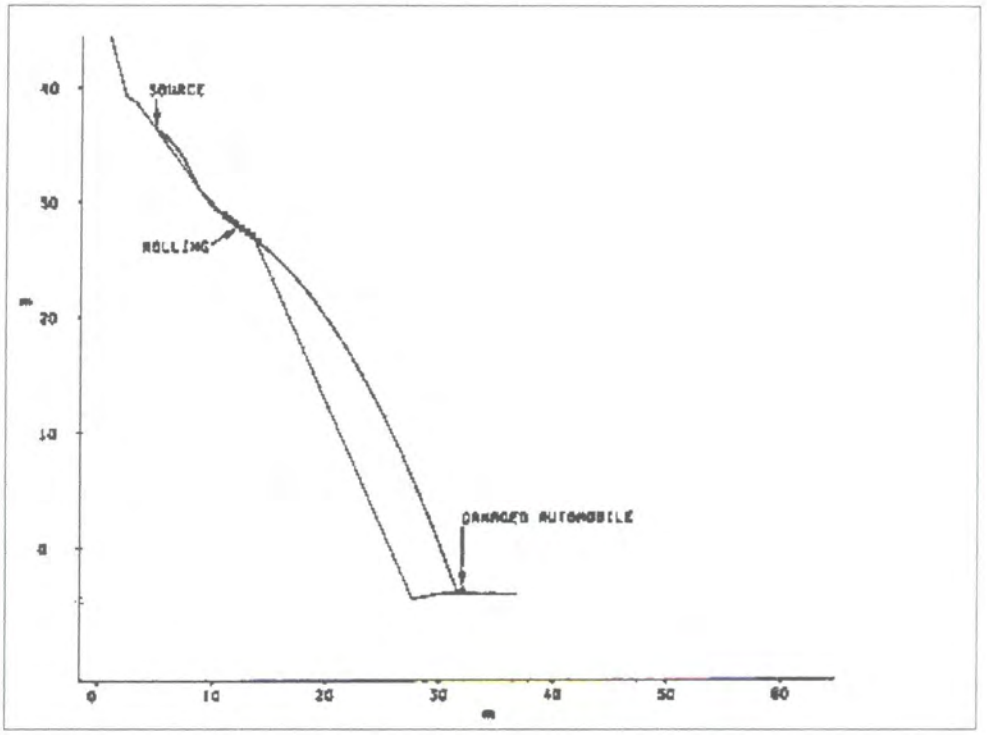

Figure 6.5: The output trajectories of Hungr and Evans' program.

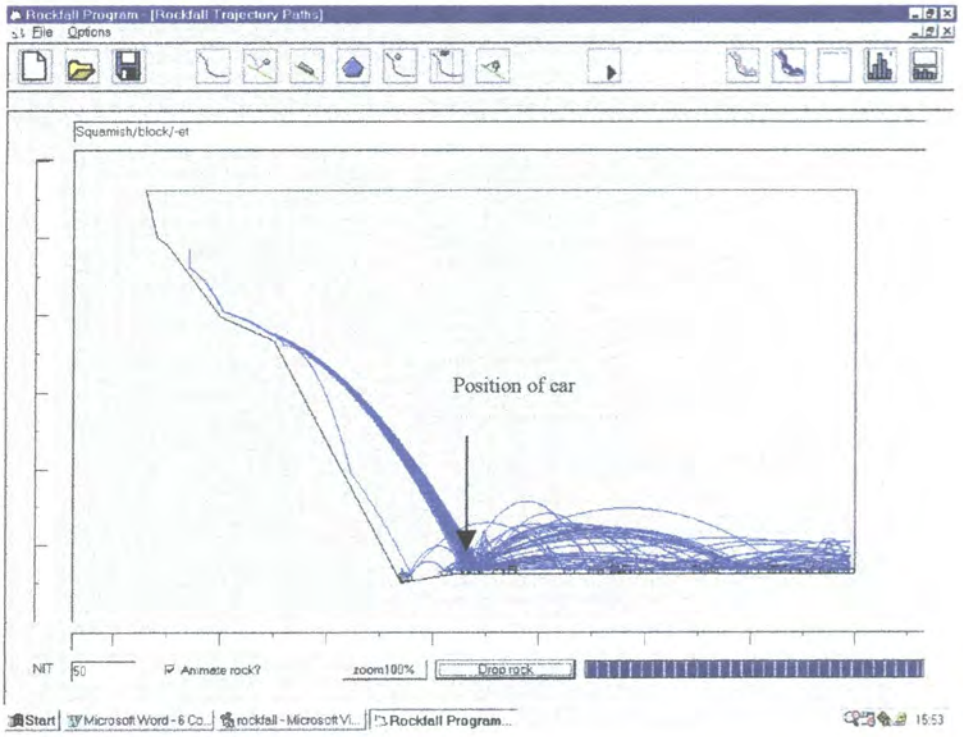

Figure 6.6: The output trajectories from GeoFall.

6.1.4 Barnhartvale

Barnhartvale is located within the city of Kamloops in the interior of British Columbia. The western part of the community is located at the foot of some prominent east facing rock slopes and associated talus. The rock is intensely jointed metavolcanics of the Cache Creek group, with prominent joint sets dipping into and out of the slope. These discontinuities form numerous detachment surfaces for fragmental rock fall.

In the spring of 1974, a boulder about a metre in diameter, fell from about 775m above sea level on to the rock slope, bounced and rolled over the talus slope and beyond its toe. The rock severely damaged a house but caused no injuries.

The incident led to scaling the rock face, removal of dangerous rocks and the excavation of a protective ditch at the base of the talus. A rock fall net was also installed but no specific details were given.

6.1.4.1 Rock fall simulation

The following rock fall simulation uses the same parameters as listed in Table 6.1. Figure 6.7 shows the trajectories of fifty simulated runs using a 1m diameter spherical rock. All of the rock trajectories have passed through the area of the damaged house situated on the outskirts of the town of Barnhartvale. The rocks have gained high kinetic energies whilst rolling down the steep mountainside.

Figure 6.8 shows the effect of the rock fall protection ditch, which has successfully stopped all of the rocks.

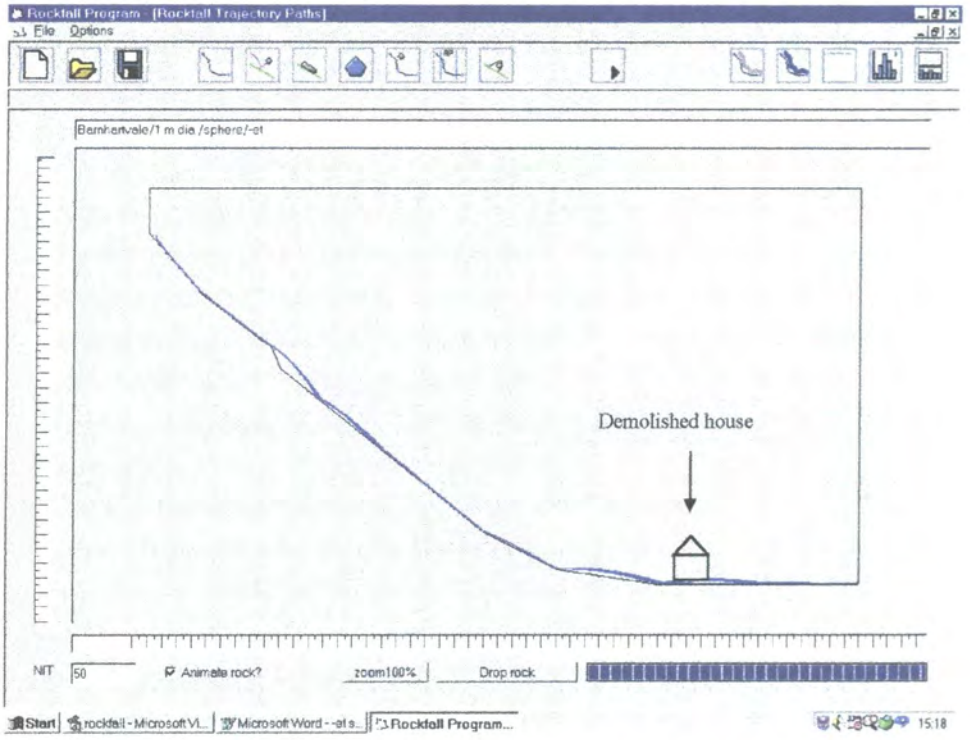

Figure 6.7: GeoFall simulation of the Barnhartvale rock fall.

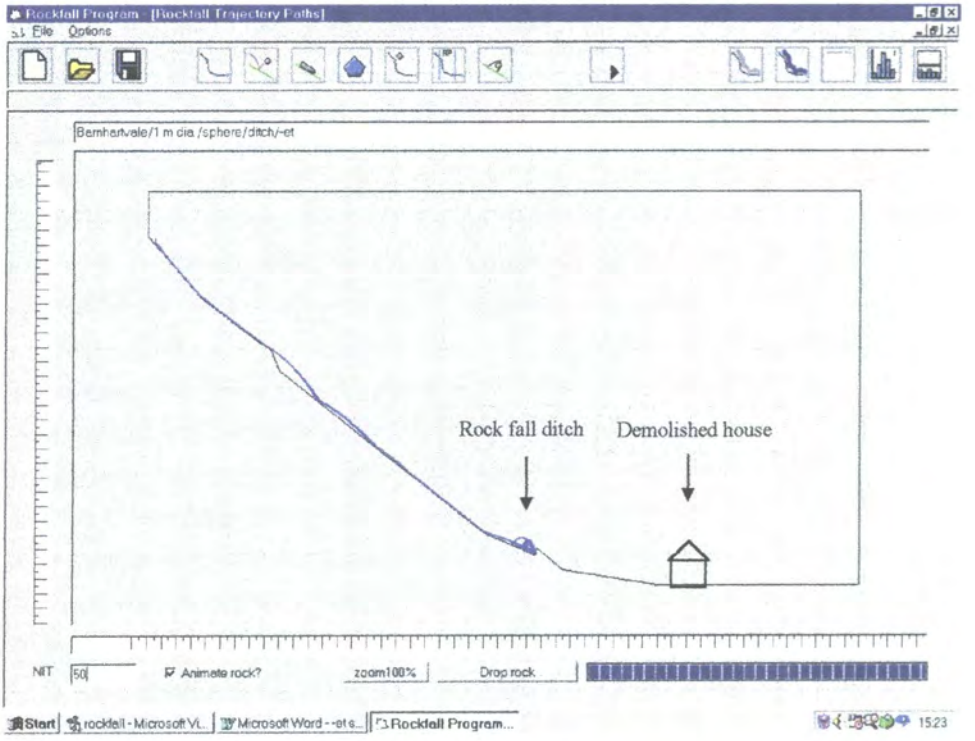

Figure 6.8: The effect of the rock fall protection ditch upon rock trajectories.

6.2 Rock fall analysis at Glenwood Canyon

In March 1985 two rock fall events damaged portions of two retaining walls under construction on Interstate 70 (I-70) in Glenwood Canyon.

The first rock fall event consisted of one 1.219 by 1.219 by 2.438m thick (4 by 4 by 8ft) block of quartzite and the second, two weeks later, of an estimated twenty to thirty irregular blocks of quartzite ranging from 0.08-0.42 m^3 (3-15 ft^3).

The severity of the rock fall damage prompted a study of the area to determine the likelihood and impact of future rock fall (Pfeiffer and Bowen, 1989). The rock fall path was traced to the base of the quartzite cliff 230m above I-70 and the source area evaluated for potential rock fall size and frequency. The slope was then analysed by Pfeiffer and Bowen using the Colorado Rock fall Simulation Program (CRSP).

6.2.1 Rock fall simulation using CRSP

Figure 6.9 shows 100 simulated rock fall runs by CRSP. The rock shape used was a 1m (3ft) radius disk, 0.6m (2ft) thick, which represents a typical rock found in the source area. All of the rocks have struck the west and east lanes of the interstate after rolling off the retaining wall.

6.2.2 Rock fall simulation using GeoFall

By using a similar rock shape and size to those of the two previous rock fall events and typical parameters for the slope material it was hoped that GeoFall would predict the impact of the rock against the retaining wall.

A disc shaped rock was used in the simulation since this most closely matches the shape of the quartzite block; the largest rock that was involved in the two previous rock fall events. Figure 6.10 shows the rock fall paths of fifty simulated runs.

In using the same input data as CRSP it was hoped that similar results would be achieved, however GeoFall cannot use the parameters used by CRSP since the formulation of the rock fall model in CRSP is not the same. CRSP does not model rolling in the same way as GeoFall and so no data is given for the rolling resistance.

Typical values have thus been used for the coefficients used in GeoFall and are shown in Table 6.2.

Outcropping Material	Normal coefficient of restitution (e_n)	Tangential coefficient of restitution (e_n)	Rolling resistance μ_r
Granitic bedrock with sparse vegetation and a thin soil cover	0.3	0.55	0.7
Talus with scattered areas of low shrubs	0.27	0.6	0.8

Table 6.2: Typical values used in the GeoFall rock fall simulation.

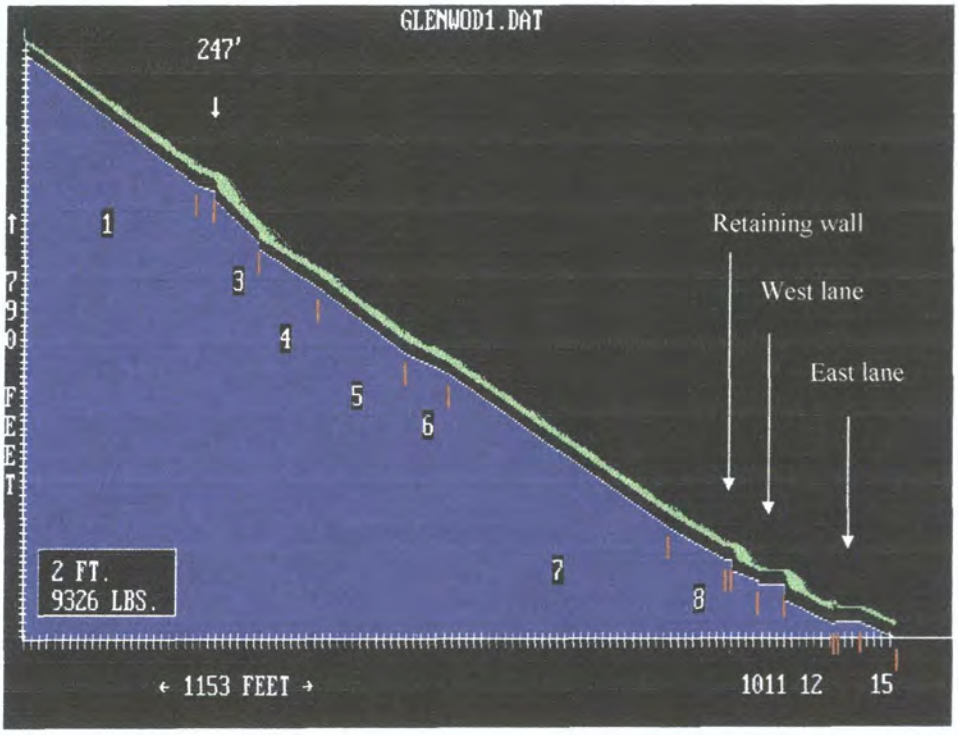

Figure 6.9: The output trajectories of CRSP for a disc shaped rock.

(Note: 1 foot (ft)=0.3128 m; 1 Lb = 0.454 Kg)

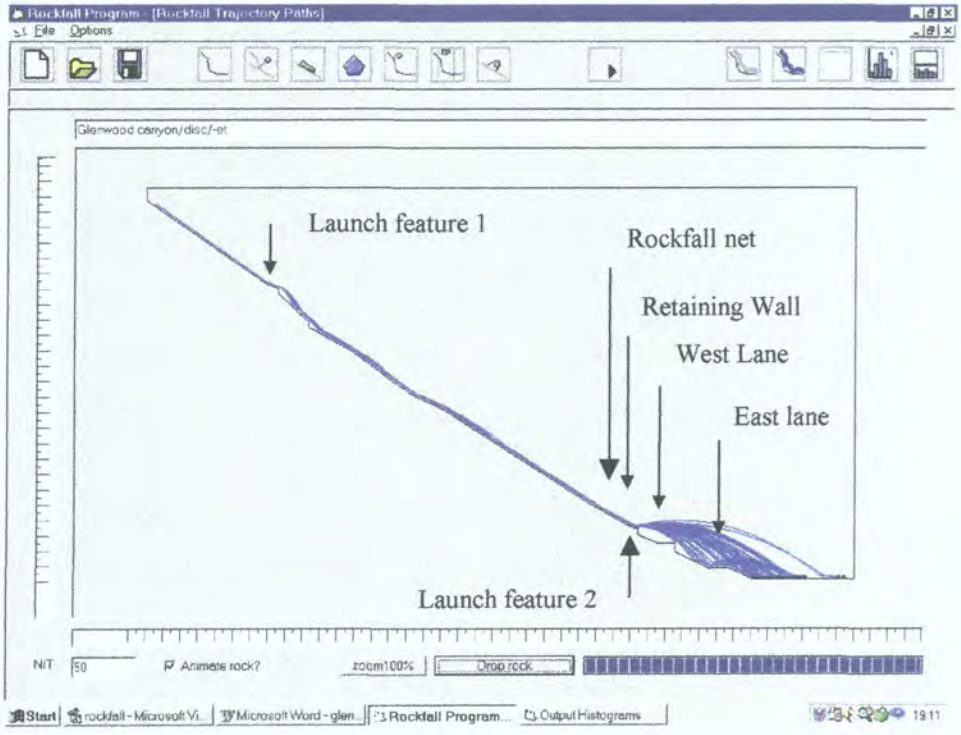

Figure 6.10: Rock fall trajectories of a disc shaped rock using GeoFall.

6.2.3 Comparison between GeoFall and CRSP

GeoFall predicts that the rock rolls or bounces down the slope until it impacts with the horizontal top of the retaining wall above the west bound lane of I-70. This second launch feature turns the roll or bounce into projectile motion. Several rocks have struck the eastbound lane at the base of the canyon.

CRSP predicts that the rock gains speed as it bounces down the granite slope from whence it loses speed as it rolls down the talus slope before it impacts on to the retaining wall. This behaviour would only be possible if the coefficients of normal and tangential restitution were unrealistically low and/or the coefficient of rolling friction was very high. It is unlikely that such a large rock rolling down a 35° talus slope would decelerate unless the rolling friction coefficient was unrealistically high. It is also possible that launch feature 2 is being ignored by CRSP and that the rock is passing through this feature rather than impacting against it.

If a rock net were to be placed before the first launch feature then the majority of the rocks would be stopped before they gained significant kinetic energies.

6.2.4 Mitigation measures chosen by the Colorado Department of Transport (CDOT).

The Colorado Department of Transport designed and constructed a rock fall net on the lower portion of the colluvial slope above the westbound lanes of I-70. The net chosen was 2.5m (8 ft) high and 44m (140 ft) long. These dimensions were chosen to accommodate the anticipated dispersal of rock fall on the convex talus slope and rock motion restricted to rolling or bounce heights of less than a meter above the slope surface. By inserting an analysis point at the location of the net the average kinetic energy of the rock was between 300 and 3400 kJ (Figure 6.11). It is likely that the capacity of the net chosen by CDOT would be insufficient to stop all of the rocks, and that two nets would be necessary.

Two nets with design values of 1500 and 750 kJ were chosen since these should theoretically stop 98% of the rocks that hit the net. Figure 6.12 shows the rock fall paths of fifty simulated runs with two, 2.5m high nets at the base of the talus slope. The rock fall nets have stopped 98% of the rocks that have either rolled or bounced into them.

If the rocks were stopped before rolling over launch feature 1 then the risk to highway users would be reduced and fewer nets would be required. An analysis point placed at the location of lauch feature 1 indicates that kinetic energies are below 300 kJ (Figure 6.13). A 1.5m high net of 500kJ capacity should be adequate to stop all of the rocks that strike it. Figure 6.14 shows fifty simulated rock fall runs with the net in place.

It is of obvious benefit to place a net in this location. The capacity and height can only realistically be determinied by assessment of the rock size and shape that is likely to hit it. This can only be assessed by inspection of the rockfall source. The net at the base of the talus is of limited use and a net closer to the rockfall source would be of greater benefit.

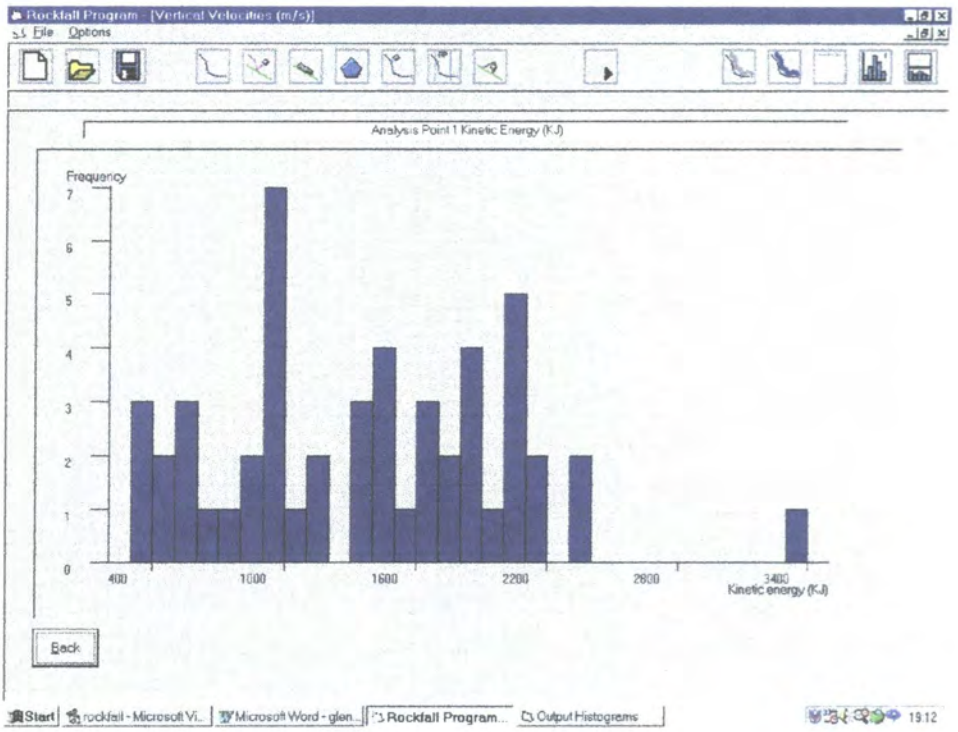

Figure 6.11: The kinetic energy of the rock at the analysis point.

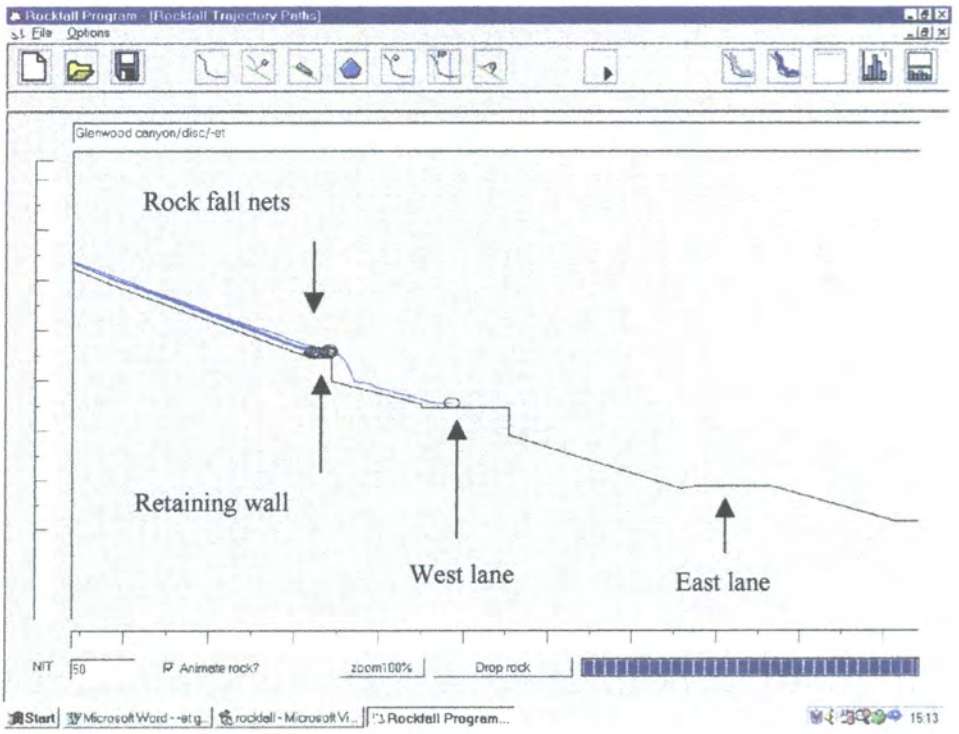

Figure 6.12: The effect two rock fall nets, 1500 and 750 kJ capacity.

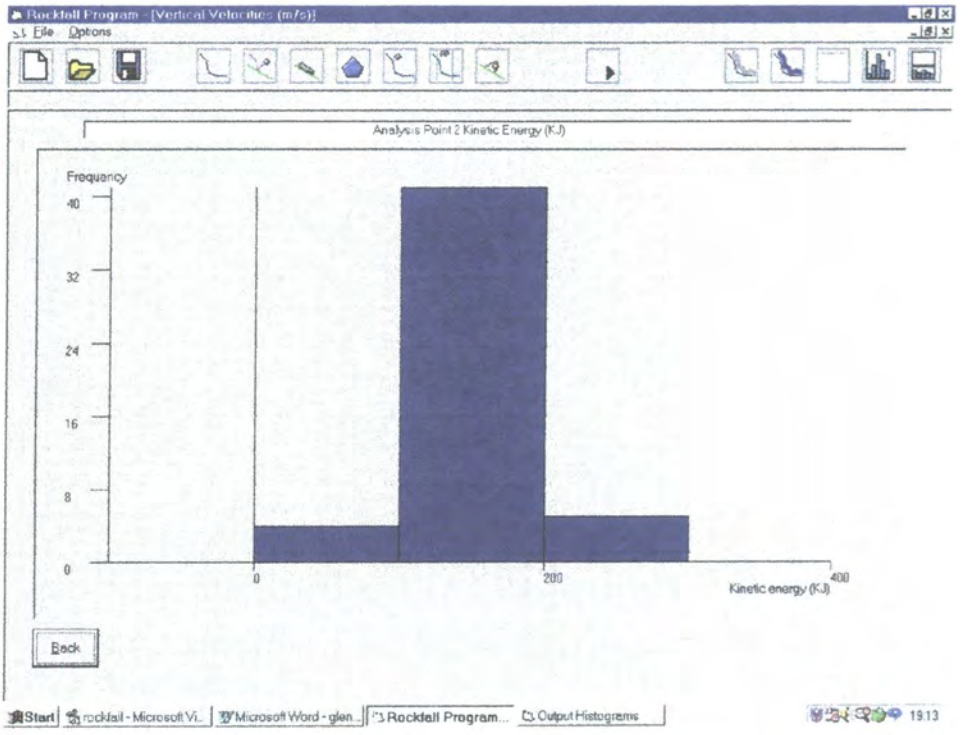

Figure 6.13: The Kinetic energy of the rock immediately before launch feature 1.

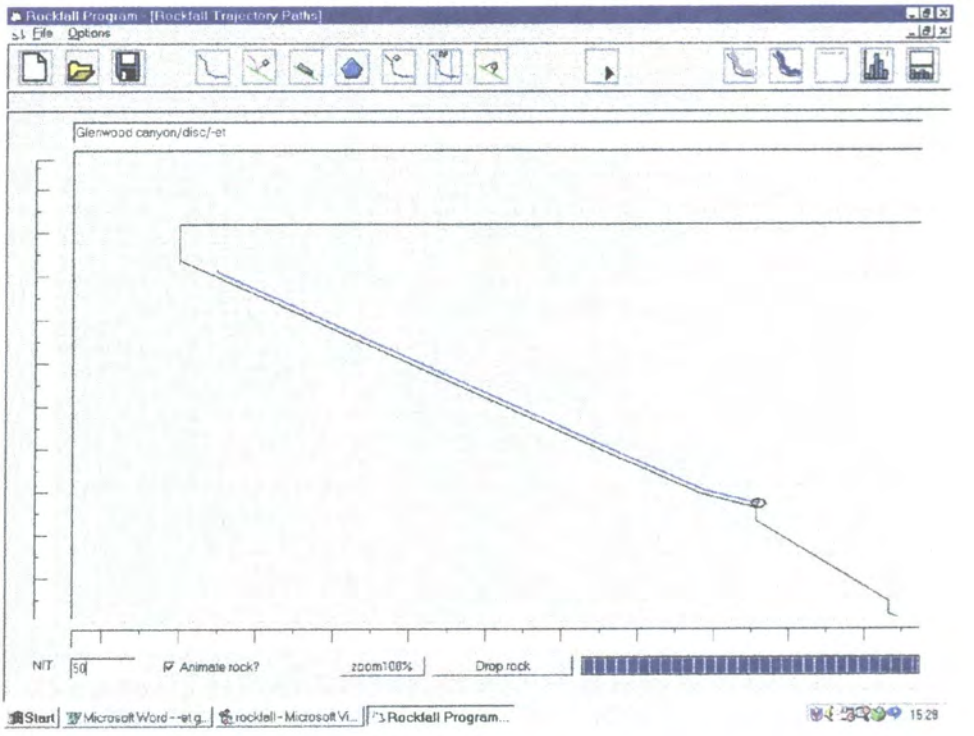

Figure 6.14. The effect of a 1.5m high 500kJ net on rock trajectories.

6.3 Rock fall analysis of limestone and chalk quarry slopes

Robotham et al. (1995) attempted to assess risk from both active and abandoned limestone and chalk quarries. On site testing was undertaken to derive the relevant coefficients for the different slope materials. The tests included dropping rock blocks to fall freely on to inclined bare rock surfaces consisting of vegetated quarry waste and also pushing rock blocks over the quarry crests. Each test was filmed to enable the determination of rock fall travel times and the values for the coefficients of restitution calculated using an in house computer simulation program. These have been listed in Table 6.1. Robotham's computer program is based on the Monte Carlo method, and models the rock as spheres.

6.3.1 Limestone slopes

A technical investigation was undertaken by the Limestone Research Group on behalf of the Department of the Environment into the stability of limestone rock slopes that have been formed by production and restoration blasting. Robotham et al. subsequently employed a computer simulation program to model rock falls from limestone quarries with similar geology to those used to determine the coefficients of restitution. Examples of the simulated rock fall trajectories for the two different slopes are shown in Figures 6.15 and 6.16, using 0.3m diameter spherical rocks.

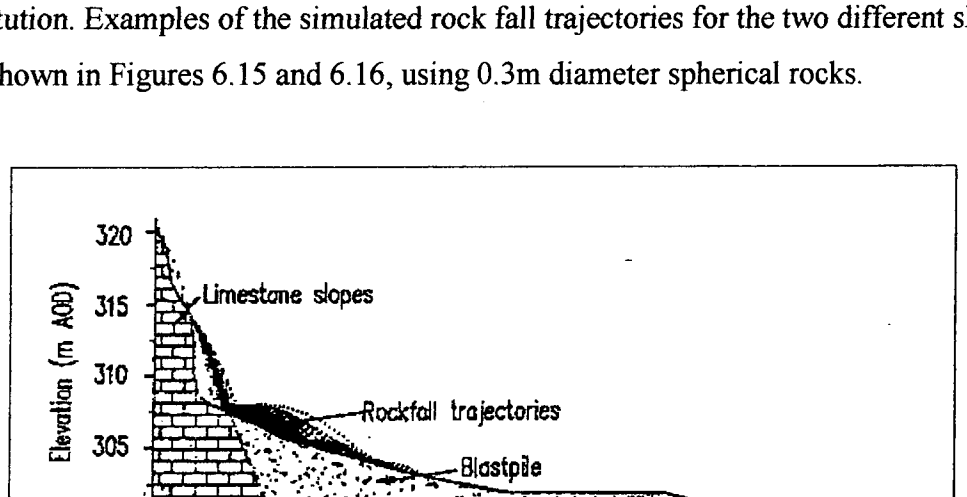

Figure 6.15: Output trajectories of Robotham's program for limestone slope 1.

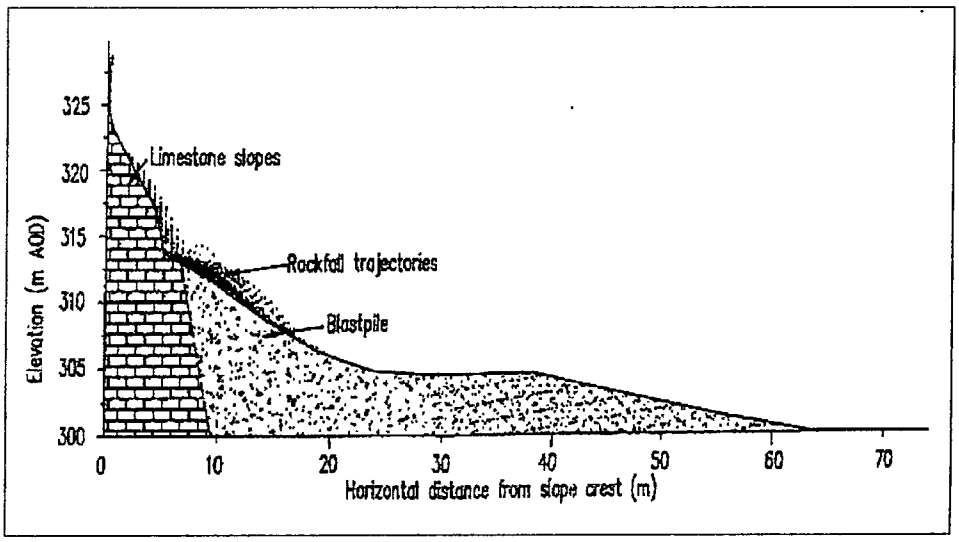

Figure 6.16: Output trajectories of Robotham's program for limestone slope 2.

Good correlation was found between the simulated trajectories using Robotham's program and those of actual rock falls that were recorded during the field tests.

The same slopes shown in Figures 6.15 and 6.16 were analysed using GeoFall, with the coefficients derived by the field tests. A rolling resistance of 0.42 for limestone bedrock and 1.0 for the vegetated scree were chosen based on values presented by Azzoni et al. (1995).

A spherical rock of 0.3m diameter was used in the following rock fall simulations. Figures 6.17 and 6.18 show the trajectory paths of fifty rocks. There is a close match between the two programs and consequently a good correlation between the GeoFall simulations and the rock falls measured in the field.

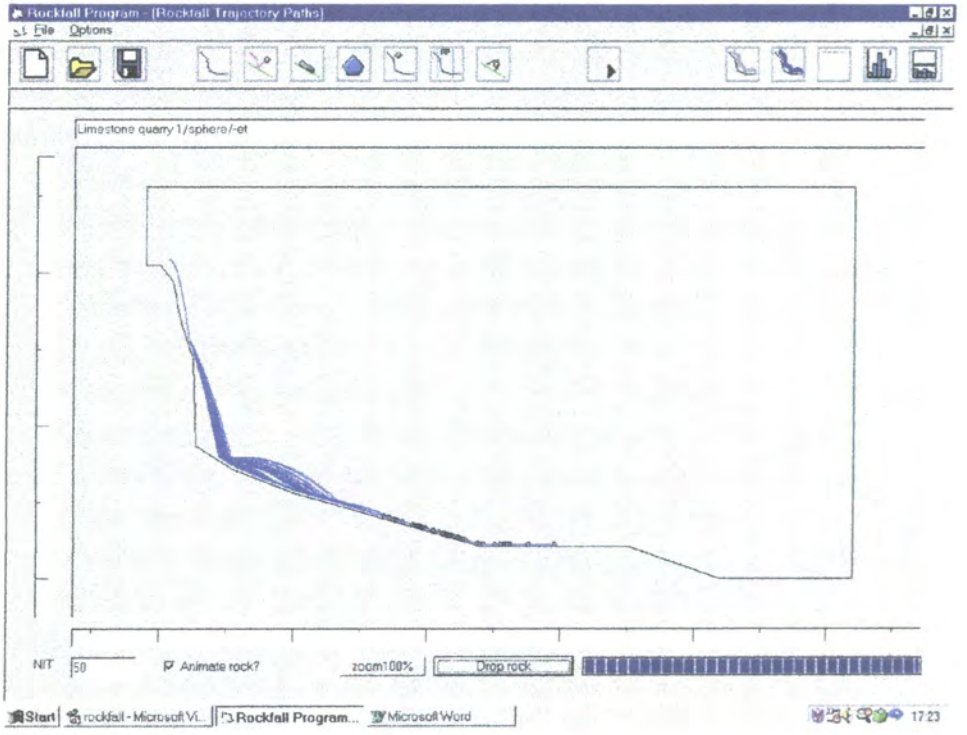

Figure 6.17: A GeoFall simulation of limestone slope 1.

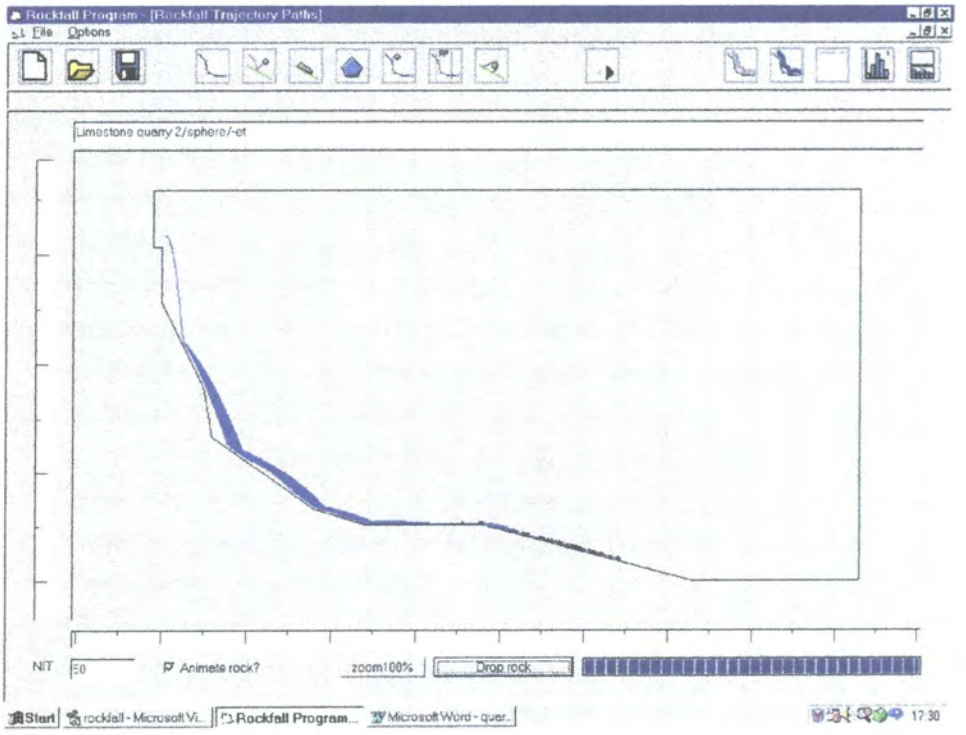

Figure 6.18: A GeoFall simulation of limestone slope 2.

6.3.2 Chalk quarry slopes

Robotham identified that there was a risk from rock fall adjacent to slopes within an old chalk quarry. Protection measures included the construction of a rock catchment ditch and a net, but these structures did not provide adequate containment.

Robotham attempted to model the rock fall in these areas to specify additional protection measures that were required. A spherical rock, 0.6m in diameter was used in the two computer simulations shown in Figures 6.19 and 6.20.

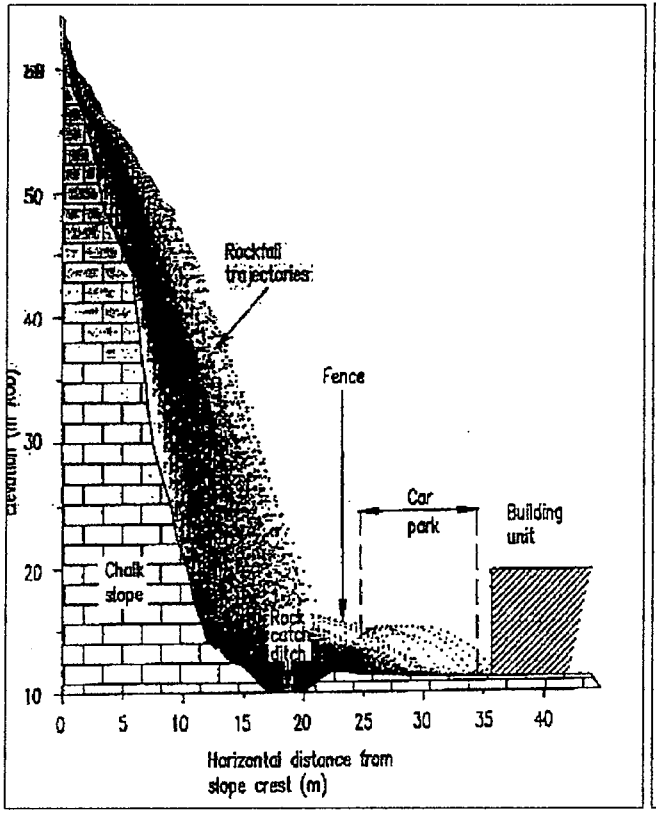

Figure 6.19
Output for chalk slope 1.

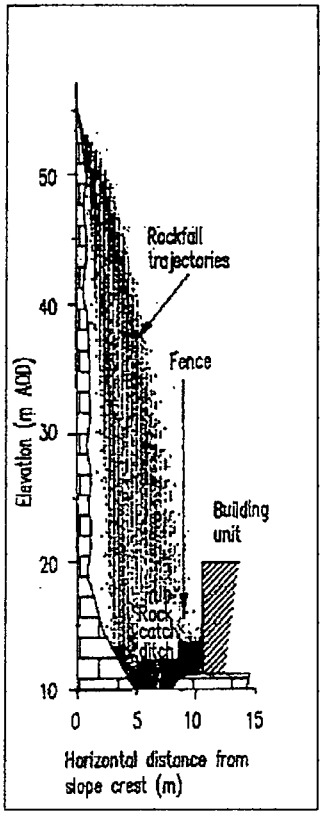

Figure 6.20
Output for chalk slope 2.

The same slopes shown in Figures 6.19 and 6.20 were analysed using GeoFall using a 0.6m diameter spherical rock. A rolling resistance of 0.4 for the chalk face and 1.0 for the vegetated chalk scree were chosen based on values presented by Azzoni et al. (1995). Figures 6.21 and 6.22 show the trajectory paths of fifty rocks. Of particular note are the rebound heights upon impact with the catchment ditch. These are both greater than those of the previous simulations shown in Figures 6.19 and 6.20 and it is possible that the coefficient of normal restitution chosen for the ditch material was a

little too high. The output trajectories of the two programs are closely matched and show a good correlation between the GeoFall simulation and the rock fall paths measured in the field.

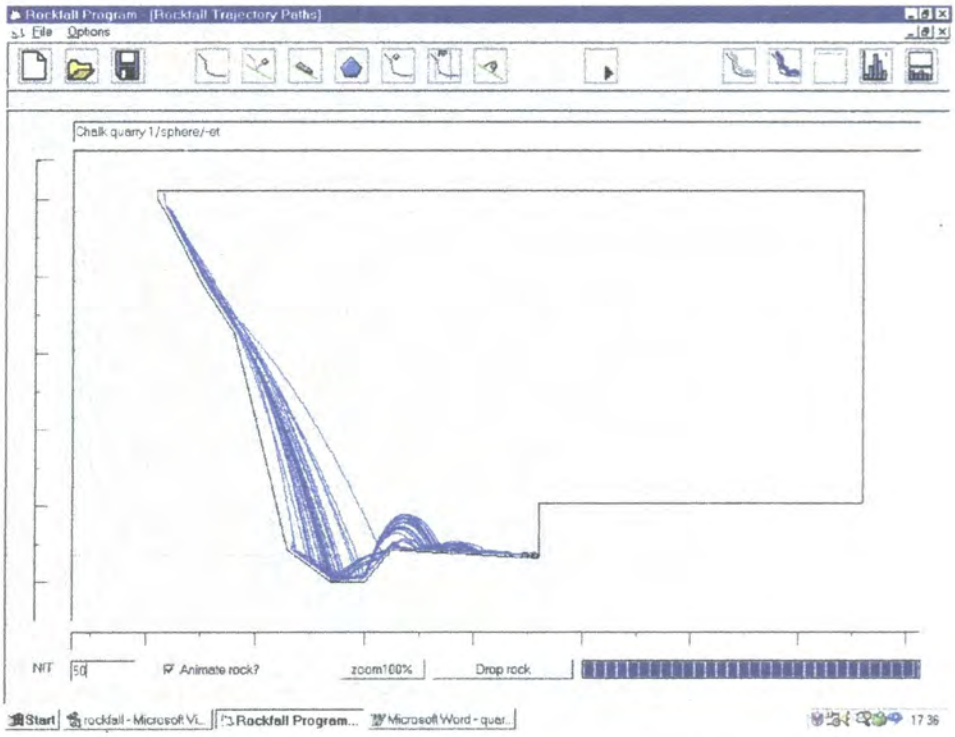

Figure 6.21: A GeoFall simulation of chalk slope 1.

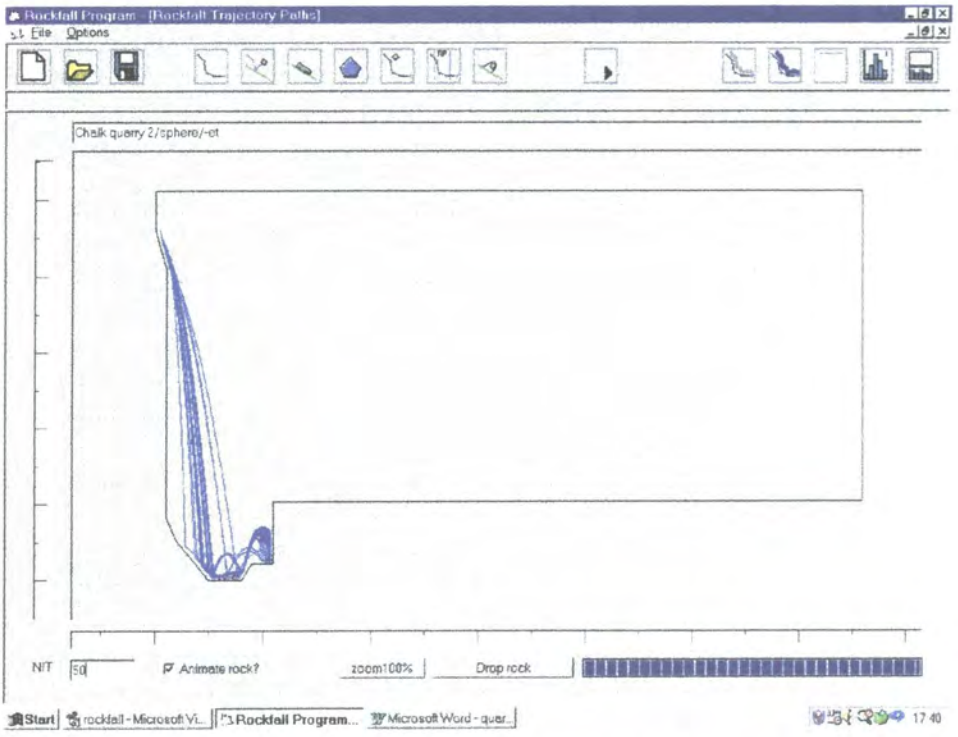

Figure 6.22: A GeoFall simulation of chalk slope 2.

6.4 Rock fall risk, hazard and mitigation at Dahekou hydropower station

Dahekou hydropower station is situated in south eastern Sichuan, China. The Sichuan Hydroelectric Investigation and Design Research Institute concentrated on the prevention of erosion rather than rock falls, which have the capacity to cause catastrophic damage to the power plant. They decided that in order to reduce the risk of rock fall from the slope two lines of flexible rock fall net were to be placed on the 145m high cliff adjacent to the dam (Zhou et al, 1996).

6.4.1 Geology

The slope is mainly composed of limestone 0.5-1m in thickness, interspersed with Ordovician shales and limestones. There are three sets of discontinuities that divide the rock mass into various block sizes.

Based upon the slope geometry the slope has been divided into three sections (Figure 6.23). The first is 420m above a reference datum, the second lies between 373-420m and the third is below 373m.

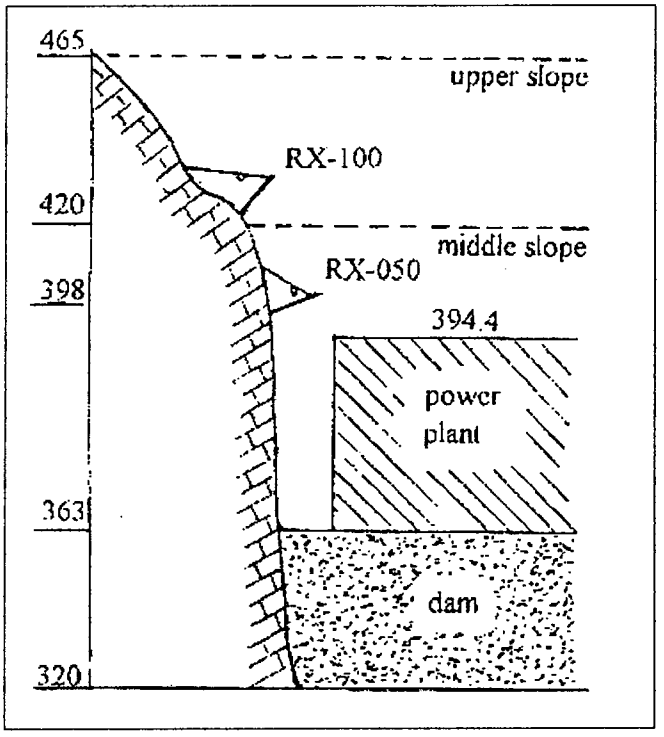

Figure 6.23: The slope cross section.

6.4.2 Rock fall history

Rock falls in the past generally originated from 420-430m above sea level. Table 6.3 shows the number of rock falls recorded in terms of rock shape and volume. The results show that the majority of the falling blocks are rectangular in shape and that 95 percent of the rock fall blocks are 0.2-1.0 m^3 in volume.

Volume (m^3)	0.2-0.5	0.5-1.0	>1.0	Total	%
Rectangle	16	33	3	52	61.2
Disc	8	10	0	18	21.2
Mixed shape	6	4	1	11	12.9
Spherical	4	0	0	4	4.7
Total	34	47	4	85	
%	40	55.3	4.7		100

Table 6.3: Historical rock falls.

Since the construction at the end of 1993, 32 further rock falls occurred. These new rock falls all originated from the upper slope between 380-465m and are shown in Table 6.4. Witnesses described the rocks as being between 0.2 and 0.7m^3 in volume and predominantly rectangular in shape.

Volume (m^3)	0.2-0.4	0.4-0.7	>0.7	Total	%
Rectangle	6	8	1	15	47
Disc	5	4	0	9	28
Mixed shape	6	2	0	8	25
Total	17	14	1	32	
%	53	43.8	3.2		100

Table 6.4: Rock falls that occurred during construction.

6.4.3 Design of mitigation measures

A program to simulate rock fall was written by Geoplan and applied to this slope. This program ignores the angular velocity component after impact. It is thus assumed based upon company expertise that this angular kinetic energy constitutes between 10-15% of the translational kinetic energy. Therefore in the design the kinetic energy after impact is calculated based upon vertical and horizontal velocities, this value is

then multiplied by a safety parameter of 1.2, the result represents the total kinetic energy. By using this method it was predicted that for the upper slope the maximum kinetic energy is 784 kJ and for the middle slope 468-492 kJ. Based upon these two design values two lines of safety net were set at 420m and 398m above sea level, to protect the power plant against rock falls from the upper and middle slope.

The first line of safety net was set at 420m, 40m in length, 5m in height and having a total capacity of 1000 kJ. The second line of safety net was set at 398m, 50m in length, 4m in height and having a capacity of 500 kJ.

6.4.4 Rock fall simulation

In order to assess the effectiveness of the remediation measures chosen by the contractor, GeoFall was used to assess the risk and effectiveness of the two chosen rock fall nets. Eight simulations were set up, four with rocks starting from the top of the upper slope and the other four starting at the top of the middle slope region. The four simulations on the upper slope region used either a $1m^3$ rectangular rock or a $1m^3$ disc shaped rock. These two rock shapes being the most common accounting for 82% of the total amount that fell. In starting the rock from the top of the slope with the largest probable rock size produces a worst case. By inserting a rock net in the position chosen by the contractor it is possible to determine the effectiveness of the net heights and capacity.

No values for the relevant slope coefficients have been produced and so typical values have been used (Table 6.5).

Outcropping material	Normal coefficient of restitution (e_n)	Tangential coefficient of restitution (e_t)	Rolling resistance μ_r	Coefficient of dynamic friction (μ_d)
Limestone bedrock	0.5	0.9	0.4	0.57

Table 6.5: Typical values for rock fall coefficients used in the GeoFall simulation.

Figure 6.24 shows the results of fifty rock fall simulations using a rectangular $1m^3$ rock. Many of the rocks have struck the top and side of the power plant, others have either struck the top of the dam or lodged on the shallow ledge after sliding or rolling down the upper slope.

A net has been included in a rock fall simulation to determine the effects of its position and capacity upon the rock fall paths. The results of fifty rock fall simulations are shown in Figure 6.24. The net has stopped all of the rocks that have struck it and only 8% of the total number of rocks have struck the roof of the power plant, none of the rocks have struck the top of the dam. The capacity of the net, 1000 kJ in this case is sufficient to stop all impacting rocks. If the net were increased in height by a metre then it would have stopped 98% of the total number of rocks.

Figure 6.26 shows the results of fifty rock fall simulations using a $1m^3$ rectangular rock that starts from the top of the middle slope region. All the rocks strike the top of the dam and several have bounced either from the slope or the dam top to impact upon the side of the power plant.

Figure 6.27 shows the effects of the rock fall protection net upon the rock fall trajectories. It is apparent that this net has stopped almost all the rocks. However kinetic energies are very close to that of the net capacity and it would take very little for a rock to penetrate the net. A safer capacity would have been 750 kJ.

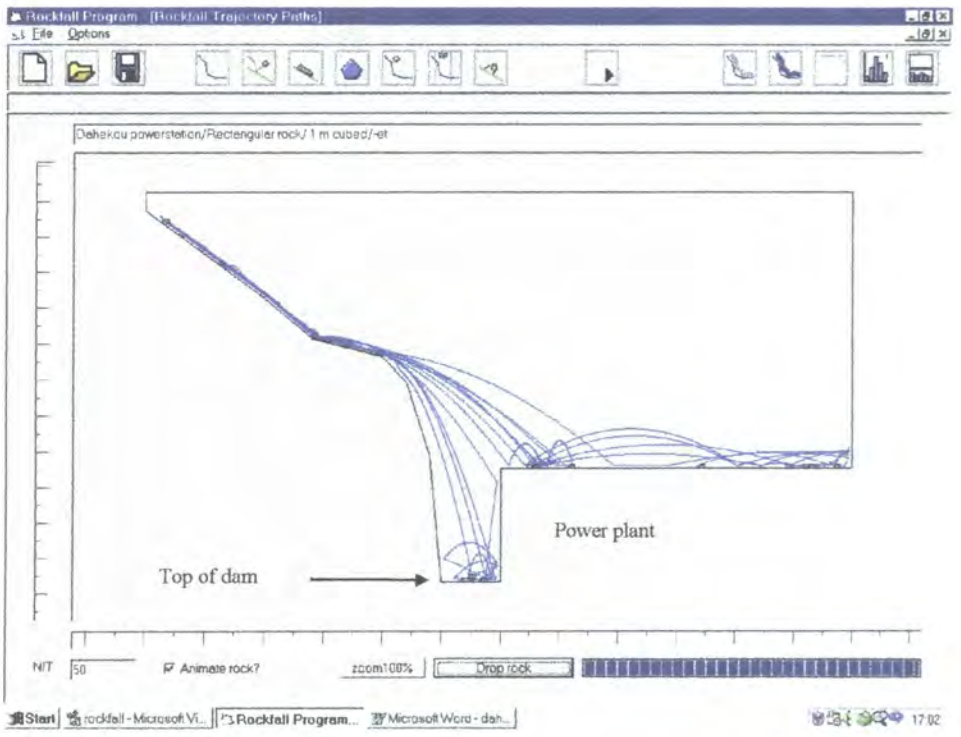

Figure 6.24: Trajectories for a $1m^3$ rectangular rock originating from the upper region without a rock fall net.

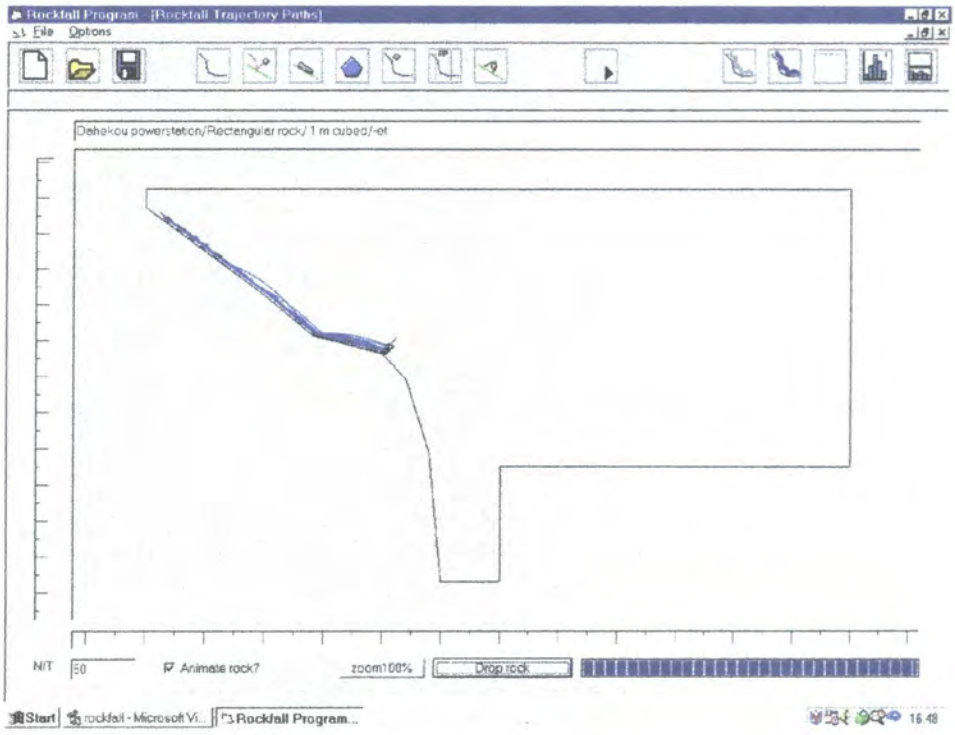

Figure 6.25: Trajectories of the $1m^3$ rectangular rocks with a 1000 kJ capacity rock fall net.

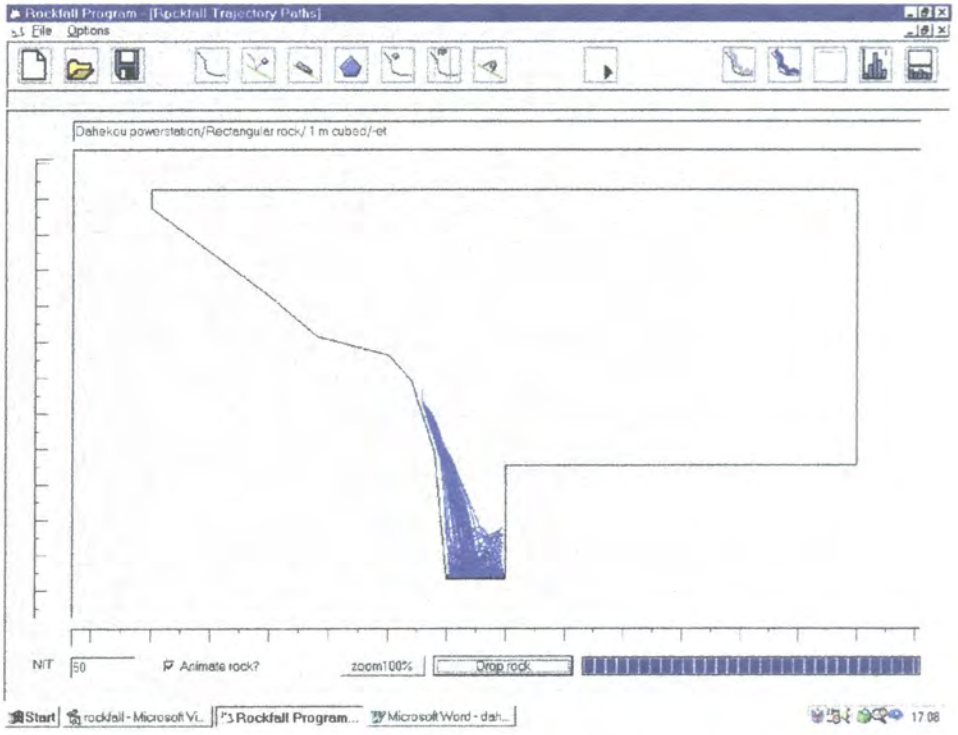

Figure 6.26: Trajectories for a $1m^3$ rectangular rock originating from the middle slope region with no rock fall net.

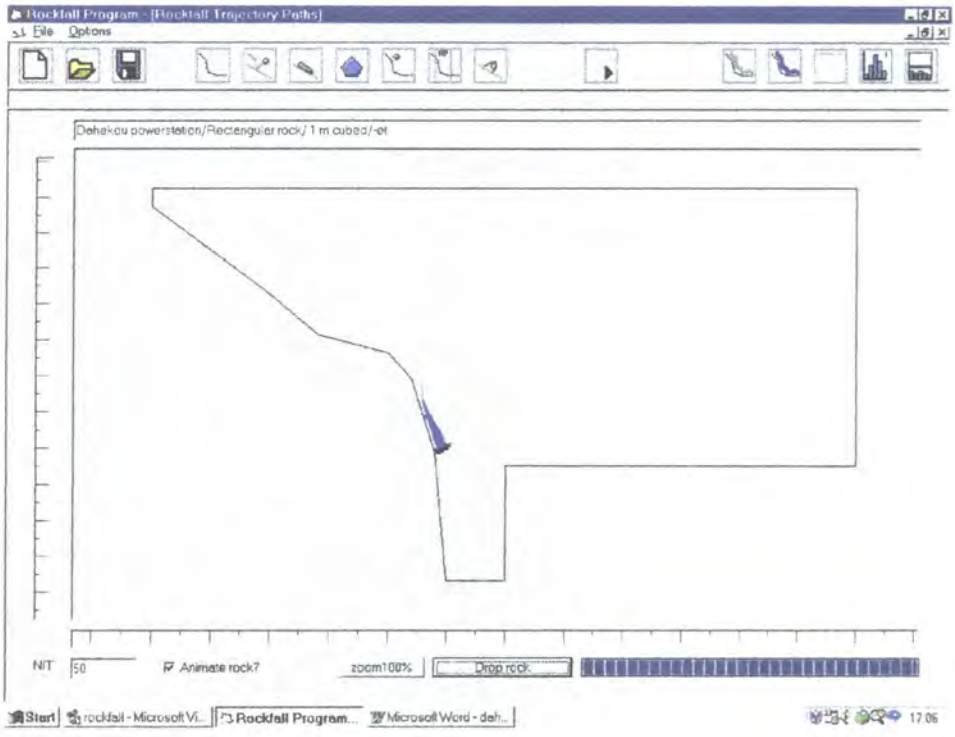

Figure 6.27: Trajectories for a $1m^3$ rectangular rock originating from the middle slope region with a 500kJ capacity rock fall net.

The previous simulations have been repeated using a $1m^3$ disc shaped rock. This is the second most common rock shape and accounts for 21.2% of the total amount of rocks that have fallen in the past. It is important to simulate this rock shape because it will most likely travel further than a rectangular rock because of its high moment of inertia and its ability to roll. Figure 6.28 shows fifty simulated rock fall trajectories starting from the upper slope region. The disc shaped rocks tend to roll down the upper slope until it hits the ledge from whence it bounces on to the roof of the power plant. This produces a worse case than the rectangular rock since not only do more rocks strike the power plant but they do so with higher kinetic energies. There is obviously a need for extra remediation measures for these types of rock. Figure 6.29 shows that the 1000 kJ net has stopped all of the rocks.

Figure 6.30 shows the results of fifty simulated rock fall runs using a $1m^3$ disc starting from the middle slope region. All of the rocks have rebounded from the top of the dam to strike the side of the power plant.

Figure 6.31 shows that the 500 kJ net has stopped all the rocks. Kinetic energies are very close to that of the net capacity and it would take very little for a rock to penetrate the net. A safer capacity would have been 750 kJ.

By using GeoFall it has been shown that the positions and heights of the two rock fall nets were highly acceptable. The capacity of the first net (1000 kJ) was acceptable and provided a small safety margin against larger rocks. The second net (500 kJ) was also acceptable but had very little margin of safety and it is recommended that this net should have possessed a capacity of 750 kJ.

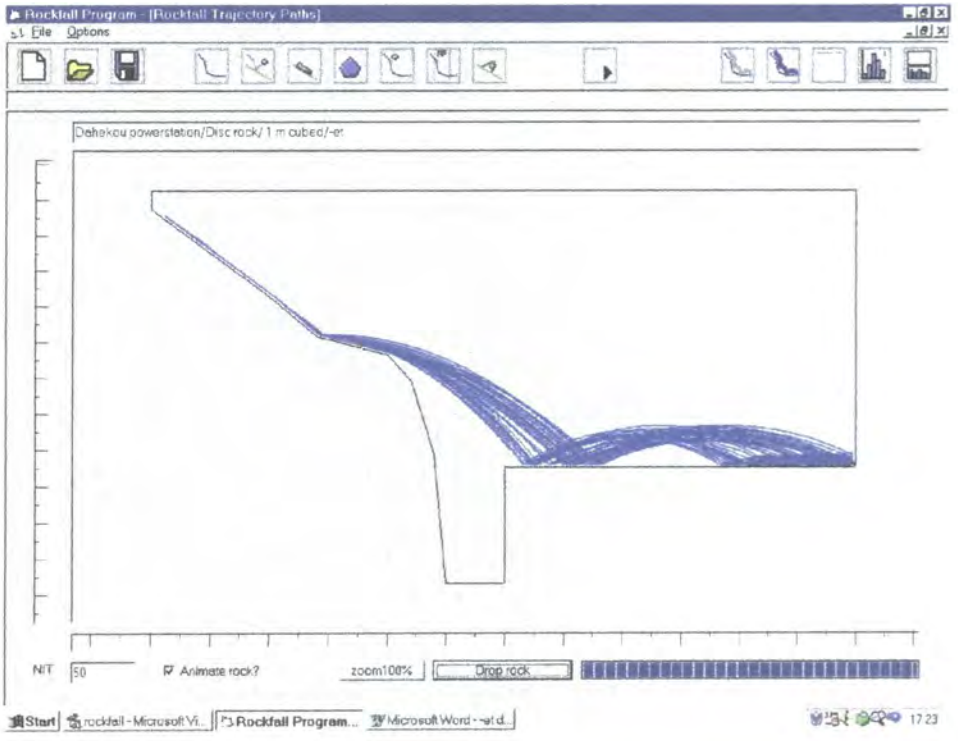

Figure 6.28: Trajectories for a $1m^3$ disc shaped rock originating from the upper slope region without a rock fall net.

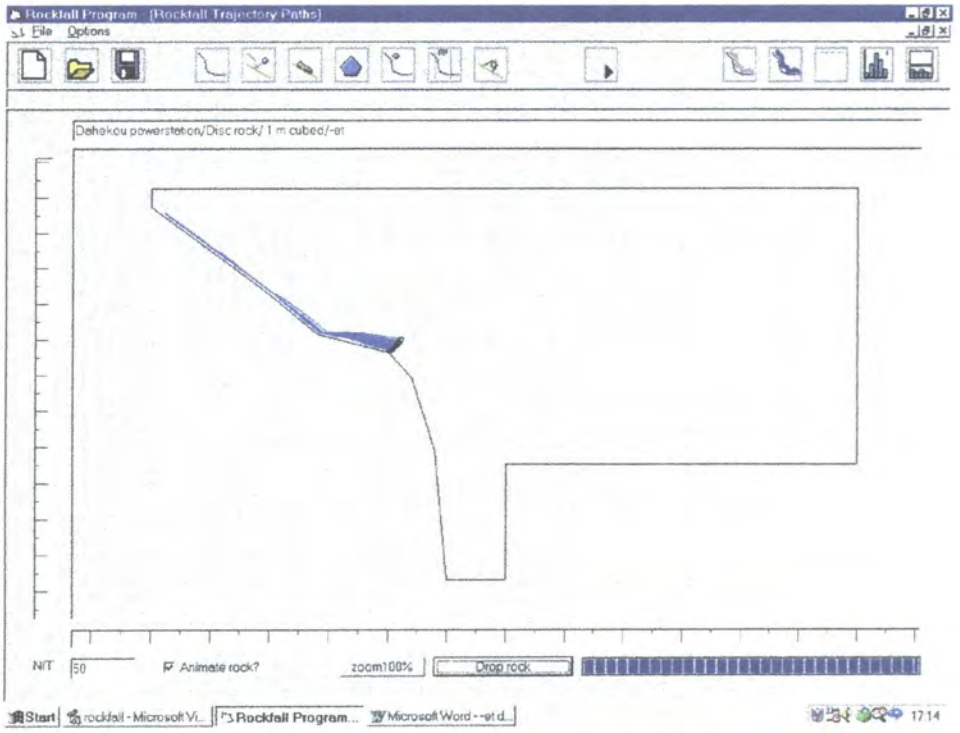

Figure 6.29: Trajectories for a $1m^3$ disc shaped rock originating from the upper slope region with a 1000 kJ capacity rock fall net.

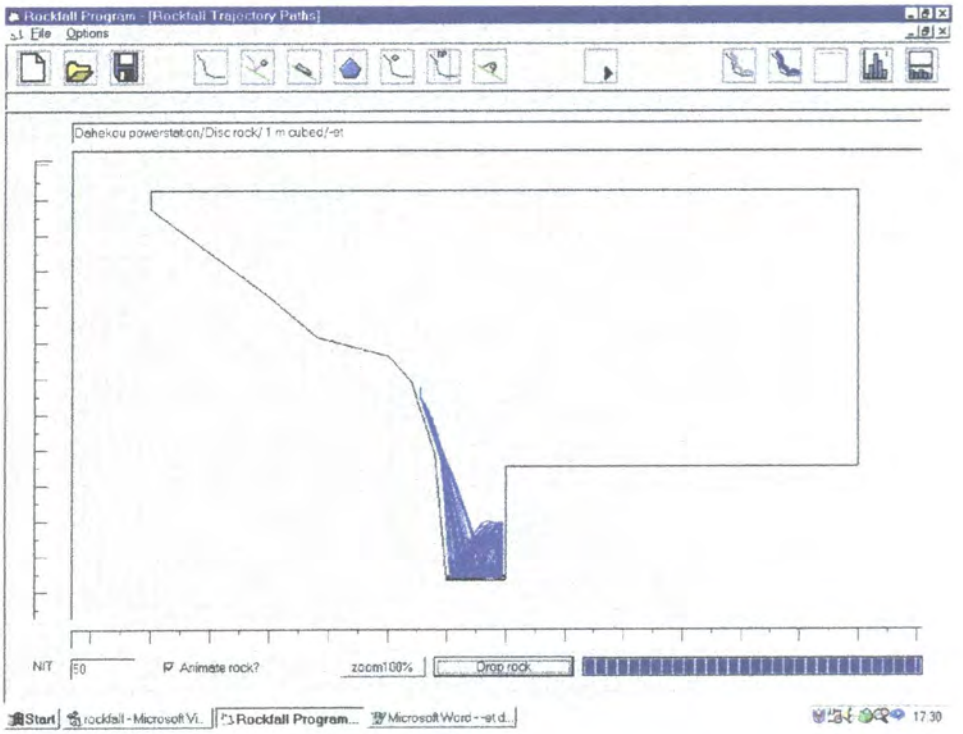

Figure 6.30: Trajectories for a $1m^3$ disc shaped rock originating from the middle slope region without a rock fall net.

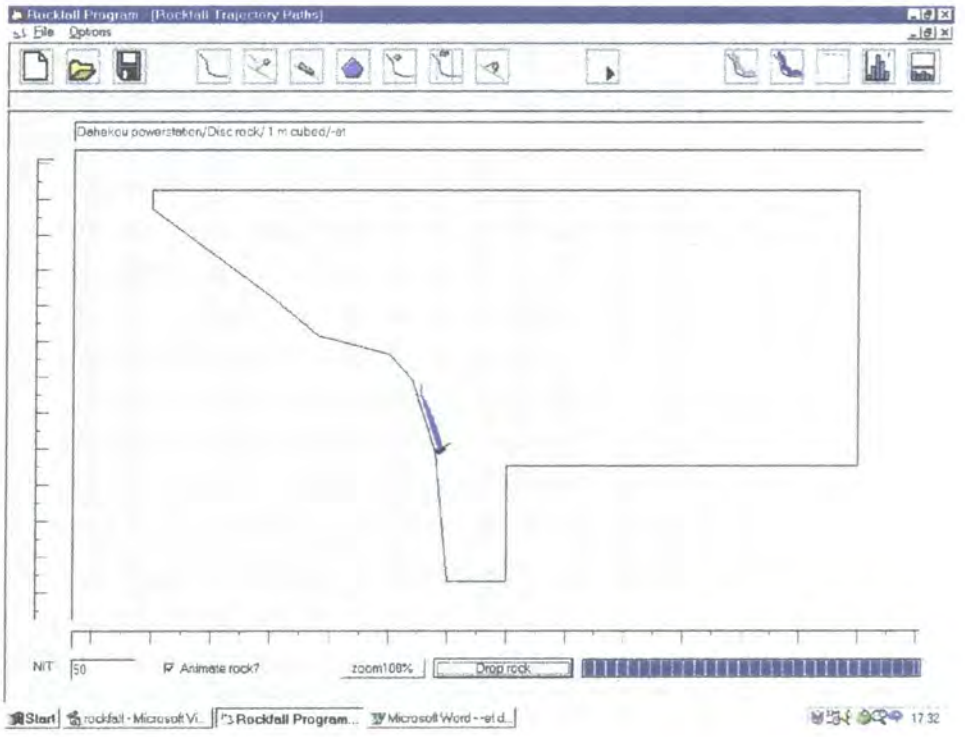

Figure 6.31: Trajectories for a $1m^3$ disc shaped rock originating from the middle slope region with a 500 kJ capacity rock fall net.

6.5 Rock fall analysis at Craig y Dref

During the summer of 1976 a ten tonne block fell from a 30m high cliff rising immediately to the north of the village of Tremadog in Gwynedd, North Wales. The block came to rest 10m from a row of cottages. There is a history of rock falls in the area known as Craig y Dref and in view of the hazard to persons and property, the Nature Conservancy Council in association with Dwyfor District Council commissioned a geotechnical survey to determine the nature and degree of stability of the area (Mercer, 1982).

6.5.1 Geology

The cliff of which Craig y Dref forms a part, trends roughly east west and extends for several kilometers. It is part of a relict coastline relating to times when the sea level was higher and in geological terms comprises a dolerite sill intruded into ordovician shales, which has subsequently been tilted during the Caledonian earth movements and now dips gently towards the north. A walkover survey by Mercer revealed that the cliff face was in very poor condition. Small to medium sized blocks ($0.5\text{-}5m^3$)

were very close to failure in a dry condition and ravelling was occuring along most of the cliff. Stunted oak trees, ivy and bracken all grow on the rock face for most of its length.

6.5.2 Remedial measures

The length of the cliff was separated in to three sections of similar geology. In the eastern section a combination of passive walling and rock anchors were considered necessary to prevent the failure of large blocks (Figure 6.32).

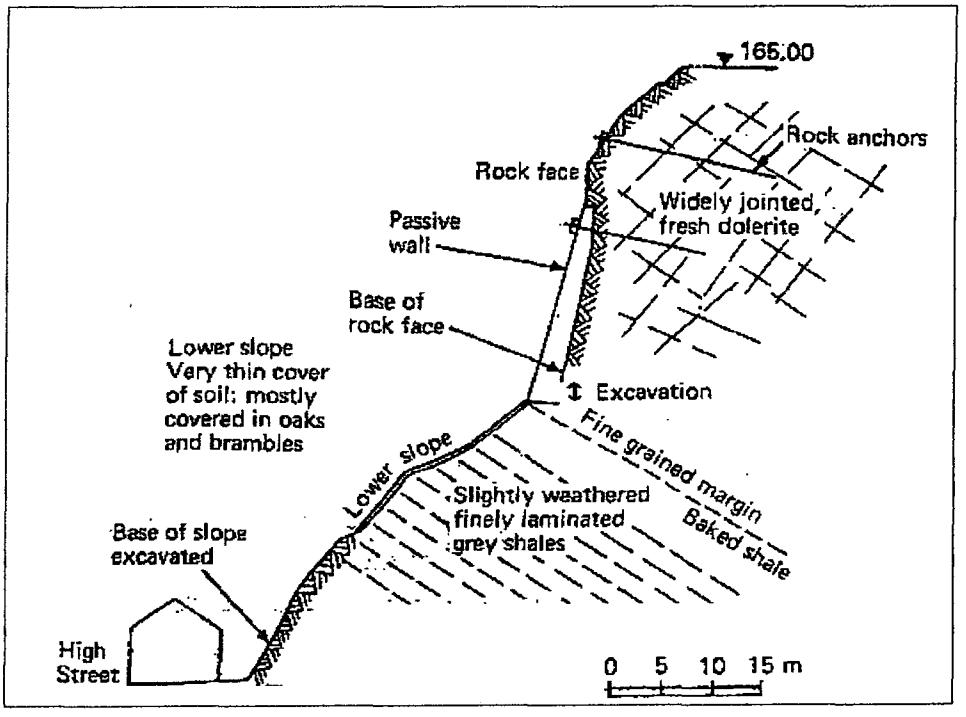

Figure 6.32: The Eastern section of the slope at Craig y Dref.

In the central section, the joint spacing was narrower and the blocks therefore smaller. In addition the cliffs diverged from the houses, but scree development was limited (Figure 6.33). Catch nets were used in this section, which extended along the base of the cliff for 200m.

The block sizes in the western section remained below $4m^3$ and the cliff diverges even furthur from the houses developing a large scree slope. In this area a 130m long gabion wall with a catch area in front of it was situated at the base of the scree immediately infront of the properties (Figure 6.34). The gabion wall was located in a densely wooded 20-40° scree slope, interspersed with narrow scree runs and large

boulders up to $15m^3$ in size. The vegetation had to be cleared, the scree runs stabilised and the large blocks reduced prior to work beginning on the foundation.

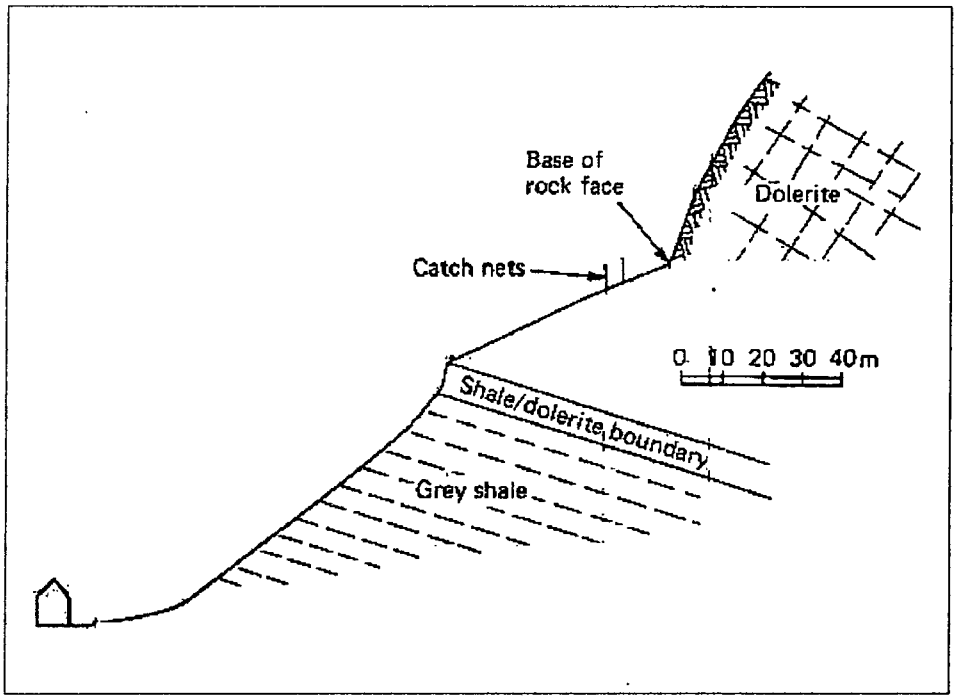

Figure 6.33: The central section of the slope at Craig y Dref.

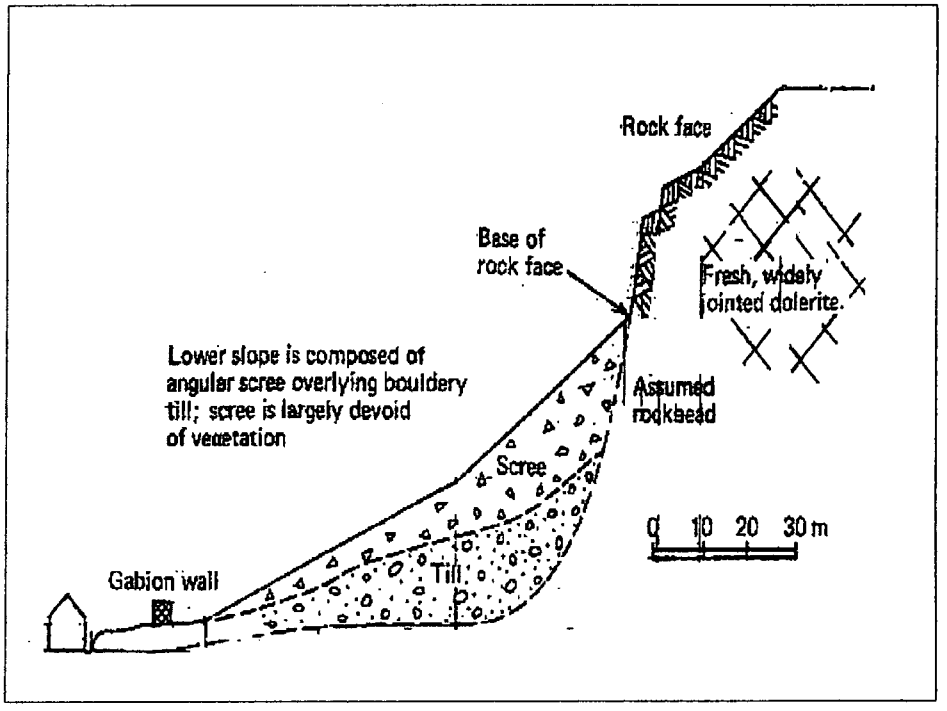

Figure 6.34: The western section of the slope at Craig y Dref.

6.5.3 Rock fall simulation

In order to test the effectiveness of the rock fall nets and gabion wall two simulations were instigated using GeoFall. Typical values of coefficients of restitution and rolling resistance have been used for both the central and western sections (Table 6.6) since no values were presented by Mercer. The eastern section has not been analysed since passive measures have been used to stabilise the slope.

Section	Outcropping Material	Normal coefficient of restitution (e_n)	Tangential coefficient of restitution (e_t)	Rolling resistance (μ_r)
Central Section	Bedrock with small trees and ivy	0.4	0.7	0.7
	Shale Dolerite boundary	0.45	0.95	
	Soil with vegetation and limited scree	0.3	0.7	
Western section	Bedrock	0.5	0.95	0.4
	Angular scree overlying till	0.3	0.7	0.45

Table 6.6: Critical values of coefficients used in the central and western sections.

6.5.3.1 Rock fall simulation for the central section

Figure 6.35 shows the results of fifty simulated rock fall runs for the central section using a 2m diameter sphere. Without some form of rock fall protection inhabitants of the buildings at the base of the slope are at great risk from rock falls. Kinetic energies of the rocks were as high as 2800 kJ at the base of the slope. In order to reduce the risk to local residents and property two lines of catch netting were placed close to the base of the dolerite cliff. The catch net comprised of polypropylene netting attached to 2.5m high posts, with ground anchored cables providing additional support. Two rock fall nets were used to prevent large boulders breaking through the first net and gaining momentum. An analysis point placed at the base of the dolerite cliff enables the kinetic energies of the rock to be ascertained (Figure 6.36).

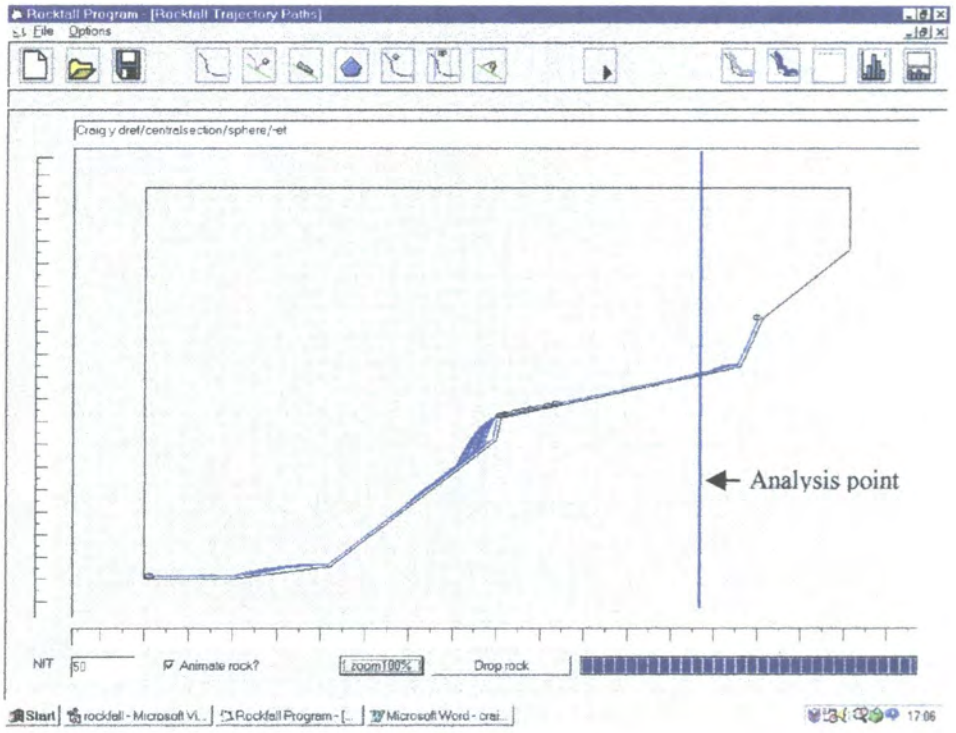

Figure 6.35: Rock trajectories for the central section.

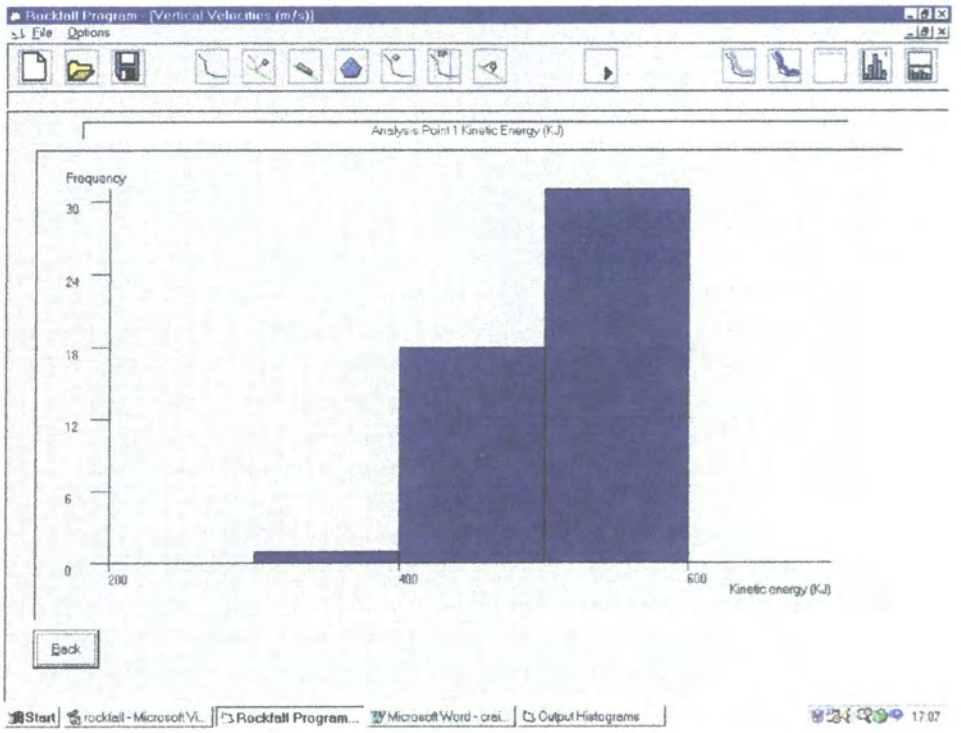

Figure 6.36: The kinetic energies of the rocks at the analysis point.

From the histogram shown in Figure 6.36, a single GeoBrugg net of 750 kJ capacity should prove sufficient to stop all the anticipated rock falls. Figure 6.37 shows the effects of the rock fall net upon the rock trajectories. It is apparent that all the rocks have been stopped by the net and that the position chosen for the net by the contractor was indeed highly suitable. The actual capacities of the rock fall net used by the contractor are unknown.

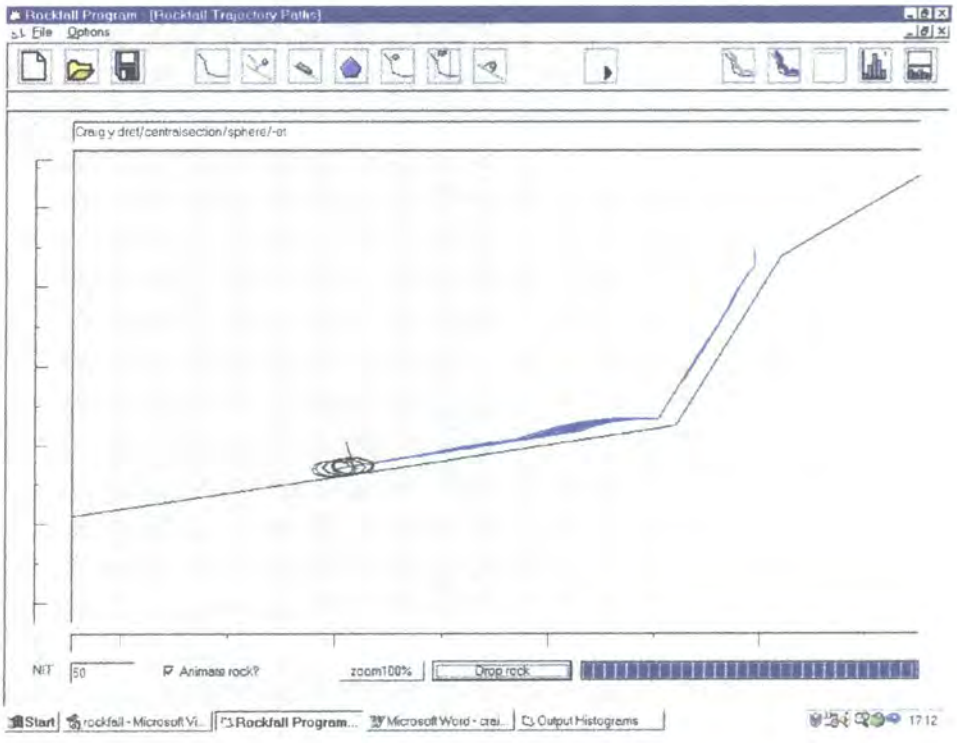

Figure 6.37: The effects a 750 kJ capacity rock fall nets on the rock trajectories.

6.5.3.2 Rock fall simulation for the western section

In the western section of Craig y Dref it was felt that a 3-5m gabion wall would prove a more economical, durable or efficient form of protection. Figure 6.38 shows fifty simulated runs on this slope using a 2m diameter sphere. It is apparent that all of the rocks have been stopped by the 3m high gabion wall and that the contractors choice of remediation measure was again highly suited to the problem.

An analysis point placed at the base of the slope prior to the wall showed that the kinetic energies of the rock varied from 1100-1400 kJ. It is possible that two rock nets would have provided the same level of protection but would of required greater routine maintenance.

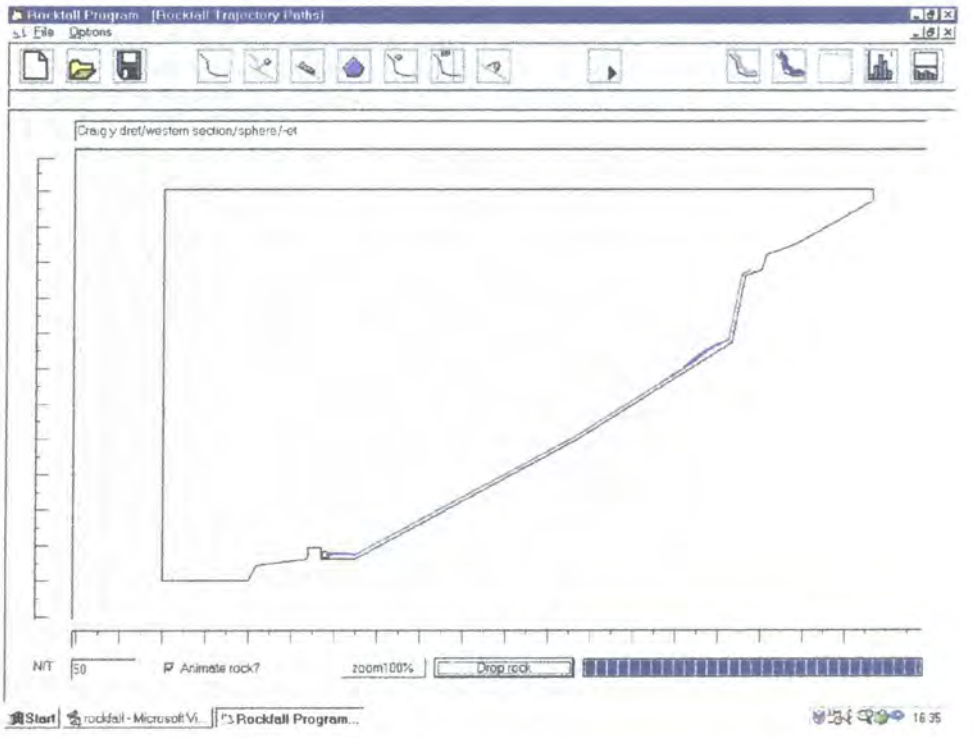

Figure 6.38: The effect of a 3 m high gabion wall on rock fall trajectories (western section).

6.6 Rock fall analysis at the ancient region of Argos, Greece

Sofianos et al. (1988) studied and attempted to simulate analytically a rock fall that occurred in Argos, Greece. The location of the rock fall site is on the western fringes of Argos town, near to the Larissa Mountains on the East Coast of the Pelopponese. Steep heavily weathered rock cliffs lie under the Byzantine monastery of Panagia Katakekrimeni. At the toe of the mountain under Katakekrimeni are the ruins of the roman Adrian aqueduct, and the town of Argos. Many parts of the heavily jointed weathered karsitic limestone face were only marginally stable and the possibility of large boulders becoming detached was extremely high. Numerous boulders were dislodged from this slope but never made it further down slope than the Adrian aqueduct. The base of the cliff was covered in small boulders and fallen rock debris and below this, a grass covered silty clay slope extends to Argos.

The last rock fall was in December 1983 during a rainstorm when a rectangular shaped boulder, 4.0 by 1.5 by 1.2m thick was dislodged from 20m above the base of the cliff below the monastery. The boulder bounced half its way down the slope and

finally came to rest approximately 7m from a house. The path of the boulder was obvious because it left numerous bounce marks (on soil that was fully saturated after the rainstorm) and crushed much vegetation. The path of the boulder was traced, from the place at which it came to rest to the position on the cliff from which it became detached. A significant portion of the boulder mass was lost during multiple collisions on other boulders at the base of the cliff.

6.6.1 Rock fall simulation

This is a difficult problem to analyse due to the lack of knowledge of restitution and friction coefficients and so typical values have been used (Table 6.7). It is further complicated by the rock fragmenting and thus the rock changing shape, mass and moment of inertia after each successive impact.

Outcropping Material	Normal coefficient of restitution (e_n)	Tangential coefficient of restitution (e_t)	Rolling resistance (μ_r)	Coefficient of dynamic friction (μ_d)
Bedrock	0.5	0.95	0.42	0.58
Bedrock covered by large blocks	0.35	0.85	0.55	0.56
Soil covered by vegetation	0.25	0.55	0.65	0.56

Table 6.7: Coefficients used by Geofall in the Argos back analysis.

The rock fall at Argos was simulated in GeoFall using a 4 by 1.5 by 1.2m thick rectangular and chamfered rock shape.

A rectangular rock gives the best possible case at Argos since it will travel less distance than a circular one. It also assumes that the rock retains its original shape and mass throughout the simulation. The trajectory paths of fifty rectangular rocks are illustrated in Figure 6.39.

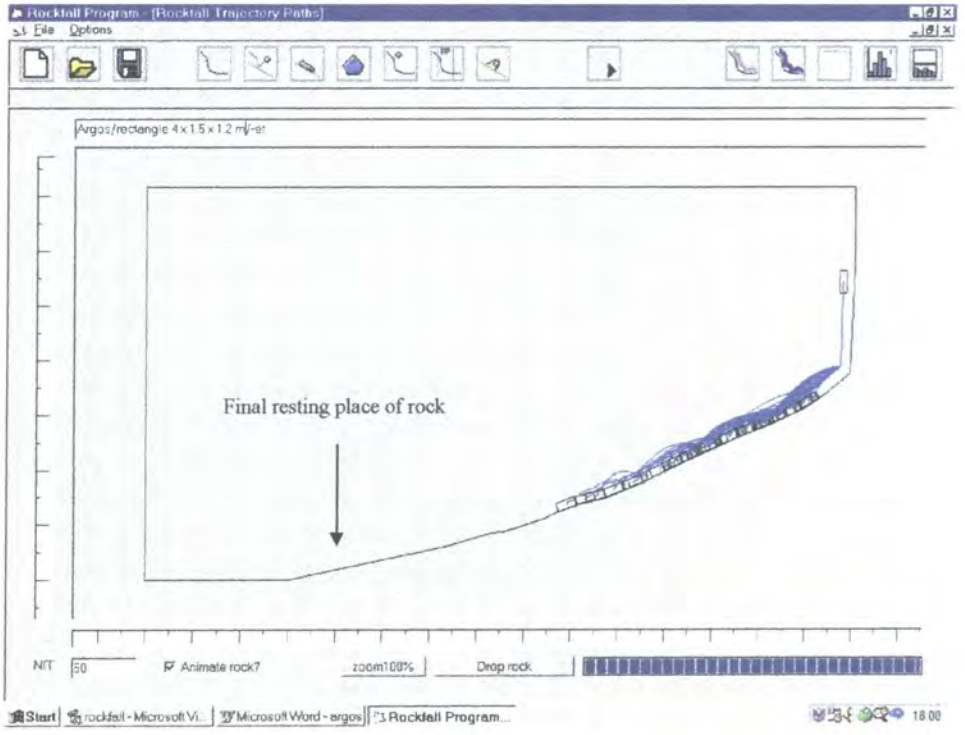

Figure 6.39: Trajectories of a 4 by 1.5 by 1.2m thick rectangular rock.

A chamfered rock (Figure 6.40) has been used in the simulation to note the effects of the rounding of the edges of the rectangular rock upon the rock path. The paths of fifty such rocks are shown in Figure 6.41.

By inspection of both Figures 6.39 and 6.41 it is apparent that the rounding effect causes the rock to travel further down the slope This is an important observation since it has always been believed that an intact rock will travel further than one which breaks upon impact. In the case of the Argos slope this was not the case. The breaking of the corners allowed the rock to roll at low angular velocities thus allowing the rock to travel further before coming to rest.

Because of the fragmentation of the rock on successive impacts it is impossible to predict the final resting-place of the rock only a range of possible positions. The rounding of the rock produced by fragmentation was a critical factor in allowing the rock to travel so far down the slope.

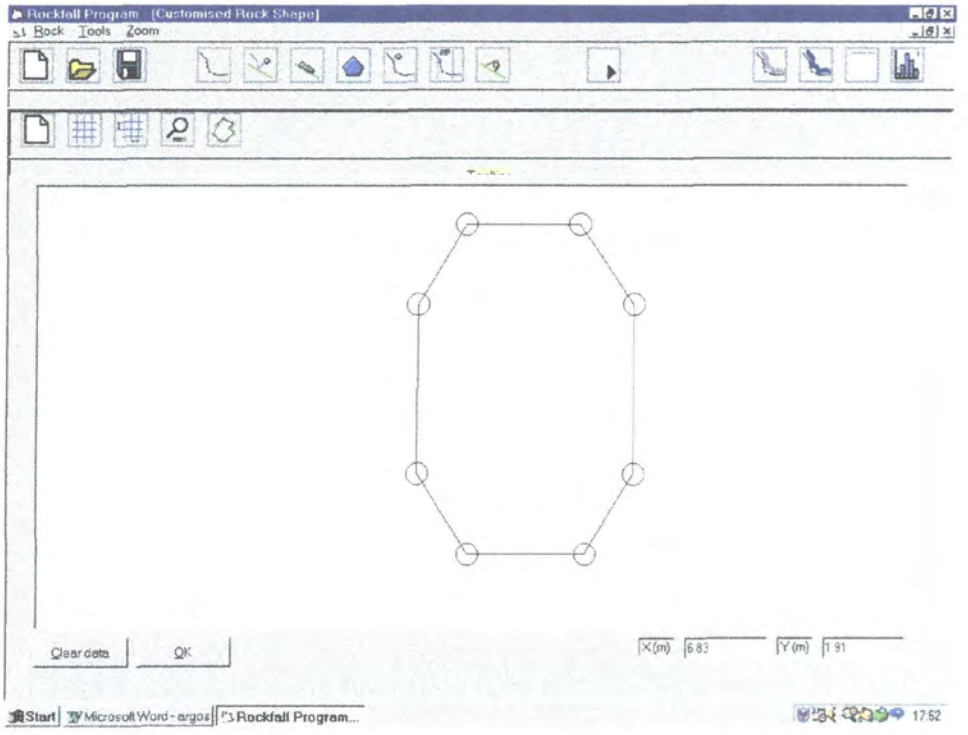

Figure 6.40: The chamfered rock shape used in the GeoFall simulation.

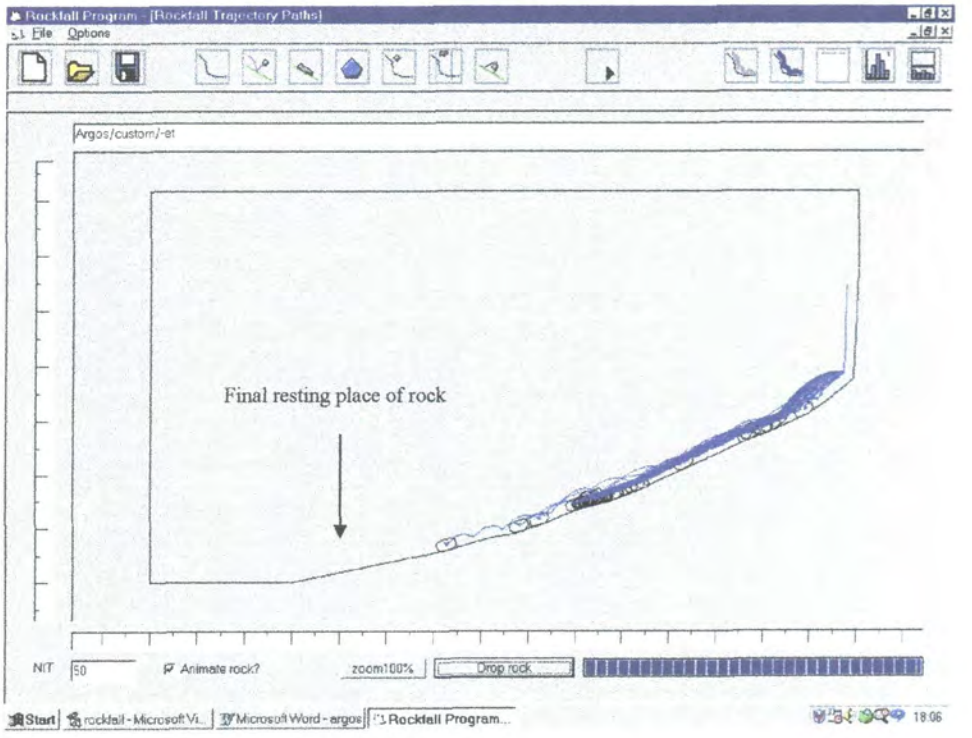

Figure 6.41: Trajectories produced by a chamfered rectangular rock.

6.7 Summary of the overall performance of GeoFall

GeoFall has accurately predicted the trajectories of all the published rockfall events described in this chapter. Where various researchers have used rock fall simulation programs to simulate the published cases, GeoFall has generally compared favourably with their output. However, it must be emphasised that when comparing the two programs, the coefficients of restitution chosen, rock shapes used, and the formulation of the programs may be different, thus accounting for any variation in the simulated trajectories. It has been shown in the Argos, Dahekou and Glenwood Canyon simulations that GeoFall is a useful design tool for the installation and placement of rock fall nets.

Chapter 7

Experimental Determination of Restitution Coefficients

7 Experimental determination of restitution coefficients

7.1 Introduction

Previous methods used to determine the coefficients of restitution have been based on either back analysis of rock fall events using computer simulation (Pfeiffer and Bowen, 1989) or in-situ filming of triggered rock falls (Azzoni et al, 1991).

If the trajectory, size and shape of a fallen rock are well defined then this data may be entered into a computer simulation program such as CRSP. The trajectory of the rock may be reproduced by varying key parameters such as the coefficients of restitution, surface roughness, rolling resistance and sliding friction such that a reasonable agreement is made between the simulated and actual rock trajectory. The resultant parameters are then considered typical of the relevant slope surface material.

The coefficients of restitution can also be calculated using in-situ testing. Usually three or more video cameras are placed along the test slope at different lateral positions depending upon the length of the slope and the morphological condition of the site. A camera is also placed in a frontal position in order to evaluate the lateral movement of the falling rock. The recorded rock fall is then analysed in the laboratory using digitisation software allowing the computation of pre and post impact velocities and rotations. From these the coefficients of restitution may be calculated.

In order to overcome the shortcomings of computer back analysis and in-situ methods a repeatable and accurate laboratory test is required, allowing the coefficients of restitution to be determined in a controlled environment.

7.2 Air table method

The method chosen to determine the coefficients of restitution for various rock types was an air table combined with video equipment. Discs of rock were cored and floated on a bed of air, which provided a frictionless surface. The discs were then fired, with no spin, at a large immobile piece of the same rock type, and the rock allowed to rebound. The pre and post impact velocities were recorded using video equipment, allowing the coefficients to be calculated using Brach's theory as outlined in section 5.3.12.

7.3 Experimental procedure

The discs of rock were cored from blocks of a red, grey and buff sandstone, limestone, a laminated Magnesian Limestone, white marble and a sand and cement mortar. Typically the disks were 54mm in diameter and 3-8mm thick. The base of each disk was polished to remove any burrs caused by the cutting wheel to allow the disc to float freely without friction on the air table surface. Because of its soft gritty texture the base of the mortar disc could not be smoothed and so a thin smooth layer of Araldite^{TM} was spread on the base to allow the rock to float unimpeded.

The air table as shown in Figure 7.1 is a wooden air chamber measuring 1m by 1m by 0.06m with a drilled PVC surface allowing the air to escape through a 20mm grid of 1mm diameter holes (Carpmael, 1995). A six pipe manifold connects the seven bar air supply to the underside of the air table, distributing the air flow evenly over the surface area. Four adjustable legs placed on each corner allow the table to be tilted and a spirit level was used to ensure that the table was level.

Figure 7.1: The air table (Carpmael, 1995)

A spring powered firing mechanism was used to propel the discs of rock. The velocity of the disc was varied by changing the distance the spring was extended, thus a spread

of velocities could be achieved. A protractor on the body of the mechanism allowed the angle of incidence to be set.

A Panasonic VHS video camera was placed on a tripod above the air table such that the plan view of the impact could be recorded. The height of the camera was adjusted such that on playback the spacing between holes shown on the portable 14" TV screen was exactly 20mm. This allowed the distances travelled by the disc to be measured off the screen without the need to scale to actual size.

A 14" portable colour television was used to monitor the playback from the video equipment. The still advance on the VHS video allowed the time to be advanced by $1/24^{th}$ of a second. Thus, the distance the rock had moved in a known period of time could be directly measured off the screen.

In an attempt to determine the coefficients of restitution for saturated rocks, discs of sandstone were placed in distilled water and left in a vacuum chamber until the stone was fully saturated. The wet disc was then tested on the air table to determine the coefficients of restitution. Unfortunately the air flow from the table caused the stone to dry and consequently the moisture content of the disc varied with time. The values determined are thus only for dry discs of rock.

7.4 The normal coefficient of restitution e_n

To calculate the normal coefficient of restitution a disc of rock was fired at a large flat immobile piece of the same rock material at an angle of incidence of 90°, with no spin as illustrated in Figure 7.2.

The coefficient of normal restitution e_n for a circular rock having no initial angular velocity ω may be calculated from Equation 5.31.

If the pre and post impact distances are measured over the same time period then the coefficient of normal restitution is the ratio of the post and pre impact distances denoted as D_n and d_n respectively.

$$e_n = \frac{D_n}{d_n} \qquad \textbf{7.1}$$

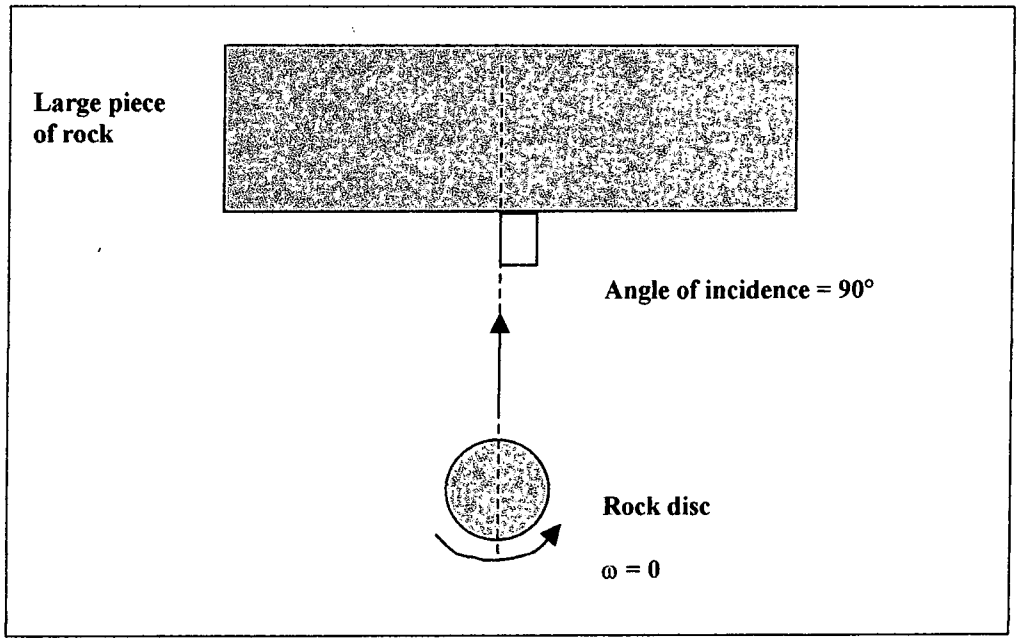

Figure 7.2: Plan view of air table.

The incident velocities were varied and a graph of incident versus rebound velocity was plotted for each given rock material as shown in Figure 7.3 for the case of a buff sandstone disc.

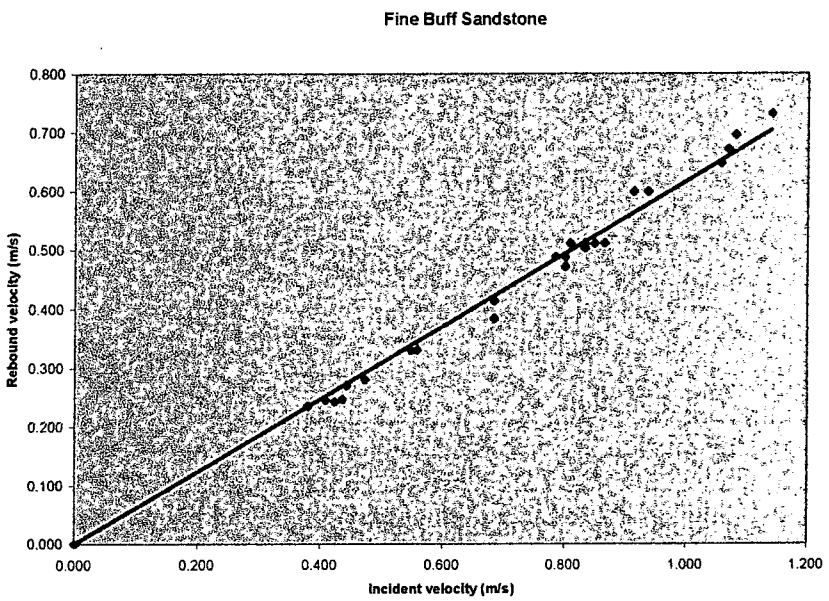

Figure 7.3: Incident versus rebound velocity for a buff sandstone disc.

This Figure shows that there is a linear relationship between incident and rebound velocity over the range of velocities 0.4-1.2 m/s used. The coefficient of normal restitution is calculated from the gradient of the straight line.

Several similar graphs have been produced for different materials and are included in Appendix 4. The calculated coefficients of normal restitution have been summarised in Table 7.1.

The measured value for e_n for each material is an upper bound since as impact velocity increases the rock will start to fragment causing localised crushing, this corresponds to a loss of energy resulting in a lower value of e_n. Typically these values of e_n would only be appropriate if a rock hit a smooth, clean and dry massive surface such that no permanent deformation, cracking or crushing of the boulder occurred.

It would be of obvious benefit to the practising engineer to be able to accurately determine the normal coefficient of restitution by means of a simple portable test or relationship between mechanical properties. Therefore, the dry density of each rock core was calculated and the pulse velocity measured using a PUNDIT machine. Each core was then crushed to obtain its dry unconfined compressive strength (UCS). Two types of Schmidt hammer were used on large pieces of the rock from which the cores were obtained.

Several graphs have been plotted using the data shown in Table 7.1 and are listed below;

a) e_n against dry density (Figure 7.4)
b) e_n against Unconfined compressive strength (Figure 7.5)
c) e_n against Schmidt hammer number (Figure 7.6)
d) e_n against Type P Schmidt hammer number (Figure 7.7)
e) e_n against PUNDIT pulse velocity (Figure 7.8)

Disc Material	e_n	Dry Density (Mg/m^3)	Unconfined Compressive Strength MPa	Schmidt hammer No.	Type P Schmidt hammer No.	PUNDIT Pulse velocity (m/s)
Mortar	0.47	1.759	6.55			2.054
Red Sandstone	0.6	2.137	55	39	126	2.511
Buff Sandstone	0.61	2.189	67.4	49.5	130	2.594
Grey Sandstone	0.62	2.398	84.8	53.9	134	2.6
Magnesian Limestone	0.66	2.415	36.8	51.8	122	1.354
Marble	0.7	2.592	135			4.537
Limestone	0.73	2.566	188			5.506

Table 7.1: Normal coefficients of restitution for various rock types.

With reference to Figure 7.4, there appears to be a good linear correlation between e_n and the dry density of the rock. This is an important observation since the determination of the dry density of the rock is straightforward and would potentially allow an engineer to estimate the normal coefficient of restitution for any rock type.

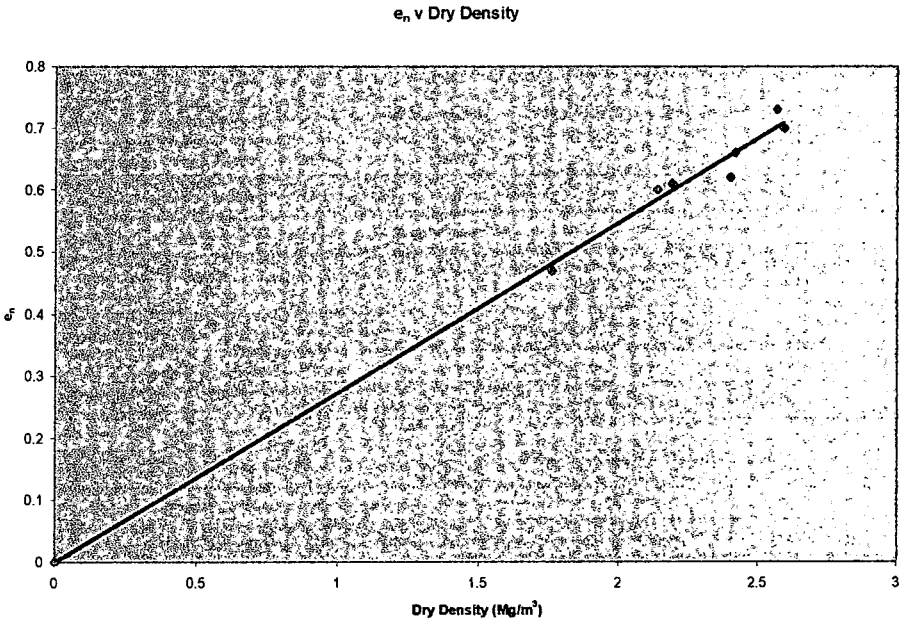

Figure 7.4 e_n against dry density.

There also appears to be a linear relationship between e_n and the unconfined compressive strength for rocks stronger than approximately 20 MPa (Figure 7.5). Below this value the normal coefficient of restitution drops off rapidly. The only anomalous value is that of the Magnesian Limestone which was heavily laminated and contained bands of soft clay. The disc tested on the air table was cored from a hard piece of the Magnesian Limestone and if the UCS core was of this harder material the UCS value would have theoretically been much higher.

Figure 7.6 shows that there is a possible linear correlation between the type P Schmidt hammer number and e_n. The anomalous value is from the Magnesian Limestone, which tended to break along the laminations when tested with the hammer. If a larger piece, of the same hardness as the disc were tested with the hammer then it would have produced a much higher rebound value.

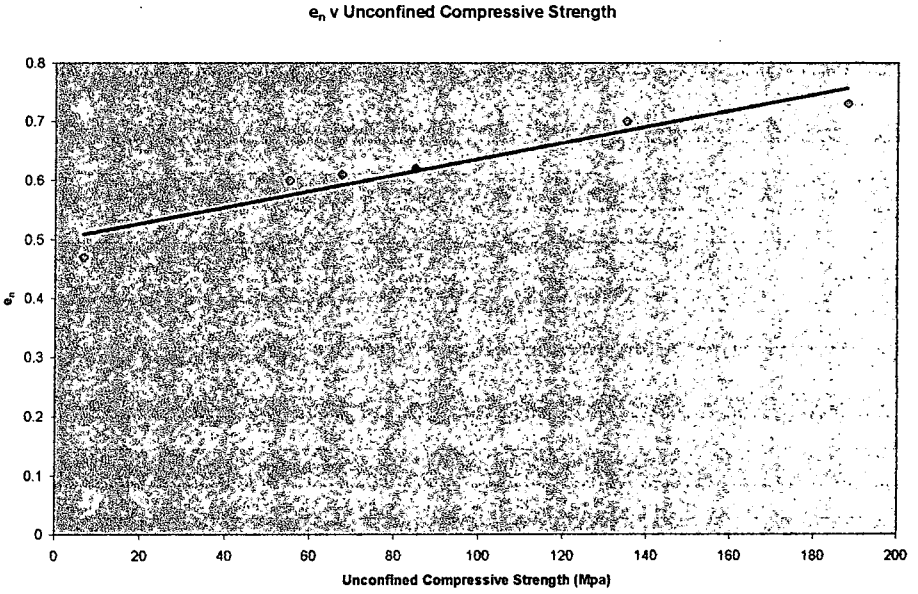

Figure 7.5: e_n against Unconfined Compressive Strength.

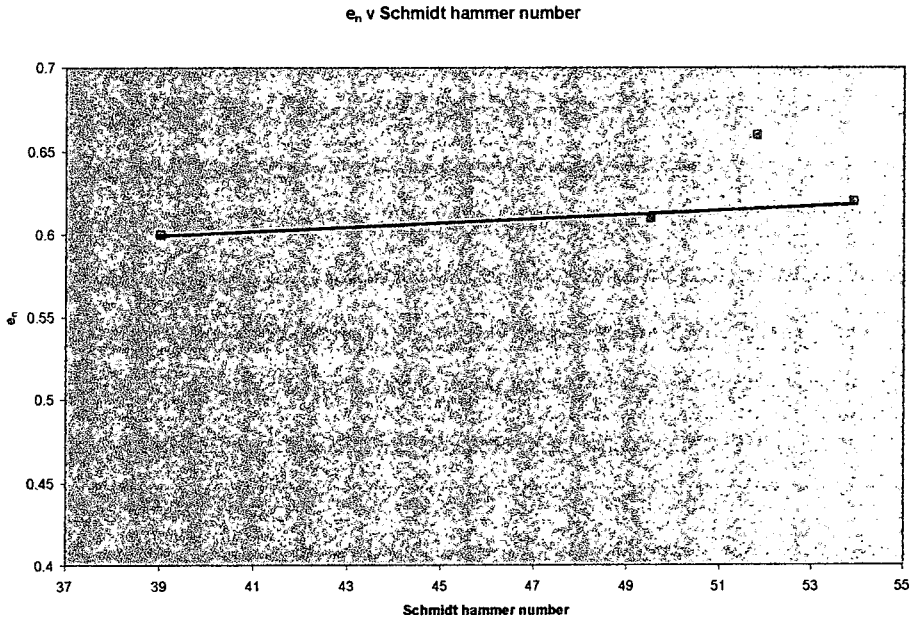

Figure 7.6. e_n against Schmidt hammer number.

Figure 7.7 shows a similar relationship to that shown in Figure 7.6, again the anomalous value is from the Magnesian Limestone.

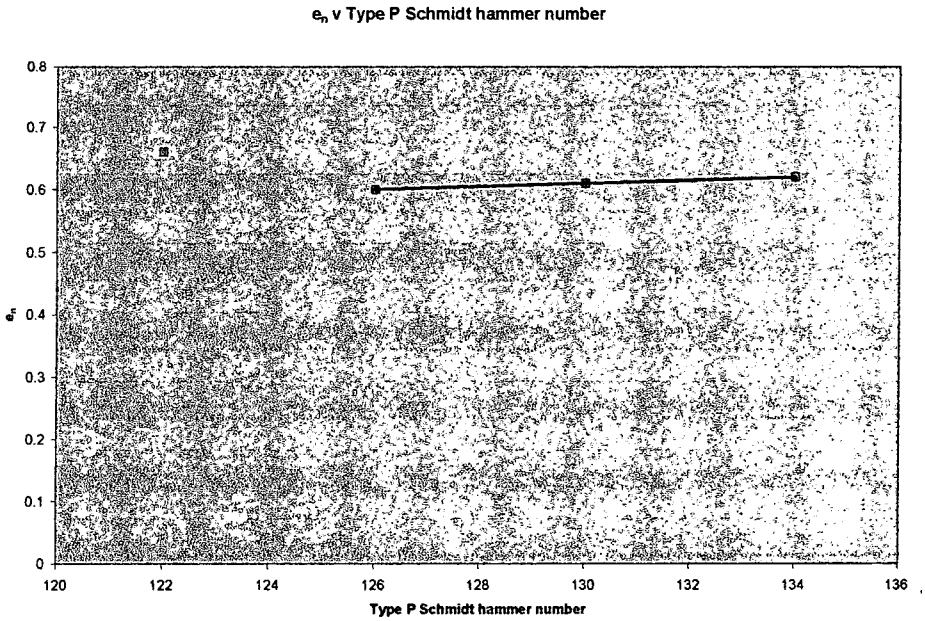

Figure 7.7. e_n against Type P Schmidt hammer number.

From the available data it would appear that there is a tentative linear relationship between e_n and the PUNDIT pulse velocity (Figure 7.8). The anomalous point is from the Magnesian Limestone. It is highly likely that the pulse velocity was low due to the laminated nature of the rock and that a core composed of the harder Magnesian Limestone would have produced a much higher pulse velocity.

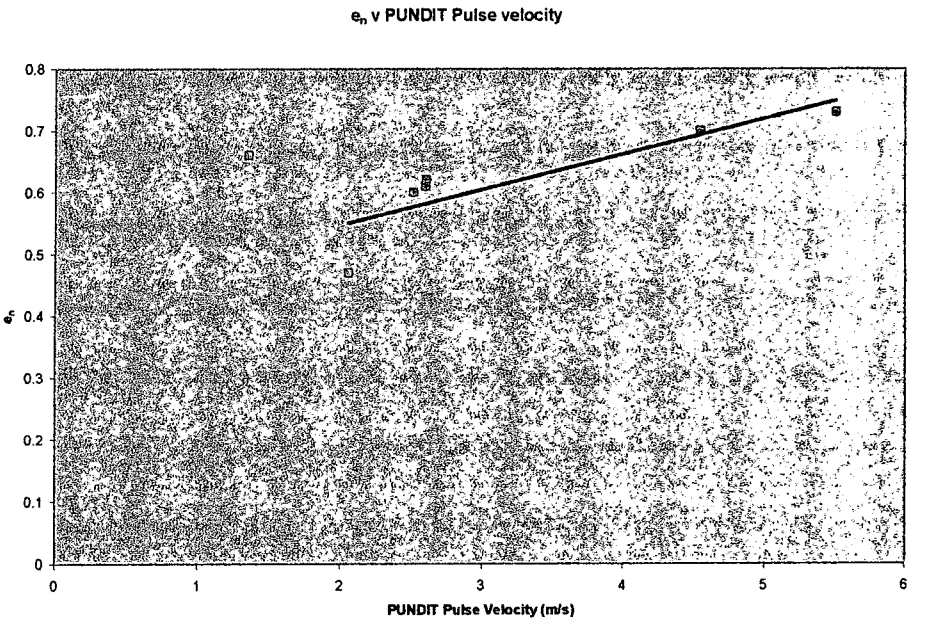

Figure 7.8: e_n against PUNDIT pulse velocity.

7.5 The Tangential coefficient of restitution e_t

The calculation for the tangential coefficient of restitution is more complex than that of the normal coefficient of restitution since the pre and post tangential impact distances must be scaled to actual size and the post impact angular velocity Ω also measured off the screen using a protractor. To eliminate the need to scale to actual size the height of the video camera was set such that the size of the grid as viewed on the playback screen measured exactly 20mm. All subsequent distance measurements off the screen were thus at actual size. Because of the time involved, the coefficient of tangential restitution was only calculated for the buff sandstone.

To calculate the tangential coefficient of restitution a disc of rock was fired at a large flat immobile piece of the same rock material at angles of incidence α, of 10°, 20°, 30°, 45°, 60° and 75° without spin as illustrated in Figure 7.9.

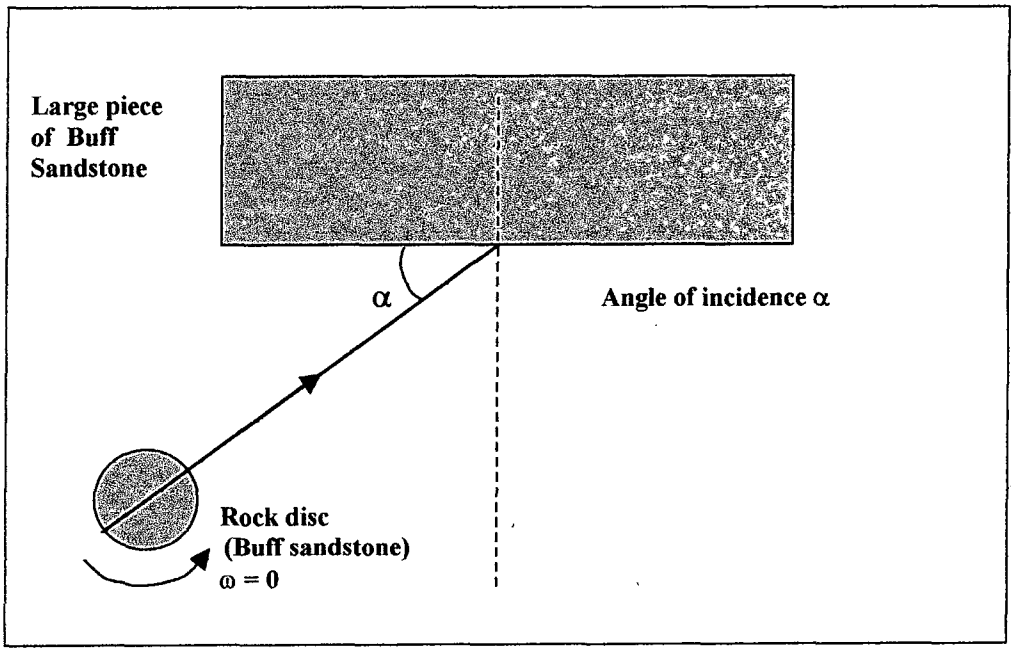

Figure 7.9: Plan view of the air table.

The tangential coefficient of restitution e_t for a circular rock of radius r having no initial angular velocity ω may be derived from Equation 5.42 to give,

$$e_t = \frac{\Omega r - V_t}{-v_t} \qquad 7.2$$

The angular velocity Ω has been plotted against the pre impact tangential velocity v_t and absolute velocity v_{abs} to determine the effects of the pre impact velocities on the post impact spin. The results of these tests are shown in Figures 7.10 and 7.11. Both graphs show that for a given angle of incidence the angular velocity Ω is directly proportional to v_t and v_{abs}.

For the graph shown in Figure 7.10 the greater the angle of incidence the greater the angular velocity Ω for a given tangential velocity v_t. Increasing the angle of incidence above 60° however causes no further increase in angular velocity for a given tangential velocity v_t.

For the graph shown in Figure 7.11 the angular velocity Ω increases with angle of incidence for a given value of tangential velocity v_t up to a maximum of 45°. Increasing the angle of incidence further causes a reduction in the angular velocity. The results for an angle of incidence of 60° closely correspond to those of 20° and those of 10° to those of 75°.

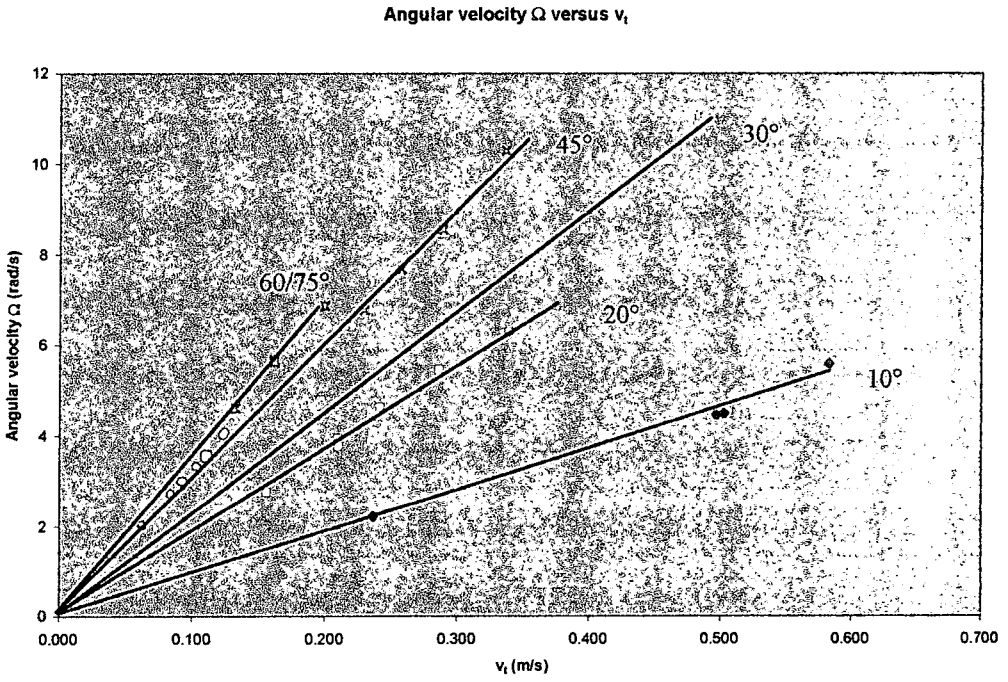

Figure 7.10: Angular velocity Ω against tangential velocity v_t.

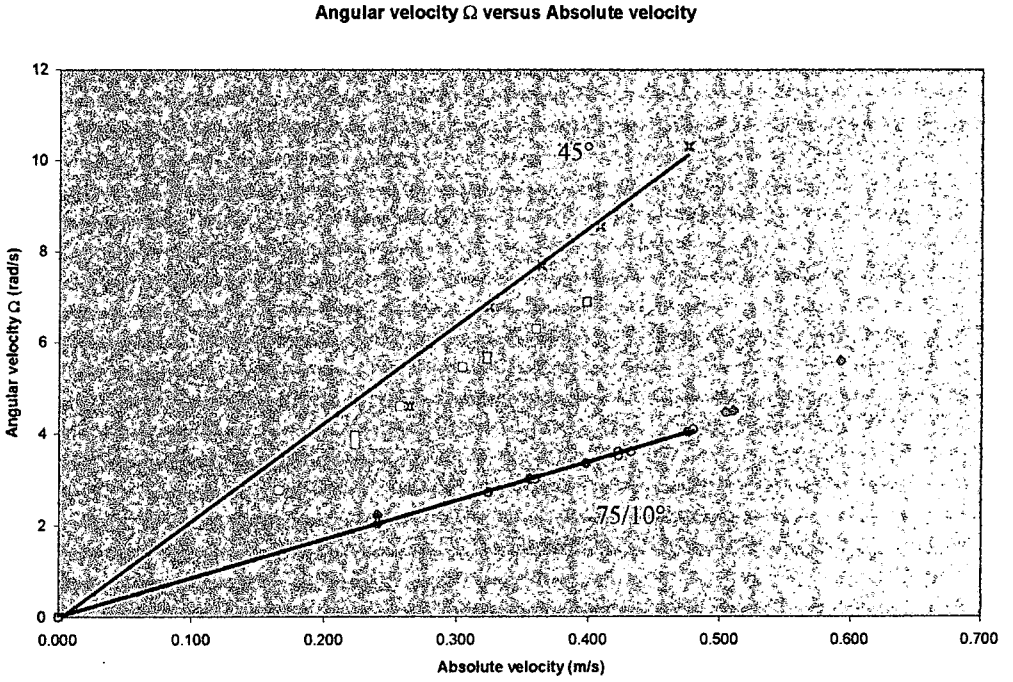

Figure 7.11: Angular velocity Ω against absolute velocity v_{abs}.

The tangential coefficient of restitution has been plotted against the angle of incidence, α and is presented in Figure 7.12.

Of importance is the fact that the tangential coefficient of restitution is not constant but varies in this case with the angle of incidence. The tangential coefficient of restitution changes from negative values at low angles of incidence to positive values at angle of incidence greater than 32°, reaching a peak value at approximately 60°.

In an attempt to explain the reason why the tangential coefficient of restitution varies with angle of incidence the final and initial velocities of the point of contact, V_{ct} and v_{ct} were calculated.

$$V_{ct} = V_t - \Omega r \qquad \textbf{7.3}$$

$$v_{ct} = v_t - \omega r \qquad \textbf{7.4}$$

A graph of e_t against v_{ct} has been plotted for the various angle of incidence and is shown in Figure 7.13.

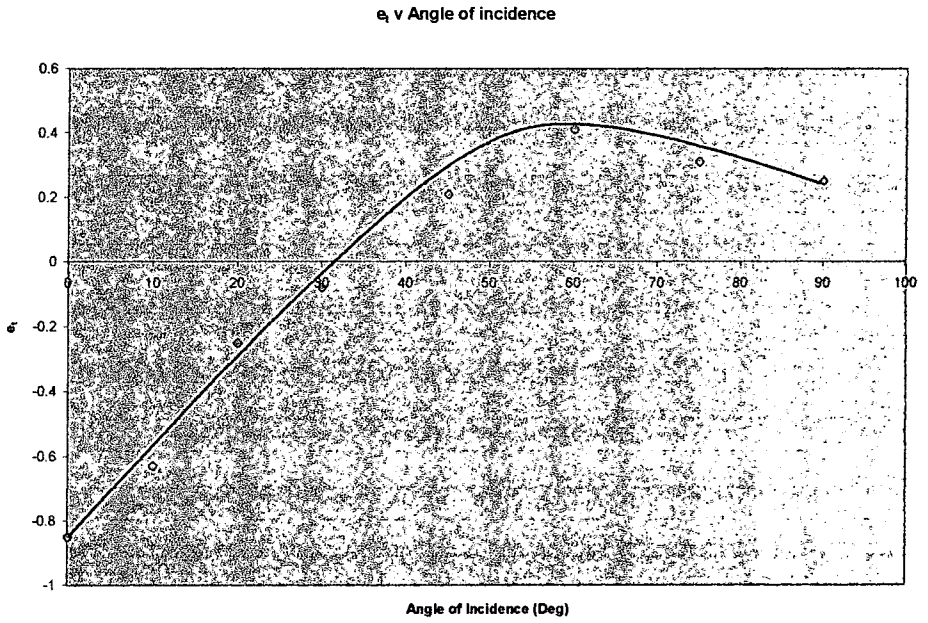

Figure 7.12: e_t against angle of incidence α.

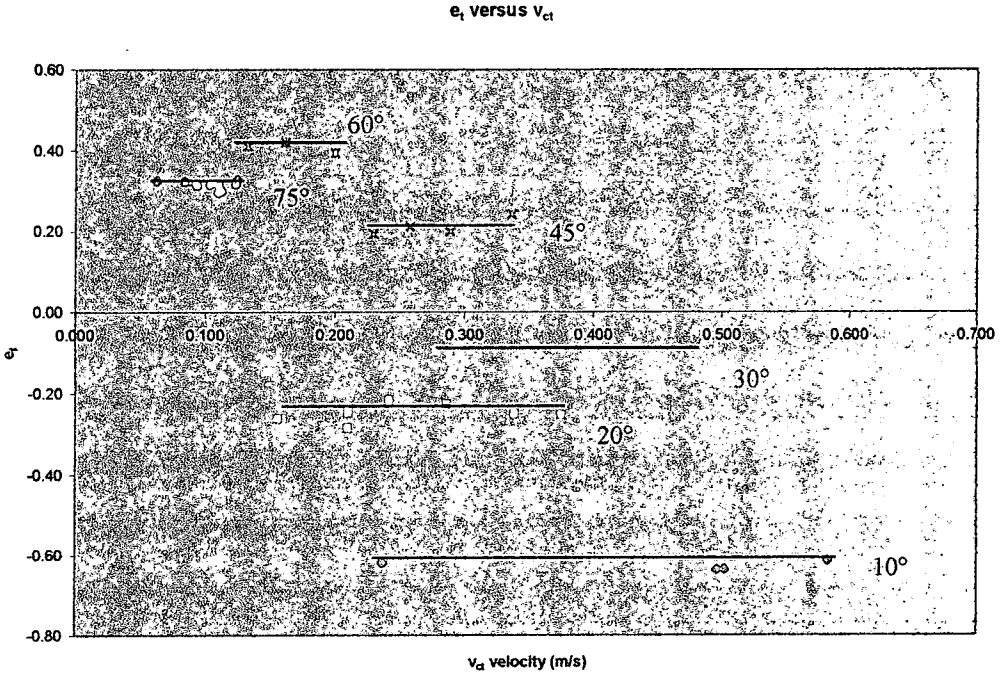

Figure 7.13: e_t against v_{ct}.

The coefficient of tangential restitution is constant for a given angle of incidence regardless of the tip velocity v_{ct}. The tangential coefficient of restitution reaches a maximum value at an angle of incidence of 60°. Increasing the angle of incidence above 60° causes a drop in e_t which has also been illustrated in Figure 7.12.

A graph of the final and initial tangential velocities of the point of contact V_{ct} and v_{ct} respectively, each divided by the initial normal velocity v_n is illustrated in Figure 7.14. The resultant curve produced is very similar to one illustrated in Brach (1991). The point at which the curve cuts the x axis defines the point at which sliding continues through separation and is an important observation. The gradient of the curve gives the tangential coefficient of restitution. As the angle of incidence approaches 0° the gradient approaches -0.84, hence the tangential coefficient of restitution is approximately -0.84 at 0°. Similarly as the angle of incidence approaches 90° the gradient of the line approaches 0.28, hence the tangential coefficient of restitution is 0.28 at 90°.

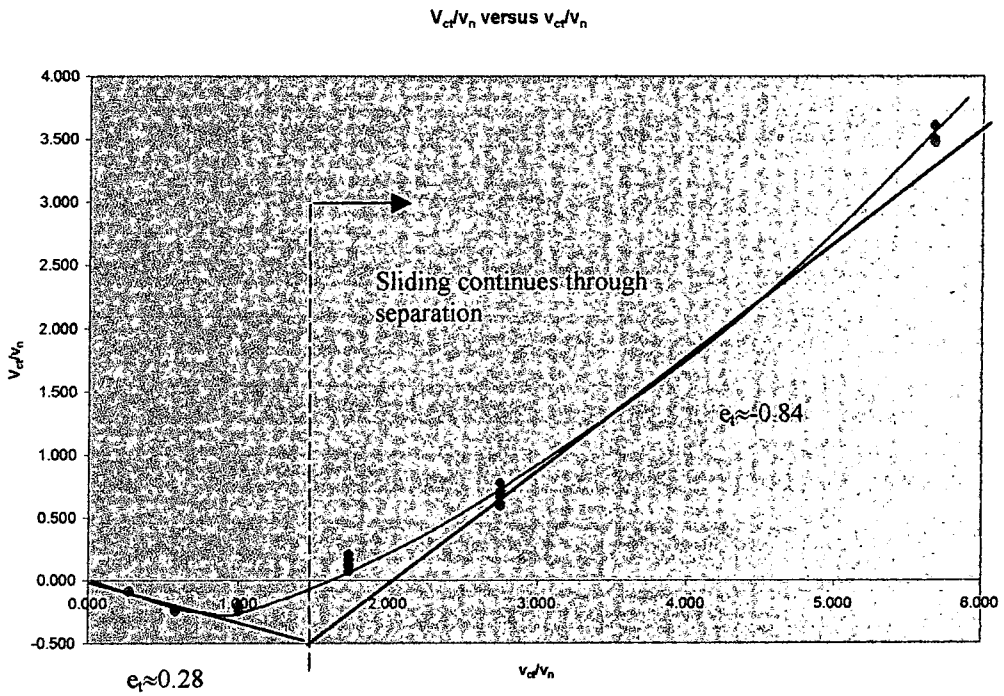

Figure 7.14: V_{ct}/v_n against v_{ct}/v_n.

These two values of e_t are hypothetical and can only be confirmed by firing a disc of rock at either 0° or 90° with a known angular velocity ω, the resultant velocities V_t and Ω measured and the tangential coefficient of restitution determined. This however is not possible with the equipment available.

7.6 Further work

Of benefit would have been apparatus that allowed a rock disc to be fired at high velocity such that the velocity or energy needed to fracture the disc could be determined. A relationship between the mass, impact energy and Unconfined Compressive Strength (UCS) could possibly have been established. This would have been advantageous since the mechanics of rock fracture and fragmentation are largely unknown.

The normal coefficients of restitution presented are for dry rock discs striking a fixed piece of the same rock type. If the rocks were tested by firing them at a dissimilar material then the change in the value of the coefficient of restitution could have been noted.

A limited range of rocks has been tested and it would be beneficial if a larger range of rock materials were tested including several igneous rock specimens.

Some tentative correlations between the normal coefficient of restitution and two types of Schmidt hammer number, the UCS of the rock, the dry density and the PUNDIT pulse velocity have been presented. It would be advantageous if these correlations could be firmly established by further testing.

The tangential coefficient of restitution was only determined for the buff sandstone due to the amount of time necessary to perform the test. Of particular note is the fact that the tangential coefficient of restitution is not a constant but varies with the angle of incidence when the disc is fired with no spin. It would have been beneficial to have fired the buff sandstone disc with different amounts of spin for a given angle of incidence. Thus a relationship between the angle of incidence, tip velocity v_{ct}, pre impact spin ω, and post impact spin Ω could have been established.

Chapter 8

Discussion

8 Discussion

This chapter presents an overall discussion of rock fall simulation programs, the importance of the choice of input parameters used and the interpretation of the program output. In particular the limitations of the rock fall simulation program GeoFall and the use of the Rock Fall Risk Assessment System (RFRAS) to determine rock fall risk have been discussed. Finally the method of determining coefficients of restitution using the air table has been discussed and the validity and interpretation of results appraised.

8.1 Rock fall simulation programs

All rock fall simulation programs have the potential to be invaluable design tools but engineering judgement and common sense must be used in the choice of the input data values and the interpretation of the program output. Since the output of the program is absolutely dependent upon the quality of the input data, it is essential that the program user is familiar with how the slope surface morphology affects the input parameters, and the formulation of the programs algorithms.

Both the normal and tangential coefficients of restitution are velocity dependent since higher impact velocities usually result in fragmentation of the rock and deformation, fracture or crushing of the slope surface material upon impact. In addition, coefficients of restitution presented in the literature generally correspond to a boulder striking a slope of the same material. It is important that the coefficients of restitution are chosen based on not only the slope surface material but also the material of the rock. If fragmentation of the rock is likely then the coefficients of restitution must be reduced to account for the additional energy loss involved in such an impact

Rolling resistance is dependant on the specific size of the rock compared with that of the slope roughness. If the slope surface is very rough and the rock is small in comparison with the surface irregularities then it is very likely that the rock will become lodged within the surface material. It has been demonstrated by Azzoni et al. (1995) that the smaller the rock is the greater the rolling resistance for any given irregular surface.

In a similar manner to that of rolling, the sliding resistance is also dependent upon the size of the rock in relation to the size of the surface irregularities.

For most cases, a 2D analysis is acceptable since it allows simulations to be run with the minimum quantity of input data. The slope cross section can be measured by levelling the slope or by measurement of contour lines on a map. The input data required for a 2D analysis is straightforward and comparatively simple to obtain. All existing 2D programs assume that there is no lateral variation in the slope profile.

A 3D analysis is usually only warranted if there is a significant lateral variation in the slope. It is possible to modify a 2D profile to account for lateral variation by using a cross section based on the estimated rock fall path rather than a simple straight cross section through the slope. This requires running several simulations and modifying the chosen slope cross section accordingly. With a 3D analysis, the amount of input data is increased greatly and in most cases, it is not worth the additional time and cost involved in collecting this data. At present there are no 3D programs that can model a rock of any arbitrary shape although one is being developed by Laboratoire IMIGIS (Leroi et al, 1996).

GeoFall was developed by the author to overcome the shortcomings of existing rock fall simulation programs. It is a general two-dimensional rock fall simulation program, which was developed over a period of approximately 14 months. The various motions of the rock are linked to form complete rock fall paths, and the rock is assumed to behave as a rigid body that remains intact during rock fall. Any slope geometry may be modelled including re-entrants and closed profiles such as caverns. Various rock fall shapes are permitted which include a sphere, disc, ellipse, and several polygonal shapes. The user may also generate any rock shape of their choosing. Translational and rotational velocities after impact are related to those before impact by coefficients of normal and tangential restitution. Rolling and sliding are also modelled by a coefficient of rolling resistance and friction, a combination roll-slide is not possible and rocks may only slide on one surface. Surface roughness is set by randomly varying the angle of the slope. Kinetic energy, velocity, bounce height envelopes and the rock fall distribution are all determined by the program at slope locations pre set by the user. The effectiveness of user defined rock fall nets may also be determined.

GeoFall is for the most part an amalgamation of the better aspects of each program that have previously been reviewed and tested. It was intended that GeoFall could be used as a design tool and as such, it was important that the program could model the effects of rock fall nets upon trajectories, something that previous programs could not do. Tumble is the only program that can model irregular shaped rocks but in testing it was shown to be unreliable, prone to error and is now unavailable to the public. None of the programs except ROXIM are capable of modelling closed slope profiles or re-entrant corners. The algorithms in GeoFall are such that slopes of any geometry may be modelled. All of the previously reviewed programs are DOS based with the exception of Rocscience. All of the DOS programs have a non-user friendly interface and therefore, Windows was chosen as the operating system for GeoFall since it is more user friendly and intuitive than DOS. Many of the existing programs use impact algorithms that are strictly only applicable to regular shapes such as discs or spheres. A new consistent theory of impact dynamics was needed in order to model the impacts of irregular rocks that may be created in GeoFall. The equations presented by Brach (1991) allow such impacts to be modelled.

At present, the slope profile can only be described by a maximum number of fifty nodes. The user may chose from 13 standard geometrical rock shapes or a customised rock defined by a maximum number of thirty nodes. A maximum of 5 analysis points and 10 rock fall nets may be placed on the slope. These default settings may only be changed by modifying the programs source code and interface. These settings have been chosen on the basis that they are very unlikely to be exceeded by the user. The greater they become the slower the program will execute. The time taken to input the parameters would also become excessive. It is possible to change these settings but in most instances, it would require not only modification of the program code but also the interface. The exception to this is the maximum number of thirty nodes that can be used to define a customised irregular polygonal rock shape. The maximum number of nodes is set by the array size and is relatively easy to change. It is considered that thirty points are more than adequate and that further refinement of the rock shape would be of little or no benefit.

Whilst GeoFall can model projectile, rolling and sliding motion it is incapable of modelling rotation whilst sliding. This type of motion cannot be analysed without assuming that a certain amount of the total kinetic energy is lost due to sliding friction

whilst the remainder is transferred into rotational and translational kinetic energy. At present, it is not possible to model a rock that is sliding with two points of the rock perimeter in contact with the slope. It is also not possible to model sliding where a facet of the rock is in contact with two or more nodes of the slope. Sliding motion is thus restricted to one facet of the rock sliding along a single slope region. It is difficult to analyse sliding where more than one point of contact is present since two or more coefficients of sliding resistance are required. In addition, the rock may rotate whilst sliding, losing contact with one or more of the points of contact.

GeoFall cannot model fracture of the rock since it is impossible to predict when a rock will fracture, the shape of the resultant fragments and the kinetic energy of each fragment after impact. Fracture could possibly be modelled by assuming that fragmentation occurs when the pre impact kinetic energy or velocity exceeds a certain value. It would then be assumed that the rock would split into a set number of fragments each possessing a percentage of the post impact kinetic energy. This percentage could be based upon the mass of each fragment. The reason rock fragmentation has not been implemented into GeoFall is that the assumptions involved are unacceptable and highly inaccurate. An intact rock will generally travel further than a rock that has fragmented and will thus usually give the worst case scenario. As shown in the Argos simulation in section 6.6 this is not always the case since rounding of a rectangular rock will allow rotation at lower kinetic energies. Thus, the possible rounding effects due to fragmentation of corners of polygonal rocks must always be considered in a rock fall simulation.

The impacts in GeoFall are modelled using the 2D equations from Brach (1991) which uses separate coefficients of normal and tangential restitution. Brach allows the impact of any rigid body against a planar fixed barrier to be modelled. His theory is both straightforward to implement and consistent.

Brach has extended his theory of impact dynamics to that of three dimensions and the implementation of this would be relatively straightforward. Unfortunately, the impact algorithms described in section 5.3.11 would have to be completely rewritten to accommodate the change to 3D. The program interface would also need to be modified to accommodate the additional data required.

The parameters used in the GeoFall simulation are such that the programs use may be extended into other areas of research. GeoFall may be used to model an impact of any

rigid body of irregular shape provided that it does not fragment or deform on impact. For example, the program may be used to simulate a metal ball bearing striking a concrete surface.

It is essential that the algorithms used in GeoFall work correctly, since the output of the program may be used as a decision making tool for Geotechnical Engineers, and much time and effort was spent on this. The program was tested in two ways. Firstly, a numerical analysis was carried out to compare the computed trajectories with those calculated by hand. Secondly, GeoFall was used to model documented rock fall events in the hope that with a sensible choice of input parameters the rock trajectory could be recreated. The output from GeoFall has also been compared with those of programs written by other researchers in the field.

Several slopes were set up in GeoFall to model projectile, rolling and sliding motion, and by using the debugging tools included in Visual Basic the position and velocity could be measured for each advancement of the time step. The velocities after 20 time steps (0.2 seconds) were then compared to those calculated by hand. The motion of the rock has been tested for all possible directions of travel. All of the computer modelled cases agreed with those calculated by hand, proving that the projectile, rolling and sliding algorithms used in the program are error free.

GeoFall has been used to model a number of rock fall events described in several published papers, in order to determine its effectiveness in modelling real life rock fall events. Actual rock fall events described in several published papers were compared with the outcome of GeoFall and those of other rock fall simulation programs. GeoFall accurately predicted the trajectories of these published rock fall events. Where various researchers have used rock fall simulation programs to simulate the published cases, GeoFall has compared favourably with their output. It must be emphasised that when comparing the two programs, the coefficients of restitution chosen, rock shapes used, and the formulation of the programs may be different, thus accounting for any variation in the simulated trajectories. It has been shown that in the Argos, Dahekou and Glenwood Canyon simulations that GeoFall is a useful design tool for the installation and placement of rock fall nets.

GeoFall was written in Visual Basic 5 because the programming language is easy to learn and the program interface may be created quickly and easily. The main disadvantage to Visual Basic is that it is an interpreted language and is not compiled

in the same manner to that of say C++ or Fortran. The consequence of this is that Visual Basic programs are slower to execute than their C++ and Fortran counterparts, especially if the program is calculation intensive which rock fall simulation programs invariably are. If the algorithms of GeoFall were rewritten in a language such as Visual C++ then the program would look more professional and also execute faster. It was decided not to rewrite GeoFall in Visual C++ because the time it would have taken simply to improve the appearance and speed of the package. The remaining time available was spent in the development of the Rock Fall Risk Assessment System and the development of the air table to determine coefficients of restitution.

8.2 Rock slope inventory systems

Previous rock slope inventory systems have concentrated on the estimation of rock fall risk to highway users. The Rock Fall Risk Assessment System (RFRAS) was developed by the author to enable the practising engineer to assess the level of rock fall risk from any rock slope, not necessarily connected with a highway. Once the risk of rock fall has been determined then the slopes at high risk of rock fall may be modelled on a rock fall simulation program such as ROXIM, CRSP or GeoFall. The simulation program thus provides an accurate means of determining the consequences of a rock fall event whilst the RFRAS determines the likelihood of a rock fall event. If more than one rock slope is to be assessed then the rating obtained from the RFRAS provides a subjective comparison between slopes, allowing a cost and benefit analysis to be made so that limited funds may be allocated accordingly.

The RFRAS based upon the RHRS developed by Pierson (1992) consists of three phases of inspection, the slope survey, and the preliminary and detailed rating phases. The slope survey allows the engineer to divide the slope into zones of approximately uniform rock fall risk. Previous rock slope inventory systems have divided the slope laterally into areas of equal rock fall risk. This assumes that the rock fall risk is uniform over the height of the rock face. This assumption is unacceptable where there is a change in overlying strata or joint orientation. Thus, a rock fall zone allows the user to define an area of the rock face that has an approximately uniform risk of rock fall. The preliminary rating acts as a coarse sift so that the detailed rating system is not applied to sites with a low rock fall risk. Initially sites of high risk have the

detailed system applied to them and sites with a moderate rock fall risk have the detailed system applied to them only if time and resources allow. The scheme uses 13 parameters with an exponential scoring system based on five grades. Each parameter is assessed as one of these grades, which represent the degree of risk and are rated exponentially as 1, 3, 9, 27 and 81. The additional grade allows a greater variation in the overall total and distinguishes the relative risk between each parameter. The detailed rating system includes 13 parameters that when assessed, evaluated and totalled will numerically differentiate slope zones from the least to the most hazardous. The RFRAS produces an overall rating in the range 21-1296 and allows the relative risk of rock fall between slopes to be assessed. It also categorises the rock fall risk as either none, low, moderate, high, or very high and the potential number of future rock falls as none, few several, many or continual.

The RFRAS was tested on 18 slopes at ten sites in County Durham. The output was used to calibrate the RFRAS total rating (V_t) into bands of rock fall risk and likely number of future rock falls. For example, V_t totals in the range of 350-705 correspond to high rock fall risk and many rock falls are likely in the future. Due to the limited number and similar geology of slopes tested, these ranges must be taken as provisional. The more slopes that are assessed with the RFRAS the better the ranges of V_t will be defined. An intensive testing of the RFRAS on slopes of varying geology in different climates is necessary to accurately calibrate the system. This detailed calibration was not possible due to limitations in resources and time.

It would have been of benefit if the RFRAS could have been calibrated such that the probability of a rock fall occurring could be determined. The rock fall simulation program could be used to calculate a probability of the falling rock striking a transportation route. Thus, the probability of the rock fall occurring multiplied by the probability of a falling rock striking a transportation route would give an overall probability of this combined event occurring. This combined probability could then be multiplied by the probability of a vehicle, train or person being on the transportation route at the time of rock fall. This would give an indication of the degree of risk from falling rocks to users of the transportation route. If the risk was deemed to be unacceptable then the degree of risk may be reduced by methods such as relocation of the route, slope stabilisation or the instalment of protection measures.

8.3 Air table

A reliable and repeatable laboratory method has been developed by the author to determine coefficients of normal and tangential restitution. Discs of rock were cored and floated on a bed of air, which provided a frictionless surface. The discs were then fired, with no spin, at a large immobile piece of the same rock type, and the rock allowed to rebound. The pre and post impact velocities were recorded using video equipment, allowing the coefficients of restitution to be calculated using Brach's theory of impact dynamics outlined in section 5.3.12.

The main limitation of the air table was the quality of the video equipment used to record the rock trajectory. A significant improvement in the accuracy of results would have been achieved if a high-speed camera linked to digitisation software were available. Unfortunately such equipment is very expensive.

Another limitation was the usable surface area of the air table. Masking tape was placed on a significant portion of the air table to increase the airflow through the uncovered surface. The increased flow rate provided greater uplift for the rock discs but restricted the distances they could travel on the air table surface.

Of benefit would have been apparatus that allowed a rock disc to be fired at high velocity such that the velocity or energy needed to fracture the disc could be determined. A relationship between the mass, impact energy and Unconfined Compressive Strength (UCS) could have possibly been established. This would have been advantageous since the mechanics of rock fracture and fragmentation are largely unknown.

The values presented for the coefficients of normal restitution (e_n) form an upper bound and in practice, the normal coefficient of restitution will be lower than those measured using the air table, due to fragmentation of the rock and deformation, fracture or crushing of the slope surface material upon impact. It is therefore not advisable to use these coefficients in a rock fall simulation program since they will be unrealistically high. Conversely, the parameters chosen for the simulation program should not exceed these upper bound values.

The normal coefficients of restitution presented are for dry rock discs striking a fixed piece of the same rock type. It is anticipated that a porous wet rock would have a lower coefficient of normal and tangential restitution since the fluid trapped in the

pores would act as a damper. The Unconfined Compressive Strength (UCS) of a rock reduces as the water content increases, therefore crushing or fracture of a wet porous rock is more likely than that of a dry porous rock. If the rocks were tested by firing them at a dissimilar material then the change in the value of the coefficient of restitution could have been noted. However, this was not done due to time constraints. A limited range of rocks has been tested and it would be beneficial if a larger range of rock materials were tested including several igneous rock specimens.

Some tentative correlations between the normal coefficient of restitution and two types of Schmidt hammer number, the UCS of the rock, the dry density and the PUNDIT pulse velocity have been presented. It would be advantageous if these correlations could be firmly established by further testing. If a reliable correlation can be established, the coefficient of normal restitution of a rock may be estimated through a simple, repeatable site or laboratory test.

The tangential coefficient of restitution was only determined for the buff sandstone due to the amount of time necessary to perform the test. Of particular note is the fact that the tangential coefficient of restitution is not a constant but varies with the angle of incidence when the disc is fired with no spin. The variation of the tangential coefficient of restitution was due to the transition of the rock from a retarding motion to that of sliding through separation which occurred at low angles of incidence. It is possible that only smooth disc shaped rocks striking a smooth surface at low angles of incidence are likely to slide through separation. Most rocks striking a rough rock slope are less likely to slide through separation due to the high friction at the point of contact. It is possible that in this situation the rocks will have a positive coefficient of tangential restitution. It has been shown using the air table that there is significantly less variation in the value of the tangential coefficient of restitution where it is positive in value. It is possible that for irregular rocks striking an irregular surface that the tangential coefficient of restitution is constant for any angle of incidence providing that the rock does not slide through separation.

It would have been beneficial to have fired the buff sandstone disc with different amounts of spin for a given angle of incidence, thus a relationship between the angle of incidence, tip velocity v_{ct}, pre impact spin ω, and post impact spin Ω could have been established. This however was not possible with the equipment available. All rock fall programs including GeoFall assume that the coefficient of tangential

restitution is constant. However, from the experimental evidence gained from using the air table it has been shown that this is not the case. It is therefore vital that a relationship between the tangential coefficient of restitution, the pre impact spin, ω and the post impact spin, Ω is established.

8.4 Rock Fall

The development of rock slope inventory systems has led to a method of determining rock fall risk to a highway user. The Rock Fall Risk Assessment System (RFRAS) was developed to assess the level of rock fall risk from any rock slope. Once the risk of rock fall has been determined using the RFRAS then slopes at high risk may be modelled on a computer simulation program such as GeoFall. The likelihood of a falling rock striking the highway, railway, footpath, house or other structure is determined by the rock fall simulation program. The likelihood of a rock fall occurring and the falling rock striking or encroaching on a structure are thus differentiated. The RFRAS determines the likelihood of a rock fall, whilst the simulation program determines whether this rock fall event is of concern. The program may then be used to determine the optimum position and capacity of protection nets in order to reduce the rock fall risk to an acceptable level. In some cases the rock fall may be of such magnitude that rock fall nets are inappropriate and as such the slope may need to be stabilised by reinforcement and rock removal methods. The overall stability of such slopes is determined using stereoscopic projection and planar and wedge failure analyses. The use of parameters determined from using an air table may be incorporated into the simulation program providing that some correction is made for the possibility of deformation, fracture or crushing of the slope material. The exact rock and slope material may be tested on the air table and as such an accurate upper bound for the normal coefficient of restitution may be determined.

Chapter 9

Conclusion and Recommendations for Further Work

9 Conclusions and Recommendations for Further Work

9.1 Overview

A general two-dimensional rock fall simulation program entitled GeoFall was developed by the author to overcome the shortcomings of existing rock fall simulation programs. A rock slope inventory system entitled the Rock Fall Risk Assessment System (RFRAS) has been developed by the author in order to determine the relative risk of rock fall between various sites and also to determine the likely number of future rock falls and the rock fall risk at any given site. A laboratory based method using an air table to float discs of rock on a bed of air was developed by the author to determine coefficients of restitution for several rock types.

9.2 GeoFall

GeoFall allows trajectories for any rock shape to be simulated on computer. The user defined rock shape may consist of up to thirty nodes joined in a linear piecewise manner. Several standard geometrical shapes such as spheres, discs, ellipses, rectangles, triangles and polygons may also be chosen. Any type of slope geometry may be modelled including re-entrant corners and closed profiles such as caverns. This combination of features is not available in any other currently available rock fall simulation program.

Projectile, rolling and sliding motion are linked to form complete rock fall paths, and the rock is assumed to behave as a rigid body that remains intact during rock fall. The impacts in GeoFall are modelled using the 2D equations from Brach (1991) which use separate coefficients of normal and tangential restitution. The equations presented by Brach allow impacts of any rock shape against an immovable planar barrier to be modelled. Rolling and sliding are also modelled by a coefficient of rolling resistance and friction respectively. Surface roughness is set by randomly varying the angle of the slope at the point of impact in the form of a ledge. Up to 10 rock fall protection nets may be placed on the slope. The net capacity may be one of three commercially available nets produced by GeoBrugg or defined by the user. The use of analysis points and the output histograms allows the user to determine optimum net capacities.

The rock fall protection net may be placed in the optimum position by examination of the rock fall trajectories.

Projectile, rolling and sliding motion of the rock have been tested for all possible directions of travel. All of the computer modelled cases agreed with those calculated by hand, proving that the projectile, rolling and sliding algorithms used in the program are error free. The program has also been tested throughout development and subjected to extreme conditions in order to test its robustness.

GeoFall has been used to model a number of rock fall events described in several published papers. GeoFall accurately predicted the trajectories of these published rock fall events. Where various researchers have used rock fall simulation programs to simulate the published cases, GeoFall has compared favourably with their output. It has been shown that in the Argos, Dahekou and Glenwood Canyon simulations GeoFall is a useful design tool for the installation and placement of rock fall nets.

GeoFall has proven to be robust and is intended to be user friendly.

9.3 The Rock Fall Risk Assessment System

The RFRAS provides a subjective comparison between slopes, allowing a cost and benefit analysis to be made so that funds may be allocated accordingly. It consists of three phases of inspection, the slope survey, and the preliminary and detailed rating phases. The slope survey allows the engineer to divide the slope into zones of approximately uniform rock fall risk. The preliminary rating acts as a coarse sift. The detailed rating phase uses 13 parameters with an exponential scoring system based on five grades. The parameters when assessed, evaluated and totalled produce an overall rating in the range 21-1296. It categorises the rock fall risk as either none, low, moderate, high, or very high and the potential number of future rock falls as none, few several, many or continual.

The RFRAS was tested on 18 slopes at ten sites in County Durham and the output data was used to calibrate the RFRAS total (V_t) into bands of rock fall risk and likely number of future rock falls.

A computer program entitled GeoRisk has been written in Visual Basic 5 to simplify the calculation of the final RFRAS total (V_t). It also determines the number of likely future rock falls and the rock fall risk.

9.4 Air table

By using an air table to float discs of various rock materials on a bed of air and using video equipment to film the impact it was possible to determine the coefficients of restitution. The normal coefficient of restitution was calculated for a cement mortar, three types of sandstone, two types of limestone and a marble. The tangential coefficient of restitution for a buff sandstone was determined for different angles of incidence. The values of the normal coefficient of restitution form an upper bound and in practice, the values will be lower due to fragmentation of the rock and deformation, fracture or crushing of the slope surface material upon impact.

9.5 Recommendations for Further Work

9.5.1 GeoFall

Whilst GeoFall can model projectile, rolling and sliding motion it is incapable of modelling rotation whilst sliding. This type of motion cannot be analysed without assuming that a certain amount of the total kinetic energy is lost due to sliding friction whilst the remainder is transferred into rotational and translational kinetic energy. At present, it is not possible to model a rock that is sliding with two points of the rock perimeter in contact with the slope. It is also not possible to model sliding where a facet of the rock is in contact with two or more nodes of the slope. Sliding motion is thus restricted to one facet of the rock sliding along a single slope region. It is difficult to analyse sliding where more than one point of contact is present since two or more coefficients of sliding resistance are required. In addition, the rock may rotate whilst sliding, losing contact with one or more of the points of contact. A useful addition to the program would be an algorithm that allowed a combination of rolling and sliding to be modelled.

GeoFall cannot model fracture of the rock since it is presently not possible to predict when a rock will fracture, the shape of the resultant fragments or the kinetic energy of each fragment after impact. This could be implemented into the program if the mechanics of rock fragmentation were better understood. More research into this field of study is thus necessary.

Rewriting GeoFall in C++ would allow a more professional interface to be developed and the code would execute faster. The program could then be made commercially available.

9.5.2 The Rock Fall Risk Assessment System

The calibration of GeoFall is based on the output of field tests carried out on eighteen slopes. The more slopes that are assessed with the RFRAS the better the ranges of V_t will be defined and the greater the accuracy of calibration. An intensive testing of the RFRAS on slopes of varying geology in different climates is necessary to accurately calibrate the system.

9.5.3 Air table

Of benefit would have been apparatus that allowed a rock disc to be fired at high velocity such that the velocity or energy needed to fracture the disc could be determined. A relationship between the mass, impact energy and Unconfined Compressive Strength (UCS) could have possibly been established.

The normal coefficients of restitution presented are for dry rock discs striking a fixed piece of the same rock type. If the rocks were tested by firing them at a dissimilar material then the change in the value of the coefficient of restitution could have been noted.

A limited range of rocks has been tested and it would be beneficial if a larger range of rock materials were tested including several igneous rock specimens.

Some tentative correlations between the normal coefficient of restitution and two types of Schmidt hammer number, the UCS of the rock, the dry density and the PUNDIT pulse velocity have been presented. It would be advantageous if these correlations could be firmly established by further testing.

The tangential coefficient of restitution was only determined for the buff sandstone due to the amount of time necessary to perform the test. Of particular note is the fact that the tangential coefficient of restitution is not a constant but varies with the angle of incidence when the disc is fired with no spin. It would have been beneficial to have fired the buff sandstone disc with different amounts of spin for a given angle of

incidence, thus a relationship between the angle of incidence, tip velocity v_{ct}, pre impact spin ω, and post impact spin Ω could have been established.

References

References

AASHTO, 1990, A policy on the geometric design of highways and streets, *American Society of Highway and Transportation Officials*, Washington DC.

Azzoni A, Rossi P.P, Drigo E, Giani G.P. & Zaninetti A, 1991, In-situ observation of rock fall analysis parameters, *Landslides*, (Ed. Senneset K.P.), Balkema, Rotterdam, 307-313

Azzoni A, La Barbera G. & Zaninetti A, 1995, Analysis and prediction of rock falls using a mathematical model, *International Journal of Rock Mechanics and Mining Science*, Vol. 32, No. 7, 709-724

Badger T.C. & Lowell S.M, 1992, Rock fall control in Washington State, Rock fall prediction and control and landslide case histories, *Transportation Research Record* 1343, 14-29

Bjerrum L. & Jorstad F.A, 1968, Stability of rock slopes in Norway, *Norwegian Geotechnical Institute*, Oslo, Publ. 79, 11

Bozzolo D. & Pamini R, 1982, Modello mathematico per lo studio della dei messi, laboratorio di fisica terrestre, *Dip. Publication Educasione*, Lugano

Bozzolo D. & Pamini R, 1986, Simulation of rock falls down a valley side, *Acta Mechanica,* Vol. 63, 113-130

Brach R.M, 1991, Mechanical impact dynamics: rigid body collisions, *Wiley Interscience Publications, New York*

Brawner C.O. & Wyllie D, 1975, Rock Slope Stability on Railway Projects, *Proceedings of the American Railway Engineering Association Regional Meeting.* Vancouver, British Colombia

Bunce C.M, Cruden D.M. & Morgenstern N.R, 1997, Assessment of the hazard of rock fall on a highway, *Canadian Geotechnical Journal*, Vol. 34, 344-356

CAN/CSA, 1991, Risk analysis requirements and guidelines, *Canadian Standards Association*, Q 634-91

Carpmael R.M.C, 1995, The study of impact, *Final Year Project Report*, University of Durham, UK

Chan Y.C, Chan C.F, and Au S.W.C, 1986, Design of a boulder fence in Hong Kong, *Proceedings of the Conference on Rock Engineering and Excavation in an Urban Environment held in Hong Kong, Institution of Mining and Metallurgy*, London, 87-96

Chau K.T, Wong R.H.C & Lee C.F, 1988, Rock fall problems in Hong Kong and some new experimental results for coefficients of restitution, *International Journal of Rock Mechanics and Mining Science*, Vol. 35, No 4/5, 662-663

Croft T & Hart D, 1988, Modelling with projectiles, *Halstead Press, New York*

Cundall P.A, 1971, A computer model for simulating progressive, large scale movements in blocky rock systems, *International Society of Rock Mechanics Symposium on Rock Fracture*, Nancy, Paper 11-8

Descoudres F. & Zimmerman H, 1987, Three dimensional calculation of rock falls, *Proceedings of the Sixth International Congress on Rock Mechanics*, Montreal, Vol. 1, 555-560

Douglas G.R, 1980, Magnitude frequency study of rock fall in Co. Antrim, N.Ireland, *Earth Surface Processes*, Vol. 5, 123-129

Falcetta J.L, 1985, Un nouveau modele de calcul de trajectoires de blocs rocheux, *Revue Francoise de Geotechnique*, Vol. 30, 11-17

Fookes P.G. & Sweeny M, 1976, Stabilisation and control of local rock falls and degrading rock slopes. *Quarterly Journal of Engineering Geology*, 1976, Vol. 9, 27-55

Fornaro M, Peila D. & Nebbia M, 1990, *Sixth International IAEG congress*, Balkema, Rotterdam, 2173-2180

Franklin J.A. & Senior S.A, 1997, RHRON: The Ontario Rock Fall Hazard Rating System, *Proceedings of IEAG International Symposium on Engineering Geology and the Environment*, Athens, Greece, 647-656

Gardner J.S, 1980, Frequency magnitude and spacial distribution of mountain rock falls and rock slides in the Highwood Pass area, Alberta, Canada, *Thresholds in Geomorphology*, Allen and Unwin, London, 267-295

Giani G.P, 1992, Rock slope stability analysis, *AA Balkema, Rotterdam*

Grosjean J, 1991, Kinematics and dynamics of mechanisms, *McGraw Hill, London*

Hearn G, Barrett R.K. & Henson H, 1995, Development of effective rock fall barriers, *Journal of Transportation Engineering*, 507-515

Hoek E, 1987, A program in BASIC for the analysis of rock falls, *Golder Associates*, Vancouver, BC.

Hoek E, 1990, Rock fall: a program in BASIC for the analysis of rock falls from slopes, *Unpublished notes.*

Huang R.Q, Wang S.T, & Zhang Z.Y, 1990, Theory and practise of geo-stress field analysis of large rock slopes, *Sixth International IAEC Congress*, Balkema, Rotterdam,

Hungr O & Evans S.G, 1988, Engineering evaluation of fragmental rock fall hazards, *Proceedings of the Fifth International Symposium on Landslides*, Lausanne, Switzerland, 685-690

Hungr O. & Evans S.G, 1993, The assessment of rock fall hazard at the base of talus slopes, *Canadian Geotechnical Journal*, Vol. 30, 620-636

Jennings J.N. & Costin A.B, 1978, Stone movement through snow creep 1963-75, Mount Twynam, Snowy Mountains, Australia, *Earth Surface Processes*, Vol. 3, 3-22

Johnson N.L & Kotz S, 1975, Continuous univariate distributions, Vol. 2 Distributions in statistics, *Wiley*, New York

Kobayashi Y, Harp E.L and Kagawa T, 1990, Simulation of rock falls triggered by earthquakes, *Rock Mechanics and Rock Engineering*, Vol. 23, 1-20

Kozanis S, 1995, Analysis of slopes version 2.05, *National Technical University of Athens*, Athens, Greece

Leroi E, Pontarollo F, Gascuel J.D. & Gascuel M.P, 1996, *Landslides*, (Ed. Senneset K.P.), Balkema, Rotterdam, Vol. 1, 271-278

Luckman B.H, 1976, Rock falls and rock fall inventory data: Some observations from Surprise Valley, Jasper National Park, Canada, *Earth Surface Processes*, Vol. 1, 287-298

McCauley M.L, Works B.W. & Naramore S.A, 1985, Rock fall mitigation, *Report FHWA/CA/TL-55-112*, Federal Highway Administration, US Department of Transportation, 147

McMillan P. & Matheson G.D, 1997, A two stage system for highway rock slope risk assessment, *International Journal of Rock Mechanics and Mining Science*, Vol. 34, No. 3-4, paper No 196.

Mercer R, 1982, The stabilisation of Craig-y-Dref, Tremadog, *Ground Engineering*, 28-32

Navarro M. & Wohl E.E, 1994, Geological hazard and risk calculation using GIS: methodology and model applied to Medelin, Columbia, *Bulletin of the Association of Engineering Geologists*, Vol. 31, No. 4, 459-481

Palassi M. & Franklin A, 1998, An expert system for evaluation and remediation of rock fall hazards in highway cuts, *Private communication*

Paronuzzi P, 1989, Probablistic approach for design optimization of rock fall protective barriers, *Quarterly Journal of Engineering Geology*, Vol. 22, 175-183

Peckover F.L, 1975, Treatment of rock falls on railway lines, *American Railway Engineering Association*, Bulletin 653, Chicago, IL, 471-503

Peckover F.L. & Kerr J.W.G, 1977, Treatment and maintenance of rock slopes on transportation routes, *Canadian Geotechnical Journal*, Vol. 14, 487-507

Peila D, Pelizza S. & Sassudelli F, 1988, Evaluation of behaviour of rock fall restraining nets by full scale tests, *Rock Mechanics and Rock Engineering*, Vol. 31, No. 1, 1-24

Pfeiffer T.J. & Bowen T.B, 1989, Computer simulation of rock falls, *Bulletin of the Association of Engineering Geologists*, Vol. 26, No. 1, 135-146

Pierson L.A, 1992, Rock fall hazard rating system, *Transportation and Research Record* 1343, 6-13

Piteau D.R, 1976, Computer rock fall model, *Publication ISMES*, Bergamo, Italy, 90-127

Ritchie A.M, 1963, Evaluation of rock fall and its control. *Highways Research Record* 17, 13-28

Robotham M.E, Wang H. & Walton G, 1995, Assessment of the risk from rock fall from active and abandoned quarry slopes, *Transactions of the Institute of Mining and Metallurgy,* (Section a), 104, 25-33

Sofianos A.I, Constantinidis C.V, Christodoulias J. & Anagnostopoulos A.G, 1988, Rock fall analysis in the ancient region of Argos, *Engineering Geology of Ancient Works, Monuments and Historical Sites,* (Ed. Marinos P. & Koukis G.), Balkema, Rotterdam, 213-217

Spang R.M, 1987, Protection against rock fall, *International Congress on Rock Mechanics,* Montreal, 1987, Vol. 1, 551-557

Statham I, 1979, A simple dynamic model of rock fall: Some theoretical principles and field experiments. *International Colloquium on Physical and Geomechanical Models.* ISMES, Bergamo, 237-258

Stevens W, 1996, Rock fall 2.0, software for the analysis of falling rocks on a steep slope. BASc. thesis, Department of Civil Engineering, *University of Toronto,* Ontario, Canada

Whiteside D.G.D, 1986, Discussion on rock fall protection measures, Conference on rock engineering in an urban environment, *Institute of Mining and Metallurgy,* Hong Kong, 490-492

Wilson J.M, 1996, ROXIM: A computer program to simulate rock fall, *Landslides,* (Ed. Senneset K.P.), Balkema, Rotterdam, 1643-1648

Wu S.S, 1985, Rock fall evaluation by computer simulation, *Transportation Research Record* 1031, 1-5

Wyllie D, 1987, Rock slope Inventory System, *Proceedings of the Federal Highway Administration Rock Fall Mitigation Seminary*, FHWA Region 10, Portland Oregon

Wyllie D.I. & Norrish N.I, 1996, Stabilisation of rock slopes, Chapter 18, Landslides investigation and mitigation, (Ed. Turner A. & Schuster R.L.), US Department of Transport, Washington DC, 474-504.

Zhou Y, Li T. & Zhou W, 1996, Assessment of risks, hazard and mitigation of rock fall in Dahekou Hydropower Station, *Landslides*, (Ed. Senneset K.P.), Balkema, Rotterdam, 435-440

Appendix 1

RFRAS Field Work

Appendix 1: RFRAS Field Work

A1.1 Slope Locations

The RFRAS has been applied to 18 slopes at ten sites in County Durham which have been listed in Table A1.1. The locations of these sites are further illustrated in Maps A1.1 to A1.6.

Slope Number	OS. Grid Reference NZ.	Location
1	433500, 540300	Running Waters
2	433500, 540300	
3	433500, 540300	
4	433500, 540300	
5	433550, 540300	Nr Running waters
6	433600, 540300	
7	366000, 382000	Nr. Wingate
8	297000, 472000	Finchale
9	292000, 473000	
10	289000, 473000	
11	333000, 442000	Pittington
12	333000, 442000	
13	334000, 455000	High Moorsley
14	358000, 485000	Eppleton quarry
15	330000, 379000	Quarrington
16	333000, 378000	
17	339000, 383000	Cassop Vale
18	374000, 375000	Wingate

TableA1.1: Slope Locations.

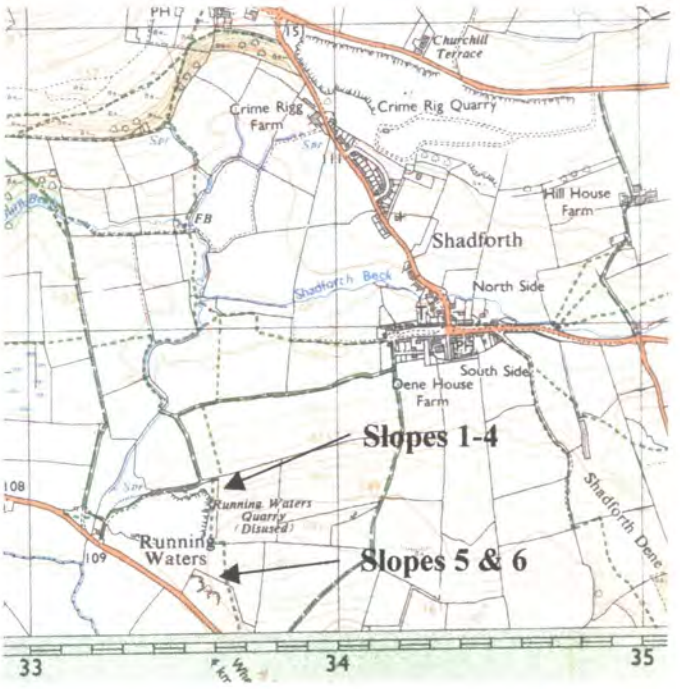

Map A1.1: Running waters quarry.

Map A1.2: Wingate quarry.

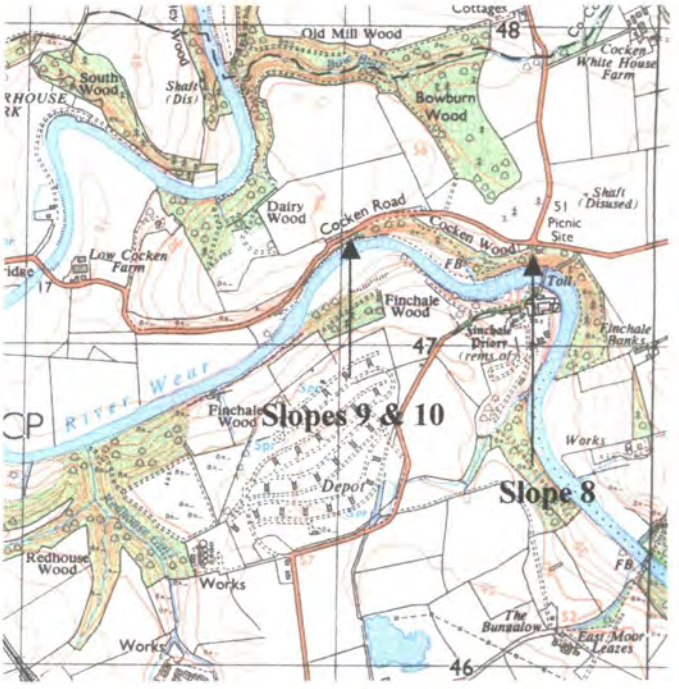

Map A1.3: Finchale.

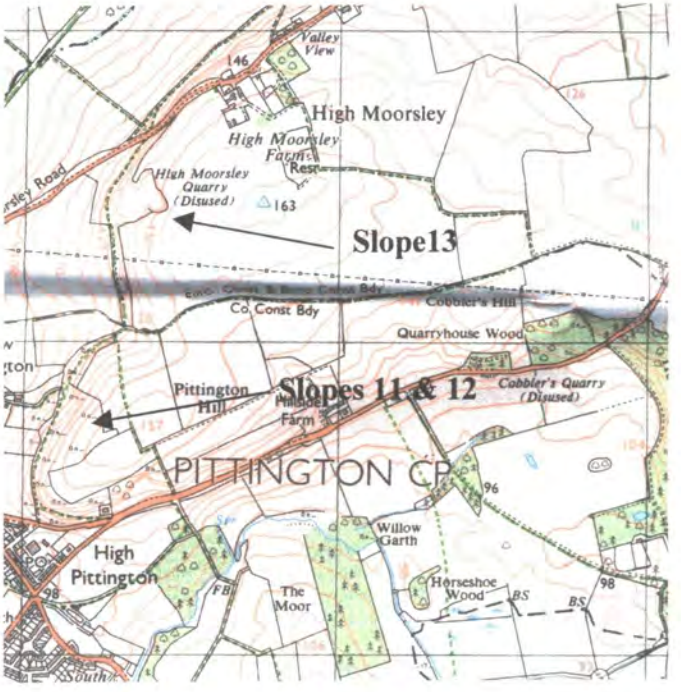

Map A1.4: Pittington and High Moorsley.

Map A1.5: Eppleton quarry.

Map A1.6: Quarrington and Cassop Vale.

A1.2 Slope photographs

Figure A1.1: Running Waters, slope 1.

Figure A1.2: Running Waters, slope 2.

Figure A1.3: Running Waters, slope 3.

Figure A1.4: Running Waters, slope 4.

Figure A1.5: Outcrop 1 Nr. Running Waters, slope 5.

Figure A1.6: Outcrop 2 Nr. Running Waters, slope 6.

Figure A1.7: Outcrop Nr. Wingate, slope 7.

Figure A1.8: Finchale, slope 8.

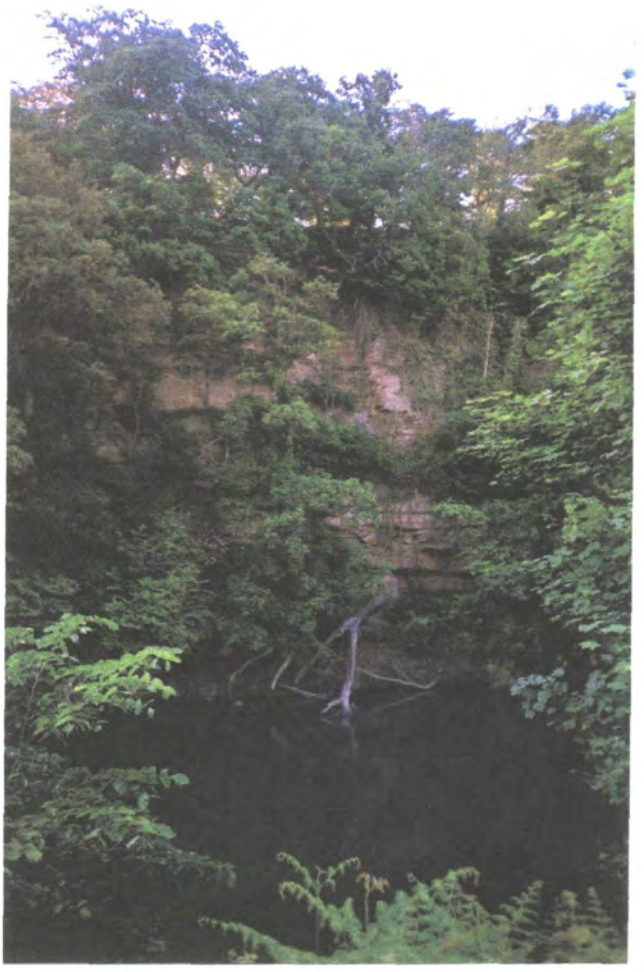

Figure A1.9: Finchale, slope 9.

Figure A1.10: Finchale, slope 10.

Figure A1.11: Pittington, slope 11.

Figure A1.12: Pittington, slope 12.

Figure A1.13: High Moorsley, slope 13.

Figure A1.14: Eppleton Quarry, slope 14.

Figure A1.15: Quarrington, slope 15.

Figure A1.16: Quarrington, slope 16.

Figure A1.17: Cassop Vale, slope 17.

Figure A1.18: Wingate, slope 18.

A1.3 Computerised Booking Sheets

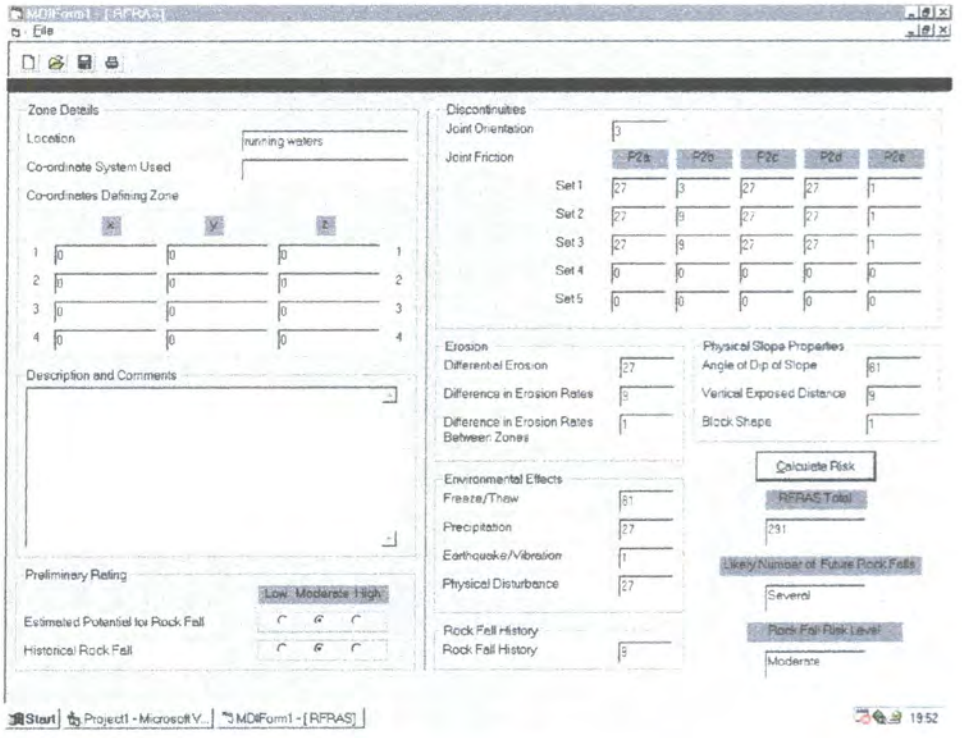

Figure A1.19: Running Waters, slope 1.

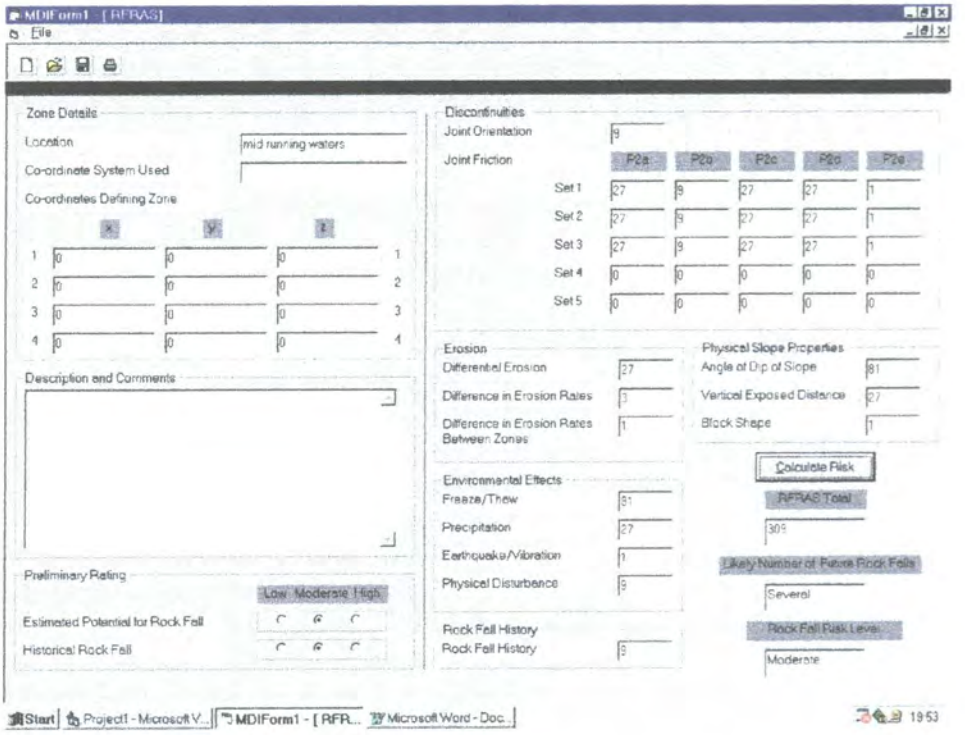

Figure A1.20: Running Waters, slope 2.

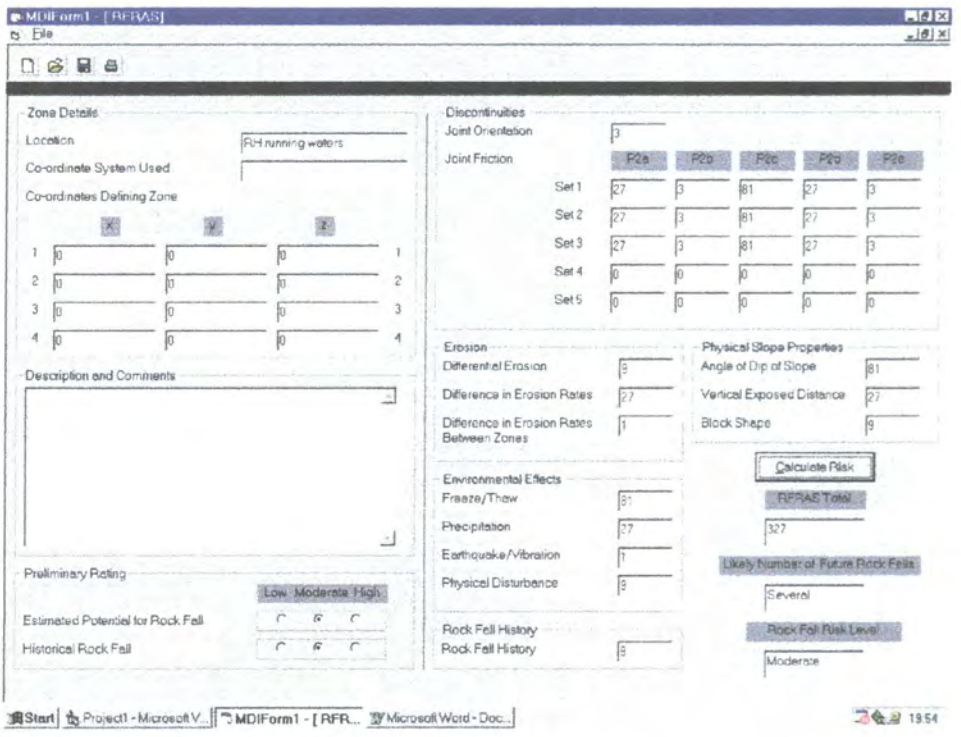

A1.21: Running Waters, slope 3.

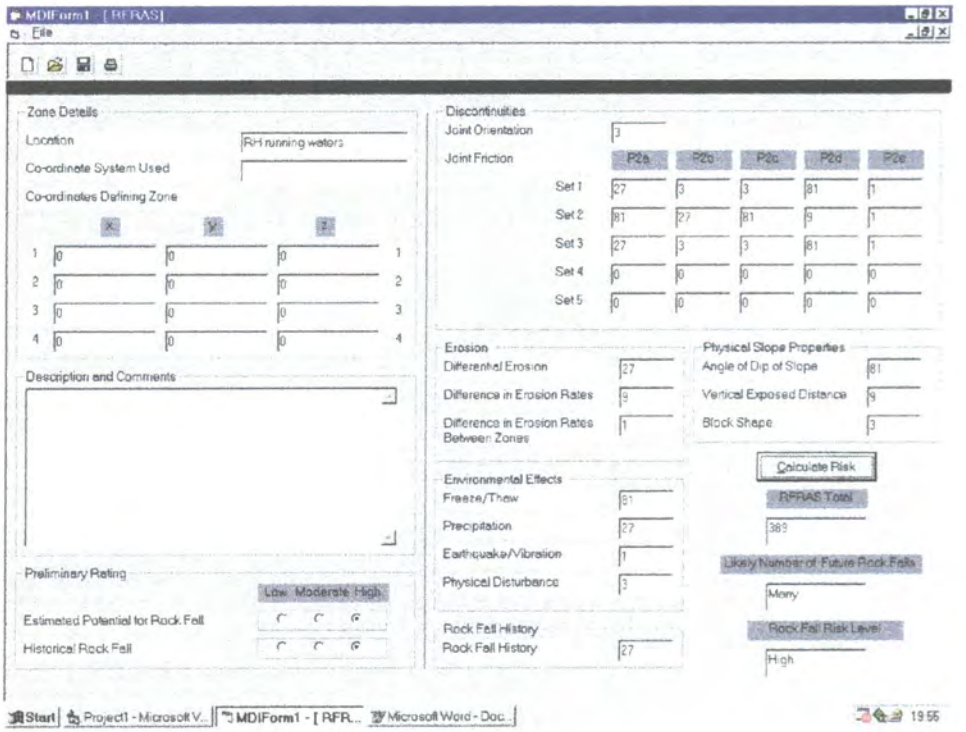

A1.22: Running Waters, slope 4.

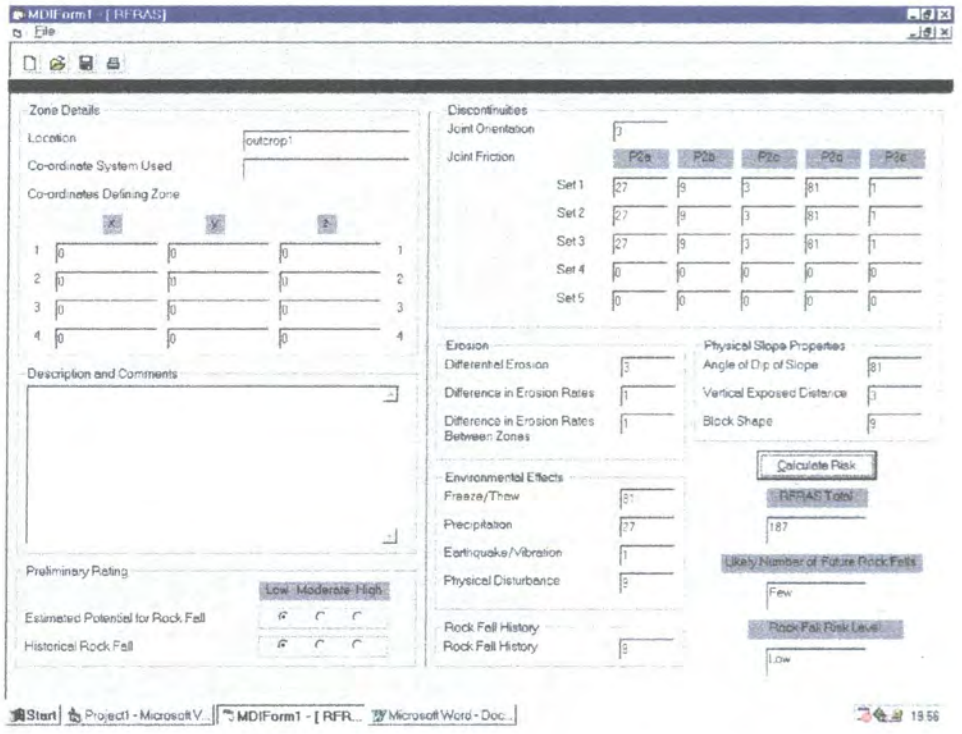

Figure A1.23: Outcrop 1 Nr. Running Waters, slope 5.

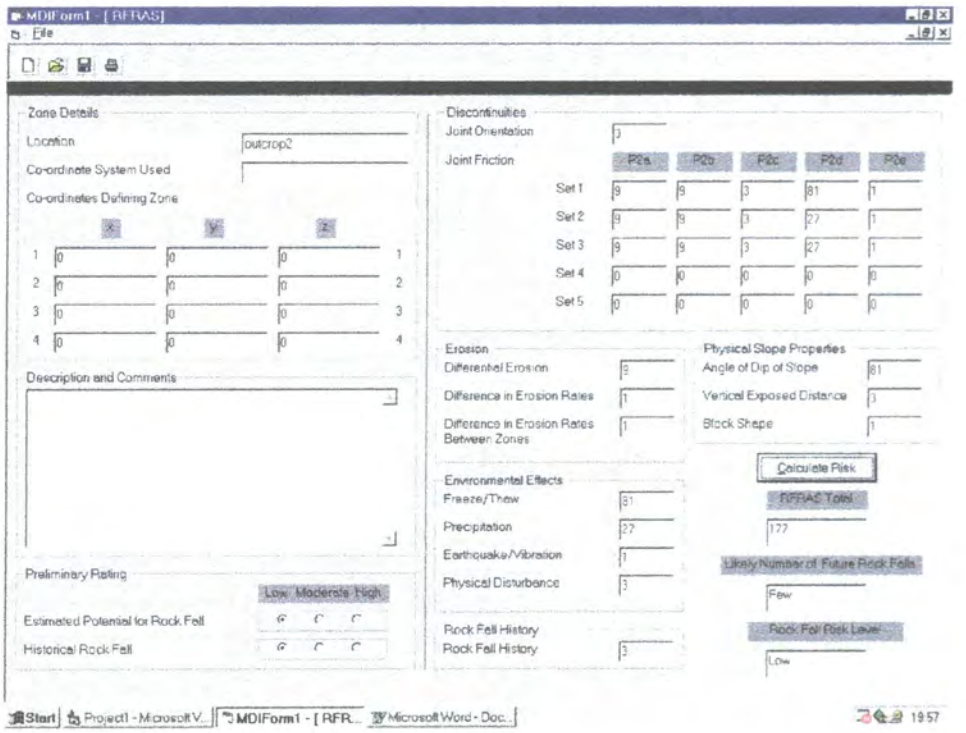

Figure A1.24: Outcrop2 Nr. Running Waters, slope 6.

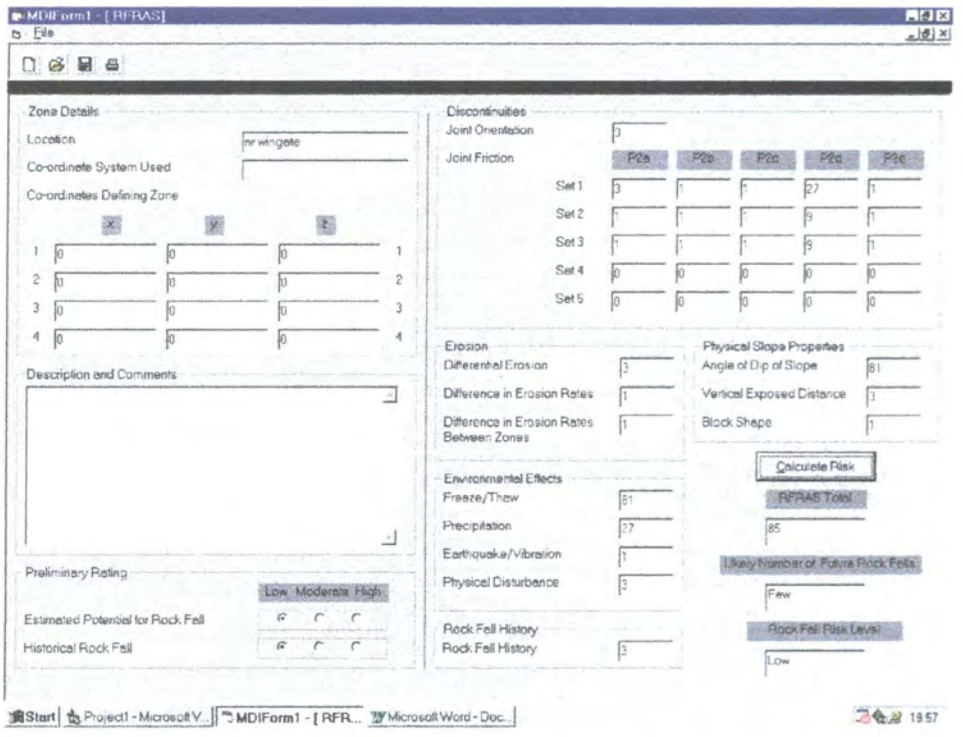

Figure A1.25: Outcrop Nr Wingate, slope 7.

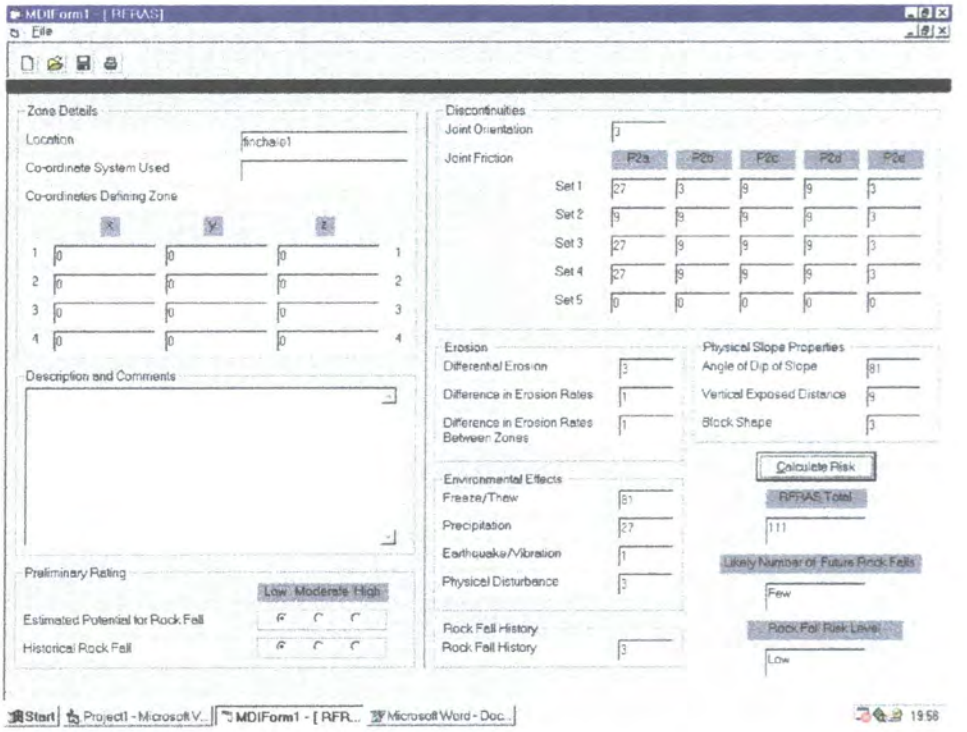

Figure A1.26: Finchale, slope 8.

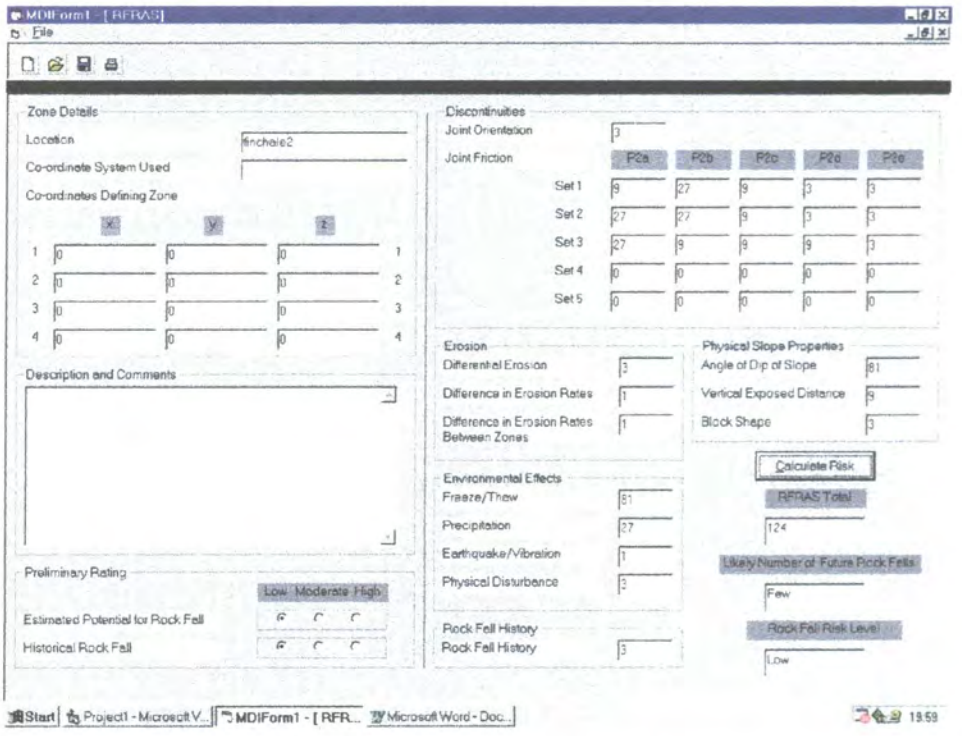

Figure A1.27: Finchale, slope 9.

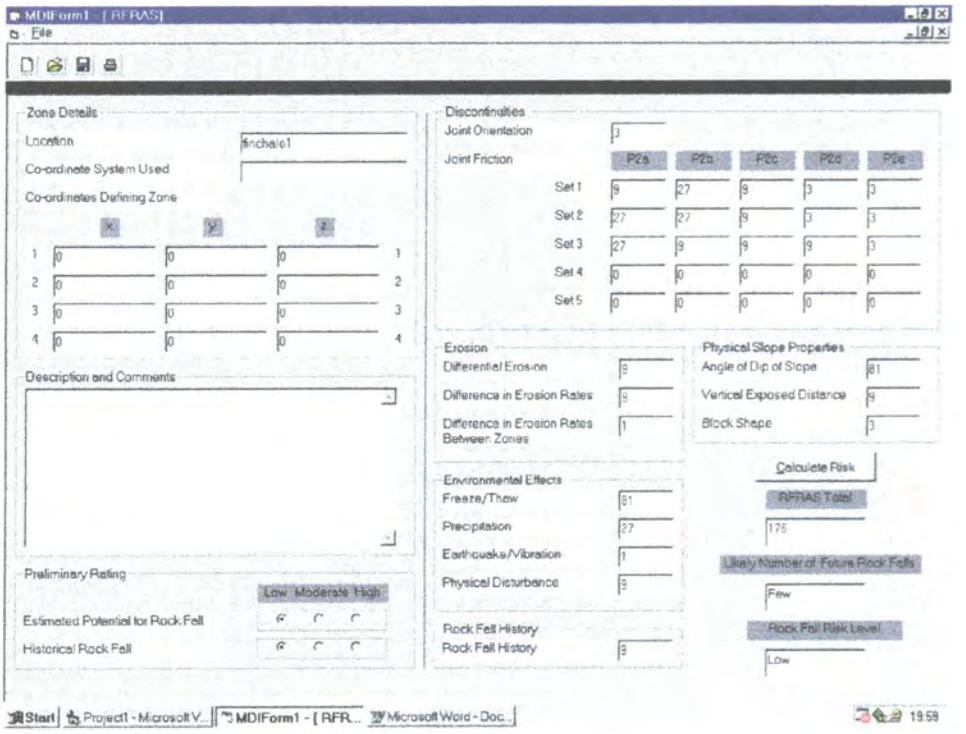

Figure A1.28: Finchale, slope 10.

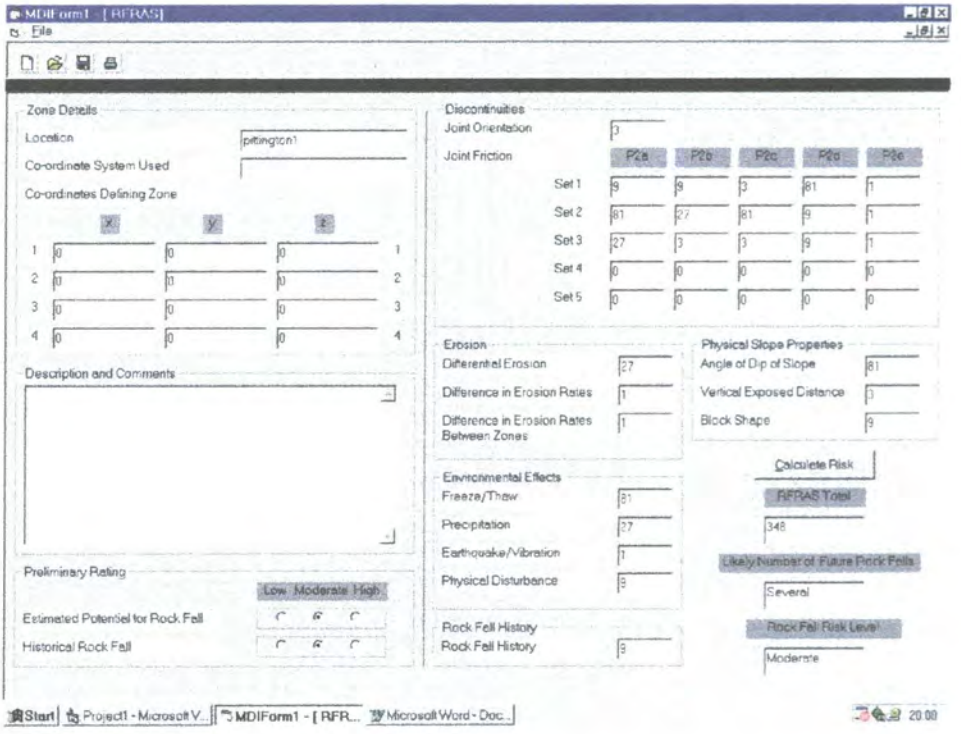

Figure A1.29: Pittington, slope 11.

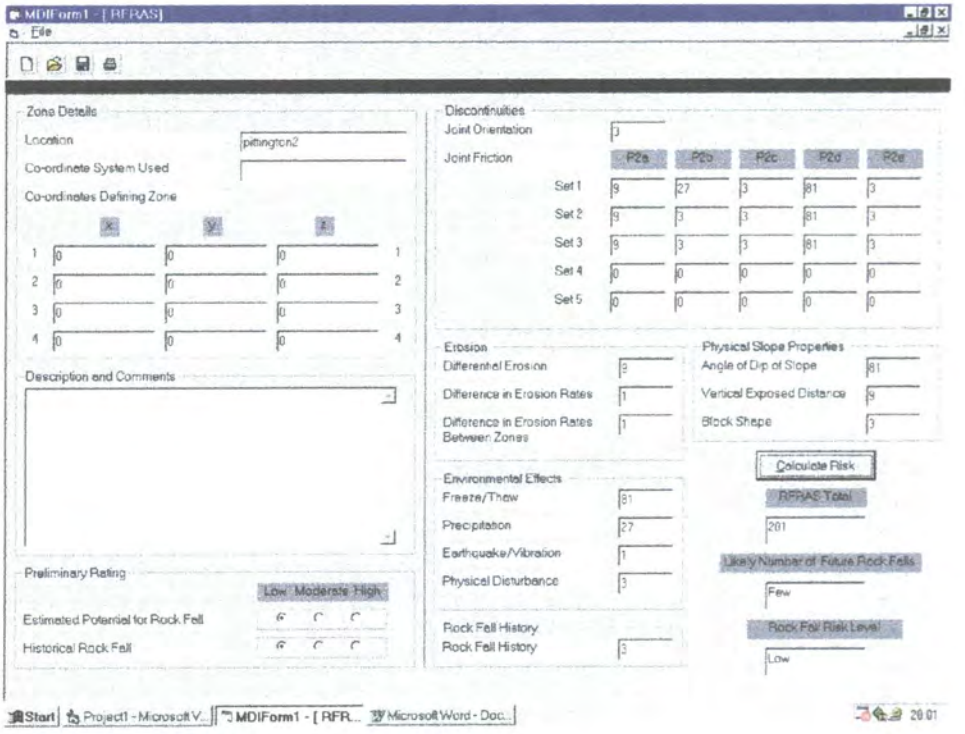

Figure A1.30: Pittington, slope 12.

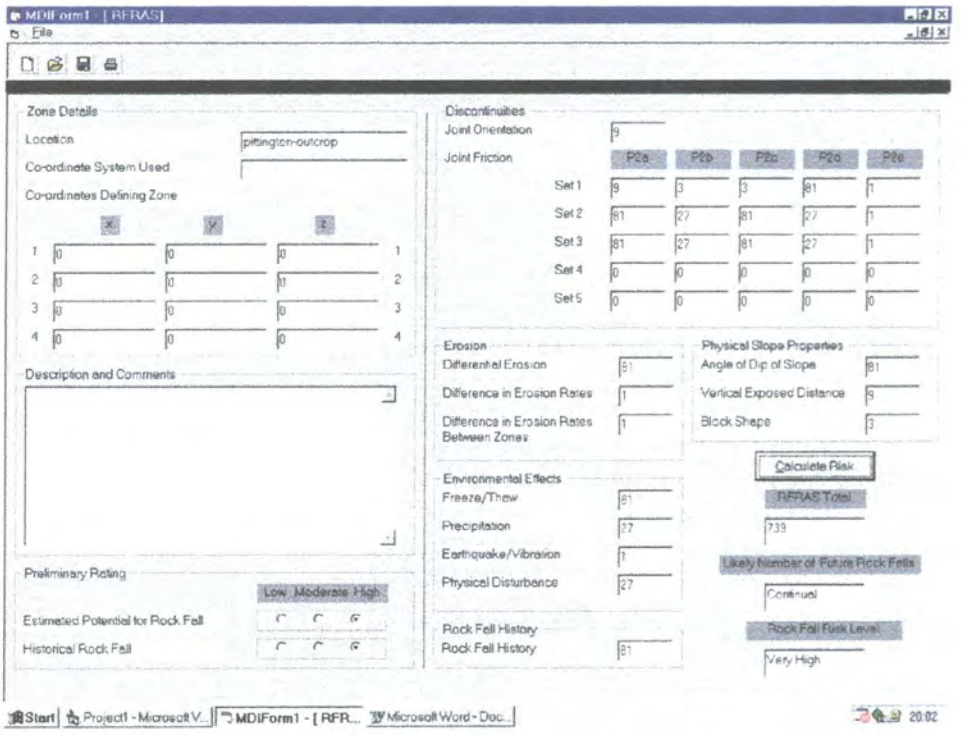

Figure A1.31: High Moorsley, slope 13.

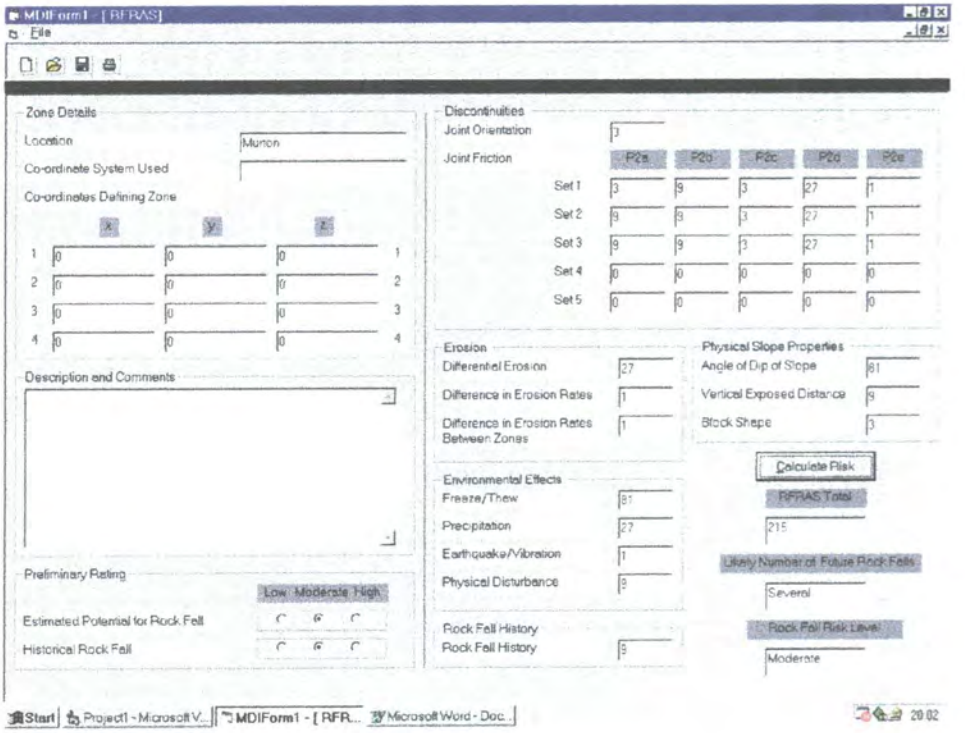

Figure A1.32: Eppleton Quarry, slope 14

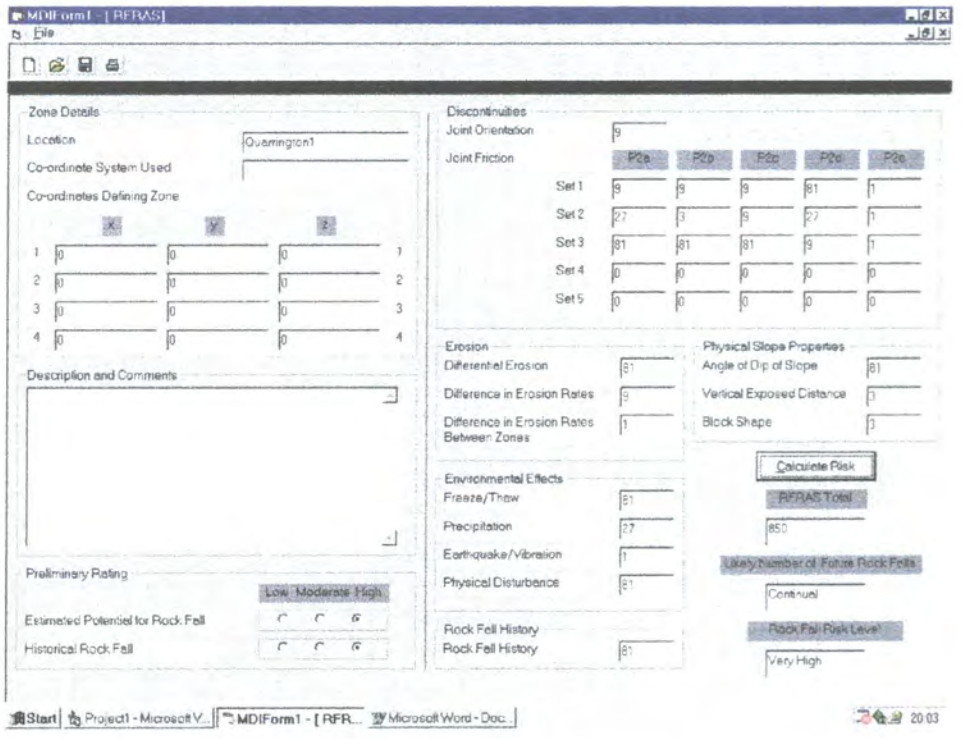

Figure A1.33: Quarrington, slope 15.

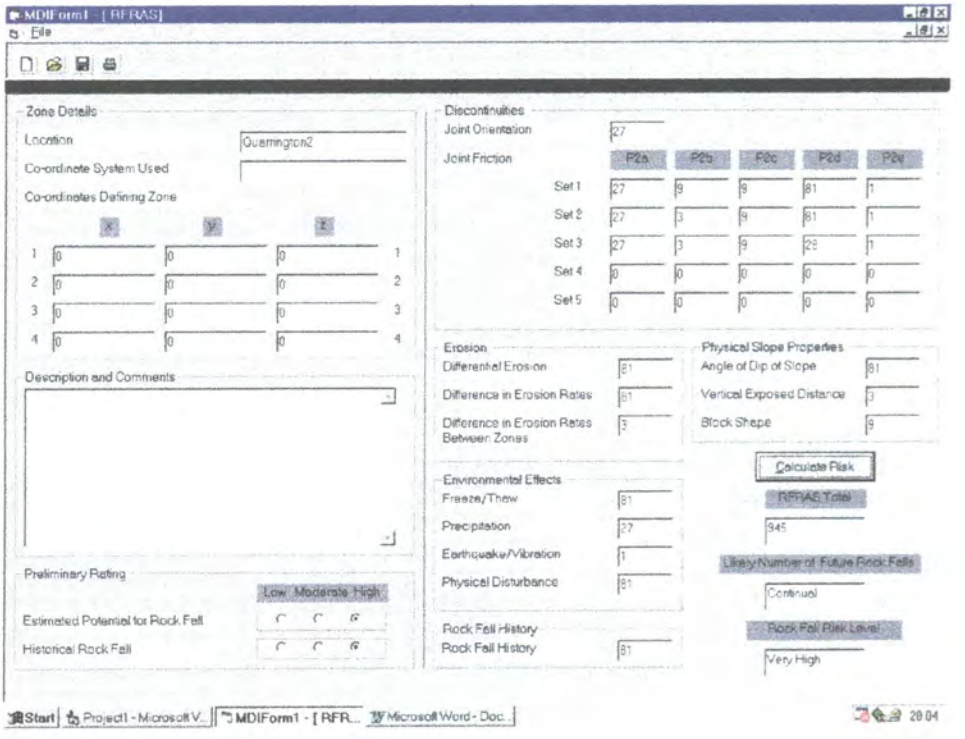

Figure A1.34: Quarrington, slope 16.

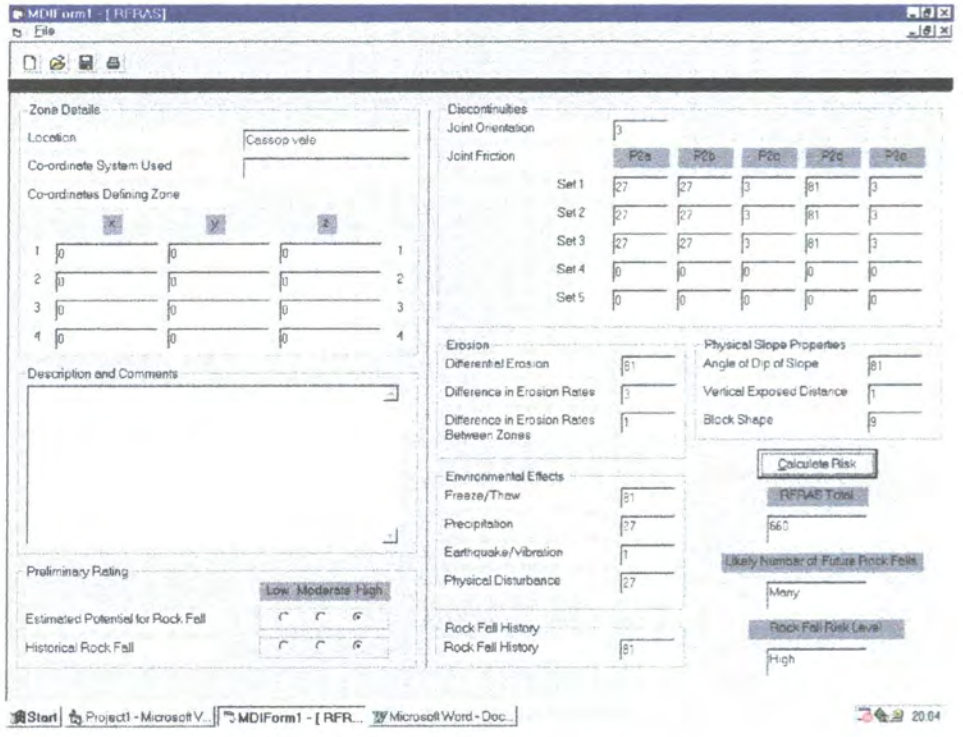

Figure A1.35: Cassop Vale, slope 17.

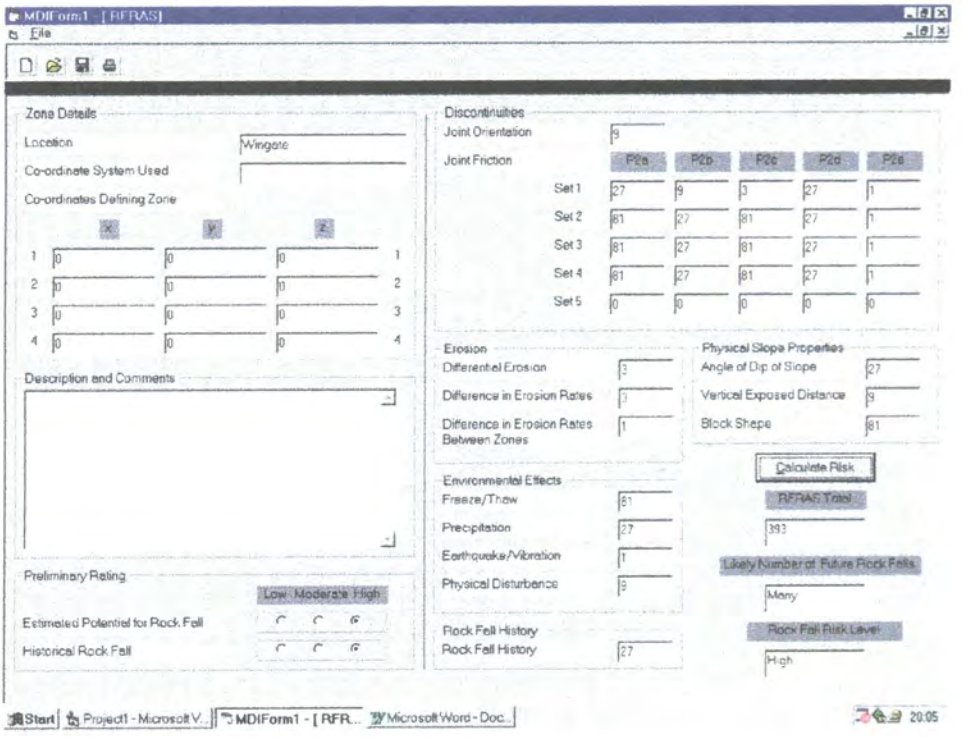

Figure A1.36: Wingate, slope 18.

Appendix 2

Users Guide to GeoFall

Appendix 2: Users guide to GeoFall

A2.1 Main program interface

Upon successful execution of the program file GeoFall.exe, the screen as illustrated in Figure A2.1 should be visible.

The interface is split into four areas from the top of the screen downwards. The first area is reserved for menu options; the second is for the tool bar. The third is used to display tool tips and the fourth is the main screen area.

The toolbar is separated into several sections, utilities, input parameters, program execute and output display.

A2.2 Utilities

The utilities section on the toolbar consists of three buttons, New, Open and Save.

A2.2.1 New

Upon pressing the New button all input data is erased and the program is reset ready for the input of new data. **Do not press this button unless you want to erase all data stored in the memory!**

A2.2.2 Open

Pressing this toolbar button brings up the pop up dialogue box as illustrated in Figure A2.2. This allows the user to open any previously saved *.rox file.

A2.2.3 Save

Pressing this toolbar button brings up the pop up dialogue box as illustrated in Figure A2.3. The destination directory and the filename may both be chosen. GeoFall file names follow standard Windows '95 naming convention. Using non-standard characters will result in an error.

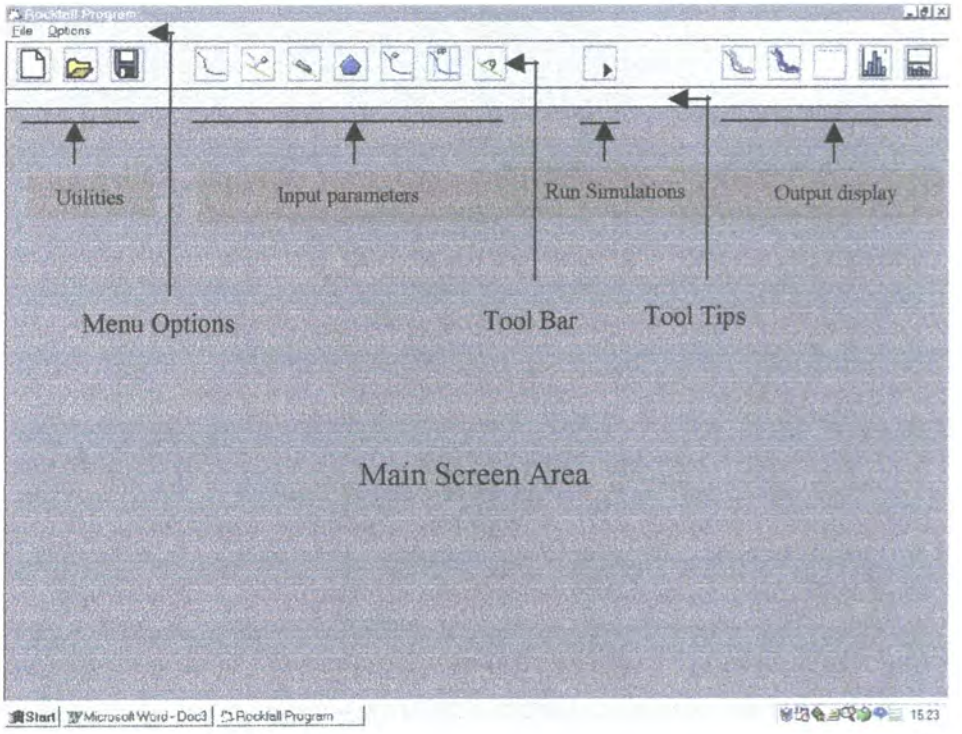

Figure A2.1: Main program interface.

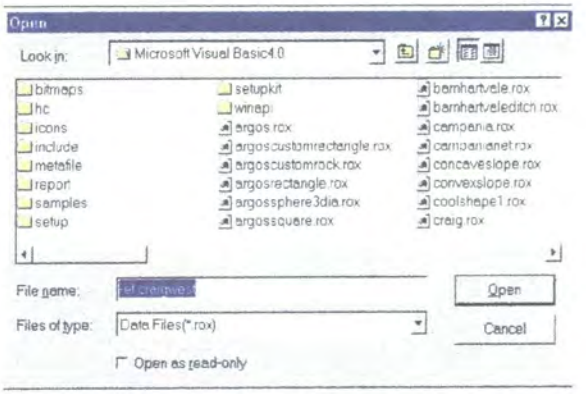

Figure A2.2: Open dialogue box.

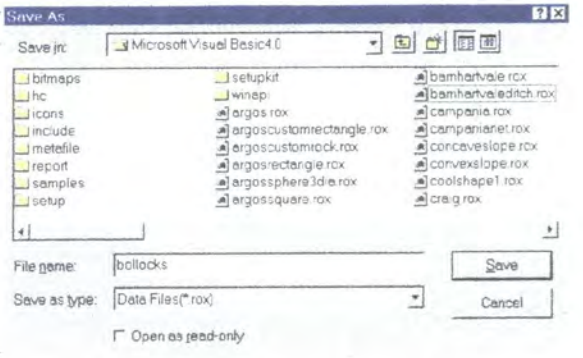

Figure A2.3: Save dialog box.

A2.3 Input parameters

The input parameter section of the toolbar consists of seven buttons. From left to right these consist of Slope co-ordinates, Slope coefficients of restitution, Coefficients of rolling and sliding, Rock type, Initial rock position, Position of analysis points and Position of nets. **It is important that the user initially inputs data from left to right.** Later on the user may wish to change some or all of the input parameters. If this is the case then data may have to be reconfirmed by clicking on the OK button on the relevant form.

A2.3.1 Slope co-ordinates

The cross section of the slope is described in a 2D Cartesian co-ordinate system. The co-ordinates of the slope are inputted such that the slope profile is generated in an anticlockwise manner (Figure A2.4). All of the co-ordinates describing the slope must both be positive and greater than zero. The slope can be described by a maximum of fifty points. Any type of slope geometry may be modelled.

A2.3.2 Coefficients of restitution

Once the data for the slope profile has been determined then data for the coefficients of restitution may be entered (Figure A2.5). The number of regions contained in the slope is automatically highlighted in red and the program on execution automatically ignores any data entered below this point. A separate deviation from the mean value for both the coefficients of normal (e_n) and tangential (e_t) restitution may be entered. This value must be positive because it is the magnitude of the deviation. The program produces a pseudo random value having a uniform probability that varies the value of the coefficient up to the maximum deviation. The deviation from the mean may be either positive or negative in sign and this is randomly determined by the program.

A2.3.3 Coefficients of rolling resistance and sliding friction,

Once the data for the slope profile has been determined then data for the coefficients of rolling resistance and sliding friction may be entered (Figure A2.6).

A2.3.4 Surface roughness

The angle of deviation in degrees for the slope region on impact may be randomly varied between set limits. The program produces a pseudo random value having a uniform probability that varies the value of the slope angle up to the maximum deviation. The deviation from the mean may be either positive or negative in sign and this is randomly determined by the program. It is recommended that the value for the slope deviation be kept below 15 degrees. If no slope variation is required then this value is set to zero by default.

A2.3.5 Rock type

Thirteen different standard geometrical rock shapes may be chosen by the user by clicking on the relevant Option button (Figure A2.7). The necessary parameters a, b, c and h may then be entered along with the density of the rock. If none of the thirteen shapes are appropriate than a custom rock shape may be generated by double clicking on the user defined Option button which brings up the screen as illustrated in Figure A2.8. The five button custom rock toolbar allows the user to define a New rock, set the Grid on or off , to set the Grid spacing, Zoom 100% or to Complete the rock shape by closing the boundary.

An example of a custom generated rock shape is illustrated in Figure A2.8. The rock consists of twelve nodes and has been drawn in an anticlockwise manner. Once the penultimate rock node has been reached then the rock shape may be closed. This is done by clicking on the right hand icon on the toolbar.
By dragging the mouse whilst the right hand button is depressed allows the user to create a zoom window.
A rock may be defined by a maximum number of thirty points or nodes.

A2.3.6 Initial position of the rock

The initial position of the rock may be set in one of two ways. The co-ordinates of the rock centroid may be typed in or by clicking the left hand mouse button on the desired location of the rock centroid (Figure A2.9).

Dragging the mouse with the right hand button depressed creates a zoom window that allows the user to zoom in on the slope. To return to the default view depress the Zoom 100% button.

The rock may be rotated by clicking on the + or - buttons. The outside buttons rotate the rock in five degree increments whilst the inner buttons rotate the buttons in one degree increments.

The initial vertical, horizontal and angular velocities may now be set.

A2.3.7 Analysis points

By inserting an analysis point, information regarding the velocity and kinetic energy of the passing rocks may be determined at that point (Figure A2.10). For each analysis point five histograms are produced. A maximum of five analysis points may be generated and the positions of these are determined by their x co-ordinate. The number of analysis points must be chosen before the corresponding x co-ordinate may be entered. This is done by clicking on the left hand button pertaining to the number of analysis points required.

A2.3.8 Rock fall nets

A total of ten rock fall nets may be placed on the slope (Figure A2.11). The location of the net is described by two sets of co-ordinates corresponding to the top and bottom of the net respectively. A net does not have to be vertical. Three commercially available nets produced by GeoBrugg may be chosen and these range in capacity from 250-1500 kJ. The user may also define the capacity of the rock net if the three commercial nets are inappropriate. All stated capacities are the maximum energy that the net may absorb by plastic deformation.

The check box in the right side of the form allows the user to include or exclude the net in the simulation.

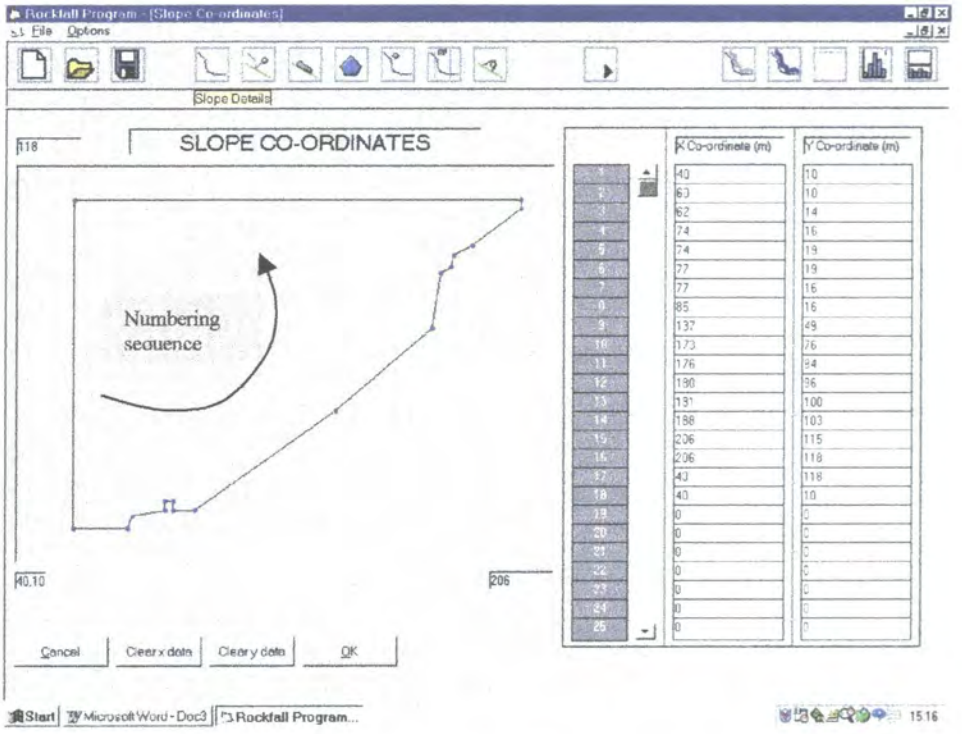

Figure A2.4: Slope co-ordinate data.

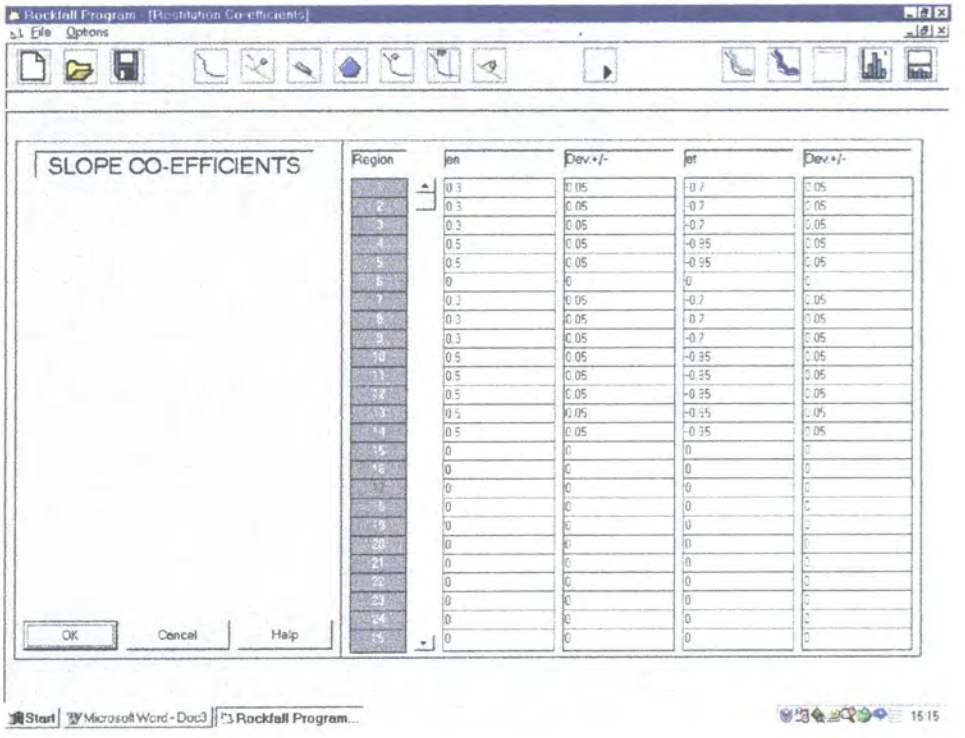

Figure A2.5: Coefficients of restitution.

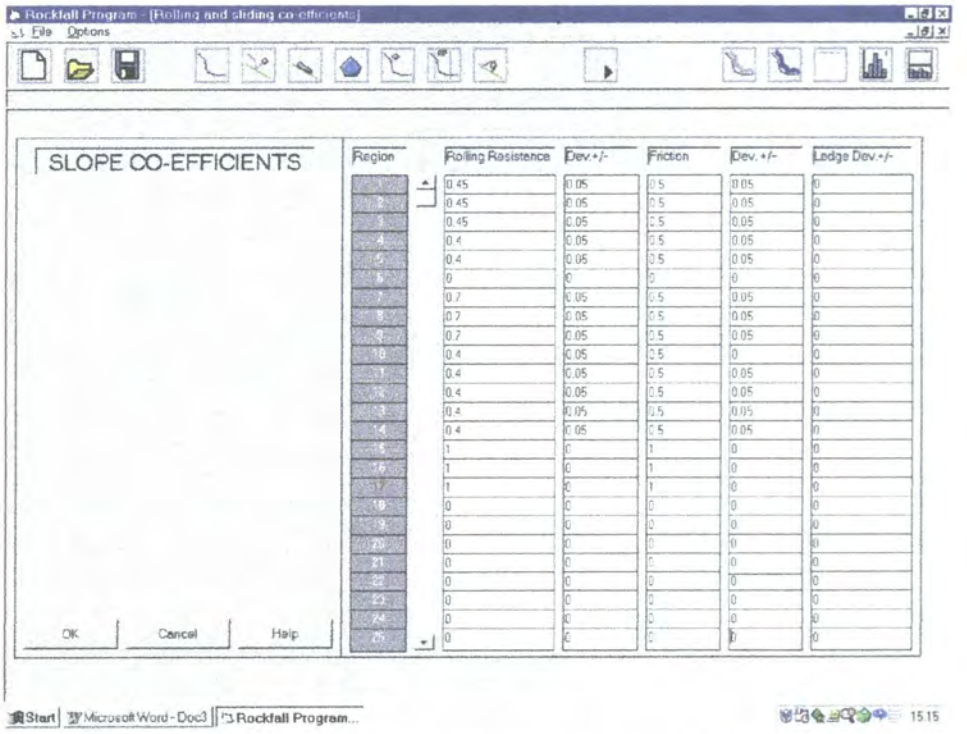

Figure A2.6: Coefficients of rolling, sliding and ledge deviation.

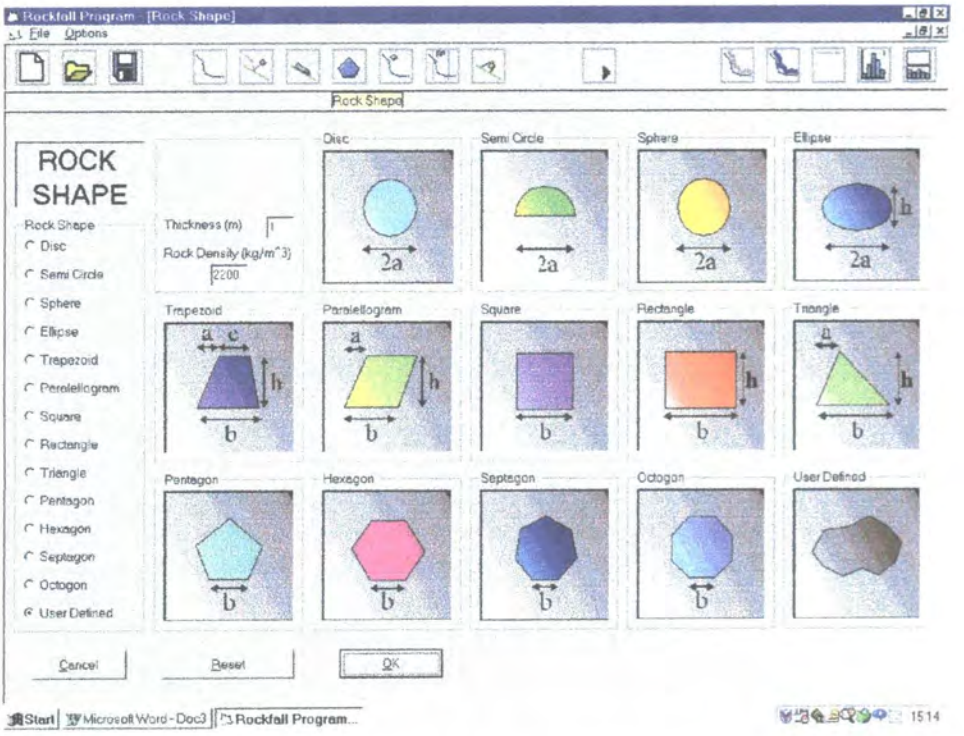

Figure A2.7: Rock shapes.

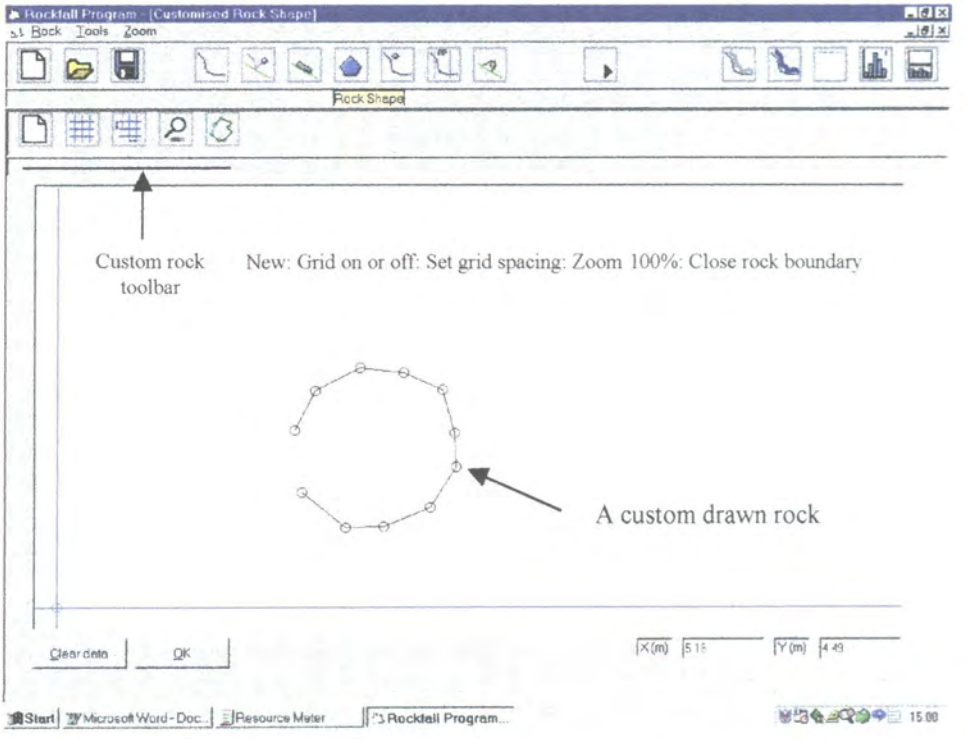

Figure A2.8: A custom generated rock.

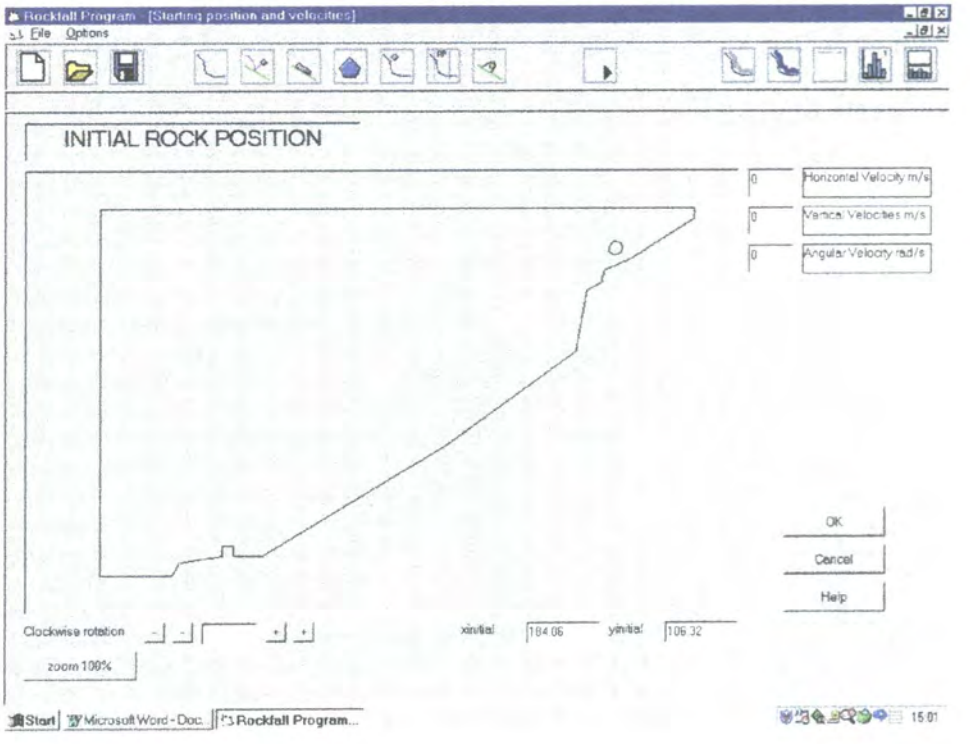

Figure A2.9. Initial position of the rock.

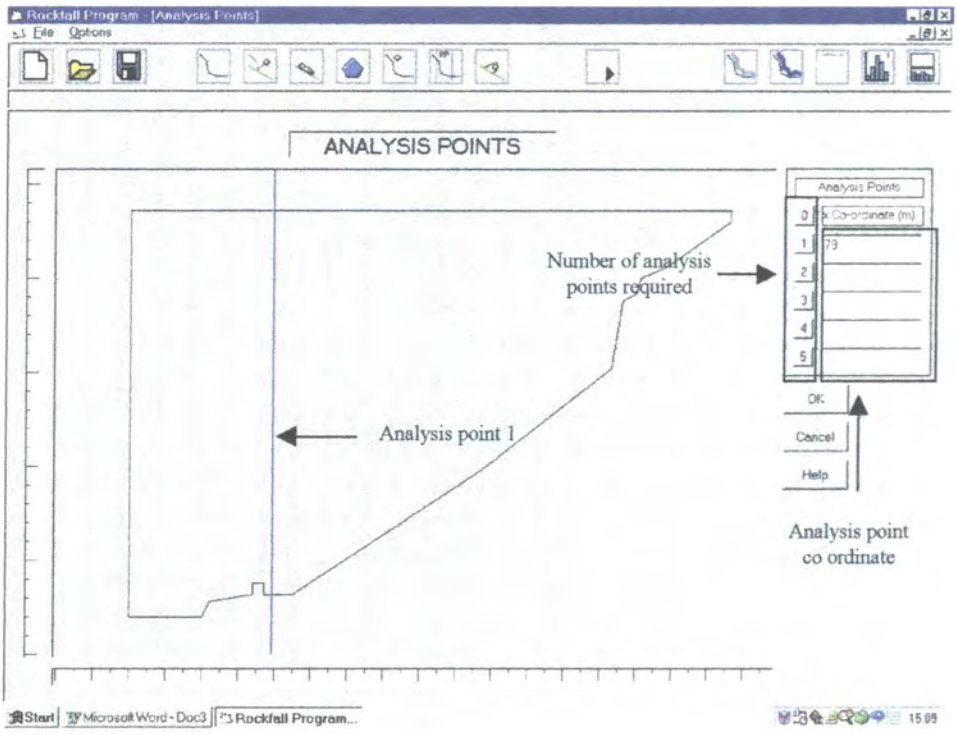

Figure A2.10. Position of analysis points.

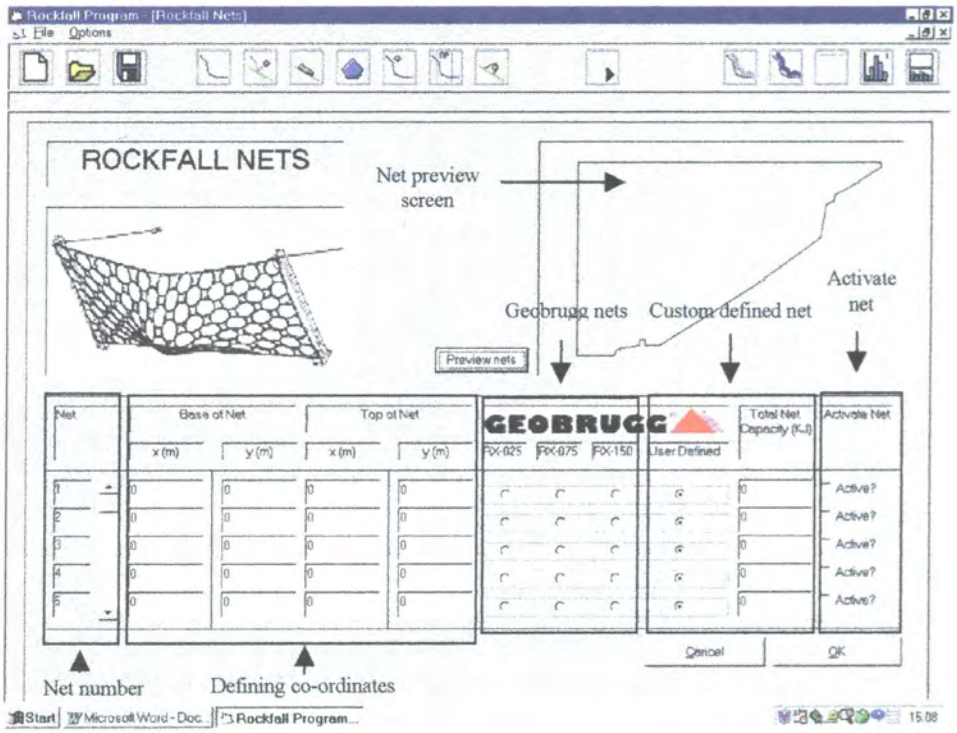

Figure A2.11: Location and capacity of rock fall nets.

A2.4 Start rock fall simulation

Once the data has been entered into the program then the rock fall simulation may be initiated by pressing the Play button on the toolbar. On successful data input the screen illustrated in Figure A2.12 should be visible.

The box labelled NIT allows the user to specify the number of iterations. There is no limit to the number in this box but the greater this number the greater the free system resources will have to be. This is dependant upon the type of computer and the amout of free RAM. Setting this parameter too high may cause the program to hang or crash. A recommended maximum value of NIT is fifty.

If the user wishes the rock to be animated then the Check box must contain a tick.

Dragging the mouse with the right hand button depressed, a zoom window is created. The user may zoom into an area on the slope before of after the rock fall simulation. Depressing the Zoom 100% button restores the display to normal.

Depressing the Drop Rock button starts the rock fall simulation. If incorrect or incomplete data has been entered then the form illustrated in Figure A2.13 will be visible. A series of check boxes on the left hand side of the form inform the user as to which data is missing. Data must be confirmed by clicking on the OK button in the relevant form. If more than one source of data is missing then they must be confirmed in sequence starting at the top and working downwards.

A progress bar shows the user the number of simulations that are complete. Figure A2.12 illustrates five rock fall trajectories using the customised rock shape described earlier.

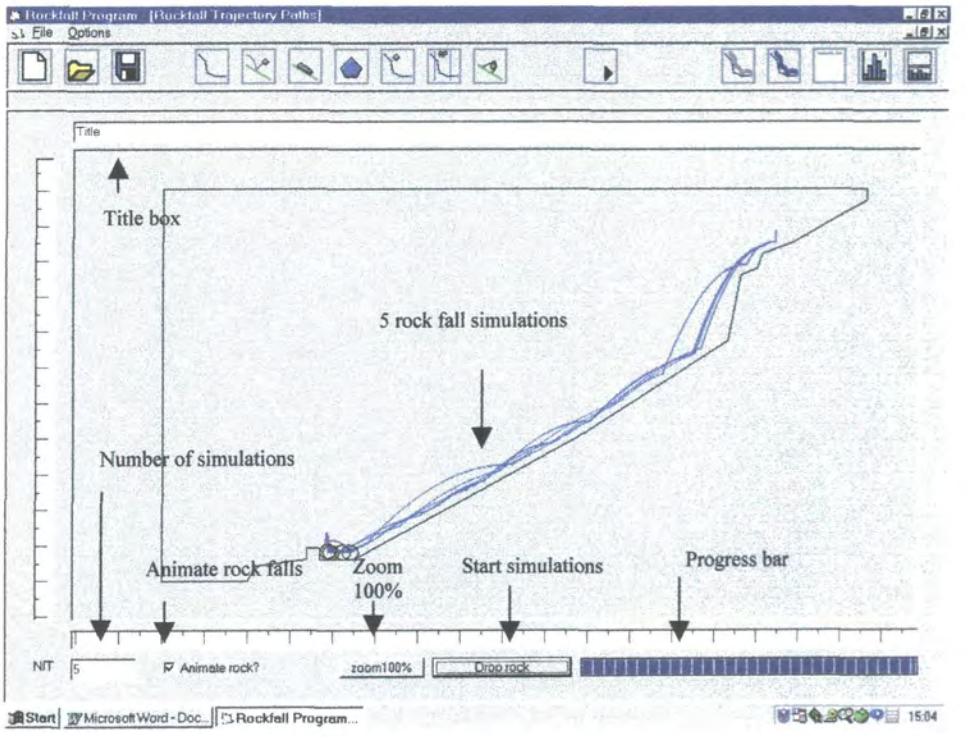

Figure A2.12: Rock fall simulation.

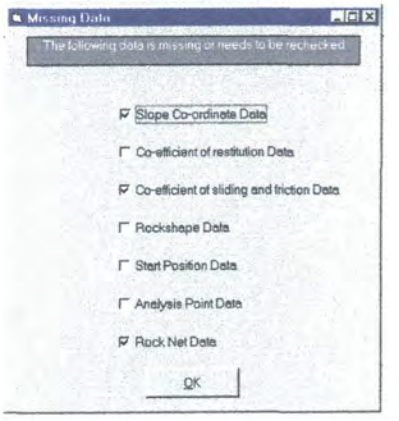

Figure A2.13: Missing data form.

A2.5 Output display

The output display section of the toolbar consists of five buttons, namely, minimum and maximum zone of influence, analysis point data, histograms and rock fall runout.

A2.5.1 Minimum and maximum zone of influence.

The minumum and maximum zones of influence for the previous five rock fall simulations are shown in Figure A2.14. The minimum zone of influence is determined by the shortest radial distance to a rock node. A circle of this radius is drawn with its centre in the position of the rock centroid. This is repeated for all the rock centroid positions which describe its trajectory. Any object within the shaded area is likely to be struck by rock fall. The maximum zone of influence is calculated using the maximum radial distance to a rock node. The procedure is then the same as for the minimum zone of influence. Anything outside the maximum zone of influence is unlikely to be struck by a rock fall. For a sphere or disc the maximum and minimum zones or influence will be identical.

A2.5.2 Analysis point data

The maximum and minimum velocities and kinetic energies for all of the rocks that cross the analysis point are presented (Figure A2.15). If no rocks pass an analysis point then the output box will contain the text "no data".

A2.5.3 Output histograms

Upon depressing the histogram button in the toolbar the pop up toolbox should appear (Figure A2.16). The number on the button refers to the analysis point number. A colour coded system is used to differentiate between output types. The blue histograms show horizontal velocity, red shows vertical velocity, green, angular velocity, purple, absolute velocity and dark blue shows kinetic energy.

The ouput histograms for the rock fall simulation illustrated in Figure A2.12 are presented in Figure A2.17.

A2.5.4 Rock fall distribution

Below the plot of the rock fall trajectories is a histogram which shows the final resting positions of the rocks (Figure A2.18). The x axis of the histogram is split into ten meter coarse intervals and five meter fine intervals. The vertical axis of the output trajectories plot is split into 25 meter coarse intervals and five meter fine intervals. These intervals are fixed and cannot be changed by the user. If a "time out error" occurs during execution of the rock fall simulation then the output of the histogram for that particular rock is shown in red, all other rock falls are shown in blue.

A2.6 Advanced options

The advanced options form is only accessible through the text menus located at the top left of the program interface screen. Figure A2.19 shows the advanced options form.

The time increment sets the time increment between calculating rock positions. The finer the increment the longer a simulation will take. It is recommended that the time increment is only changed from the default value if the rocks anticipated velocity is likely to be high.

The maximum array size is the maximum number of points which define the rock trajectory that can be stored. If the array size is too low then a "time out" error will occur.

The coefficients of restitution for the rock may be entered. These coefficents are only used if a face of the rock strikes a point on the slope.

The cut off velocities for the different modes of travel may also be set. If the velocity of the rock after impact is lower than that of the specified cut off velocity then the rocks mode of travel is altered.

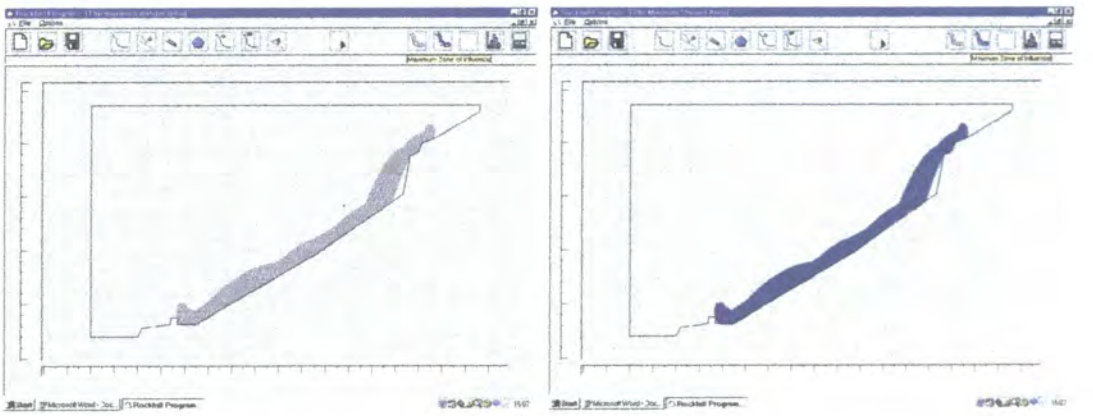

Figure A2.14: Minimum and maximum zone of influence.

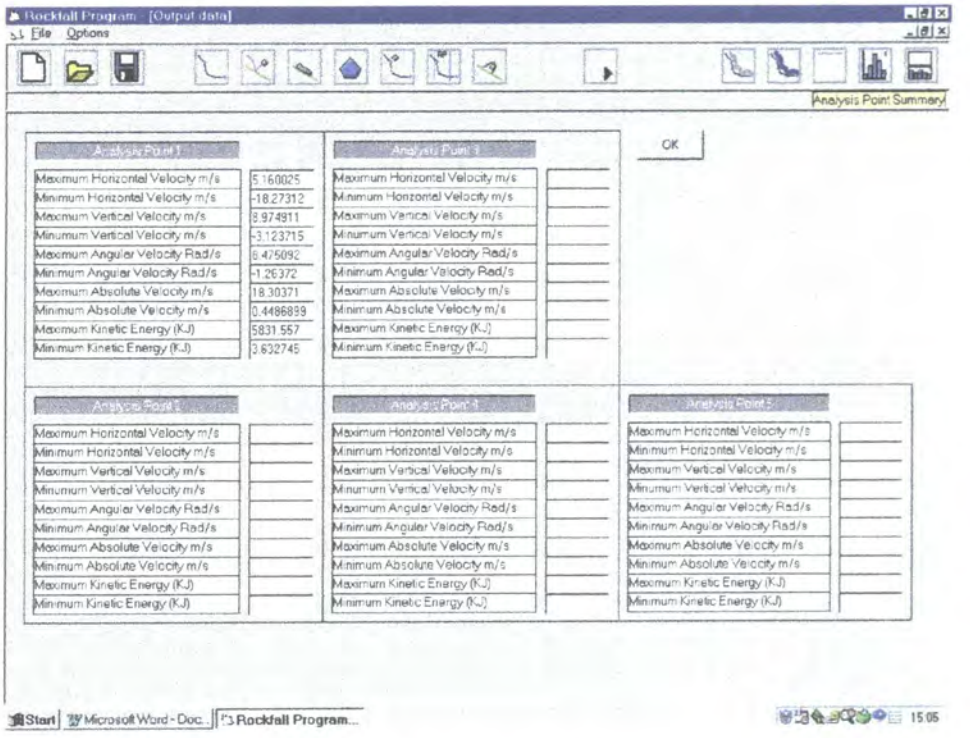

Figure A2.15: Analysis point data summary.

Figure A2.16: Output histogram toolbox.

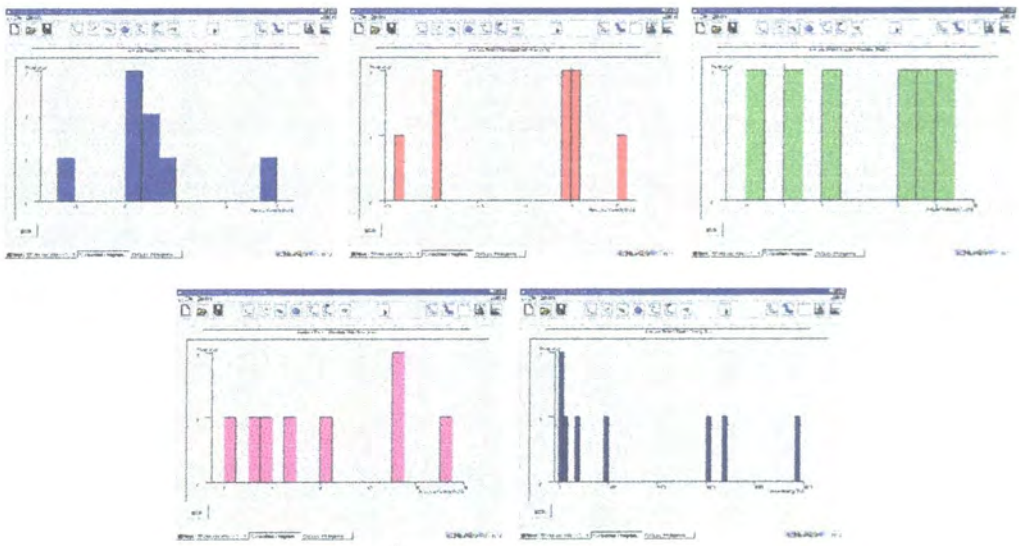

Figure A2.17: Example output histograms.

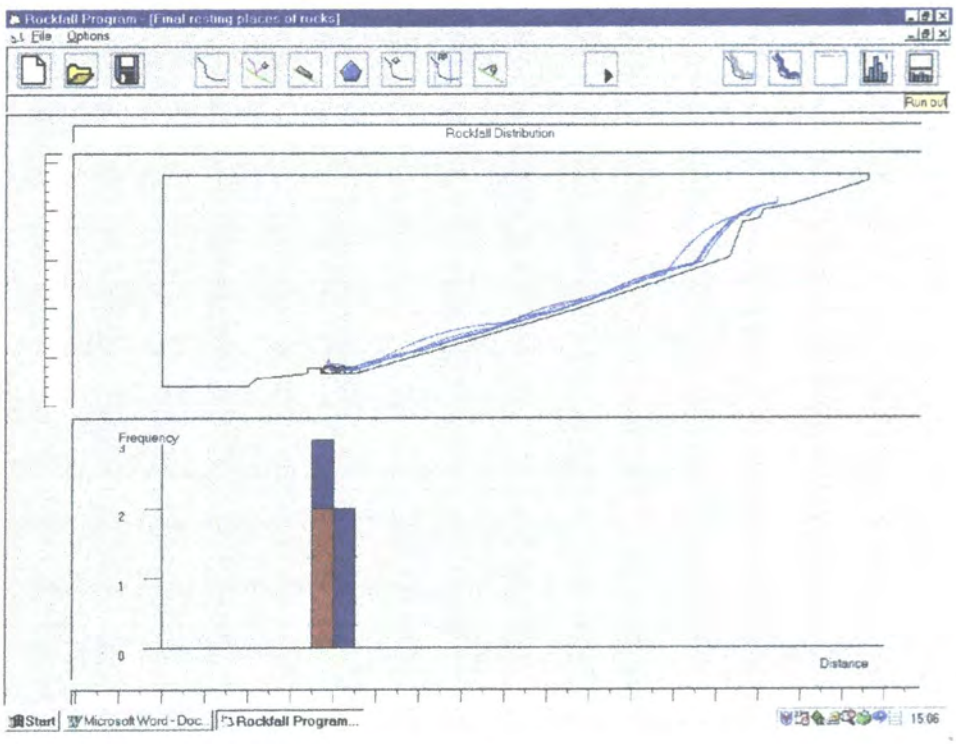

Figure A2.18: Sample rock fall distribution.

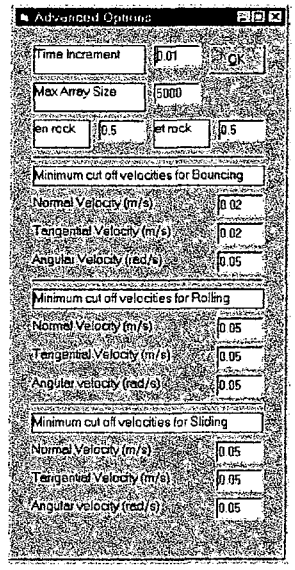

Figure A2.19: Advanced options.

A2.7 Errors

A "time out" error is caused by one or more of the following;

a) Insufficient array space.

The default array size is 5000. This allows 5000 positions of the rock to be stored in memory for each rock fall iteration. If the rock is travelling very slowly then this array space will be filled before the rock has come to rest. The user may either increase the time step or increase the array size to allow the continuance of the rock fall motion. Increasing the array size will require more system resources.

b) Too low a time step.

If the time step is too low then the array used to store the rock position will be filled. The time step may be increased or the array size increased.

c) The rock is "trapped".

Sometimes during a simulation a rock will be unable to move from its present location due to the geometry of the slope and the rocks shape. If this is the case then the rock may be trapped. This has the effect of filling the array space.

Appendix 3

GeoFall Algorithm Verification

Appendix 3: GeoFall algorithm verification

Direction of travel	Variable	GeoFall	Hand Calculation	% Error
Left to right downwards	Starting horizontal velocity (m/s)	10.000		-
	Final horizontal velocity (m/s)	10.000	10.000	0
	Starting vertical velocity (m/s)	-7.749		-
	Final vertical velocity (m/s)	-9.711	-9.711	0
	Starting centroid position (m)	22.900, 54.239		-
	Final centroid position (m)	24.900, 52.493		
Left to right upwards	Starting horizontal velocity (m/s)	16.185		-
	Final horizontal velocity (m/s)	16.185	16.185	0
	Starting vertical velocity (m/s)	4.416		-
	Final vertical velocity (m/s)	2.454	2.454	0
	Starting centroid position (m)	38.057, 34.852		-
	Final centroid position (m)	41.294, 35.539		
Right to left downwards	Starting horizontal velocity (m/s)	-10.000		-
	Final horizontal velocity (m/s)	-10.000	-10.000	0
	Starting vertical velocity (m/s)	-2.551		-
	Final vertical velocity (m/s)	-4.513	-4.513	0
	Starting centroid position (m)	82.400, 56.968		-
	Final centroid position (m)	80.400, 56.262		
Right to left upwards	Starting horizontal velocity (m/s)	-16.185		-
	Final horizontal velocity (m/s)	-16.185	-16.185	0
	Starting vertical velocity (m/s)	4.121		-
	Final vertical velocity (m/s)	2.159	2.159	0
	Starting centroid position (m)	61.458, 34.980		-
	Final centroid position (m)	58.221, 35.609		

Table A3.1: Projectile verification

Direction of travel	Variable	GeoFall	Hand Calculation	% Error
Left to right downwards μ_r=0.3	Starting horizontal velocity (m/s)	2.945		-
	Final horizontal velocity (m/s)	3.356	3.356	0
	Starting vertical velocity (m/s)	-2.454		-
	Final vertical velocity (m/s)	-2.797	-2.797	0
	Starting centroid position (m)	14.825, 47.282		-
	Final centroid position (m)	15.457, 46.755		
Left to right downwards μ_r=0.85	Starting horizontal velocity (m/s)	0.872		-
	Final horizontal velocity (m/s)	0.859	0.859	0
	Starting vertical velocity (m/s)	-0.726		-
	Final vertical velocity (m/s)	-0.716	-0.716	0
	Starting centroid position (m)	14.468, 47.583		-
	Final centroid position (m)	14.641, 47.439		
Left to right upwards μ_r=0.3	Starting horizontal velocity (m/s)	3.456		-
	Final horizontal velocity (m/s)	2.581	2.581	0
	Starting vertical velocity (m/s)	2.879		-
	Final vertical velocity (m/s)	2.150	2.150	0
	Starting centroid position (m)	51.769, 27.775		-
	Final centroid position (m)	52.368, 28.275		
Left to right upwards μ_r=0.85	Starting horizontal velocity (m/s)	3.767		-
	Final horizontal velocity (m/s)	2.467	2.467	0
	Starting vertical velocity (m/s)	3.139		-
	Final vertical velocity (m/s)	2.056	2.056	0
	Starting centroid position (m)	51.357, 27.432		-
	Final centroid position (m)	51.974, 27.947		

Table A3.2: Rolling verification

Direction of travel	Variable	GeoFall	Hand Calculation	% Error
Right to left downwards μ_r=0.3	Starting horizontal velocity (m/s)	-2.709		-
	Final horizontal velocity (m/s)	-3.120	-3.120	0
	Starting vertical velocity (m/s)	-2.257		-
	Final vertical velocity (m/s)	-2.600	-2.600	0
	Starting centroid position (m)	72.053, 44.684		-
	Final centroid position (m)	71.468, 44.197		
Right to left downwards μ_r=0.85	Starting horizontal velocity (m/s)	-0.950		-
	Final horizontal velocity (m/s)	-0.938	-0.938	0
	Starting vertical velocity (m/s)	-0.791		-
	Final vertical velocity (m/s)	-0.781	-0.781	0
	Starting centroid position (m)	72.149, 44.768		-
	Final centroid position (m)	71.960, 44.160		
Right to left upwards μ_r=0.3	Starting horizontal velocity (m/s)	-3.769		-
	Final horizontal velocity (m/s)	-2.894	-2.894	0
	Starting vertical velocity (m/s)	3.141		-
	Final vertical velocity (m/s)	2.412	2.412	0
	Starting centroid position (m)	38.720, 27.369		-
	Final centroid position (m)	38.058, 27.921		
Right to left upwards μ_r=0.85	Starting horizontal velocity (m/s)	-3.838		-
	Final horizontal velocity (m/s)	-2.538	-2.538	0
	Starting vertical velocity (m/s)	3.198		-
	Final vertical velocity (m/s)	2.115	2.115	0
	Starting centroid position (m)	27.239, 38.877		-
	Final centroid position (m)	38.245, 27.765		

Table A3.3: Rolling verification

Direction of travel	Variable	GeoFall	Hand Calculation	% Error
Right to left downwards μ_d=0.3	Starting horizontal velocity (m/s)	2.748		-
	Final horizontal velocity (m/s)	3.364	3.364	0
	Starting vertical velocity (m/s)	-2.290		-
	Final vertical velocity (m/s)	-2.805	-2.805	0
	Starting centroid position (m)	22.915, 39.896		-
	Final centroid position (m)	23.533, 39.383		
Left to right downwards μ_d=0.3	Starting horizontal velocity (m/s)	-1.791		-
	Final horizontal velocity (m/s)	-2.408	-2.408	0
	Starting vertical velocity (m/s)	-1.492		-
	Final vertical velocity (m/s)	-2.001	-2.001	0
	Starting centroid position (m)	67.446, 40.193		-
	Final centroid position (m)	67.021, 39.841		

Table A3.4: Sliding verification.

Appendix 4

Coefficients of Normal Restitution

Appendix 4: Coefficients of normal restitution (e_n)

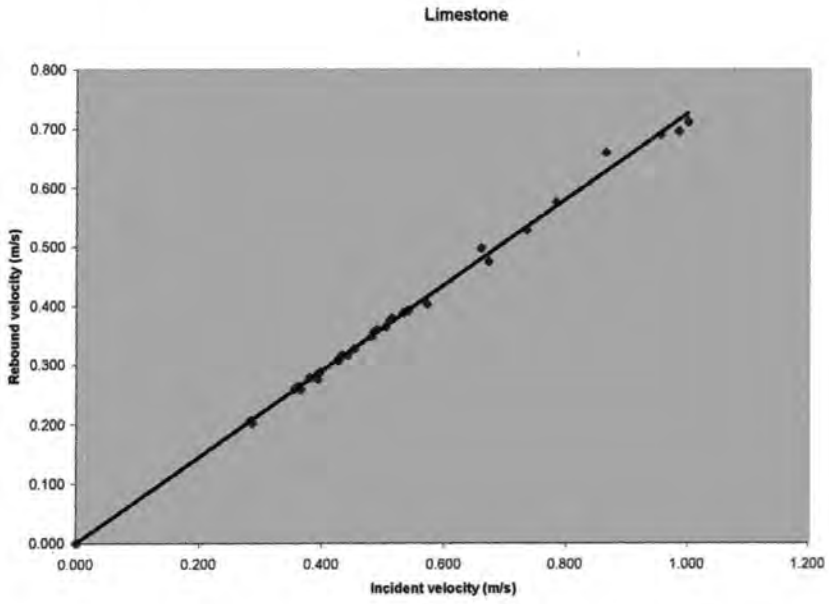

Figure A4.1: Incident v rebound velocity for a limestone disc.

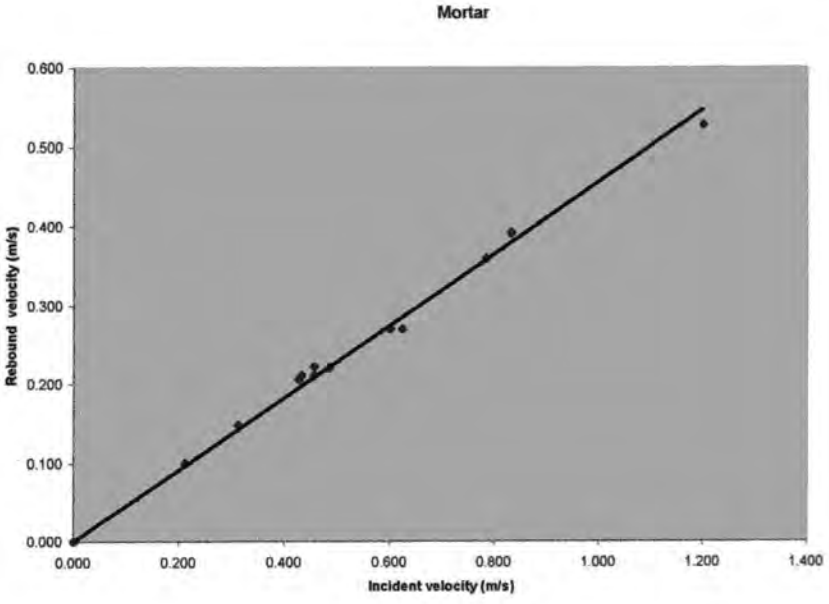

Figure A4.2: Incident v rebound velocity for a mortar disc

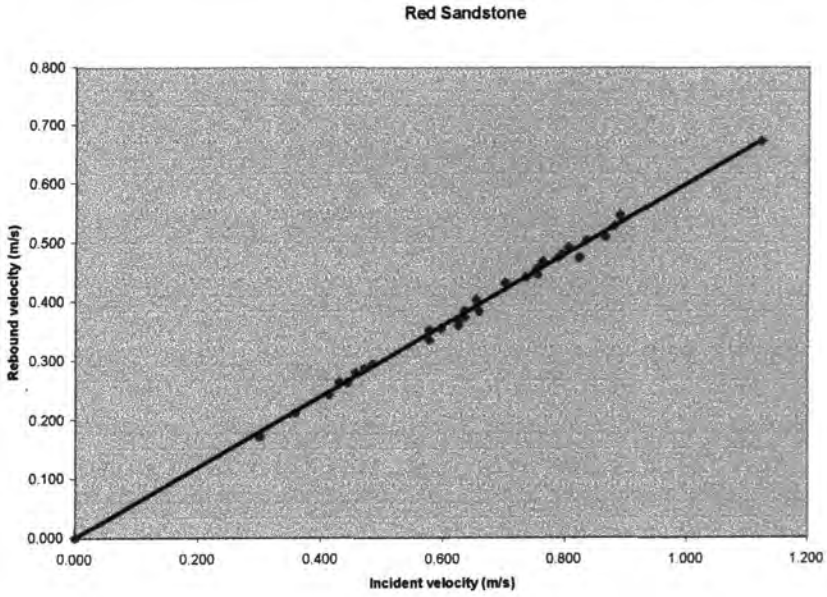

Figure A4.3: Incident v rebound velocity for a red sandstone disc.

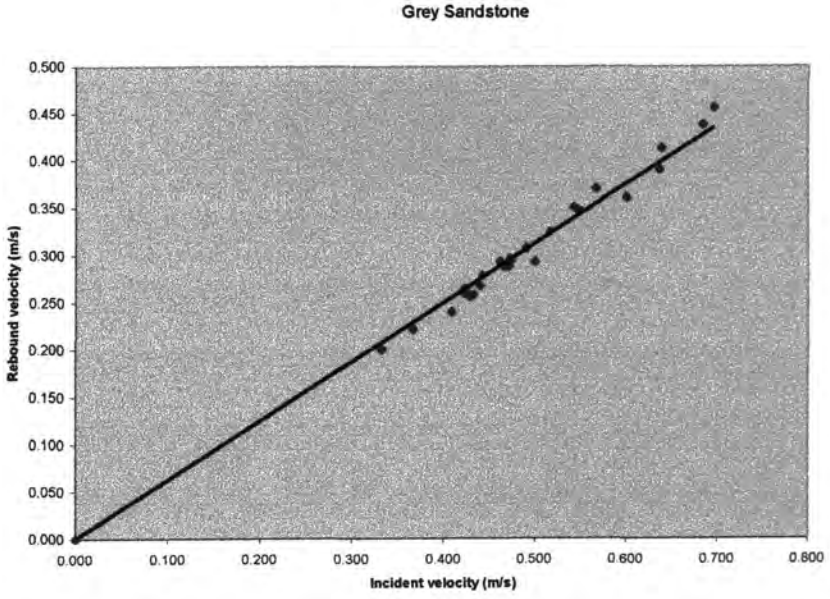

Figure A4.4: Incident v rebound velocity for a grey sandstone disc.

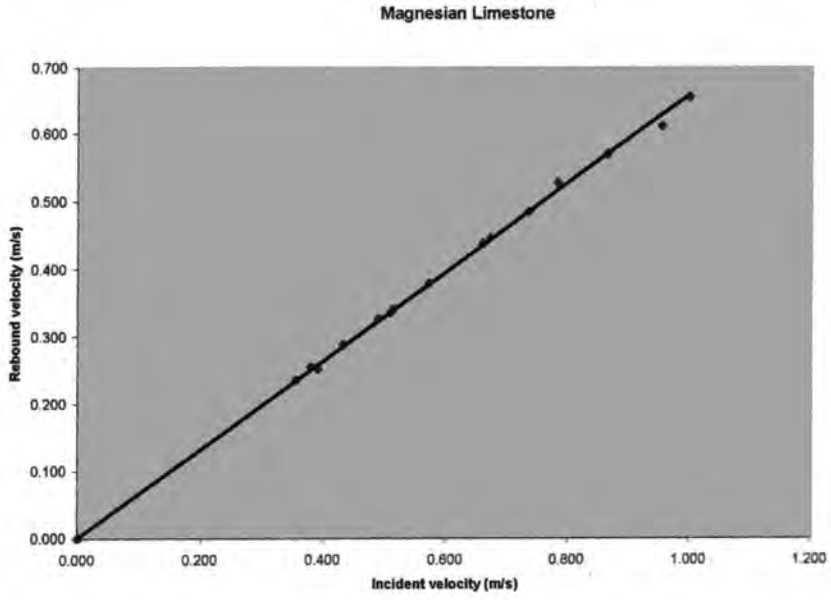

Figure A4.5: Incident v rebound velocity for a magnesian limestone disc

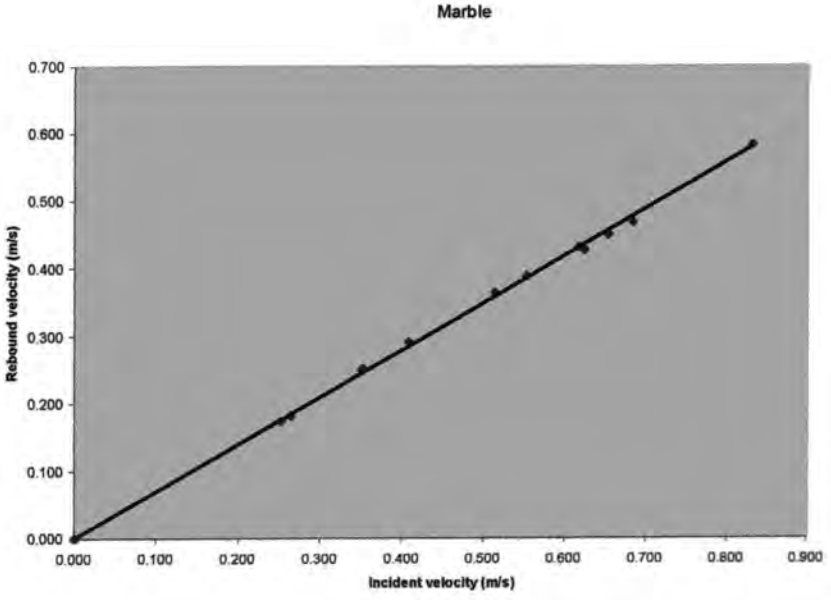

Figure A4.6: Incident v rebound velocity for a marble disc